LEVEL

A MODEL TO CALCULATE EM FIELDS IN TROPOSPHERIC DUCT ENVIRONMENTS AT FREQUENCIES THROUGH SHF

by
Sherman Marcus, Ph.D. and William D. Stuart
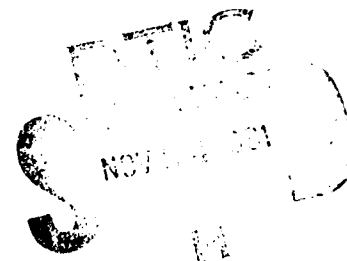of
IIT Research Institute
Under Contract to
DEPARTMENT OF DEFENSE
Electromagnetic Compatibility Analysis Center
Annapolis, Maryland 21402

SEPTEMBER 1981

FINAL REPORT

Approval for public release; distribution unlimited.

Prepared for

Electromagnetic Compatibility Analysis Center
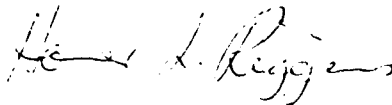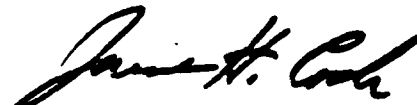North Severn, Annapolis, MD 21402

This report was prepared by the IIT Research Institute under Contract
F-19628-80-C-0042 with the Electronic Systems Division of the Air Force
Systems Command in support of the DoD Electromagnetic Compatibility Analysis
Center, Annapolis, Maryland.

This report has been reviewed and cleared for open publication and/or
public release by the appropriate Office of Information [OI] in accordance
with AFR 190-17 and DoD 5230.9. There is no objection to unlimited
distribution of this report to the public at large, or by DDC to the National
Technical Information Service [NTIS].

Reviewed by:
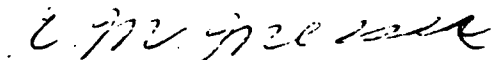
HOMER L. RIGGINS
Project Manager, IITRI

JAMES H. COOK
Assistant Director
Capability Development Department
Engineering Resources Division

Approved by:

CHARLES L. FLYNN
Colonel, USAF
Director

A. M. MESSER
Chief, Plans & Resource
Management

REPORT DOCUMENTATION PAGE	READ INSTRUCTIONS BEFORE COMPLETING FORM

1. REPORT NUMBER	2. GOVT ACCESSION NO.	3. RECIPIENT'S CATALOG NUMBER
ESD-TR-81-102	AD-A107710	

4. TITLE (and Subtitle)	5. TYPE OF REPORT & PERIOD COVERED
A MODEL TO CALCULATE EM FIELDS IN TROPOSPHERIC DUCT ENVIRONMENTS AT FREQUENCIES THROUGH SHF.	FINAL rept.
	6. PERFORMING ORG. REPORT NUMBER

7. AUTHOR(s)	8. CONTRACT OR GRANT NUMBER(s)
Sherman Marcus, Ph.D. William D. Stuart	F-19628-80-C-0042 CDRL # 10S

9. PERFORMING ORGANIZATION NAME AND ADDRESS	10. PROGRAM ELEMENT, PROJECT, TASK AREA & WORK UNIT NUMBERS
DoD Electromagnetic Compatibility Analysis Center North Severn, Annapolis, MD 21402	

11. CONTROLLING OFFICE NAME AND ADDRESS	12. REPORT DATE
	Sep 1981
	13. NUMBER OF PAGES
	226

14. MONITORING AGENCY NAME & ADDRESS(if different from Controlling Office)	15. SECURITY CLASS. (of this report)
	UNCLASSIFIED
	15a. DECLASSIFICATION/DOWNGRADING SCHEDULE

16. DISTRIBUTION STATEMENT (of this Report)

Approved for public release; distribution unlimited.

17. DISTRIBUTION STATEMENT (of the abstract entered in Block 20, if different from Report)

18. SUPPLEMENTARY NOTES

19. KEY WORDS (Continue on reverse side if necessary and identify by block number)

TROPOSPHERIC DUCTS
ELECTROMAGNETIC FIELD PREDICTION
VERTICAL REFRACTIVITY
ATMOSPHERIC WAVEGUIDE
COMPUTER MODEL (DUCT)

EIGENVALUE LOCUS

20. ABSTRACT (Continue on reverse side if necessary and identify by block number)

Non-monotonic variations of the atmospheric refractivity with height often enable energy to be propagated in a duct mode with little attenuation over long distances. A duct model employing a waveguide-mode method of analysis was developed to calculate the field strength when the refractivity variation with height is known. The developed numerical procedure methodically determines all significant eigenmodes for elevated and surface ducts at all frequencies through SHF. Computer model results for beyond-the

DD FORM 1473 EDITION OF 1 NOV 65 IS OBSOLETE

i

horizon ducts compare favorably with measurements taken at frequencies
between 65 MHz and 3.3 GHz.

ii

EXECUTIVE SUMMARY

Atmospheric ducts occur when the vertical refractivity profile has a negative gradient. Such ducts occur frequently in many parts of the world, and depend on weather conditions. In an atmospheric duct environment, electromagnetic energy may be propagated with little attenuation relative to free space over distances of hundreds of kilometers, thereby greatly increasing the potential for interference to communications and radar systems. Also, for a radar system, the coverage can be altered.

The likelihood of experiencing such a field enhancement is greater at higher radio propagation frequencies. Previously available computer models for determining ducted fields were limited in the frequencies and duct heights they were capable of considering. A mathematical model, called DUCT, has thus been developed to predict electromagnetic field levels in a duct environment for ducts at any height in the troposphere, and for propagation frequencies through SHF.

The DUCT model is based on a horizontally homogeneous waveguide-mode formulation, which was developed utilizing Fourier transform formalism. Numerical difficulties encountered by previous investigators have been overcome by the use of a unique mathematical formulation that (a) assures linear independence, even in a numerical sense, of the homogeneous form of the governing differential equation; and (b) provides flexibility for judiciously choosing the particular solution to the inhomogeneous form of this differential equation. In addition, criteria have been developed for associating specific types of modal field contributions with particular portions of the eigenvalue locus for the atmospheric waveguide, thereby providing the potential for increased computational efficiency.

Predictions of the DUCT model were compared with measurements at beyond-line-of-sight distances in both surface and elevated duct environments at frequencies between 65 MHz and 3.3 GHz. It appears to be the first model capable of predictions that compare favorably (within a few dB) with

measurements performed i.i an elevated duct environment at frequencies as high as 2201 MHz.

The effects on the fields in a duct environment, as a function of duct height, duct size, source height, observer height and propagation frequency, were ascertained by exercising the DUCT model. Predictions of fields in the presence of more than one duct in the atmosphere are also discussed.

The DUCT program is deemed to be a valid model for predicting and studying beyond-line-of-sight fields in a tropospheric duct environment, and it provides prediction capabilities for certain cases that could not be adequately treated by previously existing models.

PREFACE

The Electromagnetic Compatibility Analysis Center (ECAC) is a Department of Defense facility, established to provide advice and assistance on electromagnetic compatibility matters to the Secretary of Defense, the Joint Chiefs, of Staff, the military departments and other DoD components. The center, located at North Severn, Annapolis, Maryland 21402, is under the policy control of the Assistant Secretary of Defense for Communication, Command, Control, and Intelligence and the Chairman, Joint Chiefs of Staff, or their designees, who jointly provide policy guidance, assign projects, and estabilsh priorities. ECAC functions under the executive direction of the Secretary of the Air Force and the management and technical direction of the Center are provided by military and civil service personnel. The technical support function is provided through an Air Force-sponsored contract with the IIT Research Institute (IITRI).

To the extent possible, all abbreviations and symbols used in this report are taken from American National Standard ANSI (Y10.19 (1969) "Letter Symbols for Units Used in Science and Technology" issued by the American National Standards Institute, Inc.

Users of this report are invited to submit comments that would be useful in revising or adding to this material to the Director, ECAC, North Severn, Annapolis, Maryland 21402, Attention: XM.

TABLE OF CONTENTS

TABLE OF CONTENTS (Continued)

TABLE OF CONTENTS (Continued)

TABLE OF CONTENTS (Continued)

LIST OF ILLUSTRATIONS

Figure

TABLES OF CONTENTS (Continued)

LIST OF ILLUSTRATIONS (Continued)

LIST OF ILLUSTRATIONS (Continued)

TABLE OF CONTENTS (Continued)

LIST OF ILLUSTRATIONS (Continued)

TABLE OF CONTENTS (Continued)

LIST OF ILLUSTRATIONS (Continued)

TABLE OF CONTENTS (Continued)

LIST OF ILLUSTRATIONS (Continued)

LIST OF TABLES

LIST OF APPENDIXES

TABLE OF CONTENTS (Continued)

SECTION 1

INTRODUCTION

BACKGROUND

Duct Phenomena

It is known that the index of refraction, n, of the troposphere varies with altitude. In a "standard" atmosphere, n decreases with increasing height above the ground, approaching unity as the altitude increases. At sea level, the value of n is generally in the neighborhood of 1.000301. Usually it is more convenient to use the quantity called "refractivity" than it is to use the index of refraction. The refractivity, N, is related to n through the relationship:

$$N = (n-1) \times 10^6$$

Therefore, the refractivity of the troposphere is approximately 301 at sea level and approaches 0 as the altitude increases.

For modeling purposes, it is often more convenient to consider the earth as flat and to compensate for earth curvature through an "adjustment" of the refractivity. This adjustment is accomplished by adding a term to N which, because of Snell's law, would cause a ray to bend in such a way that its height above the "flat earth" at each point would be the same as that for a ray in an "unadjusted" refractivity environment over a curved earth. This new refractivity is called the "modified refractivity", M, and is given as:

$$M = N + \frac{z}{a} \times 10^6$$

where

      a = the radius of the earth.

      z = the height above the ground.

For a standard atmosphere, M increases with increasing height as shown in the left-hand portion of Figure 1a.

Using a geometrical optics representation (ray tracing), the right-hand portion of Figure 1a illustrates the manner in which energy would be radiated from a source (e.g., a transmitting antenna) in a refractivity environment characterized by the left-hand figure. In the illustration, r is the horizontal distance along the ground. The rays shown are bent in accordance with Snell's law, which states that a ray traced from a medium of lower refractivity to a medium of higher refractivity will bend toward the normal to the interface of the two media. Similarly, a ray traced from a medium of higher refractivity to a medium of lower refractivity will be bent away from the normal to the interface. In this case, the normal to the "interface" is in the z-direction, and the rays in Figure 1a are bent accordingly.

Notice that no energy reaches point R, far from the source, because R is located in the flat-earth representation at a point that would be beyond the horizon in the curved-earth representation.

The situation depicted above assumed a "standard" atmosphere. Now consider a case for which part of the M versus z profile changes directions, such as the situation shown in Figure 1b. Such a situation can be caused by anomalous weather conditions. In this case, a portion of the rays emanating from the source will, in accordance with Snell's law, be bent in a manner that will confine them to remain within a well-defined "layer" of the atmosphere. This layer is referred to as a "duct". Under certain conditions, waves can propagate within a duct to great distances (i.e., to beyond-line-of-sight distances) with little or no attenuation relative to free-space levels.
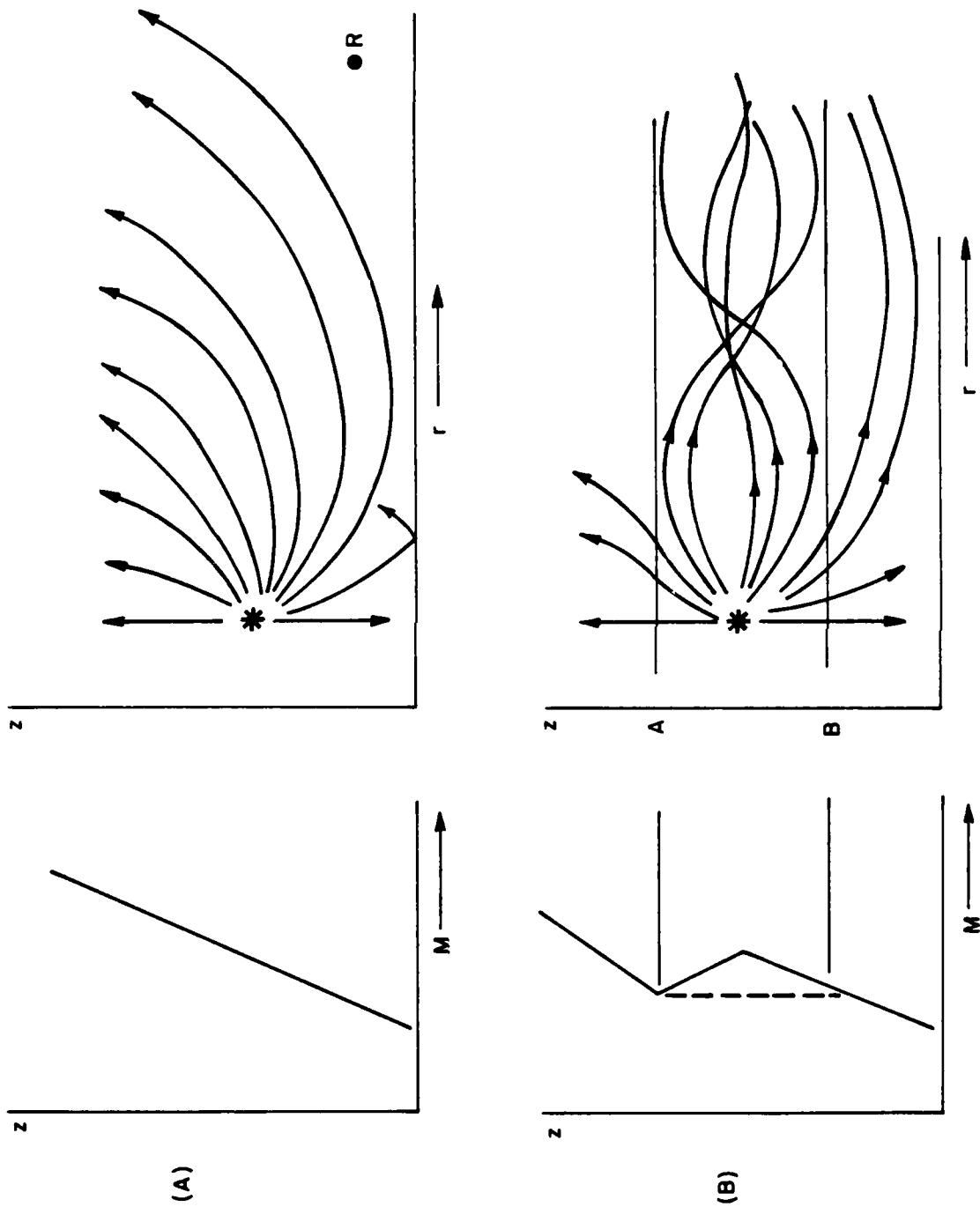
Figure 1. Geometrical optics representation of the effect of a duct on wave propagation.

The upper boundary of the duct is the height at which the modified
refractivity gradient (i.e., the ratio of the change in M to the change in z)
changes from a negative value to a positive value. This is shown as point A
in Figure 1. The lower boundary of the duct is determined by dropping a
vertical line from point A in the figure. If the vertical line intersects the
profile, the value of z at that point of intersection is the lower boundary of
the duct and the duct is said to be "elevated." For the case shown in Figure
1b, the duct will extend from the height of point B to the height of point
A. If, on the other hand, the modified refractivity profile were such that
the vertical line reached the ground without intersecting the profile curve,
the duct would be called a "surface duct" or a "ground-based duct."

Energy in a duct may be propagated with little attenuation relative to
free-space over distances of hundreds of kilometers and may subsequently
interfere with existing communications links. In order to predict whether
such interference will take place, information is required about the
characteristics of any ducts that are present and the effects of these ducts
on the propagated fields. Unfortunately, it is not possible to predict in
advance the occurrence of a duct at a particular time and in a given region.
However, statistical data is available on the occurrence of elevated and
surface ducts in different months and in different regions of the world.[1]
Reference 1 also contains statistical data related to the characteristics of
these ducts. In general, the percent of occurrence of ducts can vary from 0-
60% depending on the region and time of year. Therefore, it would be expected
that meaningful statistical data can be obtained for the propagated field
strengths observed in a duct environment. To accomplish the determination of
field strengths, the statistical duct occurrence data would be integrated with
a "deterministic" model that calculates the field strength when the duct
characteristics are known. The goal of this study was to develop such a
deterministic model.

---

[1] Ortenburger, L. N., Lawson, S. B. and Miller, G. K., Radiosonde Data
Analysis Summary Maps of Observed Data, GTE Sylvania, Inc., December 1978.

Computational Capabilities

The existence of ducts and their effects on electromagnetic wave
propagation have been recognized for a long time. Documentation of the
computations in this area first appeared at the end of World War II. A review
of the work performed at that time is available in the text edited by Kerr.[2]
That work, as in most subsequent studies, considers the propagation
environment as a waveguide. The total field strength at the location of a
receiving antenna is then the sum of the field strengths of the modes of the
waveguide. The waveguide is modeled as flat, with earth curvature compensated
by a modified refractivity. Justification for this approximation is discussed
by Pekeris.[3,4] The medium is assumed to be laterally homogeneous.

Each waveguide mode corresponds to an "eigenvalue" of the system. In
many works,[5,6] these "eigenvalues" are associated with takeoff angles of a ray
relative to the ground -- waveguide modes exist for discrete values of

---

[2] Kerr, D. E., Propagation of Short Radio Waves, MIT Radiation Laboratory
Series, Vol. 13, McGraw-Hill Book, New York, NY, 1951.

[3] Pekeris, C. L., "Wave Theoretical Interpretation of Propagation of
10-Centimeter and 3-Centimeter Waves in Low-Level Ocean Ducts,"
Proc. of the IRE, May 1947, pp. 453-462.

[4] Pekeris, C. L.,"Accuracy of the Earth-Flattening Approximation in the
Theory of Microwave Propagation," Physical Review, Vol. 70,
Nos. 7 and 8, 1 and 15 October 1946, p. 518.

[5] Pappert, R. A., and Goodhart, C. L., Waveguide Calculations of Signal
Levels in Tropospheric Ducting Environments, TN 3129, Naval Electronics
Laboratory Center, San Diego, CA, 25 February 1976.

[6] Budden, K. G., The Wave-Guide Mode Theory of Wave Propagation,
Prentice Hall, Englewood Cliffs, NJ, 1961.

such angles, which are referred to as "eigenangles". Whether the eigenvalues
are associated with angles or with any other physical parameter, they are
obtained as the roots of a complex equation called a modal equation.
Therefore, a major part of any computation is dedicated to determining these
roots.

Computations of the lowest order waveguide modes in a duct environment
and the behavior of the corresponding fields were considered by Wait and
Spies.[7] Dresp[8] developed a usable program that computed field strengths in,
above, and below a duct. He modeled the earth as cylindrical; once a general
solution was obtained, he showed that it can be approximated with the aid of
the modified refractivity as the solution for the flat-earth case. Although
the formulation by Dresp was mathematically elegant, his program was limited
to the determination of 20 waveguide modes. In addition, his results were not
verified by comparison with measured data.

Pappert and Goodhart (see Reference 5) developed a code that was verified
using measured data for a surface duct. Skillman and Woods[9] found that the
Pappert and Goodhart program predictions adequately reflected measurements at
frequencies below 450 MHz, taken in an elevated duct environment. However,
they found that the Pappert and Goodhart model failed to provide predictions
for comparison with measurements at 2.2017 GHz.

---

[7] Wait, J. R., and Spies, K. P., "Internal Guiding of Microwaves by an
Elevated Tropospheric Layer," Radio Science, Vol. No. 4, April 1969,
pp. 319-326.

8 Dresp, M. R., Tropospheric Duct Propagation at VHF, UHF, and SHF, MITRE
Technical Report MTR-3114, Vols. I and II, MITRE Corporation,
Bedford, MA, October 1975.

[9] Skillman, J. L., and Woods, D. R., "Experimental Study of Elevated Ducts,"
Proc. of Conference on Atmospheric Refractivity Effects Assessment,
Technical Document 260, Naval Ocean Systems Center, San Diego, CA,
15 June 1979.

Inherent limitations can be found in the Pappert and Goodhart model. One such limitation involves the uncertainty in any calculation that all significant modes have been found; that is, it is possible in their model to miss eigenvalues.[10] An attempt was made to utilize a more effective search method with their model, but an extensive modification of the mathematical formulation of the basic model was required, making its implementation impractical.

Another limitation of the Pappert and Goodhart model is the requirement that a "reference height" be specified, and the final result is dependent in some instances on this reference height. Since the specification of the reference height requires some physical insight into the particular problem under consideration, the Pappert and Goodhart model may be employed only by users with such knowledge. In this case, the model is not user-oriented. In addition, no user's guide is available for the Pappert and Goodhart model.

The computational capabilities noted above assumed a laterally homogeneous model. Cho and Wait[11] performed work in which only piecewise homogeneity was assumed, and the modes in each homogeneous section were determined. However, no user-oriented computer code for accomplishing this has been developed.

A major obstacle in developing any computer program that uses a waveguide model is the calculation of all significant modes. The number of modes increases as the frequency and duct height increases. In some cases, thousands of modes are necessary to adequately describe the fields; this

---

[10] Goodhart, C. L., and Pappert, R. A., Application of a Root Finding Method for Tropospheric Ducting Produced by Trilinear Refractivity Profiles, Technical Report 153, Naval Ocean Systems Center, San Diego, CA, 12 September 1977.

[11] Cho, S. H., and Wait , J. R., Analytical Study of Whispering Gallery Transmission in a Non-Uniform Tropospheric, Interim Report, Cooperative Institute for Research in Environmental Sciences, University of Colorado, Boulder, CO, 30 December 1976.

further complicates the problem of determining all significant modes. In the hope of overcoming the problem, Cho, et al.[12] attempted to utilize a hybrid approach to the problem in which a waveguide and geometrical optics series may be used to describe the fields. In such a case, a single geometrical optics term may be used to replace a vast number of terms in the waveguide mode series. They obtained good results for a duct formed by an ideal refractivity profile. However, this method is not applicable to more general refractivity profiles.

OBJECTIVE

The objective of this work was to develop a user-oriented deterministic computer model to compute the fields propagated in a homogeneous duct environment for all frequencies and ducts of interest.

APPROACH

Documentation was reviewed on existing computational capabilities for predicting propagated fields in a duct environment. Such capabilities were found lacking for the frequencies associated with elevated ducts, principally because of the inability to determine all the waveguide modes required to describe the fields. After extensive analysis, it was found that this inability stemmed from the facts that:

1.   The mathematical functions, which are solutions to the field equations in the duct environment, became linearly dependent (in a numerical sense) for the most significant values of the argument of these functions; and

---

[12] Cho, S. H., Migliora, C. G. and Felsen, L. B., "Hybrid Ray-Mode Formulation of Tropospheric Propagation," Proc. of Conference on Atmospheric Refractivity Effects Assessment, Technical Document 260, Naval Ocean Systems Center, San Diego, CA, 15 June 1979.

2.   The value of these mathematical functions could be exponentially large or small, thereby exceeding the capacity of common high-speed computers.

These problems were overcome by:

1.   Expressing the solutions to the field equations as linear combinations of these functions in a manner that assures linear independence in a numerical sense; and

2.   Utilizing a unique method for computationally expressing exponentially large or small numbers.

It was decided that a Fourier transform formulation of the problem would result in a modal equation that was most compatible with an available and efficient eigenvalue "search" method. This formulation also provided a flexibility, heretofore unavailable, for obtaining the field solution in a numerically efficient manner. A computer code was developed based on this approach.

The adequacy of the mathematical approach and the corresponding computer model was verified by comparing computed results with those of other codes and with documented measurements. Once this was successfully accomplished, the code was used to analyze the eigenvalues and the fields for different duct configurations, different frequencies, and different heights of the transmitting and receiving antennas.

ORGANIZATION OF REPORT

    The analytical and numerical basis of a computer program, called DUCT, which has been used sucessfully in predicting propagated field strengths in a DUCT environment, is described herein. A synopsis of the individual sections follows.

Section	Contents
2	Mathematical formulation.
3	Numerical procedures used to determine the eigenvalues of the modal equation.
4	Numerical procedures utilizing the eigenvalues to determine the fields.
5	Comparison of predictions of the DUCT program with measurements.
6	Analysis of eigenvalue results and relation of specific eigenvalues to particular field contributions.
7	Analysis of results of fields for different parameters of interest.
Appendix A	Review of some characteristics of the modified Hankel functions of order one-third.
Appendix B	Basis for an efficient method for evaluating the modal equation, which is in the form of a determinant.

    Section 5 is independent of Sections 2, 3, and 4 so that the reader who is interested only in verification aspects may skip directly to Section 5. Sections 6 and 7 may also stand alone, although Section 3 would be beneficial for a complete understanding of Section 6.

SECTION 2
MATHEMATICAL FORMULATION

GENERAL

In this section, the problem of electromagnetic propagation in an atmospheric duct is mathematically formulated. This is accomplished for horizontally polarized radiation by using a second-order partial differential equation to describe the variation of a component of the magnetic Hertz (vector) potential. The solution of this equation is obtained by utilizing Fourier transform formalism to cast the partial differential equation into the form of an ordinary differential equation, and by solving the latter equation in terms of unknown coefficients. These coefficients are determined using the boundary and radiation conditions of the system. The solution for the Hertz potential is obtained in the form of an integral that is evaluated with the aid of complex function theory in terms of a series of waveguide modes.

The above process is generalized to include vertically polarized radiation. Alternative mathematical formulations are introduced in succeeding sections that will prove useful in required numerical evaluations.

REFRACTIVITY PROFILE

The index of refraction of a medium is given by:

$$n(z) = \sqrt{\mu_r \epsilon_r} = \sqrt{\epsilon_r(z)} \tag{1}$$

where ϵ_r and μ_r are the relative permittivity and permeability of the medium. It is assumed that $\mu_r = 1$ everywhere. In what follows, n is only a function of the height z above the ground. The refractivity N is defined as:

$$N = (n-1) \times 10^6 \tag{2}$$

11

and is numerically a more convenient parameter than n.

It is often mathematically convenient to utilize a rectangular coordinate system to describe atmospheric wave propagation. In such a formalism, it has been found that the earth curvature may be accounted for by appropriately modifying the index of refraction of the atmosphere. This modification is accomplished by adding a term to n which would cause a ray to bend in such a way that its height above the "flat earth" at each point would be the same as if it were a straight ray over a curved earth. The modified index of refraction, m, is then given by (see Reference 2):

$$m(z) = n(z) + z/a \tag{3}$$

where a is the radius of the earth in the same units as z.

The modified refractivity is defined as:

$$M = (m-1) \times 10^6 \tag{4}$$

The modified index of refraction will have a profile (i.e., a variation with height) such as that shown by the dashed line on the right side of Figure 2. To make the problem mathematically tractable, this general profile will be approximated by a piecewise linear profile with L sections, such as that shown by the solid lines on the right side of Figure 2. In the figure, L = 3 has been used. Each section will represent an atmospheric layer, or region, the boundaries of which are parallel to a flat earth located at z = 0.

The interface between the ith and ith+1 layer $(1 \leq i \leq L-1)$ is located at $z = z_i$, with the layer i = 1 closest to the ground. This is illustrated in Figure 2, for the case L = 3. Each layer is assumed to be horizontally homogeneous, with a modified index of refraction given by:

$$m_i(z) = \frac{z - H_i}{2} \tan \alpha_i + 1,$$

$$= M_i(z) \times 10^{-6} + 1 \;, \; 1 \leq i \leq L \tag{5}$$

12
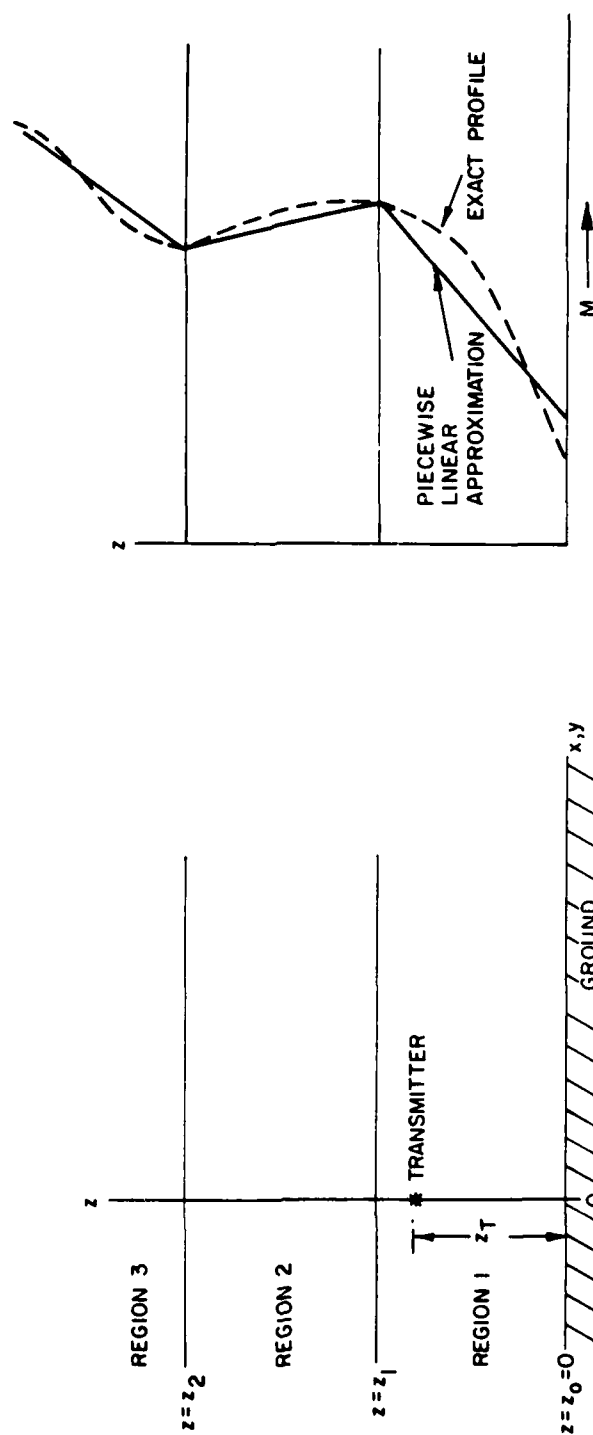
Figure 2.   Coordinate system definition and sample profile of modified index of refraction.

where H_i is the value of z at which $m_i(z)$ would equal unity, and the slope $\tan \alpha_i/2$ is assumed small:

$$| \tan \alpha_i | \ll 1 \tag{6}$$

From Equations 5 and 6,

$$m_i^2(z) \approx 1 + (z-H_i) \tan \alpha_i , \quad 1 \le i \le L \tag{7}$$
$$= 1 + 2 M_i(z) \times 10^{-6}$$

The modified index $m_i(z)$ is assumed to be continuous across the interfaces between the layers (see Figure 2):

$$m_i(z_i) = m_{i+1}(z_i) , \quad 1 \le i \le L-1 \tag{8}$$

MAGNETIC HERTZ POTENTIAL

It can be assumed that horizontally polarized wave propagation is due to a radiating magnetic dipole $\vec{p} = p \hat{z}$ oriented in the z-direction and located at $x = y = 0$, $z = z_T$ (see Figure 2). In a laterally homogeneous medium, the wave propagation due to such a dipole exhibits axial symmetry (about a vertical axis through the radiating dipole), and may be obtained from the z-component Π_z of the magnetic Hertz potential vector $\vec{\Pi}$. Thus:

$$\vec{\Pi}(x,y,z) = \Pi_z(x,y,z) \hat{z} \tag{9}$$

$$\vec{E} = -j\omega\mu_o \nabla \times \vec{\Pi}$$

and

$$\vec{H} = \nabla \times \nabla \times \vec{\Pi} \tag{11}$$

14

where $\omega = 2\pi f$

f = the propagation frequency,

μ_o = the permeability in vacuum,

and an $e^{j\omega t}$ time dependence is assumed.

DIFFERENTIAL EQUATION

In each atmospheric layer, Π_z satisfies the partial differential equation:

$$\nabla^2 \Pi_i + k_o^2 m_i^2(z) \; \Pi_i = -p \; \delta(x)\delta(y)\delta(z - z_T), \; 1 \leq i \leq L \tag{12}$$

where

Π_i = the value of Π_z in the ith layer

k_o = the free-space wave number determined by $\quad k_o^2 = \omega^2 \mu_o \epsilon_o$

p = the magnetic dipole strength

δ = the Dirac delta function.

The Laplacian operator ∇^2 is defined as:

$$\nabla^2 = \frac{\partial^2}{\partial x^2} + \frac{\partial^2}{\partial y^2} + \frac{\partial^2}{\partial z^2}$$

In the ground, Π_z satisfies the equation:

$$\nabla^2 \Pi_g + k_o^2 n_g^2 \; \Pi_g = 0 \; , \; z \leq 0 \tag{13}$$

where

Π_g is the value of Π_z in the ground and

n_g is the constant refractive index of the ground.

This is given by:

$$n_g{}^2 = \varepsilon_g - \frac{j\sigma_g}{\varepsilon_o \omega}$$

where ε_g and σ_g are the ground values for the permittivity and conductivity, respectively.

A solution is sought to Equation 13 in the ground and to Equation 12 in each atmospheric layer, subject to the boundary conditions at the ground and at each layer interface that the tangential components of $\vec{E}$ and $\vec{H}$ are continuous across the boundary. Using Equations 7, 10 and 11, it may be shown[13] that these conditions may be written:

$$\left. \begin{array}{l} \Pi_i = \Pi_{i+1} \\[2mm] \dfrac{\partial \Pi_i}{\partial z} = \dfrac{\partial \Pi_{i+1}}{\partial z} \end{array} \right\} \quad \text{on} \quad z = z_i, \; 1 \le i \le L-1 \qquad (14)$$

$$\left. \begin{array}{l} \Pi_g = \Pi_i \\[2mm] \dfrac{\partial \Pi_g}{\partial z} = \dfrac{\partial \Pi_i}{\partial z} \end{array} \right\} \quad \text{on} \quad z = 0 \qquad (15)$$

---

[13] Tyras, G., _Radiation and Propagation of Electromagnetic Waves,_ Academic Press, New York, NY, 1969.

An additional requirement on the solutions obtained is that the radiation conditions be satisfied. That is, Π_g must represent an outgoing wave as $z \to -\infty$, and Π_i must represent an outgoing wave as $z \to +\infty$.

FOURIER TRANSFORM FORMULATION

The partial differential Equations 12 and 13 may be reformulated as ordinary differential equations with the aid of Fourier transform theory (see Reference 13). The double Fourier transform of $\Pi(x,y,z)$ is defined as:

$$\tilde{\Pi}(\mu,\nu,z) = \int_{-\infty}^{\infty} dx\, e^{-j\mu x} \int_{-\infty}^{\infty} dy\, e^{-j\nu y}\, \Pi(x,y,z) \tag{16}$$

with the inverse transform given by:

$$\Pi(x,y,z) = \frac{1}{(2\pi)^2} \int_{-\infty}^{\infty} d\mu\, e^{j\mu x} \int_{-\infty}^{\infty} d\nu\, e^{j\nu y}\, \tilde{\Pi}(\mu,\nu,z) \tag{17}$$

Taking the double Fourier transform of Equations 12 through 15 yields:

$$\left\{ \frac{d^2}{dz^2} + k_o^2 \left[m_i^2(z) - \frac{\rho^2}{k_o^2} \right] \right\} \tilde{\Pi}_i = -p\, \delta(z - z_T) \; , \; 1 \le i \le L \tag{18}$$

$$\left[\frac{d^2}{dz^2} + k_o^2 \left(n_g^2 - \frac{\rho^2}{k_o^2} \right) \right] \tilde{\Pi}_g = 0 \tag{19}$$

$$\left. \begin{array}{l} \tilde{\Pi}_i = \tilde{\Pi}_{i+1} \\[2mm] \dfrac{d\tilde{\Pi}_i}{dz} = \dfrac{d\tilde{\Pi}_{i+1}}{dz} \end{array} \right\} \quad z = z_i \; , \quad 1 \le i \le L-1 \tag{20}$$

17

$$\tilde{\Pi}_g = \tilde{\Pi}_1$$

$$z = 0 \qquad\qquad (21)$$

$$\frac{d\tilde{\Pi}_g}{dz} = \frac{d\tilde{\Pi}_1}{dz}$$

where

$$\rho^2 \equiv \mu^2 + \nu^2$$

Thus solutions are sought for $\tilde{\Pi}_i$ and $\tilde{\Pi}_g$ in Equations 18 and 19, subject to the boundary conditions in Equations 20 and 21 and to the radiation conditions. Once these solutions are found, they may be used in Equation 17 to find the Hertz potential in each medium which, in turn, may be used in Equations 10 and 11 to find the electromagnetic field vectors.

SOLUTION OF EQUATIONS

In Ground

The solution to Equation 19 is:

$$\tilde{\Pi}_g = A_g \, e^{j\gamma z} \qquad\qquad (22)$$

where

$$\gamma = k_o \sqrt{n_g^2 - (\rho^2/k_o^2)} \qquad\qquad (23)$$

and A_g is a function of the parameter ρ. $\tilde{\Pi}_g$ satisfies the radiation condition for large negative values of z, since it represents an outgoing wave in this region. To assure that $\tilde{\Pi}_g \to 0$ as $z \to -\infty$, the branch of γ is chosen so that:

$$\text{Im } \gamma < 0. \tag{24}$$

In Atmosphere

The complete solution to Equation 18 will be given by the sum of the general solution of the homogeneous equation and a particular solution of the inhomogeneous equation. The homogeneous form of Equation 18 may be written:

$$\left(\frac{\partial^2}{\partial q_i^2} + q_i \right) \widetilde{\Pi}_i = 0 \tag{25}$$

where

$$q_i(z) = \left(\frac{k_o}{\lceil \tan \alpha_i \rceil} \right)^{2/3} \left[m_i^2(z) - \frac{\rho^2}{k_o^2} \right] \tag{26}$$

and Equation 7 was used. Equation 25 is known as the Stokes Equation and its solutions are given in terms of Airy functions or in terms of modified Hankel functions of order 1/3. For purposes at hand, it is more convenient to utilize the latter.
Thus:

$$\widetilde{\Pi}_i = A_i h_1(q_i) + B_i h_2(q_i) , \quad 1 \le i \le L \tag{27}$$

where

$$h_1(q) = \left(\frac{2}{3} q^{3/2} \right)^{1/3} H_{1/3}^{(1)} \left(\frac{2}{3} q^{3/2} \right) \tag{28}$$

$$h_2(q) = \left(\frac{2}{3} q^{3/2}\right)^{1/3} H_{1/3}^{(2)}\left(\frac{2}{3} q^{3/2}\right) \qquad (29)$$

are the modified Hankel functions of order 1/3 of the first and second kind, respectively, and are tabulated in the literature.[14] $H_{1/3}^{(1)}$ and $H_{1/3}^{(2)}$ are Hankel functions of order 1/3 of the first and second kind, respectively.

The A_i and B_i in Equation 27 are not functions of z, but depend on the parameters μ and ν. Their values are determined from the boundary conditions. In order to satisfy the radiation condition for large z in the Lth medium:

$$A_L \equiv 0 \qquad (30)$$

The solution (Equation 27 with Equation 30) for the homogeneous form of Equation 18 represents the entire solution for every layer except the one in which the transmitting dipole is located. That is, only for the layer containing $z = z_T$ is Equation 18 inhomogeneous. Assuming this to be the Pth layer, a particular solution of the inhomogeneous equation in this layer is:

$$\tilde{\Pi}_P = \frac{P}{W_{q_P}} \cdot \begin{cases} h_1[\,q_P(z)\,]\, h_2[\,q_P(z_T)\,], & z < z_T \\ h_2[\,q_P(z)\,]\, h_1[\,q_P(z_T)\,], & z > z_T \end{cases} \qquad (31)$$

where W is the constant Wronskian for h_1 and h_2 given by:

---

[14]Harvard Computational Laboratory, Tables of Modified Hankel Functions of Order One-Third and of Their Derivatives, Harvard University Press, Cambridge, MA, 1945.

$$W = W(h_1, h_2) = h_1(q) \, h_2^{'}(q) - h_2(q) \, h_1^{'}(q) = -\frac{4j}{\pi} \left(\frac{3}{2}\right)^{1/3} \qquad (32)$$

and the primes indicate the derivative with respect to the argument of the function. Thus:

$$h_m^{'}(q) = \frac{\partial h_m(q)}{\partial q} \quad , \quad m = 1, 2 \qquad (33)$$

and

$$q_p^{'}(z) = \frac{\partial q_p}{\partial z} = \left(\frac{k_0}{|\tan \alpha_p|}\right)^{2/3} \tan \alpha_p \qquad (34)$$

where Equations 26 and 7 were used. That Equation 31 is a solution may be verified by substituting it into Equation 18, integrating each term from $z_T - \varepsilon$ to $z_T + \varepsilon$ and letting $\varepsilon \to 0$. Since $\tilde{\Pi}_p$ is assumed finite at $z = z_T$, this yields:

$$\frac{d \tilde{\Pi}_p}{dz} \left|\begin{array}{l} z_T + \varepsilon \\ \\ z_T - \varepsilon \end{array}\right. = -p \qquad (35)$$

which produces an identity when Equation 31 is used.

Equation 31 may be written more conveniently as:

$$\tilde{\Pi}_p = R_p \, h_1(q_{p<}) \, h_2(q_{p>}) \qquad (36)$$

where

$$q_{P<} = q_P \, [\min \, (z, z_T)]$$

$$q_{P>} = q_P \, [\max \, (z, z_T)]$$

and

$$R_P = \frac{p}{Wq_P}$$

It will be noticed that, when $P = L$ and z becomes large, the dependence of $\tilde{\Pi}_P$ on z is through $h_2[q(z)]$. Therefore, the solution of $\tilde{\Pi}_P$, given in Equation 36, represents an outgoing wave as $z \to \infty$, and therefore is consistent with the radiation condition.

Combining the general solution (Equation 27) of the homogeneous equation with a particular solution (Equation 36) of the inhomogeneous equation yields:

$$\tilde{\Pi}_i = A_i h_1(q_i) + B_i h_2(q_i) + R_i h_1(q_{i<}) h_2(q_{i>}) \delta_{iP}, \quad 1 \le i \le L \qquad (37)$$

which, along with Equation 30, is the complete solution of Equation 18 in each layer. δ_{iP} is the Kroneker delta function defined as:

$$\delta_{iP} = \begin{cases} 1 & , \quad i = P \\ 0 & , \quad i \ne P \end{cases}$$

DETERMINATION OF COEFFICIENTS

The coefficients A_g in Equation 22 and A_i, B_i in Equation 37 must now be obtained from the boundary conditions. In the equations which follow, the notation q_{ij} is used to indicate the value of q_i on the boundary at $z = z_j$, with z_o denoting ground level. Thus:

$$q_{ij} = q_i(z_j) \tag{38a}$$

Also, let

$$q_{iT} = q_i(z_T) \tag{38b}$$

Substituting Equations 22 and 37 in each of Equations 21 yields:

$$A_g = A_1 \, h_1(q_{10}) + B_1 \, h_2 \, (q_{10}) + R_1 \, h_1 \, (q_{10}) \, h_2(q_{1T}) \, \delta_{1P}$$

and

$$j\gamma A_g = \acute{q}_1 \quad [A_1 \, \acute{h}_1 \, (q_0) + B_1 \, \acute{h}_2 \, (q_0) + R_1 \, \acute{h}_1 \, (q_0) \, h_2 \, (q_T) \, \delta_P]$$

from which A_g may be eliminated, resulting in:

$$A_1[h_1{'}(q_{10}) - G \, h_1(q_{10})] + B_1[h_2{'}(q_{10}) - G \, h_2(q_{10})] \tag{39}$$
$$= -h_2(q_{1T}) \, R_1 \delta_{1P}[\, h_1{'}(q_{10}) - G \, h_1(q_{10})]$$

where

$$G = \frac{j\gamma}{q_1^{'}}$$ (40)

Substituting Equation 37 in each of Equations 20 yields:

$$A_i h_1(q_{ii}) + B_i h_2(q_{ii}) + R_i h_1(q_{iT}) h_2(q_{ii}) \delta_{iP}$$

$$= A_{i+1} h_1(q_{i+1,i}) + B_{i+1} h_2(q_{i+1,i})$$

$$+ R_{i+1} h_1(q_{i+1,i}) h_2(q_{i+1,T}) \delta_{i+1,P}$$

and

$$A_i h_1^{'}(q_{ii}) + B_1 h_2^{'}(q_{ii}) + R_i h_1(q_{iT}) h_2^{'}(q_{ii}) \delta_{iP}$$

$$= \frac{q_{i+1}^{'}}{q_i^{'}} \quad A_{i+1} h_1^{'}(q_{i+1,i}) + B_{i+1} h_2^{'}(q_{i+1,i})$$

$$+ R_{i+1} h_1^{'}(q_{i+1,i}) h_2(q_{i+1,T}) \delta_{i+1,P}$$

These equations may be recast into the more convenient form:

$$A_i h_1(q_{ii}) + B_i h_2(q_{ii}) - A_{i+1} h_1(q_{i+1,i}) - B_{i+1} h_2(q_{i+1,i})$$

$$= R_{i+1} h_1(q_{i+1,i}) h_2(q_{i+1,T}) \delta_{i+1,P}$$ (41a)

$$- R_i h_1(q_{iT}) h_2(q_{ii}) \delta_{iP}$$

24

ECAC-TN-81-032

$$A_i h_1^{\prime}(q_{ii}) + B_i \, h_2^{\prime}(q_{ii}) - A_{i+1} \frac{q_{i+1}^{\prime}}{q_i^{\prime}} h_1^{\prime}(q_{i+1,i})$$

$$+ B_{i+1} \frac{q_{i+1}^{\prime}}{q_i^{\prime}} h_2^{\prime}(q_{i+1,i})$$

(41b)

$$= R_{i+1} \frac{q_{i+1}^{\prime}}{q_i^{\prime}} h_1^{\prime}(q_{i+1,i}) \, h_2(q_{i+1,T}) \, \delta_{i+1,P}$$

$$- R_i h_1(q_{iT}) \, h_2^{\prime}(q_{ii}) \, \delta_{iP}, \quad 1 < i \le L - 1$$

Equations 41, 39 and 30 represent 2L equations in the 2L unknowns A_i, B_i, $1 \le i \le L$.

As an illustration of the system of equations which must be solved to obtain the unknown coefficients, Equations 30, 39 and 41 are written in the following form, assuming $L = 3$ and $P = 1$:

$$A_1 \hat{h}_1(q_{10}) + B_1 \hat{h}_2(q_{10}) \qquad\qquad = -R_1 h_2(q_{1T})\hat{h}_1(q_{10})$$

$$A_1 h_1(q_{11}) + B_1 h_2(q_{11}) - A_2 h_1(q_{21}) - B_2 h_2(q_{21}) \qquad = -R_1 h_1(q_{1T}) h_2(q_{11})$$

$$A_1 h_1^{\prime}(q_{11}) + B_1 h_2^{\prime}(q_{11}) - A_2 q_R^{\prime} h_1^{\prime}(q_{21}) - B_2 q_R^{\prime} h_2^{\prime}(q_{21}) \qquad = -R_1 h_1(q_{1T}) h_2^{\prime}(q_{11})$$

$$A_2 h_1(q_{22}) + B_2 h_2(q_{22}) - B_3 h_2(q_{32}) = 0$$

$$A_2 h_1^{\prime}(q_{22}) + B_2 h_2^{\prime}(q_{22}) - B_3 q_D^{\prime} h_2^{\prime}(q_{32}) = 0$$

(42)

where

$$q_R^{\prime} = q_2^{\prime}/q_1^{\prime} \, , \quad q_D^{\prime} = q_3^{\prime}/q_2^{\prime} \, .$$

and

25

$$\hat{h}_m(q_{10}) \cong h_m{}'(q_{10}) - G\, h_m(q_{10}) \ , \quad m = 1,2 \tag{42a}$$

If P were not equal to 1, then the system of equations would be the same as that shown in Equation 42 except for the *right* hand side of the equations. This will be discussed *further* in Section 4.

It is seen that this system of equations may be expressed in matrix forms as:

$$\alpha \ \xi = \beta \tag{43}$$

where

$$\alpha = \begin{bmatrix}
\hat{h}_1(q_{10}) & \hat{h}_2(q_{10}) & 0 & 0 & 0 \\
h_1(q_{11}) & h_2(q_{11}) & -h_1(q_{21}) & -h_2(q_{21}) & 0 \\
h_1{}'(q_{11}) & h_2{}'(q_{11}) & -q_R{}'h_1{}'(q_{21}) & -q_R{}'h_2{}'(q_{21}) & 0 \\
0 & 0 & h_1(q_{22}) & h_1(q_{22}) & -h_2(q_{32}) \\
0 & 0 & h_1{}'(q_{22}) & h_2{}'(q_{22}) & -q_D{}'\,h_2{}'(q_{32})
\end{bmatrix}$$

$$\tag{44}$$

$$\xi = \begin{bmatrix} A_1 \\ B_1 \\ A_2 \\ B_2 \\ B_3 \end{bmatrix} \tag{45}$$

and

$$\beta = R_1 \begin{bmatrix}
-h_2(q_{1T}) \ \hat{h}_1(q_{10}) \\
-h_1(q_{1T}) \ h_2(q_{11}) \\
-h_1(q_{1T}) \ h_2{}'(q_{11}) \\
0 \\
0
\end{bmatrix} \tag{46}$$

26

The solution for any one of the unknown coefficients may be obtained through
the use of determinants. Thus:

$$A_i = \frac{|T_{Ai}|}{|\alpha|} \;,\; B_i = \frac{|T_{Bi}|}{|\alpha|} \tag{47}$$

where, for $1 \leq i \leq L-1$, T_{Ai} is the matrix obtained by replacing the column of
α in Equation 44 containing the coefficients of A_i (in Equation 42) by the
vector β; and for $i = L$, $|T_{Ai}| \equiv 0$. T_{Bi}, $1 \leq i \leq L$, is the matrix obtained by
replacing the column of α containing the coefficients of B_i by the vector β.
Thus, for example:

$$T_{A2} = \begin{bmatrix} \hat{h}_1(q_{10}) & \hat{h}_2(q_{10}) & -R_1 h_2(q_{1T}) \hat{h}_1(q_{10}) & 0 & 0 \\ h_1(q_{11}) & h_2(q_{11}) & -R_1 h_1(q_{1T}) h_2(q_{11}) & -h_2(q_{21}) & 0 \\ h_1'(q_{11}) & h_2'(q_{11}) & -R_1 h_1(q_{1T}) h_2'(q_{11}) & -q_R' h_2'(q_{21}) & 0 \\ 0 & 0 & 0 & h_2(q_{22}) & -h_2(q_{32}) \\ 0 & 0 & 0 & h_2'(q_{22}) & -q_D' h_2'(q_{32}) \end{bmatrix}$$

The notation $|T|$ indicates the determinant of the matrix T.

SOLUTIONS IN INTEGRAL FORM

Using Equation 47 in Equation 38 yields:

$$\tilde{\Pi}_i(\mu,\nu,z) = \tilde{\Pi}_i(\rho,z) = \frac{|T_{Ai}| \, h_1(q_i) + |T_{Bi}| \, h_2(q_i)}{|\alpha|} + R_i h_1(q_{i<}) h_2(q_{i>}) \delta_{iP} \;,$$

$$1 \leq i \leq L \tag{48}$$

27

which may be used in Equation 17 to obtain:

$$\Pi_i(x,y,z) = \frac{1}{(2\pi)^2} \int_{-\infty}^{\infty} d\mu \; e^{j\mu x} \int_{-\infty}^{\infty} d\nu \; e^{j\nu y} \; \tilde{\Pi}_i(\rho,z) \qquad (49)$$

Since μ and ν enter $\tilde{\Pi}_i$ as ρ, Equation 49 may be written (References 2 and 13):

$$\Pi_i(r,z) = \frac{1}{2\pi} \int_0^{\infty} \rho \; d\rho \; J_0(\rho r)\tilde{\Pi}_i = \frac{1}{4\pi} \int_C \rho \; d\rho \; H_0^{(2)}(\pi r) \; \tilde{\Pi}_i(\rho,z) \qquad (50)$$

where C is the contour in the complex ρ-plane shown as the solid line in Figure 3.

As discussed in Reference 2, Equation 50 is valid only when there are no singularities of $\tilde{\Pi}_i(\rho,z)$ in the first quadrant of the complex ρ-plane, and when:

$$\int_{C^+} \rho \; d\rho \; H_0^{(1)}(\rho r) \; \tilde{\Pi}_i(\rho,z) \to 0 \; , \qquad (51)$$

where C^+ is the quarter-circle contour of infinite radius lying in the first quadrant of the ρ-plane. Both these conditions may be shown to hold.
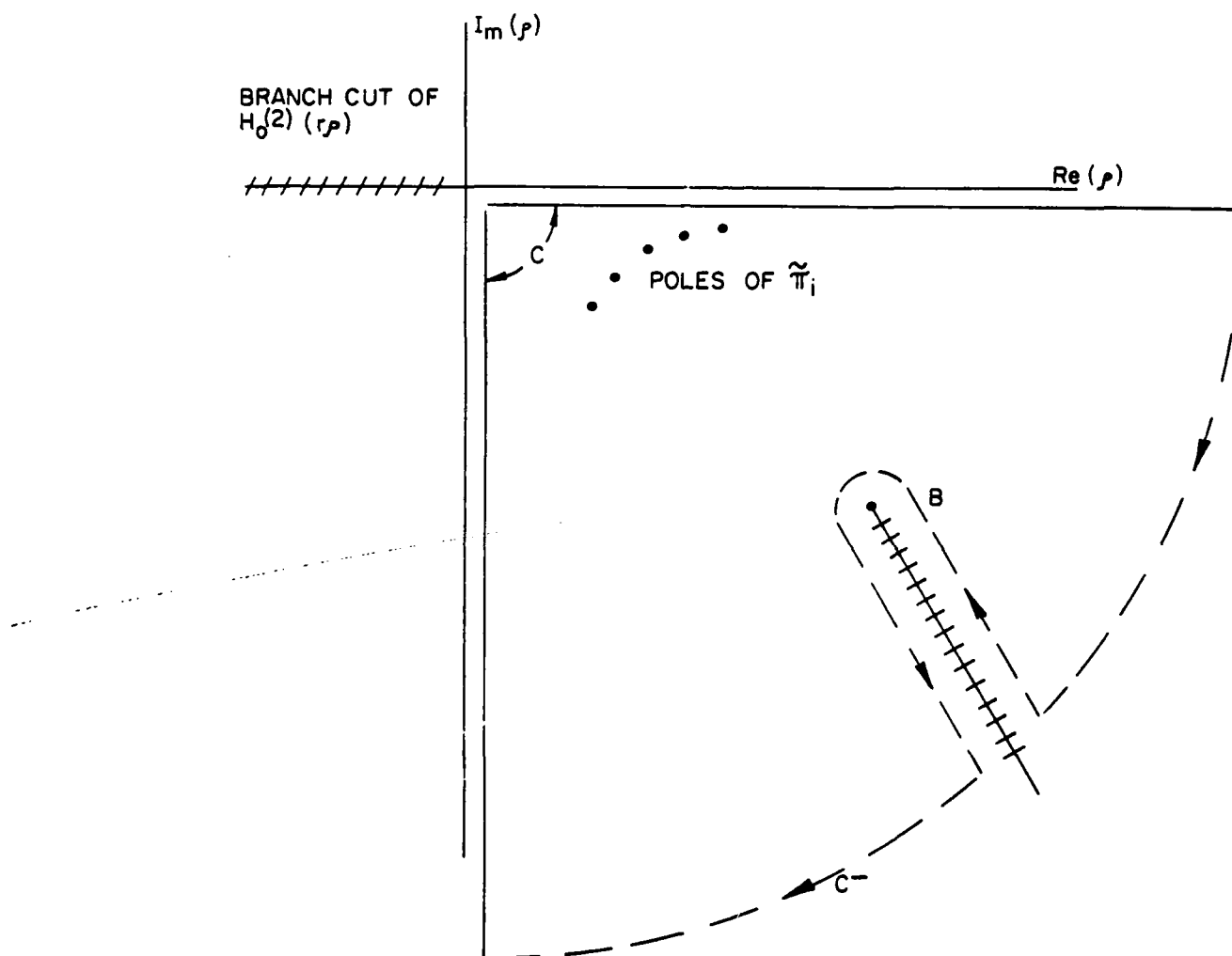
Figure 3. Contour for integral of Equation 50.

SOLUTIONS IN TERMS OF WAVEGUIDE MODES

By closing the contour C of the integral in Equation 50, the residue theorem of complex variables may be used:

$$\Pi_i(r,z) = -\frac{2\pi j}{4\pi} \sum_n \text{Res}_n + \frac{1}{4\pi} \left(\int_{C^-} + \int_B \right) \rho \, d\rho \, H_0^{(2)}(\rho r) \, \widetilde{\Pi}_i(\rho,z) \quad (52)$$

where the factor $\sum_n \text{Res}_n$ is the sum of the residues of $\rho \, H_0^{(2)}(\rho r) \, \widetilde{\Pi}_i(\rho,z)$ at the poles of $\widetilde{\Pi}(\rho_i,z)$; the contour C^- (see Figure 3) is the quarter circle of infinite radius lying in the fourth quadrant; and the contour B encloses the branch cut which is present as a result of the radical in the expression for γ in Equation 23. No other branch cuts are present within the contour of integration shown in Figure 3 since the only branch points of the functions $h_1(q)$ and $h_2(q)$ are at infinity (see Reference 14). The integral will vanish over contour C^- in Equation 52 as in Equation 51. The integral over contour B represents the surface wave contribution to the total field, and is assumed to be small relative to the other field contributions. Therefore, it will be ignored as well. Equation 52, therefore, becomes:

$$\Pi_i(r,z) = -\frac{j}{2} \sum_n \text{Res}_n \qquad\qquad (53)$$

where the residues correspond to waveguide modes[15].

An expression for the residues in Equation 53 will now be derived. Since the function $H_0^{(2)}(\rho r)$ has no poles in the complex ρ-plane, the only poles of the integrand $\rho \, H_0^{(2)}(\rho r) \, \widetilde{\Pi}_i(\rho,z)$ will be those of $\widetilde{\Pi}_i(\rho,z)$. But since $h_i[q(\rho)]$ and $h_2[q(\rho)]$ have no poles in the ρ-plane, it is seen from

---

[15]Wait, J.R., Electromagnetic Waves in Stratified Media, Pergamon Press, New York, NY, 1962.

Equation 48 that the only poles of $\widetilde{\Pi}_i$ will be those for which $|\alpha| = 0$. Therefore,

$$\text{Res}_n\left(\rho\ H_0^{(2)}(\rho r)\ \widetilde{\Pi}_i(\rho,z)\right) = \text{Res}_n\left\{\frac{\rho\ H_0^{(2)}(\rho r)\ \left(|T_{Ai}|\ h_1(q_i) + |T_{Bi}|\ h_2(q_i)\right)}{|\alpha|}\right\}$$

or from the well-known techniques[16] for evaluating residues:

$$\text{Res}_n = \rho_n\ H_0^{(2)}(\rho_n r)\ \frac{\left[|T_{Ai}|\ h_1(q_i) + |T_{Bi}|\ h_2(q_i)\right]_{\rho\ =\ \rho_n}}{\frac{\partial|\alpha|}{\partial\rho}\Big|_{\rho\ =\ \rho_n}} \tag{54}$$

where ρ_n is the nth value of ρ for which $|\alpha| = 0$.

For all cases of interest, $|\rho_n r| \gg 1$, so that $H_0^{(2)}(\rho_n r)$ may be approximated asymptotically as:

$$H_0^{(2)}(\rho_n r) \simeq e^{j\pi/4}\ \sqrt{\frac{2}{\pi\rho_n r}}\ e^{-j\rho_n r} \tag{55}$$

Using Equations 54 and 55, Equation 53 may be written:

$$\Pi_i(r,z) = -j\ \sqrt{\frac{1}{2\pi r}}\ e^{j\pi/4}\ \sum_n \frac{\sqrt{\rho_n}}{\left(\frac{\partial|\alpha|}{\partial\rho}\right)_{\rho\ =\ \rho_n}}\ \left[|T_{Ai}|\ h_1(q_i) + |T_{Bi}|\ h_2(q_i)\right]_{\rho\ =\ \rho_n}\ e^{-j\rho_n r}$$

$$= -j\ \frac{1}{\sqrt{2\pi r}}\ e^{j\pi/4}\ \sum_n \lambda_n\ E_n\ e^{-j\rho_n r} \tag{56}$$

---

[16]Churchill, R.V., <u>Introduction to Complex Variables and Applications</u>, p. 122, McGraw Hill Book Co., New York, NY, 1948.

where

$$\lambda_n \equiv \frac{\sqrt{\rho_n}}{\left(\dfrac{\partial |\alpha|}{\partial \rho}\right)_{\rho = \rho_n}} \tag{57}$$

is referred to as an excitation function, and:

$$E_{ni} = E_{ni}(\rho_n, z, z_T) = \left[|T_{Ai}| \, h_1(q_i) + |T_{Bi}| \, h_2(q_i) \right]_{\rho = \rho_n} \tag{58}$$

may be referred to as a height-gain function. The functional dependence on z occurs through $h_1(q_i)$ and $h_2(q_i)$ (see Equation 26). The parameter z_T enters through $|T_{Ai}|$ and $|T_{Bi}|$.

ELECTRIC FIELD RELATIVE TO FREE-SPACE

Although the value of $\vec{E}$ may be obtained from Equation 56 by using Equation 10, it is often more convenient to determine the magnitude of the electric field relative to free-space:

$$A = \frac{|\vec{E}|}{|\vec{E}_{fs}|} \tag{59}$$

where $|\vec{E}_{fs}|$ is the magnitude of the field that would be obtained at the same receiving location and using the same source, but with the propagation taking place in empty space (i.e. in a vacuum). The value of A will now be shown to be proportional to Π_i for the problem under consideration.

In free-space, the z-component of the magnetic Hertz potential is given
by:

$$\Pi_{fs} = \frac{p}{4\pi} \frac{e^{-jk_0 r}}{r} = \frac{R_P \, W \, q_P'}{4\pi} \frac{e^{-jk_0 r}}{r} \tag{60}$$

where Equation 37 was used and q_P' is obtained from Equation 34 using the
parameters of the actual environment (i.e., not the free-space environment).

When the Hertz potential vector is given by Equation 9, Equation 10 may
be used to obtain:

$$\vec{E} = E_\theta \hat{\Theta} = j\omega\mu \frac{\partial \Pi_z}{\partial r} \hat{\Theta} \tag{61}$$

in cylindrical coordinates. Using Equation 60 in Equation 61 yields:

$$E_{\theta fs} \approx \frac{k_0 \omega\mu \, R_P \, W \, q_P'}{4\pi} \frac{e^{-jk_0 r}}{r} \tag{62}$$

where higher order terms in $1/r$ were neglected. Applying Equation 56 to
Equation 61 results in:

33

$$E_{\theta i} = \frac{-j\omega\mu}{(2\pi r)^{1/2}} e^{j\pi/4} \sum_n \rho_n \lambda_n E_n e^{-j\rho_n r} \approx \frac{-jk_0\omega\mu}{(2\pi r)^{1/2}} e^{j\pi/4} \sum_n \lambda_n E_n e^{-j\rho_n r} \quad (63)$$

where it was assumed that:

$$\rho_n \approx k_0 \quad (64)$$

for all ρ_n of interest. In Section 3, the approximation given in Equation 64 is shown to be valid for the work described herein. By comparing Equations 56 and 63, it is seen that:

$$E_{\theta i} = k_0 \omega\mu \Pi_i \quad (65)$$

Defining:

$$\beta_0 = \frac{2(2\pi r)^{1/2}}{R_p W q_p'} = \frac{2(2\pi r)^{1/2}}{p} = 2(2\pi r)^{1/2} \quad (66)$$

and using Equations 62 and 65 in Equation 59 yields:

$$A = \frac{4\pi r \left|\Pi_i\right|}{R_p W q_p'} = \beta_0 \left|\sum_n \lambda_n E_n e^{-j\rho_n r}\right| \quad (67a)$$

where Equation 56 was used. A dipole strength of unity was assumed in
Equation 66.

In Equation 67a, Π_i represents a sum of complex numbers taking full
account of the phase of each term. That representation will be referred to as
a "coherent sum", a "mode sum", or a "vector sum." It is also useful to
define the relative field that would be obtained if the phase of each term
were completely random instead of well-defined. This will be denoted as $\overline{A}$,
where:

$$\overline{A} = \beta_o \sqrt{\sum_n \left| \lambda_n E_n e^{-j\rho_n r} \right|^2} \tag{67b}$$

which is similar to the result that would be obtained if the power
contribution of each mode were added, rather than the field contribution.
Therefore, the representation used in Equation 67a will be referred to as the
"power sum" or "incoherent sum."

In terms of dB relative to free-space, A and $\overline{A}$ are written as:

$$A_{dB} = 20 \log_{10} A \tag{67c}$$

and

$$\overline{A}_{dB} = 20 \log_{10} \overline{A} \tag{67d}$$

In most works on this subject (e.g., References 2, 5, and 8), the
function E_n defined in Equation 58 is written in the form:

$$E_n = u(\rho_n, z) \; u(\rho_n, z_T) \tag{68}$$

which demonstrates the reciprocity between the transmitter and receiver. Using Equation 68 in Equation 66 would result in precisely the formulation used by Dresp [17] (see also Reference 8). Although it is elegant in its representation, the form of Equation 58 is more desirable for the numerical formulation of this problem.

VERTICALLY POLARIZED PROPAGATION

As shown in Reference 2, the magnetic Hertz potential, and the definitions in Equations 10 and 11 for the electromagnetic field vectors, are consistent with Maxwell's equations when Equation 1 holds (i.e., when the variation in refractive index occurs only through a variation of ε_r but not of μ_r). For vertically polarized propagation, on the other hand, an electric Hertz potential $\vec{\Pi}^{(e)}$ must be used, from which the field vectors are obtained through:

$$\vec{H} = j\varepsilon\omega \; \nabla \times \vec{\Pi}^{(e)} \tag{69}$$

and

$$\vec{E} = \nabla \times \nabla \times \vec{\Pi}^{(e)} \tag{70}$$

---

[17]Dresp, M.R., Tropospheric Duct Propagation at VHF, UHF and SHF, MITRE Technical Report MTR-3114, Vols. I and II, MITRE Corporation, Bedford, MA, October 1975.

As shown in Reference 2, these definitions are only approximately consistent with Maxwell's equations. The approximation, however, is considered to be a good one for the duct problems of interest.

The mathematical formulation using the electric Hertz potential $\vec{\Pi}^{(e)}$ is identical to the formulation using the magnetic Hertz potential, with the following exceptions:

1. The magnetic dipole strength p in Equation 12 should be replaced by:

$$p \rightarrow \frac{-jp^{(e)}}{\omega\varepsilon_0 n^2(z_T)} \tag{71}$$

where $p^{(e)}$ is the strength of an electric dipole oriented with its axis in the z direction. This will also affect the value of R_p in Equation 37.

2. The first of Equations 15 should be changed to:

$$n_g^2 \Pi_g^{(e)} = n_1^2(0) \Pi_1^{(e)} \text{ on } z = 0 \tag{72}$$

3. The first of Equations 21 should be changed to:

$$n_g^2 \tilde{\Pi}_g^{(e)} = n_1^2(0) \Pi_1^{(e)} \text{ on } z = 0 \tag{73}$$

4. Equation 40 should be changed to:

$$G = \frac{j\gamma}{q_1'} \frac{n_1^2(0)}{n_g^2} \tag{74}$$

Of those listed above, Equation 74 is the only change that in practice will affect the calculations. This may be concluded from the fact that β_o (Equation 67) is proportional to $1/R_p$, and E_n (Equation 58) is proportional to R_p (through the dependence of $|T_{Ai}|$ and $|T_{Bi}|$ on R_p). Since the final result is dependent on the product $\beta_o E_n$, the value of R_p is therefore of no consequence. Also, Equations 72 and 73 are manifested in Equation 74.

ALTERNATIVE REPRESENTATION

General Solution of Homogeneous Equation

The general solution to Equation 25 may be given in terms of Airy functions, or in terms of modified Hankel functions, which are linear combinations of Airy functions. The general solution to Equation 25 could similarly be written in terms of linear combinations of the modified Hankel functions. This will be very useful in later sections. Thus:

$$\tilde{\Pi}_i = A_i \, K_1(q_i) + B_i \, K_2(q_i) \tag{75}$$

would be a valid general solution of Equation 25, where:

$$K_1(q_i) = c_{11i} h_1(q_i) + c_{12i} h_2(q_i) \tag{76}$$

$$K_2(q_i) = c_{21i} h_1(q_i) + c_{22i} h_2(q_i) \tag{77}$$

38

The subscript i is placed on the constants c_{mn} to indicate that there is no need for these constants to be identical in each layer. The c_{mni} would have to be such as to make the $K_1(q_i)$ linearly independent.

It is convenient to set:

$$c_{21i} = 0, \quad c_{22i} = 1 \text{ for } i = L \tag{78}$$

so that $\widetilde{\Pi}_L$ in Equation 75 would satisfy the radiation condition when Equation 30 holds. It is also convenient to define:

$$c_{11i} = 1, \qquad c_{12i} = 0$$
$$c_{21i} = -e^{4\pi j/3}, \qquad c_{22i} = 1, \quad i < L \tag{79}$$

and

$$c_{11L} = 1, \qquad c_{12L} = -e^{-4\pi j/3} \tag{80}$$

Substituting Equations 78 through 80 into Equations 76 and 77 yields:

$$K_1(q_i) = h_1(q_i)$$
$$K_2(q_i) = h_2(q_i) - e^{4\pi j/3} h_1(q_i), \quad i < L \tag{81}$$

and

$$K_1(q_i) = h_1(q_i) - e^{-4\pi j/3} h_2(q_i)$$
$$K_2(q_i) = h_2(q_i), \quad i = L \tag{82}$$

As shown in APPENDIX A, these definitions have the effect of assuring that the modulus of the two solutions $K_1(q_i)$ and $K_2(q_i)$ are not both exponentially large for any value for which $\mathrm{Im}(q_i) > 0$.

Using Equations 81 and 82 in Equation 32, it may be seen that the Wronskian for K_1 and K_2 (as defined above) is identical to the Wronskian for h_1 and h_2:

$$W\{K_1, K_2\} = W\{h_1, h_2\} = -\frac{4j}{\pi}\left(\frac{3}{2}\right)^{1/3} \tag{83}$$

Particular Solution of Inhomogeneous Equation

A particular solution of Equation 18 was given in Equation 34. By substitution in Equation 33, it may be seen that both of the following particular solutions are also valid:

$$\tilde{\Pi}_p = \begin{cases} R_p \, K_1(q_{p<}) \, K_2(q_{p>}) & \tag{84} \\[2em] -R_p \, K_1(q_{p>}) \, K_2(q_{p<}) & \tag{85} \end{cases}$$

where K_1 and K_2 are given by Equations 81 and 82. However, notice that Equation 85 will not satisfy the radiation condition when $P = L$.

Mode Series Solution

Using the K_i-representation rather than the h_i-representation, all terms in the mode series solution remain the same as those derived above, except h_i is replaced by K_i. Thus, from Equation 58:

$$E_n = \left[|T_{Ai}| \; K_1(q_i) + |T_{Bi}| \; K_2(q_i) \right]_{\rho \; = \; \rho_n} \tag{86}$$

The substitution of K_i for h_i would also take place in the expressions for T_{Ai}, T_{Bi} and α in Equations 44 and 47.

SECTION 3

DETERMINATION OF THE EIGENVALUES

GENERAL

The major computational effort required to obtain the solution given in
Equation 66 is determined by the eigenvalues $\rho = \rho_n$ which are the zeroes of
the determinant of α (see Equation 44). That is, the equation:

$$G_0(\rho_n) = |\alpha(\rho_n)| = 0 \tag{87}$$

must be solved for the ρ_n. The variable ρ enters the matrix α in Equation 44
through the arguments q_{ij} of h_1 and h_2, where:

$$q_{ij} = q_i(z_j) = \left(\frac{k_0}{|\tan \alpha_i|}\right)^{2/3} \left[1 - \frac{\rho^2}{k_0^2} + (z_j - H_i) \tan \alpha_i\right] \tag{88}$$

and where Equations 7 and 26 were used. z_j is the height of the interface
between the jth and jth+1 atmospheric layer, with $z_0 \equiv 0$ representing the
ground level.

CHANGE OF VARIABLES

Instead of searching for solutions of Equation 87 in ρ-space, the search
may be carried out for any convenient function of ρ. In the waveguide mode
literature, the variable:

$$\Theta_n = \sin^{-1}\left(1 - \frac{\rho_n^2}{k_0^2}\right)^{1/2} \tag{89}$$

is often used (see Reference 5), where Θ is interpreted as a plane wave angle
of incidence with respect to the horizontal at a given reference height.
Dresp (see Reference 8) searches for eigenmodes using the variable:

$$\lambda_n = 1 - \frac{\rho_n^2}{k_0^2} \tag{90}$$

For numerical and analytical reasons which will become clear later, it is more convenient to search for the roots of Equation 87 in "q_{10}-space". That is, it is more convenient to write Equation 87 as:

$$G_1(q_{10}) = \left| \alpha \left(q_{10}^{(n)} \right) \right| = 0 \tag{91}$$

where, from Equation 88:

$$q_{10} = \left(\frac{k_0}{\lceil \tan \alpha_1 \rceil} \right)^{2/3} \left(1 - \frac{\rho^2}{k_0^2} - H_1 \tan \alpha_1 \right) \tag{92}$$

Thus

$$1 - \frac{\rho^2}{k_0^2} = \frac{q_{10}}{\left(\dfrac{k_0}{\lceil \tan \alpha_1 \rceil} \right)^{2/3}} + H_1 \tan \alpha_1 \tag{93}$$

and

$$\rho = k_0 \sqrt{1 - H_1 \tan \alpha_1 - \frac{q_{10}}{\left(\dfrac{k_0}{\lceil \tan \alpha_1 \rceil} \right)^{2/3}}} \tag{94}$$

44

Using Equation 93 in Equation 88 yields:

$$q_{ij} = q_{10}\, t_i + s_{ij}, \quad 1 \leqslant i \leqslant L, \quad j = i-1, i \tag{95}$$

where

$$t_i = \left(\left|\tan \alpha_1\right| / \left|\tan \alpha_i\right|\right)^{2/3} > 0 \tag{96}$$

and

$$s_{ij} = \left(k_0 / \left|\tan \alpha_i\right|\right)^{2/3} \left(H_1\, \tan \alpha_1 - H_i\, \tan \alpha_i + z_j\, \tan \alpha_i\right) \tag{97}$$

The t_i and s_{ij} are all real constants.

It should be noted from Equation 34 that:

$$q_i'(z) = \left(k_0 / \left|\tan \alpha_i\right|\right)^{2/3} \tan \alpha_i \tag{98}$$

is not a function of ρ (and therefore not a function of q_{10}).

The roots of ρ_n of interest were shown to lie in the fourth quadrant of the complex ρ-plane. By straightforward conformal mapping using Equation 92, the corresponding roots $q_{10}^{(n)}$ will lie in the upper half of the complex q_{10}-plane.

The relationship between the q_{ij} and q_{10} may be obtained from Equation 95. Figure 4 illustrates this relationship for two arbitrary values of q_{10} using a refractivity profile of the form shown in Figure 5. Figure 6 illustrates the relationship using the refractivity profile of the form shown in Figure 7.

NUMERICAL INSTABILITIES IN h_i REPRESENTATION

It was shown in the previous section that the matrix elements in Equation 44 may contain the functions h_1 and h_2, or alternatively, may contain functions that are linear sums of h_1 and h_2 (such as the functions K_1 and K_2 in Equations 76 and 77). It can also be shown that use of the h_1 and h_2 functions result in numerical instabilities of the determinant $|\alpha|$ when q_{10} is near the negative real axis and has a large magnitude. Section 6 shows that the roots in this region of the complex q_{10}-plane contribute most to fields within the duct. Therefore, numerical instabilities in this region cannot be tolerated.

From the asymptotic expansions of $h_1(q)$ and $h_2(q)$ for large $|q|$, given in Reference 14 and APPENDIX A:

$$h_2(q) = e^{4\pi j/3}h_1(q) + F(q), \quad \frac{\pi}{2} < \arg(q) < \pi \tag{99}$$

For $|q|$ large and $2\pi/3 < \arg(q) < \pi$, $h_1(q)$ is exponentially large while $F(q)$ is exponentially small. Thus:

$$h_2(q) \approx e^{4\pi j/3}h_1(q), \quad \frac{2\pi}{3} < \arg(q) < \pi, \quad |q| \gg 1 \tag{100}$$

If Equation 100 were to hold, say, for $q = q_{10}$ and $q = q_{11}$ (which would be the worst case in branch B of Figure 4), and if Equation 100 were substituted into

46
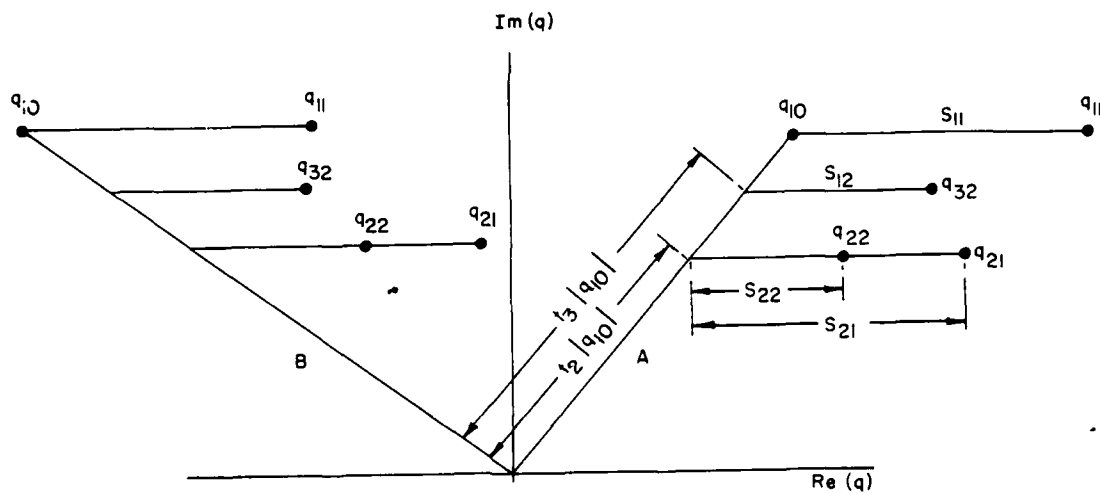
Figure 4.   Relationship between q_{ij} and q_{10} in complex q-space for refractivity profile of Figure 5.
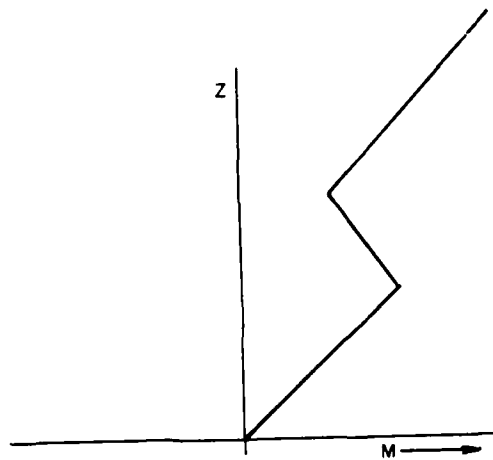
Figure 5.   Refractivity profile producing elevated duct.
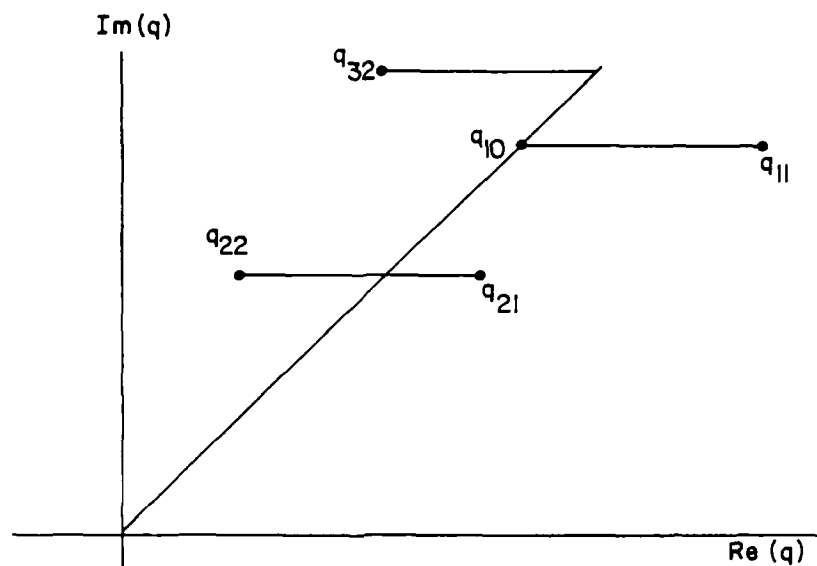
Figure 6. Relationship between q_{ij} and q_{10} in complex q-space for refractivity profile of Figure 7.
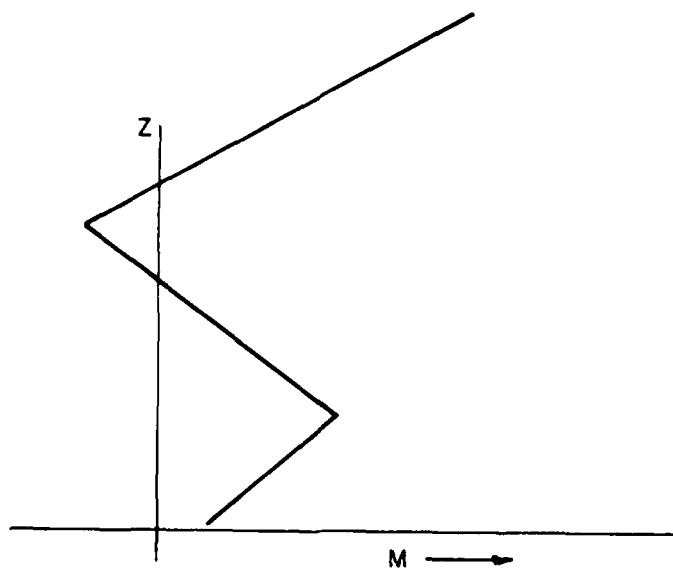
Figure 7. Refractivity profile producing surface duct.

Equation 44, then the first two columns of the matrix α would be linearly dependent. That is, each term in the second column would be equal to the corresponding term in the first column multiplied by the constant factor $e^{4\pi j/3}$. This is sufficient to make α singular, so that:

$$\left| \alpha(q_{10}) \right| \approx 0, \quad \text{all } q_{10},$$

thereby making it impossible to locate discrete roots of Equation 91. Of course, the matrix α is not singular in an analytical sense since the term $F(q)$, albeit small, makes Equation 100 only an approximation. Nevertheless, the matrix α would be singular in a "numerical" sense, and would preclude the use of numerical techniques to obtain the discrete roots $q_{10}^{(n)}$.

Pappert and Goodhart (see Reference 5) utilized a formulation employing the functions $h_1(q)$ and $h_2(q)$. They avoided the numerical instabilities described above by a "switching" procedure: They argued that, for values of q for which Equation 100 holds, the fields are evanescent. Since the general solution of Equation 25 was shown to be given by Equation 27:

$$\tilde{\Pi}_i = A_i h_1(q_i) + B_i h_2(q_i), \quad 1 \leqslant i \leqslant L, \tag{101}$$

an evanescent solution may be obtained from Equation 101 by letting:

$$A_i = - B_i e^{4\pi j/3}$$

so that

$$\tilde{\Pi}_i = B_i \left[h_2(q_i) - e^{4\pi j/3} h_1(q_i) \right] \tag{102}$$

which, from Equation 99, may be written:

$$\widetilde{\Pi}_i = B_i \ F(q_i) \tag{103}$$

As stated above, in the region of the q-plane in which Equation 100 holds, $F(q)$ is exponentially small and therefore is an evanescent field.

As described by Pappert and Goodhart (see Reference 10), the "solution-switching" between Equation 101 and Equation 102 causes a discontinuity in the function of which the roots are sought [$G(q_{10})$ in the case at hand]. In turn, this could lead to missing or duplicating a root already found.

CHOICE OF ALTERNATIVE REPRESENTATION

The discussion above indicates the desirability of a solution in terms of functions that

1. will not be exponentially large simultaneously in the root-search region; and

2. will reduce without "switching" to the form of Equation 103 when Equation 100 is valid.

Functions that satisfy these conditions are the pair $h_1(q)$ and $F(q)$, where $F(q)$ is defined from Equation 99. Thus:

$$\widetilde{\Pi}_i = A_i \ h_i(q_i) + B_i \ F(q_i) \tag{104}$$

The validity of using functions other than h_1 and h_2 was discussed in Section 2.

In a region where the field is evanescent, A_i would be expected to approach 0, thus leaving an equation in the form of Equation 103. That $F(q_i)$

is exponentially small when $|q|$ is large and $\pi < \arg(q) < \pi/2$ was noted following Equation 99, so that in this subregion of the q_{10}-plane, $h_1(q)$ and $F(q)$ are not both exponentially large. $h_1(q)$ is never exponentially large in the remainder of the upper half of the q_{10}-plane as shown in APPENDIX A. Thus Equation 104 is well suited for numerical determination of the roots of Equation 91. It has the disadvantage, however, of not satisfying the radiation condition. Since the radiation condition need only be satisfied for the solution in the uppermost region $(i = L)$, the form:

$$\tilde{\Pi}_L = B_L\, h_2(q_L) \tag{105}$$

will again be used in this region.

The functions used in the solutions given in Equations 104 and 105 are identical to the functions $K_1(q_i)$ and $K_2(q_i)$, as defined in Equations 81 and 82. Therefore:

$$\tilde{\Pi}_i = A_i\, K_1(q_i) + B_i\, K_2(q_i) \tag{106}$$

BOUNDS ON SEARCH REGION - MODE ATTENUATION

As discussed previously, the eigenvalues of Equation 91 will lie in the upper half of the q_{10}-plane (i.e., in the region $\text{Im}(q_{10}) > 0$). Thus the lower bound of this region is the real axis. Although a discussion of the left and right boundaries of the search region will be postponed for a later section (Section 6), an upper bound of the search region will be obtained here in terms of the maximum attenuation of the strength of a mode per unit length.

From Equation 66, it is seen that each modal contribution to the total field has an exponential dependence $e^{-j\rho_n r}$. Since the ρ_n are complex with $\text{Im}(\rho_n) < 0$, the amplitude of each mode will fall off exponentially. Thus, if:

$$\rho_n = a + jb,\quad b < 0$$

then

$$e^{-j\rho_n r} = e^{br} e^{-jra}$$

Since b is negative, $e^{-j\rho_n r}$ will decrease in amplitude as r increases. Typical values of r are generally large enough to make $e^{-j\rho_n r}$ negligible for all $|b|$ greater than some positive number. The relative decrease in the field contribution from the nth mode over a single unit of length is given by:

$$\left| \frac{e^{-j\rho_n r(r+1)}}{e^{-j\rho_n r}} \right| = \left| e^{-j\rho_n} \right|$$

so that the loss in dB would be given by:

$$L_n = -20 \log_{10} \left| e^{-j\rho_n} \right| = -20 \log_{10}(e^b) = -20 \ b \ \log_{10} e \tag{107}$$

Suppose a maximum value of L_n is specified, say L_{max}. Then roots ρ_n will be sought, such that:

$$-b \ (20 \ \log_{10} e) < L_{max}$$

or

$$b = \text{Im}(\rho_n) > \frac{L_{max}}{20 \ \log_{10} e} \tag{108}$$

Equation 108 represents a bound on the region in ρ-space for which the mode attenuation per unit length would not exceed L_{max}. This condition must now be converted to q_{10}-space. To accomplish this, Equation 92 is written:

$$q_{10}^{(n)} = \left(\frac{k_0}{|\tan \alpha_1|} \right)^{2/3} (\lambda_n - H_1 \tan \alpha_1) \tag{109}$$

where

$$\lambda_n = 1 - \frac{\rho_n^2}{k_0^2}$$

and

$$|\lambda_n| \ll 1 \tag{110}$$

under the assumption that $|\rho_n| \approx |k_0|$, which will be shown to be valid later. Thus:

$$\rho_n = k_0 \sqrt{1 - \lambda_n} \approx k_0 \left(1 - \frac{\lambda_n}{2} + \ldots\right) \tag{111}$$

where Equation 110 was used to obtain the Taylor series expansion in Equation 111.

Therefore,

$$\lambda_n \approx 2\left(1 - \frac{\rho_n}{k_0}\right) \tag{112}$$

In particular,

$$\mathrm{Im}(\lambda_n) \approx -\frac{2}{k_0} \mathrm{Im}(\rho_n) \tag{113}$$

Using Equation 113 in Equation 109 yields:

$$\mathrm{Im}\left(q_{10}^{(n)}\right) = -\left(\frac{k_0}{|\tan \alpha_1|}\right)^{2/3} \frac{2}{k_0} \mathrm{Im}(\rho_n) \tag{114}$$

53

and using Equation 114 in Equation 108 results in:

$$Im(q_{10}) < U \qquad (115)$$

where

$$U = \frac{2}{k_0} \left(\frac{k_0}{|\tan \alpha_1|} \right)^{2/3} \frac{L_{max}}{20 \log_{10} e} \qquad (116)$$

Therefore, U as defined in Equation 116 will be used as an upper bound of the search region, with L_{max} being specified. Thus the search for eigenvalues will be carried out in the band in the q_{10}-plane defined by:

$$0 < Im (q_{10}) < U \qquad (117)$$

SEARCH METHOD

The procedure used to find the zeroes of:

$$G_1(q_{10}) = |\alpha(q_{10})| = 0 \qquad (118)$$

in the complex plane is described by Morfitt and Shellman [18] and reviewed in Reference 10. The procedure will be denoted herein as the MODESRCH method.

---

[18] Morfitt, D.G., and Shellman, C.H., MODESRCH, An Improved Computer Program for Obtaining ELF/VLF/LF Mode Constants in an Earth - Ionosphere Waveguide, Interim Report 77T prepared for Defense Nuclear Agency, Naval Electronics Laboratory Center, San Diego, CA, 1 October 1976.

54

The method assumes that the function G_1 is analytic everywhere within the region of search, and thus does not permit the presence of poles in this region. The function $G_1(q_{10})$ satisfies these conditions.

The MODESRCH method was applied by Pappert and Goodhart (see Reference 10) to the ducting problem, where their modal equation was in the form:

$$G_2(\Theta) = 0 \tag{119}$$

where θ is related to q_{10} and ρ through Equation 89. Their formulation of the problem differed from the one being presented here in that the function G_2 is obtained from the fundamental equation of waveguide propagation:

$$G_2(\Theta) = R_d(\Theta) \, R_u(\Theta) - 1 \tag{120}$$

where R_d and R_u are the reflection coefficients "looking downward" and "looking upward", respectively, from a given reference height. Equation 120 does not lend itself to application of the root-finding method to be discussed below because it contains poles in the region of search. The function $G_2(\theta)$, therefore, had to be manipulated to produce a pole-free function. This fact, together with the problems they encountered in solution-switching between the forms of Equations 101 and 102, detracted from the desirability of applying this MODESRCH method to their formulation.

Since the formulation of the problem presented in this report does not suffer from the difficulties encountered by Pappert and Goodhart [i.e. $G_1(q_{10})$ is pole-free and no solution-switching is required], the MODESRCH method was chosen to locate the roots of Equation 118.

The method utilizes the following fact from complex functional analysis: In a finite region of the complex q-plane in which no poles of $G_1(q)$ are present and in which the only zeroes of $G_1(q)$ are simple zeroes, lines of

constant phase [i.e., arg(G) = const] may end only at the boundary of the
region or at a zero of $G_1(q)$. Figure 8 (taken from Reference 10) illustrates
a rectangular region being searched. This figure shows that a line AB of
constant phase on which arg(G) = 0 has its ends at a zero of the function and
at the boundary of the region. The line HG, on which arg(G)= 0, has both its
ends on the boundary of the region. It is impossible for a line of constant
phase to have each end at a zero of G(q).

The MODESRCH method thus starts from the upper left-hand corner of a
"search rectangle" in the q-plane, and searches along the left-hand boundary
of the rectangle until a value of q is found at which arg[G(q)] = const = 0 or
arg(G) = 180°. Say a phase contour arg(G) = 0 is found at the point A, as in
Figure 8. This contour is then followed until it either exits the search
rectangle or until it ends at a point within the rectangle. If it ends at a
point within the rectangle, that point must be a zero of the function. Such
is the case in Figure 8, with the zero located at point B. Since a phase
contour arg(G) = 180° must also intersect that zero, this contour is followed
until it exits the search rectangle (point C in the figure). The point at
which this contour exits the rectangle is stored, in order to assure that it
will not be followed again later in the search process. The search then
resumes again at the point A, and the boundary is traversed counter-clockwise
until another value of q is found at which arg(G) = 0 or arg(G) = 180°. The
next such point in Figure 8 is point C. But this contour will not be followed
since it has been previously investigated. Therefore, the search continues
until the contour arg(G) = 0 is reached at point D, a zero is found at point
E, and the contour arg(G) = 180° exits the rectangle at point F. The search
resumes again at D, and the rectangle is traversed until point G is reached at
which arg(G) = 0. This contour is seen to exit the rectangle at point H
without passing through a zero of the function. The search resumes at point G
and the remainder of the rectangle is traversed without finding any additional
contours arg(G) = 0 or arg(G) = 180° which have not been previously
investigated.
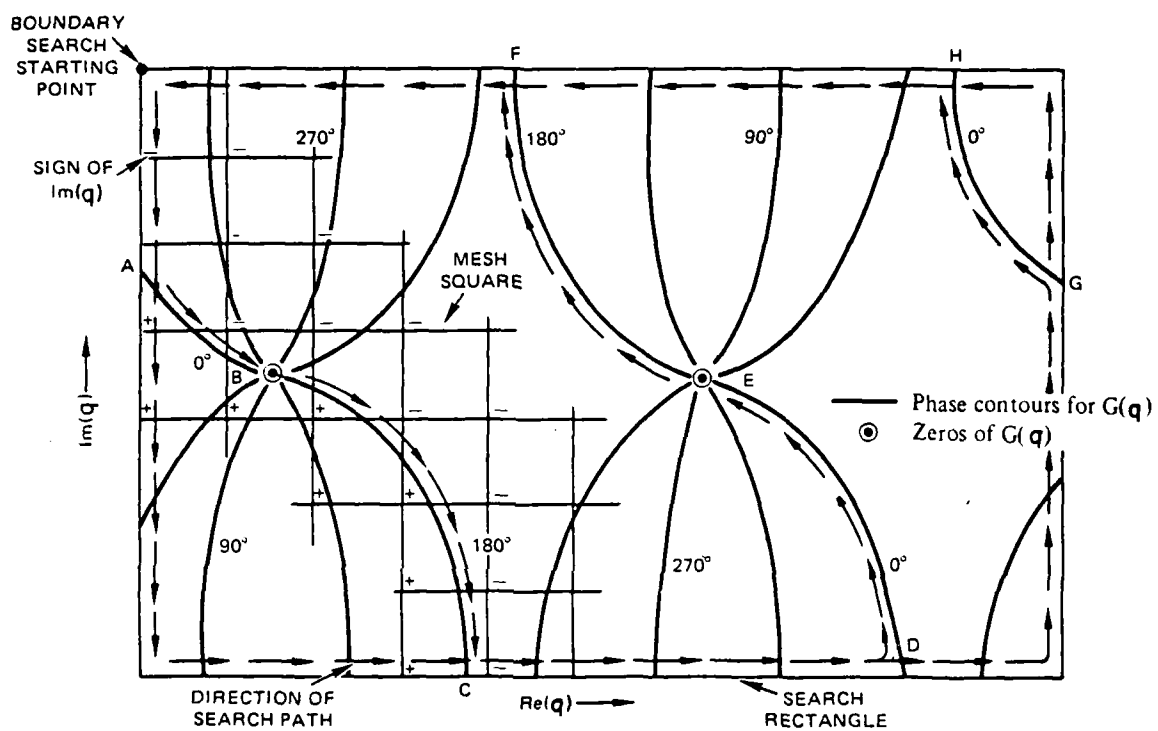
Figure 8.   Root finding method for a function G(q).

The procedure just described is accomplished numerically by dividing the
search rectangle into mesh squares of side length Δt as shown in Figure 8, and
by investigating the sign of $Im(G)$ at the corners of the mesh. A change of
sign between two adjacent corners indicates that a phase contour $arg(G) = 0$ or
a phase contour $arg(G) = 180°$ passes between these two corners. A change in
sign of $Re(G)$ between the corners of a mesh square through which the $0°$ or
$180°$ phase contour passes, or between the corners of an adjacent mesh square,
indicates that the phase contour $arg(G) = 90°$ or $arg(G) = 270°$ is nearby and
thus a zero is in the vicinity. The approximate location q_o of the zero
within a mesh square is obtained by an interpolation procedure. The precise
location of the zero is obtained using the Newton Raphson[19] method:

$$q_{i+1} = q_i - \Delta q_i, \quad i = 0, 1, 2, \ldots \qquad (121)$$

where

$$\Delta q_i = \frac{G(q_i)}{G'(q_i)} \qquad (122)$$

The iteration in Equation 121 ends when the magnitude of the correction Δq_i
to the previous approximation becomes less than a specified small positive
number, i.e. when:

$$|\Delta q_i| < \varepsilon \qquad (123)$$

[19]Pennington, R.H., Introductory Computer Methods and Numerical Analysis,
Macmillian Co., p. 236 ff, New York, NY.

APPLICATION OF MODESRCH

As mentioned above, the MODESRCH method for determining the roots of the modal equation requires the definition of a "search rectangle" in the q_{10}-plane where the roots are sought. The upper and lower limits of this rectangle were given in Equation 117. It is shown in Section 6 that a left limit may be determined as well. However, instead of defining the left and right sides of a search rectangle in which all the roots should lie, it is convenient to perform the search in subregions. This will have the advantage of requiring less computer storage space for the searching subroutine. The subregions are defined as shown in Figure 9. From Equation 117, the lower bound is at $Im(q_{10}) = 0$ and the upper bound at $Im(q_{10}) = U$. [The MODESRCH program (Reference 18) automatically increases the search region slightly for numerical reasons.] The first subregion will be the rectangle defined by $-4 < Re(q_{10}) < 4$. Thereafter, subregions of 4 units width are searched, moving to the left of the imaginary axis, then to the right, then to the left, etc., as shown in Figure 9. The search ends when two successive regions are encountered which contain no roots.
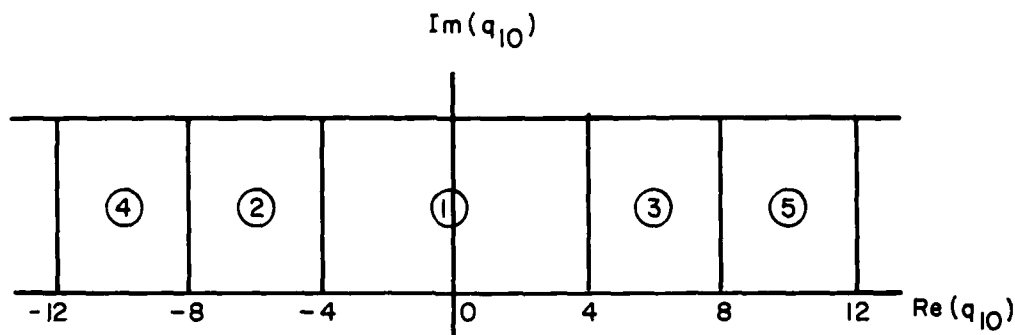
Figure 9. Subregions of q_{10} plane for root-finding method.

The size Δt of the sides of the mesh square in each subregion is about .1:

$$\Delta t \approx .1 \tag{124}$$

and the value of ε in Equation 123 is:

$$\varepsilon = \Delta t/1000. \tag{125}$$

However, if, after searching the first subregion, there is any indication that Δt is too large, it is automatically made smaller.

NUMERICAL REPRESENTATION OF K_1 AND K_2 - EXPONENTIAL REPRESENTATION OF COMPLEX NUMBERS

The functions $K_1(q)$ and $K_2(q)$, defined in Equations 81 and 82, are numerically evaluated for large values of $|q|$ (i.e., $|q| > 4.2$) using the asympotic expansions given in (Reference 14) and summarized in APPENDIX A. For small values of $|q|$ (i.e., $|q| < 4.2$) a power series is used (Reference 14). In APPENDIX A, it is seen that for large values of $|q|$ the magnitudes of K_1 and K_2 have an exponential dependence (see Equations A-11 and A-12), so that it is possible for $|K_1|$ and $|K_2|$ to become exponentially large and to exceed the upper numerical limit which a high-speed computer can consider. It is this fact which prompted Pappert and Goodhart (Reference 3) to "switch" to a solution of the form of Equation 102 when $|q|$ becomes very large. Since the formula presented here avoids "switching", a different scheme must be used to permit evaluation of K_1 and K_2 even when $|q|$ is exponentially large. This scheme will be defined in the following:

Instead of using two "words" to describe a value of the complex function K_1 (or K_2) (i.e., a real value and an imaginary value), three words will be used. These will represent a real value, an imaginary value and a real exponent. Thus for example:

$$K_1 = \overline{K}_1 \, e^{E_1} \qquad (126)$$

where

$\overline{K}_1$ is a complex number and

E_1 is a real number

The value of E_1 will be given by one of the exponents in Equation A-12. The values of $|\overline{K}_1|$ and E_1 will be small enough for a computer to handle in a single precision mode. This representation using three numbers to describe a complex number will be referred to as an "exponential representation."

All arithmetic using the functions K_1 and K_2 will be carried out without evaluating e^E when E is large. Thus, if:

$$z_a = \overline{z}_a e^{E_a}, \quad z_b = \overline{z}_b e^{E_b} \qquad (127)$$

then the product:

$$z_c = z_a \, z_b \qquad (128)$$

will be evaluated by:

$$\overline{z}_c = \overline{z}_a \overline{z}_b, \quad E_c = E_a + E_b \qquad (129)$$

where

$$z_c = \bar{z}_c e^{E_c} \tag{130}$$

The sum:

$$z_d = z_a + z_b \tag{131}$$

is evaluated as:

$$\bar{z}_d = \bar{z}_a + \bar{z}_b e^{(E_b - E_a)}, \tag{132a}$$

$$E_d = E_a, \quad E_a > E_b$$

or

$$\bar{z}_d = \bar{z}_a e^{(E_a - E_b)} + \bar{z}_b, \tag{132b}$$

$$E_d = E_b, \quad E_a < E_b$$

The multiplication of $\bar{z}_b$ with $e^{(E_b - E_a)}$ in Equation 132a is carried out, as is the corresponding multiplication in Equation 132b.

Only when a final answer is required is a complex number z_c obtained by carrying out the multiplication indicated in Equation 130.

The summation procedure in Equations 132a and 132b for complex numbers in the exponential representation is valid for two numbers. Numerical difficulties may arise, however, when more than two numbers must be summed. To illustrate this, consider the following three numbers:

$$z_a = 2e^{300}$$

$$z_b = 3e^4 \tag{133}$$

$$z_c = -2e^{300}$$

62

The sum of these numbers is obviously $S = 3e^4 = 163.79$. However, when summed in the above order, Equation 132 yields:

$$S_1 = z_a + z_b = (2 + 3e^{-296})\, e^{300} \approx 2e^{300} \tag{134a}$$

and

$$S + S_1 + z_c = (2-2)e^{300} = 0 \tag{134b}$$

which does not agree with the actual result. The reason for this disagreement is the fact that a computer would evaluate $2 + 3e^{-296}$ as 2, thus losing the second term.

The problem described above may be overcome by carrying out the sum in the order of decreasing exponents and, if in the partial sum $S_n = \overline{S}_n e^{E_n}$ the value $\overline{S}_n = 0$, setting $E_n = 0$. The example above would then be carried out as:

$$S_1 = z_a + z_c + z_b \tag{135a}$$

so that

$$S_1 = z_a + z_c = (2 - 2)e^{300} - 0e^{300} = 0e^0 \tag{135b}$$

and

$$S = S_1 + z_b = e^4 (3 + 0e^{-4}) = 3e^4 \qquad (135c)$$

EVALUATION OF THE MODAL DETERMINANT

Determination of the roots of Equation 118 required the evaluation of the determinant of the matrix α which, for $L = 3$, is given in Equation 44 with h_1, h_2 replaced by K_1, K_2. Thus:

$$|\alpha| = \begin{vmatrix} \hat{K}_1(q_{10}) & \hat{K}_2(q_{10}) & 0 & 0 & 0 \\[2em] K_1(q_{11}) & K_2(q_{11}) & -K_1(q_{21}) & -K_2(q_{21}) & 0 \\[2em] K_1'(q_{11}) & K_2'(q_{11}) & -\dfrac{q_2'}{q_1'} K_1'(q_{21}) & -\dfrac{q_2'}{q_1'} K_2'(q_{21}) & 0 \\[2em] 0 & 0 & K_1(q_{22}) & K_2(q_{22}) & -K_2(q_{32}) \\[2em] 0 & 0 & K_1'(q_{22}) & K_2'(q_{22}) & -\dfrac{q_3'}{q_2'} K_2'(q_{32}) \end{vmatrix}$$

$$(136)$$

where

$$\hat{K}_m(q_{10}) = K_m'(q_{10}) - G\, K_m(q_{10}), \quad m = 1, 2 \qquad (136a)$$

During the mode searching procedure the value of $|\alpha|$ must be determined numerous times. An efficient method should be used to accomplish this. However, the standard elimination methods require many summing operations

which should be avoided as much as possible when expressing the K_1, K_2 functions in terms of the exponential representation described above. The evaluation method should also take maximum advantage of the presence of zeroes in the matrix of Equation 136.

APPENDIX B describes a method for accomplishing this in which the total number of multiplication operations required in the evaluation of the modal determinant is on the order of 8(L-1), where L is the number of layers in the atmosphere. This compares with (2L-1)! multiplication operations required when evaluating the determinant using a cofactor expansion.

It is also possible using the method described in APPENDIX B, to avoid any summation operations until all terms in the sum have been evaluated. The total number of terms to be summed will be 2^{2L-1}, and the method described following Equation 134 is used to accomplish this.

EVALUATION OF THE DERIVATIVE OF THE MODAL DETERMINANT

Part of the MODESRCH method for determining the roots of $G_1(q_{10})$ in Equation 118 involves the use of the Newton-Raphson method (see Reference 19) described by Equations 121 and 122. Since Equation 122 includes the derivative $G_1'(q_{10})$, this derivative must be evaluated.

If all the elements $a_{ij}(q)$ of an N-by-N matrix α are functions of a variable q, then the derivative of the determinant of α with respect to q is the sum of N determinants, each one having the elements of a different row replaced by the derivative of the elements of that row. Thus, for example, for a 3-by-3 matrix given by:

$$\alpha_0 = \begin{pmatrix} a_{11} & a_{12} & a_{13} \\ a_{21} & a_{22} & a_{23} \\ a_{31} & a_{32} & a_{33} \end{pmatrix} \tag{137}$$

the derivative of its determinant would be:

$$
\frac{d|\alpha_0|}{d_q} = \begin{vmatrix} a_{11}' & a_{12}' & a_{13}' \\ a_{21} & a_{22} & a_{23} \\ a_{31} & a_{32} & a_{33} \end{vmatrix} + \begin{vmatrix} a_{11} & a_{12} & a_{13} \\ a_{21}' & a_{22}' & a_{23}' \\ a_{31} & a_{32} & a_{33} \end{vmatrix} + \begin{vmatrix} a_{11} & a_{12} & a_{13} \\ a_{21} & a_{22} & a_{23} \\ a_{31}' & a_{32}' & a_{33}' \end{vmatrix} \quad (138)
$$

The above rule for obtaining the derivative of a determinant may be easily applied to $|\alpha|$ in Equation 136. The derivatives of the individual elements are obtained using the formula:

$$
\frac{\partial K_m(q_{ij})}{\partial q_{10}} = \frac{\partial K_m(q_{ij})}{\partial q_{ij}} \frac{\partial q_{ij}}{\partial q_{10}} = K_m'(q_{ij}) t_i, \quad 1 \leq i \leq L, \quad j = i - 1, \quad i, m = 1 \quad (139)
$$

where Equations 95 and 96 were used and the prime indicates differentiation with respect to the argument q_{ij}. Also:

$$
\frac{\partial}{\partial q_{10}} K_m'(q_{ij}) = K_m''(q_{ij}) t_i = - q_{ij} K_m(q_{ij}) t_i \quad (140)
$$

where, from Equations 25 and 75, the fact was used that $K_m(q_{ij})$ is a solution of the equation:

$$
\frac{\partial^2 K_m'(q_{ij})}{\partial q_{ij}^2} + q_{ij} K_m(q_{ij}) = 0 \quad (141)
$$

Equations 139 and 140 may be applied in Equation 136 to determine the derivative of $|\alpha|$ with respect to q_{10} according to the rule given in Equation 138.

66

Each of the individual determinants in Equation 138 will be evaluated using the same method as that used to evaluate $|\alpha|$. As previously discussed, each determinant is composed of a sum of terms and, for numerical reasons, this sum must be evaluated in order of decreasing exponents of the terms (see Equation 135). However, since the derivative of a determinant is represented in Equation 138 by the sum of determinants, it might appear that the use of the summation scheme should be postponed until all terms of all the determinants in Equation 138 are evaluated. That is, in Equation 138, each determinant is composed of the sum of six terms. To avoid numerical errors, it would appear that the summation method should not be applied separately to each set of six terms representing the value of each determinant, but rather it should be applied to the eighteen terms representing the entire summation in Equation 138 (three determinants with six terms for each determinant). Although this is possible to accomplish, it would be extremely time consuming, particularly when the size of the matrix becomes larger.

The number of terms in the total sum representating the determinant derivative may be made to be the same as the number of terms in the representation of any individual determinant of which that derivative is composed. (That is, in the example of Equation 138, the determinant derivative $d|\alpha_0|/dq$ may be expressed for cases of interest as a sum of only six elements.) This stems from the fact that the exponent in the exponential representation of $K_m(q_{ij})$ is equal to the exponent in the exponential representation of $K_m{}'(q_{ij})$. That is, if:

$$K_m(q_{ij}) = \overline{K_m(q_{ij})}\, e^{E_m(q_{ij})} \qquad\qquad (142)$$

then

$$K_m{}'(q_{ij}) = \overline{K_m{}'(q_{ij})}\, e^{E_m(q_{ij})} \qquad\qquad (143)$$

with the E_m being the same in both equations. It should be noted that the notation of Equation 126 was followed so that $\overline{K_m'(q_{ij})}$ is _not_ necessarily equal to the derivative of $\overline{K_m(q_{ij})}$. The fact that the E_m are the same in Equations 142 and 143 may be seen from examining the derivatives of the asymptotic expansion of K_m in APPENDIX A.

Thus in each of the determinants of which $\partial|\alpha_1|/\partial q_1$ is composed, the value of the exponent of the (i,j) term would be identical. This fact will lead to the terms of the sums representing each determinant having the same exponents *for each determinant*. To illustrate this, Equation 138 will be used with:

$$a_{ij} = \overline{a_{ij}}\, e^{E_{ij}} \tag{144}$$

$$a_{ij}' = \overline{a_{ij}'}\, e^{E_{ij}} \tag{145}$$

Then, from Equation 138:

$$\frac{d|\alpha_0|}{\partial q} = S_1 + S_2 + S_3$$

where

$$S_1 = b_{11}e^{\epsilon_1} + b_{12}e^{\epsilon_2} + b_{13}e^{\epsilon_3} + b_{14}e^{\epsilon_4} + b_{15}e^{\epsilon_5} + b_{16}e^{\epsilon_6}$$

$$S_2 = b_{21}e^{\epsilon_1} + b_{22}e^{\epsilon_2} + b_{23}e^{\epsilon_3} + b_{24}e^{\epsilon_4} + b_{25}e^{\epsilon_5} + b_{26}e^{\epsilon_6}$$

$$S_3 = b_{31}e^{\epsilon_1} + b_{32}e^{\epsilon_2} + b_{33}e^{\epsilon_3} + b_{34}e^{\epsilon_4} + b_{35}e^{\epsilon_5} + b_{36}e^{\epsilon_6} \tag{146}$$

where the ε_i's are the same for S_1, S_2 and S_3, $1 \le i \le 6$.
Since these ε_i's are the same, the respective terms may be summed without incurring numerical difficulties. Thus:

$$\frac{d|\alpha_0|}{dq} = c_1 e^{\varepsilon_1} + c_2 e^{\varepsilon_2} + c_3 e^{\varepsilon_3} + c_4 e^{\varepsilon_4} + c_5 e^{\varepsilon_5} + c_6 e^{\varepsilon_6} \tag{147}$$

where

$$c_1 = b_{1i} + b_{2i} + b_{3i}, \quad 1 \le i \le 6 \tag{148}$$

From Equations 146 and 147 it is seen that, using the summation scheme for exponential representation, the number of terms to be summed in order to obtain the determinant derivative is the same as the number which must be summed for the determinant itself.

SAMPLE RESULTS

A method has been described above for numerically determining the roots in q_{10}-space of the modal determinant given in Equation 136. For the refractivity profile shown in Figure 10, the results for the case of transmission frequency of 2.2017 GHz are shown in Figure 11. The value of L_{max} used in Equation 107 was .375 dB/km.

Each "dot" in the figure represents a mode. For comparison purposes, an illustration of the same modes in a space similar to one utilized in Reference 7 is also included as Figure 12. Figure 12 plots the location of the roots in terms of $Re(\theta)$ with θ given in Equation 89, and the mode attenuation per kilometer defined by Equation 107.

69
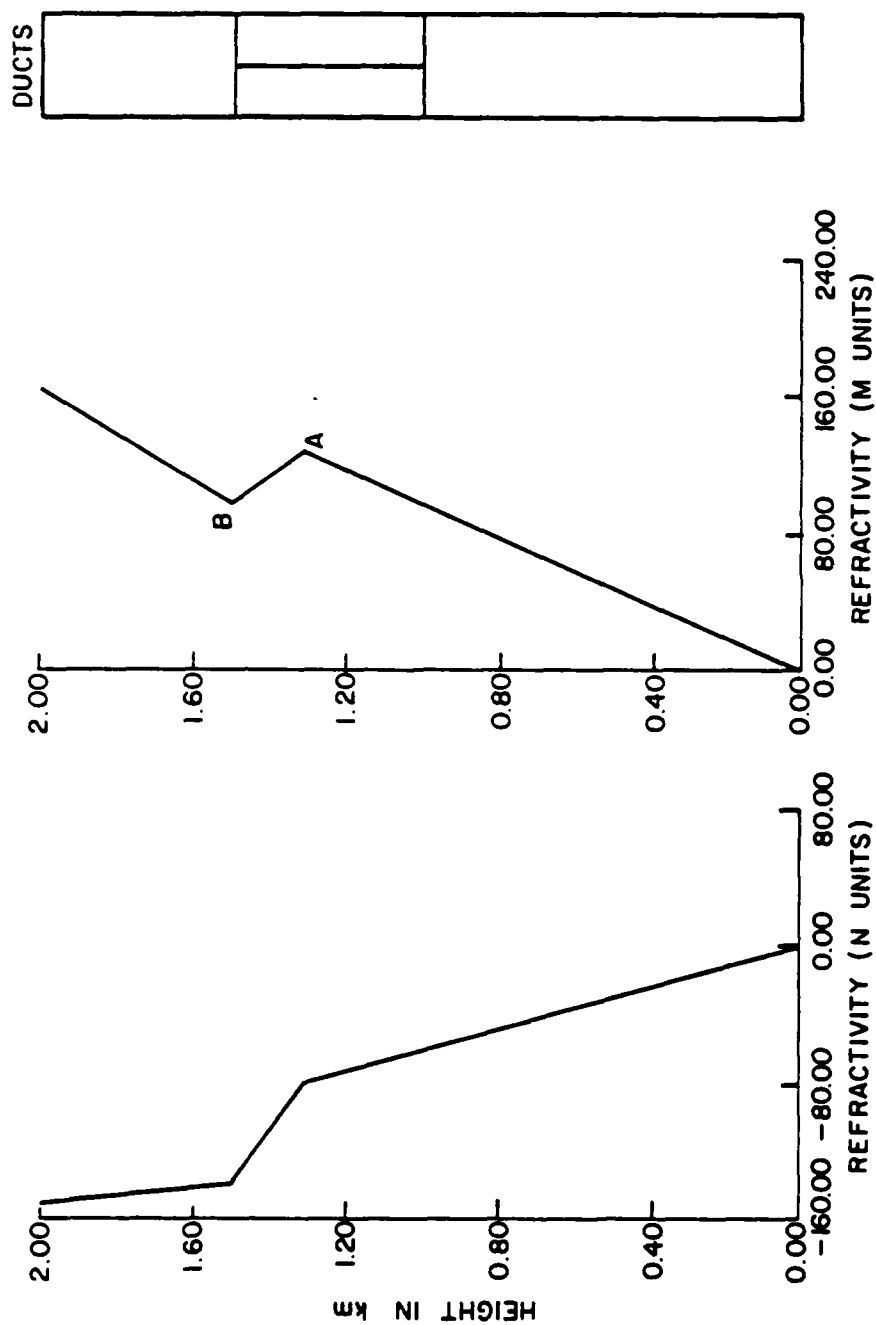
Figure 10. Refractivity profile used to obtain results of Figure 11.
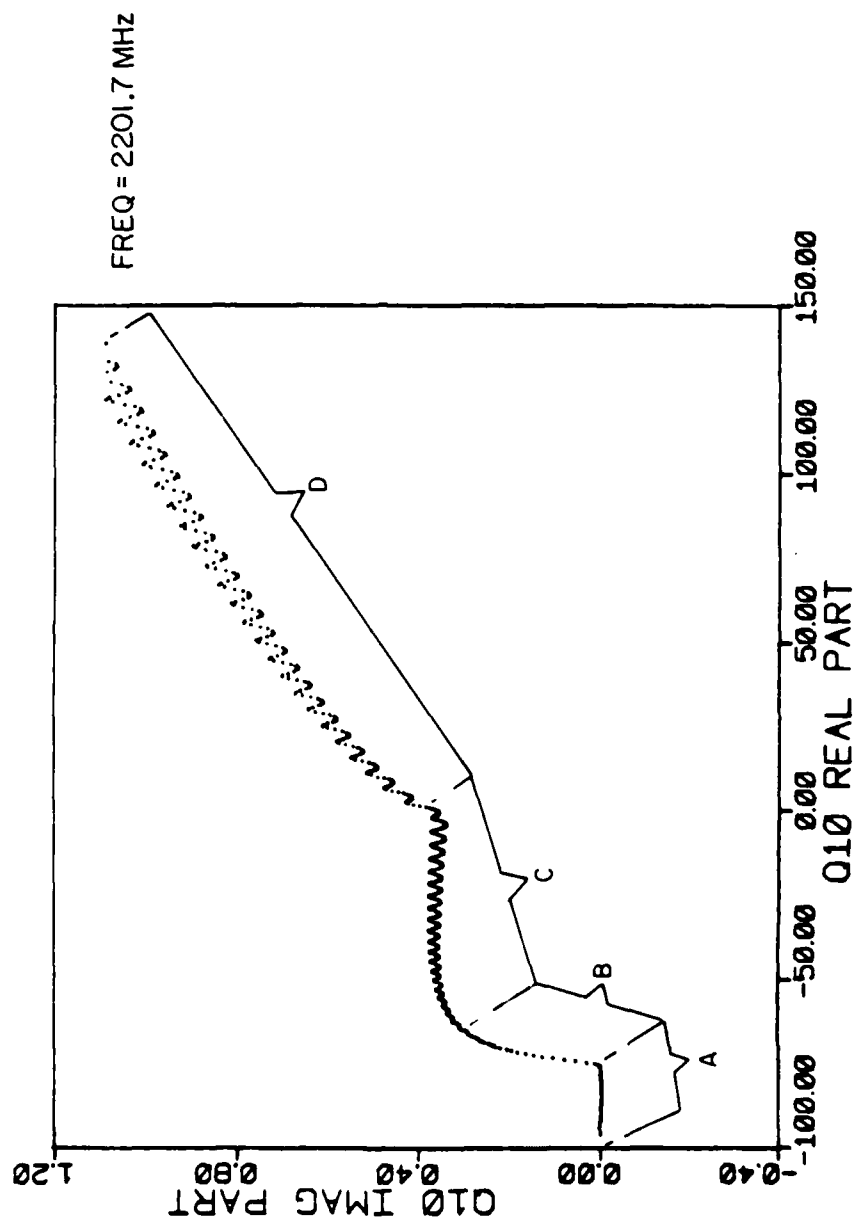
Figure 11. Eigenvalues obtained in q_{10}-space using refractivity profile of Figure 10.

In Figures 11 and 12, the corresponding regions in which the roots lie
are indicated. Thus the roots lying in region A of the q_{10}-plane in Figure 11
correspond to the roots lying in region A of the complex plane shown in
Figure 12. The approximate number of roots in each region are:

Region	No. of roots
A	34
B	35
C	67
D	344

An interesting result in the comparison of the two figures is the large
variation in root-spacing that occurs from region to region in Figure 12.
Thus the 34 roots in region A in Figure 11 are essentially located at a
"point" on the scale of Figure 12. Similarly, the 67 roots in region C in
Figure 11 are all clustered in a relatively small region of Figure 12. The
magnified plot of the roots shown in Figure 13 (corresponding to Figure 12),
demonstrates this to be true. The reason for this behavior is that the
abscissa, $Re(\theta)$, is an entirely different quantity from the ordinate,
attenuation/km. Indeed, had the roots been plotted in a θ-plane in which the
axes were $Re(\theta)$ and $Im(\theta)$, then the behavior would have been appreciably
better. Nevertheless, it is to be noted that this poor behavior was not
observed in similar plots presented in Reference 9. This is probably due to
the difference in mathematical formulation in Reference 9, including
specifications of a "reference height" within the duct (see Section 5).

It is apparent from Equation 89 that, for all the roots of interest, the
corresponding values of ρ_n are very close to the value of k_0, because of the
smallness of the values of θ for the roots in Figure 12.
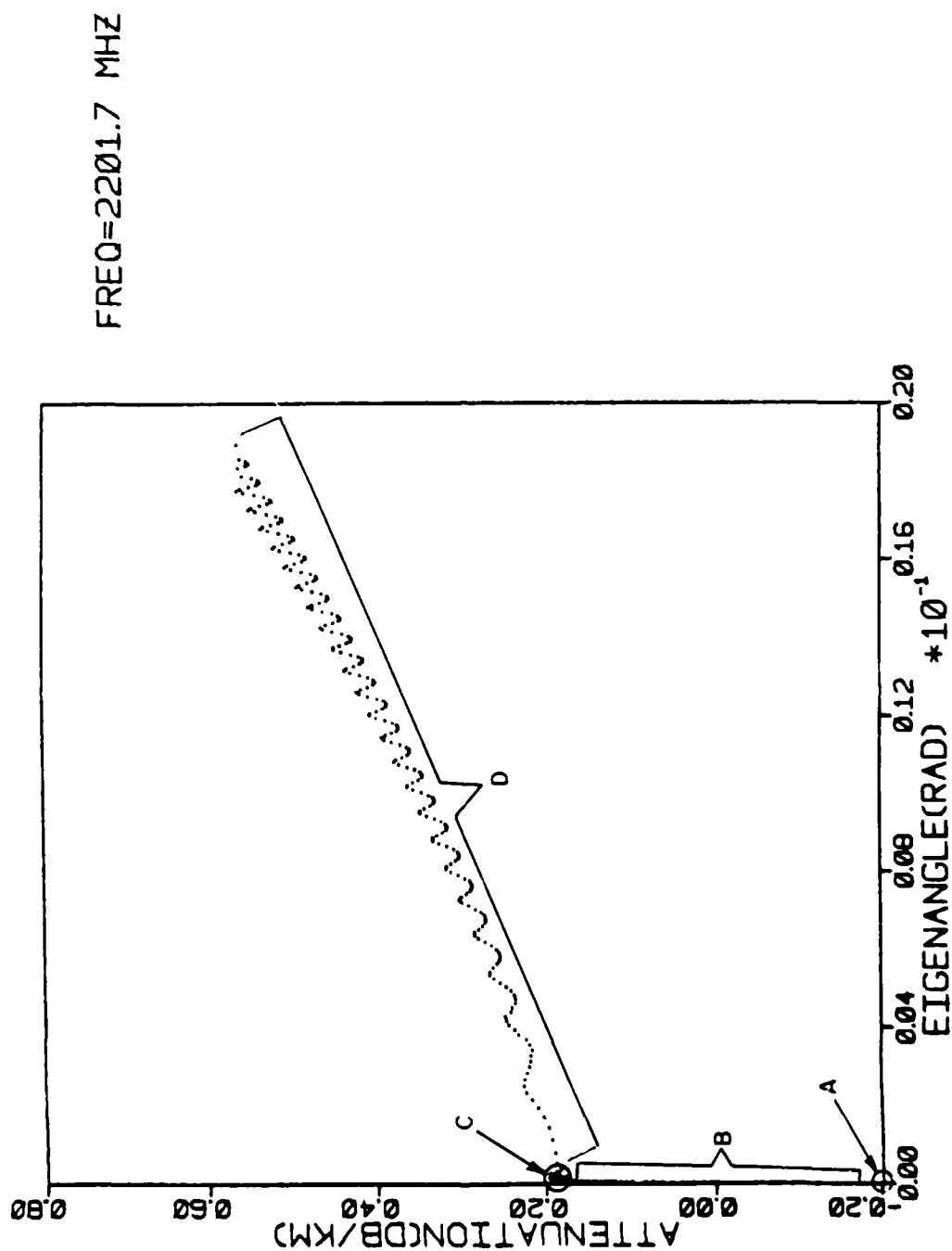
Figure 12.   Eigenvalues obtained in θ-space using refractivity profile of Figure 10.
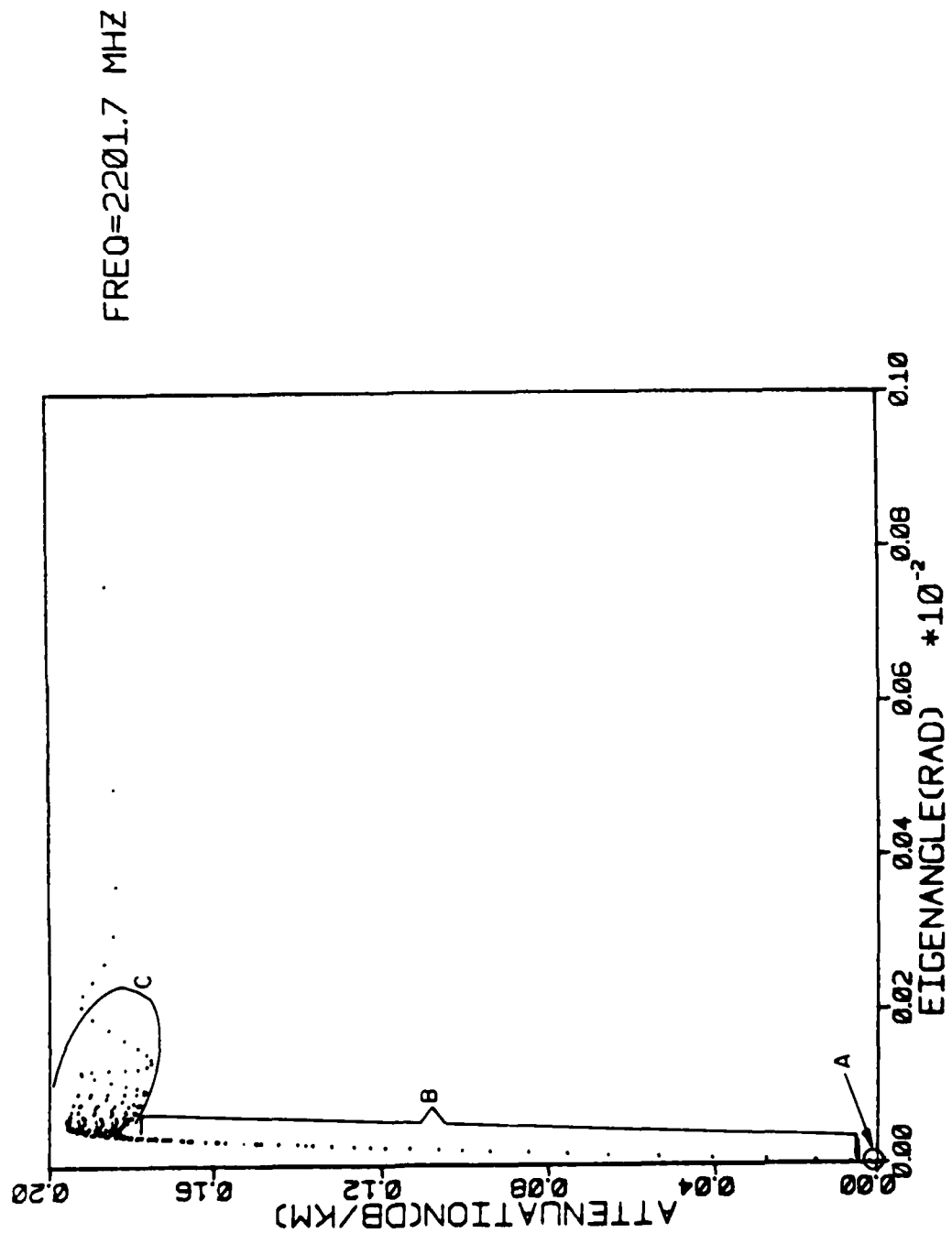
Figure 13. Magnification of a subregion of the eigenvalues shown in Figure 12.

NORMALIZATION OF REFRACTIVITY PROFILE

It will now be shown that the roots $q_{10}^{(n)}$ obtained for a given refractivity profile $M(z)$ are identical to the roots that would be obtained for a profile with the same refractivity gradients, but normalized so that $M(0) = 0$. That is, the roots would be the same for the two refractivity profiles shown in Figure 14.

Using Equation 7, let the unnormalized modified refractivity be given by:

$$2\,M_i(z) \cdot 10^{-6} = (z - H_i)\tan\alpha_i, \quad 1 \leqslant i \leqslant L \tag{149}$$

Then a modified refractivity profile $\overline{M}_i(z)$ with the same gradients (characterized by $\tan\alpha_i$) would be given by:

$$2\,\overline{M}_i(z) \cdot 10^{-6} = (z - \overline{H}_i)\tan\alpha_i, \quad 1 \leqslant i \leqslant L \tag{150}$$

Since it is desired that $\overline{M}_i(z)$ have the value 0 when $z = 0$:

$$\overline{H}_i \equiv 0 \tag{151}$$

Since $M_i(z)$ and $\overline{M}_i(z)$ have the same gradients, the difference Δ between $2M_i(z) \times 10^{-6}$ and $\overline{2M}_i(z) \times 10^{-6}$ at each value of z will be constant. Thus:

$$\frac{\Delta}{2 \times 10^{-6}} = M_i(z) - \overline{M}_i(z) = \text{const} = M_i(0) - \overline{M}_i(0) = M_1(0)\,\frac{H_i\,\tan\alpha_1}{2 \times 10^{-6}} \tag{152}$$
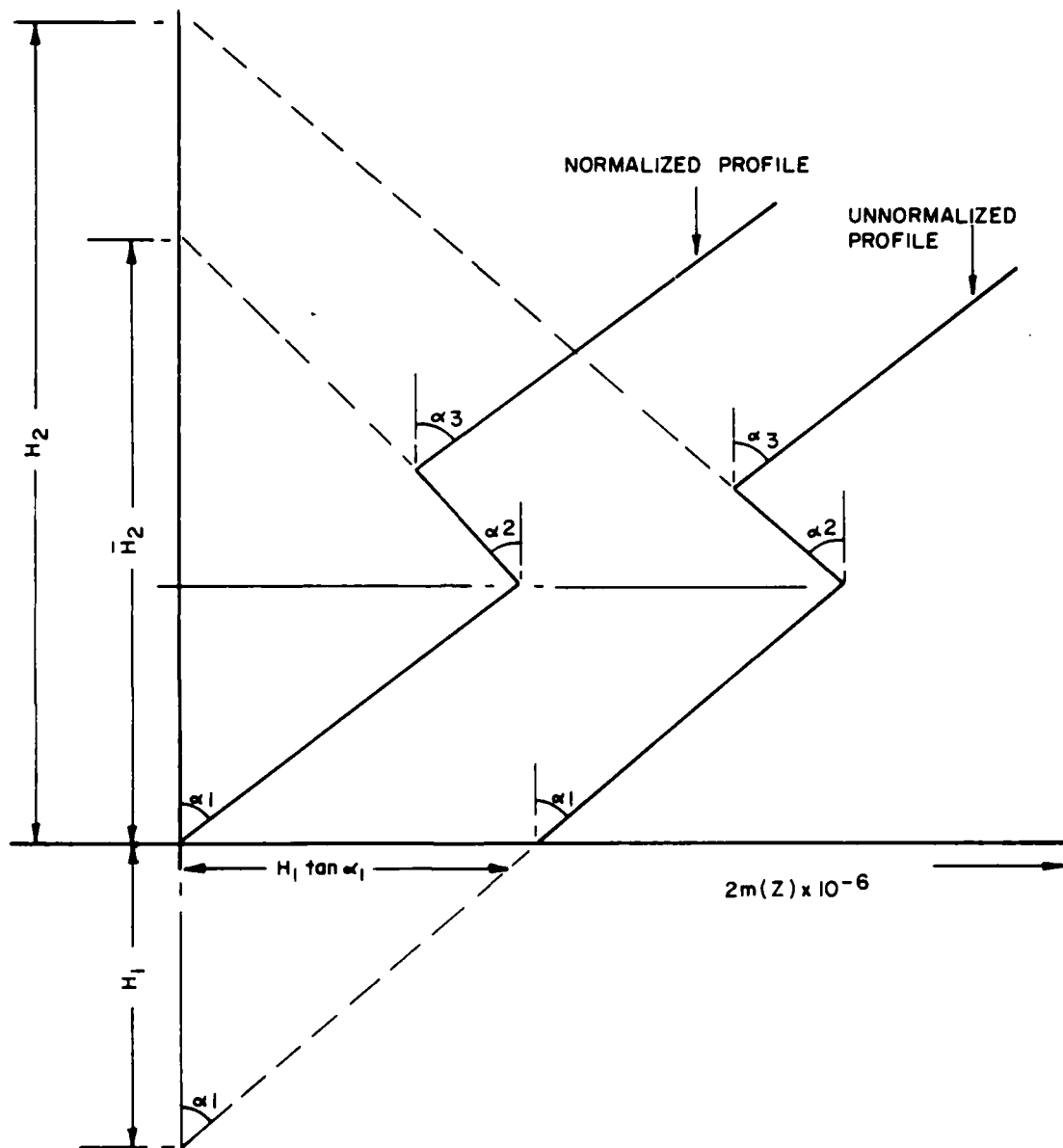
Figure 14.   Illustration of an unnormalized and a corresponding normalized
             refractivity profile.

or, using Equations 149 and 150 in Equation 152,

$$(Z - H_i) \tan \alpha_i - (Z - \overline{H}_i) \tan \alpha_i = - H_1 \tan \alpha_1$$

or

$$H_1 \tan \alpha_1 - H_i \tan \alpha_i = - \overline{H}_i \tan \alpha_i \tag{153}$$

Now the eigenvalues of the modal determinant for the refractivity profile $M_i(z)$ will be the same as the eigenvalues of the modal determinant for the refractivity profile $\overline{M}_i(z)$ if the q_{ij}, $1 \le i \le L$, $j = i-1,i$ are the same for each profile. For the profile $M_i(z)$ given by Equation 149, the values of q_{ij} will be given by Equations 95 to 97, with Equation 97 representing the dependence of q_{ij} on the H_i as:

$$s_{ij} = \left(\frac{k_0}{|\tan \alpha_i|} \right)^{2/3} [H_1 \tan \alpha_1 - H_i \tan \alpha_i + z_j \tan \alpha_i] \tag{154}$$

For the profile $\overline{M}_i(z)$ given by Equations 150 and 151, the values of q_{ij} will be given by Equation 95 to 97 but with:

$$s_{ij} = \left(\frac{k_0}{|\tan \alpha_i|} \right)^{2/3} [- \overline{H}_i \tan \alpha_i + z_j \tan \alpha_i] \tag{155}$$

But from Equation 153, the value of s_{ij} in Equation 155 is the same as the value of s_{ij} in Equation 154. Therefore, the values of q_{ij} are the same for the two profiles, and thus the values of q_{10} are also the same.

It is emphasized here that the fact that the values of $q_{10}^{(n)}$ are the same for the normalized and unnormalized profiles does _not_ imply that the fields obtained in Equations 67 for the two profiles would be the same. In

general, these fields would not be the same for the two profiles since, although the $q_{10}^{(n)}$ are the same, the ρ_n are not. The ρ_n affect the value of $e^{-j\rho_n r}$ and λ_n in Equations 67.

SECTION 4

NUMERICAL DETERMINATION OF THE FIELDS

RELATIVE FIELDS IN TERMS OF $q_{10}{}^{(n)}$

Once the zeroes of the modal determinant of the problem are found, the electric field magnitude relative to free space due to a transmitter at height z_T may be determined from Equation 67a at a height z_R and distance r from the transmitter. Thus

$$A = \beta_0 \; \sum_n \; \lambda_n \; E_n \, e^{-j\rho_n r} \tag{156}$$

where, from Equations 57, 58 and 66:

$$\beta_0 = 2 \sqrt{2\pi r} \tag{157}$$

$$\lambda_n(\rho_n) = \frac{\sqrt{\rho_n}}{\left(\dfrac{\partial |\alpha|}{\partial \rho}\right)_{\rho \, = \, \rho_n}} \tag{158}$$

$$E_n(\rho_n, \, z_r, \, z_T) = \left[|T_{AR}(q_T)| k_1(q_R) + |T_{BR}(q_T)| k_2(q_R) \right]_{q_{10} \, = \, q_{10}{}^{(n)}} \tag{159}$$

In Equation 156, ρ_n is obtained from the eigenvalue $q_{10}{}^{(n)}$ through Equation 94:

$$\rho_n = k_0 \sqrt{1 - H_1 \tan \alpha_1 - \frac{q_{10}^{(n)}}{|\tan \alpha_1|^{2/3}}} \qquad (160)$$

Equation 158 may be expressed in terms of $q_{10}^{(n)}$ by writing:

$$\lambda_n = \frac{\sqrt{\rho_n}}{\left[\left(\frac{\partial |\alpha|}{\partial q_{10}} \frac{\partial q_{10}}{\partial \rho} \right) \right]_{\rho = \rho_n, \ q_{10} = q_{10}^{(n)}}}$$

But, from Equation 92,

$$\frac{\partial q_{10}}{\partial \rho} = -\frac{2\rho}{k_0^2} \left(\frac{k_0}{|\tan \alpha_1|} \right)^{2/3}$$

Therefore

$$\lambda_n = -\frac{k_0^2}{2 \sqrt{\rho_n} \left(\frac{k_0}{|\tan \alpha_1|} \right)^{2/3} \left(\frac{\partial |\alpha|}{\partial q_{10}} \right)_{q_{10} = q_{10}^{(n)}}} \qquad (161)$$

The value of ρ_n in Equation 161 may be obtained from Equation 160 and the value of $\partial |\alpha| / \partial q_{10}$ may be obtained using the method discussed by Equations 137 to 148.

The factors λ_n, E_n and $\exp(-j\rho_n r)$ in Equation 156 are evaluated using the exponential representation illustrated in Equation 126, and the product of these factors is evaluated using Equations 127 to 129.

Referring to Equation 159, the q_R are defined using Equations 95 to 97 by:

$$q_R = q_{10} t_R + S_R$$
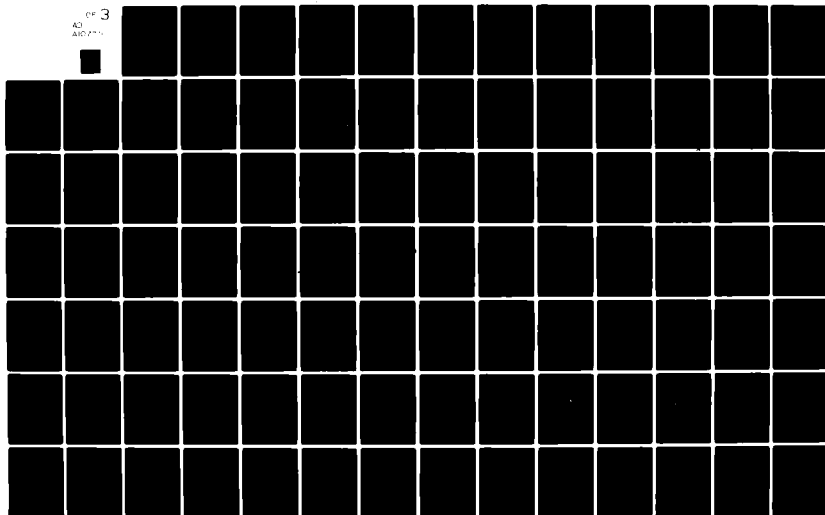
where

$$t_R = \left(\frac{|\tan \alpha_1|}{|\tan \alpha_R|} \right)^{2/3} \tag{163}$$

and

$$S_R = \left(\frac{k_0}{|\tan \alpha_R|} \right)^{2/3} \left[H_1 \tan \alpha_1 - H_R \tan \alpha_R + z_R \tan \alpha_R \right] \tag{164}$$

where z_R is the height of the receiver located in region R. If the transmitter is at a height z_T which is located in region T, then q_T is given by Equations 162 to 164 with R replaced by T. The values of q_R and q_T used in Equation 159 are those for which $q_{10} = q_{10}^{(n)}$ in Equation 162.

DEFINITIONS OF THE MATRICES T_{AR} AND T_{BR}

Equation 159 requires the values of the determinants $|T_{AR}|$ and $|T_{BR}|$. The matrices T_{AR} and T_{BR} will first be considered. These were discussed briefly following Equation 47. For clarity, they will be redefined here using the K_i solutions rather than the h_i solutions.

81

The modal matrix for a three-layer atmosphere is given by (see Equation 136):

$$\alpha = \begin{pmatrix} \hat{K}_1(q_{10}) & \hat{K}_1(q_{10}) & 0 & 0 & 0 \\ K_1(q_{11}) & K_2(q_{11}) & -K_1(q_{21}) & -K_2(q_{21}) & 0 \\ K_1'(q_{11}) & K_2'(q_{11}) & -\dfrac{q_2'}{q_1'} K_1'(q_{21}) & -\dfrac{q_2'}{q_1'} K_2'(q_{21}) & 0 \\ 0 & 0 & K_1(q_{22}) & K_2(q_{22}) & -K_2(q_{32}) \\ 0 & 0 & K_1'(q_{22}) & K_2'(q_{22}) & -\dfrac{q_3'}{q_2'} K_2'(q_{32}) \end{pmatrix}$$

$$(165)$$

where, as in Equation 136a,

$$\hat{K}_m(q_{10}) = K_m'(q_{10}) - G\, K_m(q_{10}), \quad m = 1, 2 \tag{166}$$

As in Equation 46, a vector β_T is defined which represents the contribution to the boundary conditions of the particular solution of the inhomogeneous differential Equation 18. The subscript T indicates the region in which the transmitter is located $(1 \le T \le L)$. For the example of $L = 3$,

$$\beta_1 = \begin{pmatrix} \beta_{11} \\ \beta_{12} \\ \beta_{13} \\ 0 \\ 0 \end{pmatrix} \tag{167}$$

$$\beta_2 = \begin{pmatrix} 0 \\ \beta_{21} \\ \beta_{22} \\ \beta_{23} \\ \beta_{24} \end{pmatrix} \tag{168}$$

82

$$\beta_3 = \begin{pmatrix} 0 \\ 0 \\ 0 \\ \beta_{31} \\ \beta_{32} \end{pmatrix} \tag{169}$$

The values of the β_{Tm} will be given below. Thus, when the transmitter is in region 1, Equation 167 is used; when the transmitter is in region 2, Equation 168 is used; and when the transmitter is in region 3, Equation 169 is used.

The matrix T_{AR} is constructed by replacing the first column of the Rth pair of columns of α by the vector β_T, $1 \le R \le L-1$, and the matrix T_{BR} is constructed by replacing the second column of the Rth pair of columns of α by β_T, $1 \le R \le L-1$. The matrix T_{AL} is not considered as explained following Equation 47. The matrix T_{BL} is constructed by replacing the last column of α by the vector β_T.

Thus, T_{A1} is formed by replacing the first column of α by β_T; and T_{A2} is formed by replacing the third column of α by β_T. T_{B1} is formed by replacing the second column of α by β_T; T_{B2} is formed by replacing the fourth column of α by β_T; and T_{B3} is formed by replacing the fifth column of α by β_T.

A discussion of the elements of the β_T vector follows. The elements of β_T for $T = 1$ were given in Equation 46 using the solutions in terms of the h_i.

Suppose the solution of the inhomogeneous differential equation in region 1 were given in terms of Equation 84:

$$\widetilde{\Pi}_1 = R_1 \ K_1(q_{1<}) \ K_2(q_{1>}) \tag{170}$$

where $q_{1<}$ and $q_{1>}$ are defined following Equation 36. Then the elements of β_1 may be given in terms of the K_i solutions as:

$$\beta_{11} = - \ R_1 \ K_2(q_{1T}) \hat{K}_1(q_{10})$$

$$\beta_{12} = - \ R_1 \ K_1(q_{1T}) K_2(q_{11}) \tag{171}$$

$$\beta_{13} = - \ R_1 \ K_1(q_{1T}) K_2'(q_{11})$$

where the β_{1m} refer to the corresponding elements in the vector of Equations 167. If the solution were given by Equation 85:

$$\widetilde{\Pi}_1 = - \ R_1 \ K_1(q_{1>}) K_2(q_{1<}) \tag{172}$$

then the following set of values of the β_{1m} would be valid:

$$\beta_{11} = R_1 \ K_1(q_{1T}) \hat{K}_2(q_{10})$$

$$\beta_{12} = R_1 \ K_2(q_{1T}) K_1(q_{11}) \tag{173}$$

$$\beta_{13} = R_1 \ K_2(q_{1T}) K_1'(q_{11})$$

In an entirely similar manner, if the solution in region 2 is given by:

$$\widetilde{\Pi}_2 = R_2 \, K_1(q_{2<})K_2(q_{2>}) \tag{174}$$

then the elements of β_2 are:

$$\beta_{21} = R_2 \, K_2(q_{2T})K_1(q_{21})$$

$$\beta_{22} = R_2 \, \frac{q_2'}{q_1'} \, K_2(q_{2T})K_1'(q_{21})$$

$$\beta_{23} = - \, R_2 \, K_1(q_{2T})K_2(q_{22})$$

$$\beta_{24} = - \, R_2 \, K_1(q_{2T})K_2'(q_{22}) \tag{175}$$

and if the solution is given by:

$$\widetilde{\Pi}_2 = -R_2 \, K_1(q_{2>})K_2(q_{2<}) \tag{176}$$

then

$$\beta_{21} = - \, R_2 \, K_1(q_{2T})K_2(q_{21})$$

$$\beta_{22} = - \, R_2 \, \frac{q_2'}{q_1'} \, K_1(q_{2T})K_2'(q_{21})$$

$$\beta_{23} = R_2 \, K_2(q_{2T})K_1(q_{22})$$

$$\beta_{24} = R_2 \, K_2(q_{2T})K_1'(q_{22}) \tag{177}$$

In region 3, if the solution is given by:

$$\widetilde{\Pi}_3 = R_3 \, K_1(q_{3<})K_2(q_{3>}) \tag{178}$$

85

then the elements of β_3 are:

$$\beta_{31} = R_3 \ K_2(q_{3T})K_1(q_{32})$$

$$\beta_{32} = R_3 \ \frac{q_3'}{q_2'} \ K_2(q_{3T})K_1'(q_{32})$$

(179)

and if the solution is given by:

$$\tilde{\Pi}_3 = - R_3 \ K_1(q_{3>})K_2(q_{3<})$$

(180)

the elements of β_3 are:

$$\beta_{31} = - R_3 \ K_1(q_{35})K_2(q_{32})$$

$$\beta_{32} = - R_3 \ \frac{q_3'}{q_2'} \ K_1(q_{35})K_2'(q_{32})$$

(181)

In region 3, the solution $\tilde{\Pi}_3$ must satisfy the radiation condition, thus precluding the use of Equations 180 and 181. In region 3, therefore, β_3 will be defined using Equation 179.

Theoretically, either Equations 171 or 173 may be used to define β_1; and either Equations 175 or 177 may be used to define β_2. Numerically, however, there is often a strong preference as to which expression for β_1 and β_2 to choose. The basis of the choice will be somewhat similar to the basis used to choose Equation 179 instead of Equation 181 to define the vector β_3 in region 3. Just as in region 3 the form of the solution is used which "best satisfies" the boundary and radiation conditions, so too the form of the solution which most closely characterizes the field in each respective region will be used. Heuristically, the general solution will have to "work harder" to satisfy the boundary conditions when the particular solution is farther from the exact solution. Conversely, the general solution will be more numerically correct if the particular solution more closely characterizes the field in the region of interest.

To determine which solution best characterizes the field in a given region, the following general information will be used, and verified in Section 7. In a duct environment,

1. The only instance in which the field in region T could be much less at the upper boundary of the region than at the height at which the transmitter is located, is when $\tan \alpha_T < 0$, $T > 1$ and the field will be that due to the "trapped modes" (see Section 6).

2. "Trapped modes are those for which the eigenvalues $q_{10}^{(n)}$ lie near the negative real axis, which implies from Equations 162 through 164 that $q_{T<}^{(n)}$ and $q_{T>}^{(n)}$ will lie near the real axis.

From Equations 162 through 164:

$$\text{Re}(q_{T<}) < \text{Re}(q_{T>}) \text{ when } \tan \alpha_T > 0 \qquad (182)$$

$$\text{Re}(q_{T<}) > \text{Re}(q_{T>}) \text{ when } \tan \alpha_T < 0 \qquad (183)$$

When $\text{Re}(q_{10}) << 0$, it may be seen from APPENDIX A and Equations 182 and 183 that:

$$\left| K_1(q_{T<}) \right| > \left| K_1(q_{T>}) \right|, \tan \alpha_T > 0 \text{ when } \left| K_1(q_{T<}) \right| >> 1 \qquad (184)$$

$$\left| K_1(q_{T>}) \right| > \left| K_1(q_{T<}) \right|, \tan \alpha_T < 0 \text{ when } \left| K_1(q_{T>}) \right| >> 1 \qquad (185)$$

when

$$|K_2(q_{T<})| \sim |K_2(q_{T>})| \sim 1 \tag{186}$$

From Equations 184 to 186, for $\tan \alpha_T > 0$, it may be concluded that the field in region T due to trapped modes will not be appreciably less at the upper boundary of the region than at any point within the region when the solution in that region is given by:

$$\tilde{\Pi}_T \sim K_1(q_{T>})K_1(q_{T<}), \quad \tan \alpha_T > 0 \tag{187}$$

For $\tan \alpha_T < 0$, the field may be appreciably less at the upper boundary of region T than at any other point within the region when the solution in that region is given by:

$$\tilde{\Pi}_T \sim K_1(q_{T>})K_2(q_{T<}), \quad \tan \alpha_T < 0 \tag{188}$$

Therefore, from item (1), the particular solution of the differential equation will be given by:

$$\tilde{\Pi}_T = R_T \cdot \begin{cases} K_1(q_{T<})K_2(q_{T>}), & \tan \alpha_T > 0 \text{ or } T = 1 & \tag{189a} \\ \\ - K_1(q_{T>})K_2(q_{T<}), & \tan \alpha_T < 0 \text{ and } T \neq 1 & \tag{189b} \end{cases}$$

The values of the elements in the vector β_T will be determined based on whether the solution is given by Equation 189a or by Equation 189b. Thus, the elements of β_1 will always be given by Equation 171. The elements of β_2 will be given by Equation 175 if $\tan \alpha_2 > 0$ and by Equation 177 when $\tan \alpha_2 < 0$.

All evaluations of the $|T_{AR}|$ and $|T_{BR}|$, as well as of E_n in Equation 159, are carried out using exponential representation.

EVALUATION OF THE DETERMINANTS $|T_{AR}|$ AND $|T_{BR}|$

The form of the matrices T_{AR} and T_{BR} (i.e., the locations of their zero elements) depends on the value of R and the value of T. The value of T would affect whether β is given by Equation 167, 168 or 169. The value of R would affect the column of α (Equation 165) which the vector β replaces to form T_{AR} or T_{BR}.

It is clear from the three-layer example used in Equations 165, 167, 168 and 169 that, if R = T, the zero elements of T_{AR} and T_{BR} are in the same location as the zero elements of α. The same algorithm used to evaluate $|\alpha|$ (see APPENDIX B) will then also be applicable to the evaluation of $|T_{AR}|$ and $|T_{BR}|$.

To demonstrate the general evaluation procedure when R ≠ T, only a single example will be used, with the application to other cases being straightforward. For this example, T = 1, R = 2 will be used, and the determinant $|T_{A2}|$ will be evaluated. In this case, the matrix T_{A2} will have the form:

$$
T_{A2} = \begin{pmatrix}
\hat{K}_1(q_{10}) & \hat{K}_1(q_{10}) & \beta_{11} & 0 & 0 \\
K_1(q_{11}) & K_1(q_{11}) & \beta_{12} & -K_2(q_{21}) & 0 \\
K_1'(q_{11}) & K_2'(q_{11}) & \beta_{13} & -\dfrac{q_2'}{q_1'} K_2'(q_{21}) & 0 \\
0 & 0 & 0 & K_2(q_{22}) & -K_2(q_{32}) \\
0 & 0 & 0 & K_2'(q_{22}) & -\dfrac{q_3'}{q_2'} K_2'(q_{32})
\end{pmatrix}
$$

$$(190)$$

Now comparing T_{A2} with α, it is seen that T_{A2} has non-zero elements in the same locations as the non-zero elements of α, except T_{A2} has the element β_{11} at a position in which the matrix α has a zero. But from the definition of a determinant in terms of a cofactor expansion, it may be shown that:

$$
|T_{A2}| = |T_{A2}|_{\beta_{11} = 0} + |T_{A2}|_{\beta_{12} = \beta_{13} = 0}
\tag{191}
$$

Now $|T_{A2}|_{\beta_{11} = 0}$ has non-zero elements in the same locations as the non-zero elements of $|\alpha|$, and may therefore be evaluated using the same procedures as those used to evaluate $|\alpha|$ (APPENDIX B). The second term on the right side of Equation 191 may be written as the product of β_{11} and its cofactor:

$$
|T_{A2}|_{\beta_{12} = \beta_{13} = 0} = \beta_{11} |M(\beta_{11})|
\tag{192}
$$

where $M(\beta_{11})$ indicates the matrix which is the minor of β_{11}, and is given by:

90

$$
M(\beta_{11}) = \begin{pmatrix}
K_1(q_{11}) & K_2(q_{11}) & -K_2(q_{21}) & 0 \\[2ex]
K_1'(q_{11}) & K_2'(q_{11}) & -\dfrac{q_2'}{q_1'} K_2'(q_{21}) & 0 \\[2ex]
0 & 0 & K_2(q_{22}) & -K_2(q_{32}) \\[2ex]
0 & 0 & K_2'(q_{22}) & -\dfrac{q_3'}{q_2'} K_2'(q_{32})
\end{pmatrix} \qquad (193)
$$

The determinant of $M(\beta_{11})$ (also called the cofactor of β_{11}) is just the product of the determinants of the upper left 2-by-2 matrix and the lower right 2-by-2 matrix:

$$
|M(\beta_{11})| = \begin{vmatrix}
K_1(q_{11}) & K_2(q_{11}) \\[2ex]
K_1'(q_{11}) & K_2'(q_{11})
\end{vmatrix} \times \begin{vmatrix}
K_2(q_{22}) & -K_2(q_{32}) \\[2ex]
K_2'(q_{22}) & -\dfrac{q_3'}{q_2'} K_2'(q_{32})
\end{vmatrix} \qquad (194)
$$

The evaluation of the determinants on the right side of Equation 194 is straightforward. However, the first determinant may be identified as tne Wronskian given in Equation 83, so that this determinant need not be numerically calculated.

Substituting Equation 194 into Equation 192, the result may be used in Equation 191 to evaluate $|T_{A2}|$.

SECTION 5

VERIFICATION OF CALCULATION METHOD

GENERAL

A method is presented in the previous sections for calculating the fields relative to free space in a duct environment. The method has been programmed in a computer model called DUCT. In this section, the predictions using DUCT are compared with measured fields in an environment containing surface ducts and in an environment containing elevated ducts. In each case, the measured fields are compared with:

(1) the mode sum predictions (Equation 67c) in which the phase of each modal contribution is fully taken into account; and

(2) the power sum predictions (Equation 67d) in which the phase of each modal contribution is assumed to be random.

SURFACE DUCTS

Measurements in an environment containing a surface duct were documented in several references[20,21] (see also Reference 5). The refractivity profile used to calculate the fields is illustrated in Figure 15. It is the same as that used by Pappert and Goodhart as an approximation to the profile observed over the propagation path during the period in which the measurements were made. It is normalized to zero at the ground. In Section 3, it was shown that this normalization does not affect the location of the eigenvalues

---

[20] Pappert, R.A., and Goodhart, C.L., "Case Studies of Beyond-the-Horizon Propagation in Tropospheric Ducting Environments," Radio Science, Vol. 12, No. 1, pp. 75-87, January-February 1977.

[21] Pappert, R.A., and Goodhart, C.L., "A Numerical Study of Tropospheric Ducting at HF," Radio Science, Vol. 14, No. 5, pp. 803-813, September-October 1979.
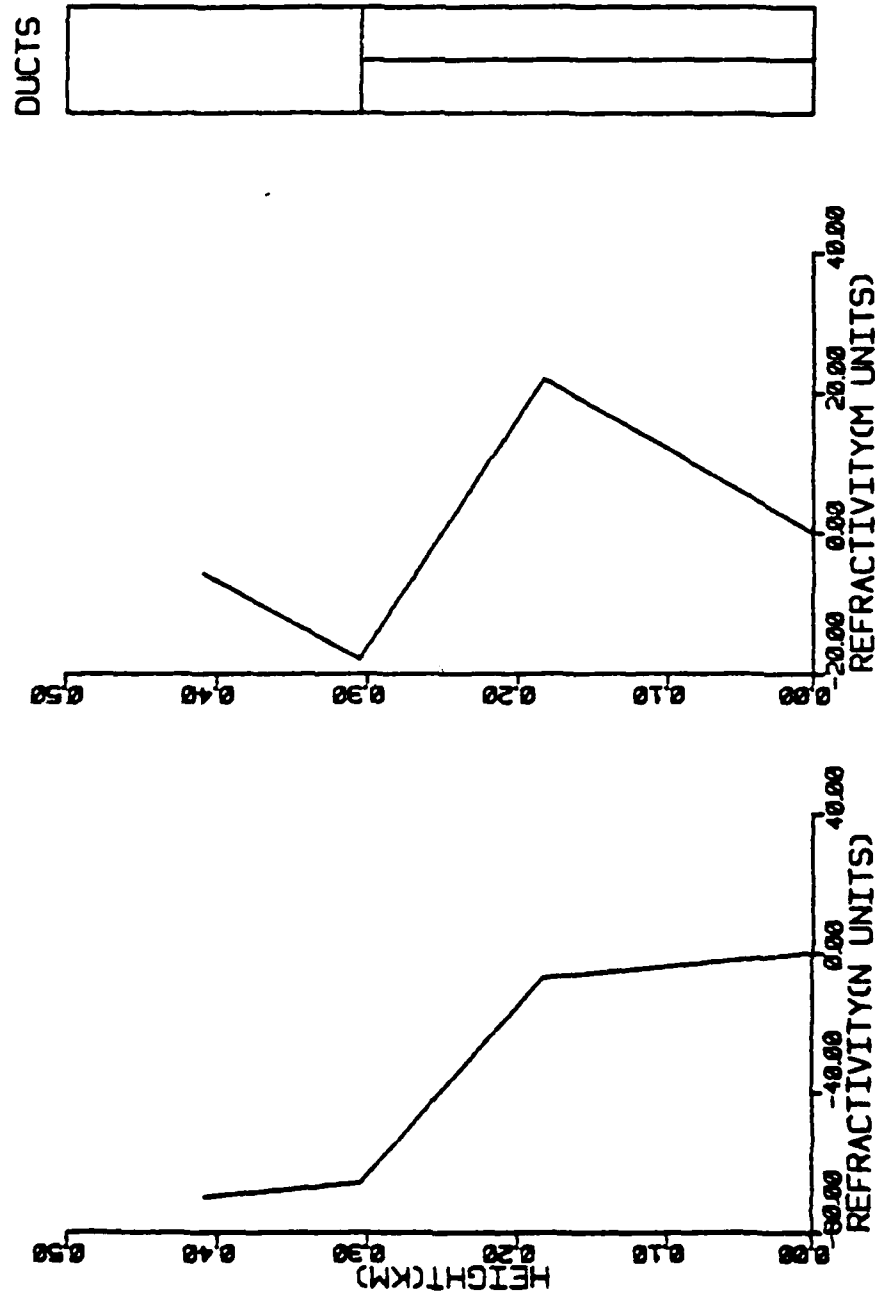
Figure 15.   Refractivity profile producing surface duct for comparison of DUCT predictions with measurements.

94

$q_{10}^{(n)}$, but it might affect the value of the fields. The effect of profile normalization on the calculated field is discussed in Section 7.

Comparison of DUCT predictions and measurements are given at frequencies of 65 MHz, 170 MHz, 520 MHz and 3300 MHz; at distances 111.2 km and 222.4 km; for receiver heights 30.5 m and 152.4 m; and for transmitter heights that varied continuously from the ground to about 500m. Computationally, it is more convenient to set the transmitter heights at 30.5 m and 152.4 m and have the receiver heights vary continuously. It was verified that the computed results using these propagation circuits were identical to those for which the transmitter and receiver locations are reversed, as should be the case from Equation 68.

The comparison of DUCT predictions with mesurements for different parameters are found in Figures 16 to 19. The figures denote the location (height) of the duct by a vertical dashed line and the height of the transmitter by a large asterisk. Also denoted under the heading "normal" is the range of relative fields over the heights shown that would be obtained if the duct were not present. This field is the median field due to troposcatter effects and was taken from Reference 5.

Figures 16 to 19 show an overall excellent agreement between measurements and predictions, particularly since the prediction model is based on idealized assumptions (e.g., lateral homogeneity) that only approximate reality. The predictions are significantly closer to the measured data than they are to the corresponding median troposcatter fields. In Section 7, the divergence of the power-sum solutions from the mode sum solutions for higher frequencies and at higher altitudes is discussed.
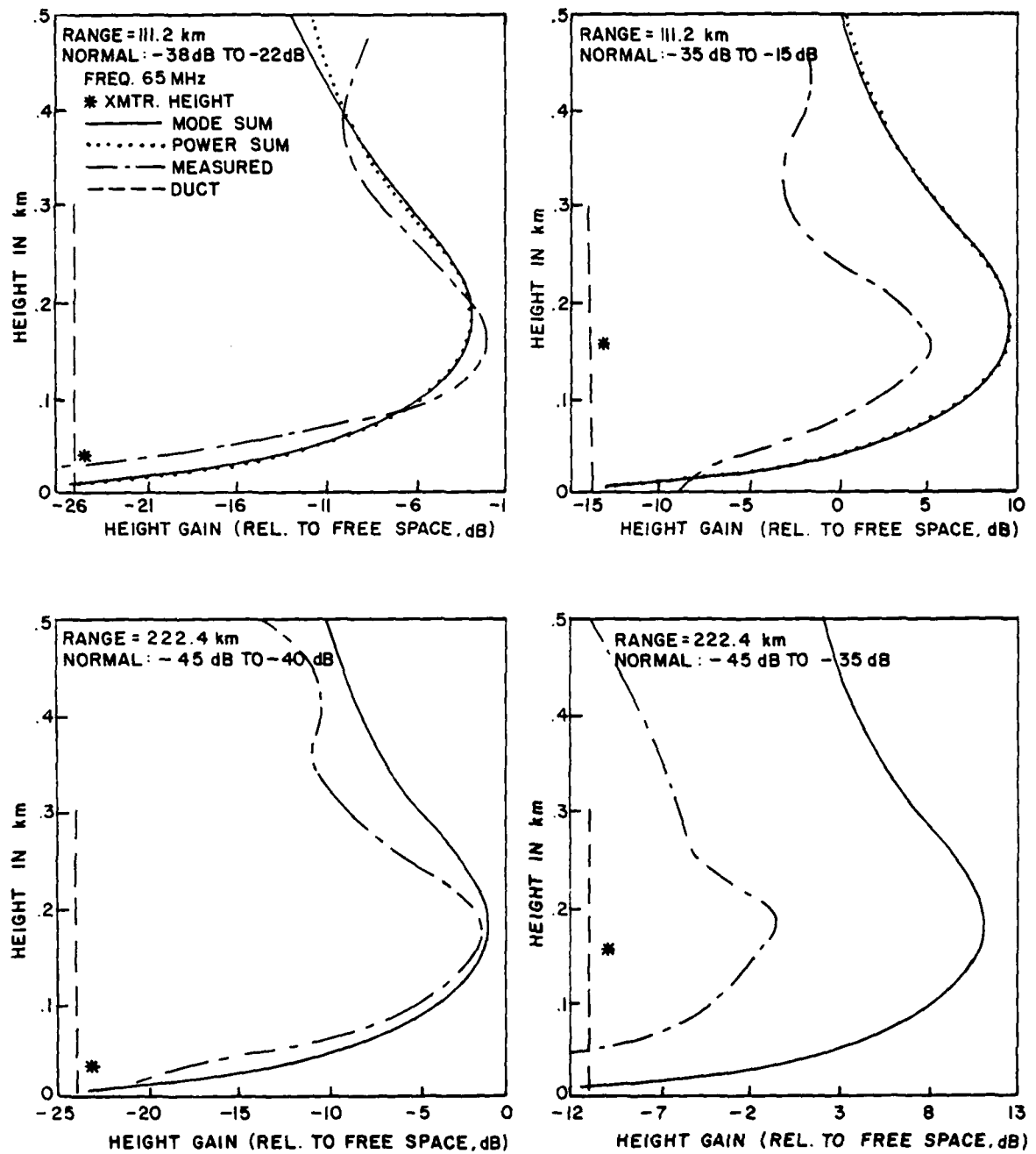
Figure 16.   Comparison of predictions with measurements for surface duct,
              f = 65 MHz.   (Mode sum and power sum predictions are identical
              for the bottom two figures.)

96

Figure 17.   Comparison of predictions with measurements for surface duct,
             f = 170 MHz.

Figure 18.   Comparison of predictions with mesurements for surface duct,
             f = 520 MHz.
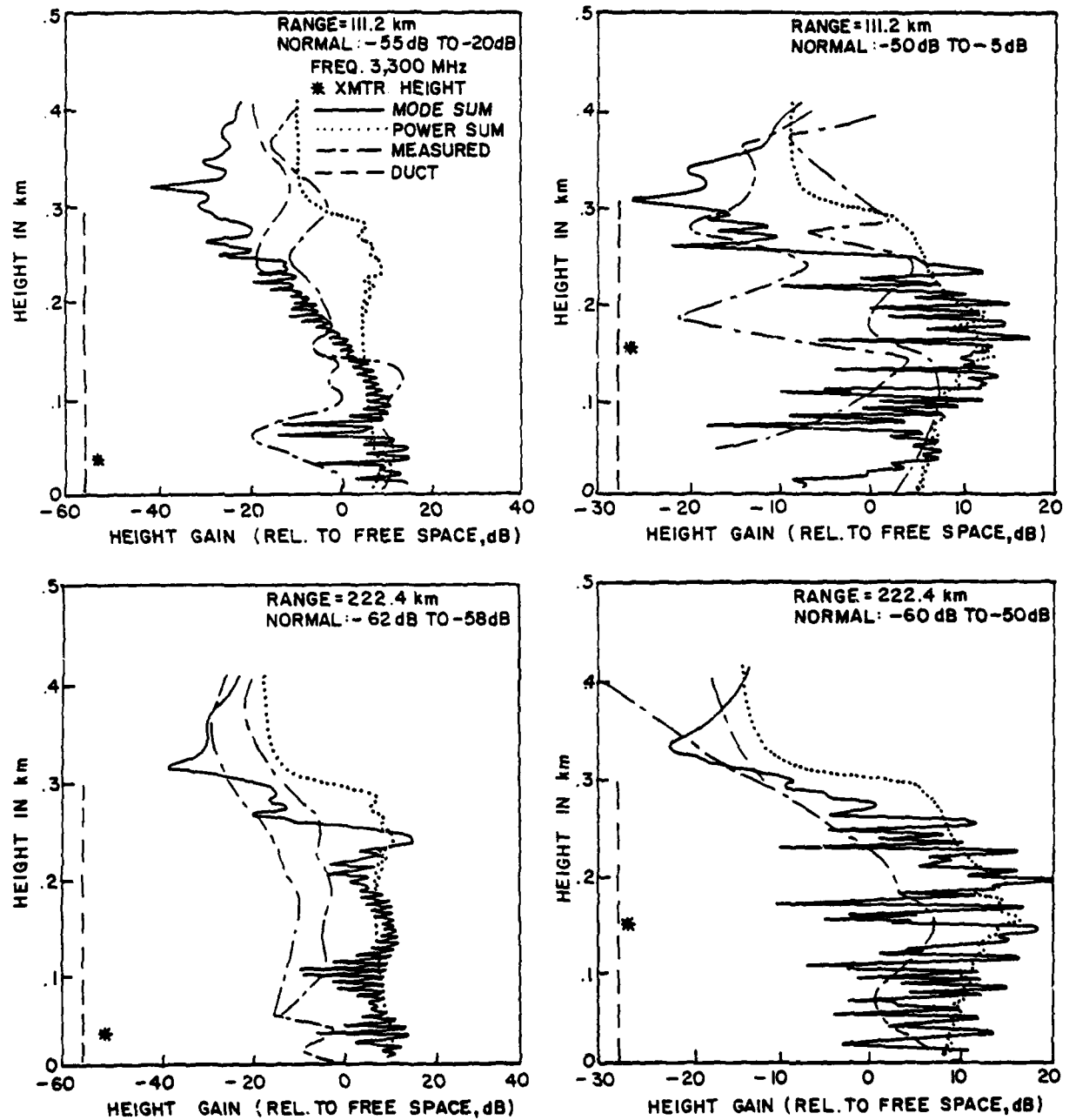
Figure 19. Comparison of predictions with measurements for surface duct,
f = 3300 MHz.

The mode-sum predicted values in Figures 16 to 19 are essentially identical to the predicted values of Pappert and Goodhart (References 5 and 20). The method of Pappert and Goodhart, however, requires specification of a reference height D at which the reflection coefficients of Equation 120 are calculated. They indicate that using their formulation of the problem, their results can be different for different reference heights. In Reference 5, they present two examples in which the predictions using D= 0 are different from those using D = 182.9 m. These are shown in Figure 20 in which they are compared with the results using the DUCT program. In both cases, the DUCT predictions are in agreement with the D = 182.9 m results which Pappert and Goodhart state are preferable to the D = 0 results and which agree with the measurements more closely.

ELEVATED DUCTS

Measurements in an environment containing an elevated duct were documented by Skillman and Woods (Reference 9). They compared their measurements with predictions obtained using the method of Pappert and Goodhart (Reference 5). The refractivity used here to calculate the fields is illustrated in Figure 21. The refractivity is the same as that used by Skillman and Woods as an approximation of the profile observed over the propagation path during the period in which the measurements were made. It is normalized to zero at the ground.

Comparisons of predictions with measurements are given in Figure 22 for f = 449.2 MHz and in Figure 23 for f = 2201.7 MHz. The predictions obtained for the 449.2-MHz case were the same as those obtained by Skillman and Woods. However, Skillman and Woods did not obtain predictions for the 2201.7-MHz case.

The overall agreement between the measurements and predictions shown in Figures 22 and 23 is considered excellent. The divergence of the power sum solution from the mode sum solution in the region above the duct is even more pronounced in these results for an elevated duct than they were for the surface-duct cases considered above. This is discussed further in Section 7.
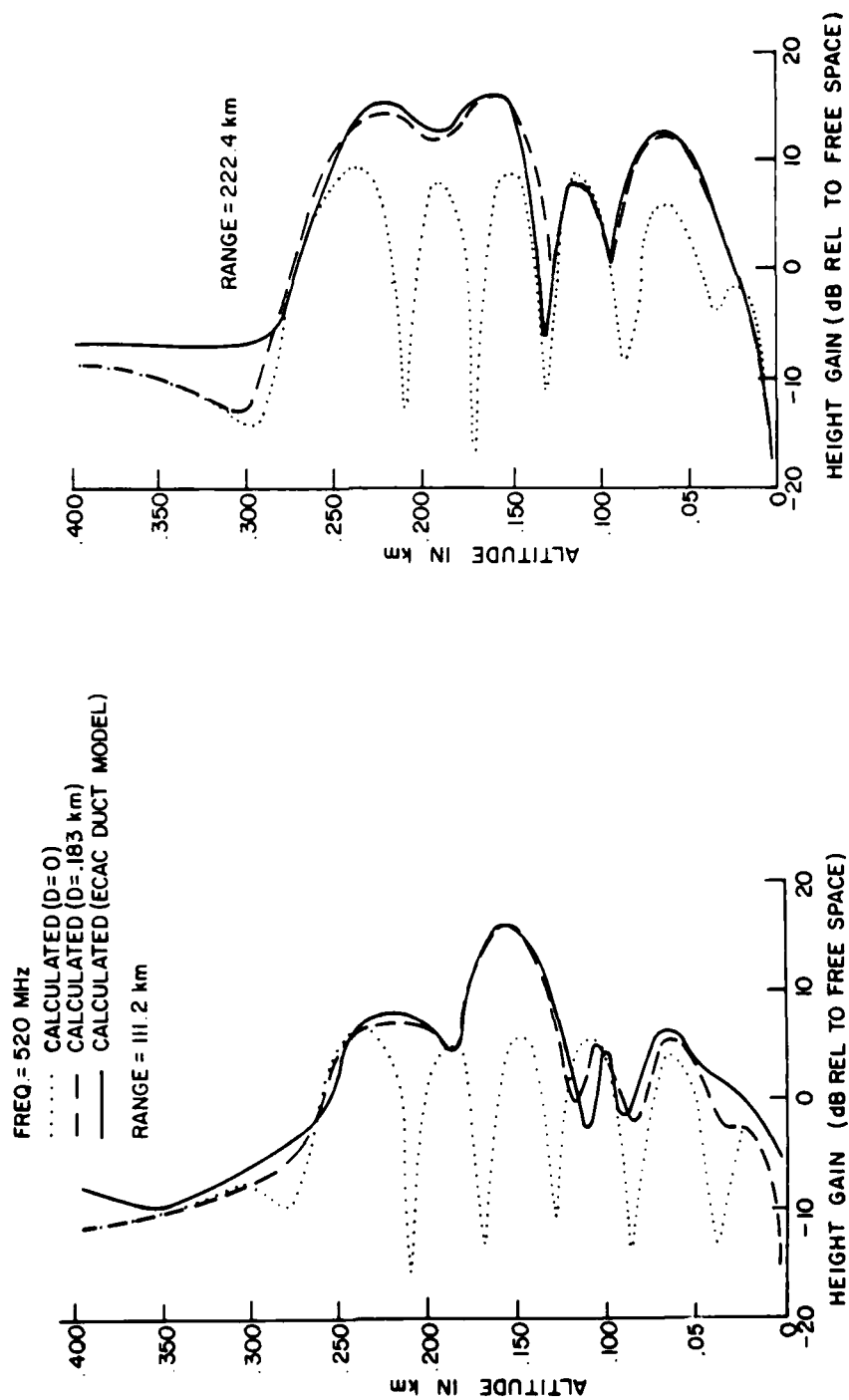
Figure 20. Comparison of NOSC predictions for two reference heights (D) with ECAC predictions, transmitter height = .154 km.
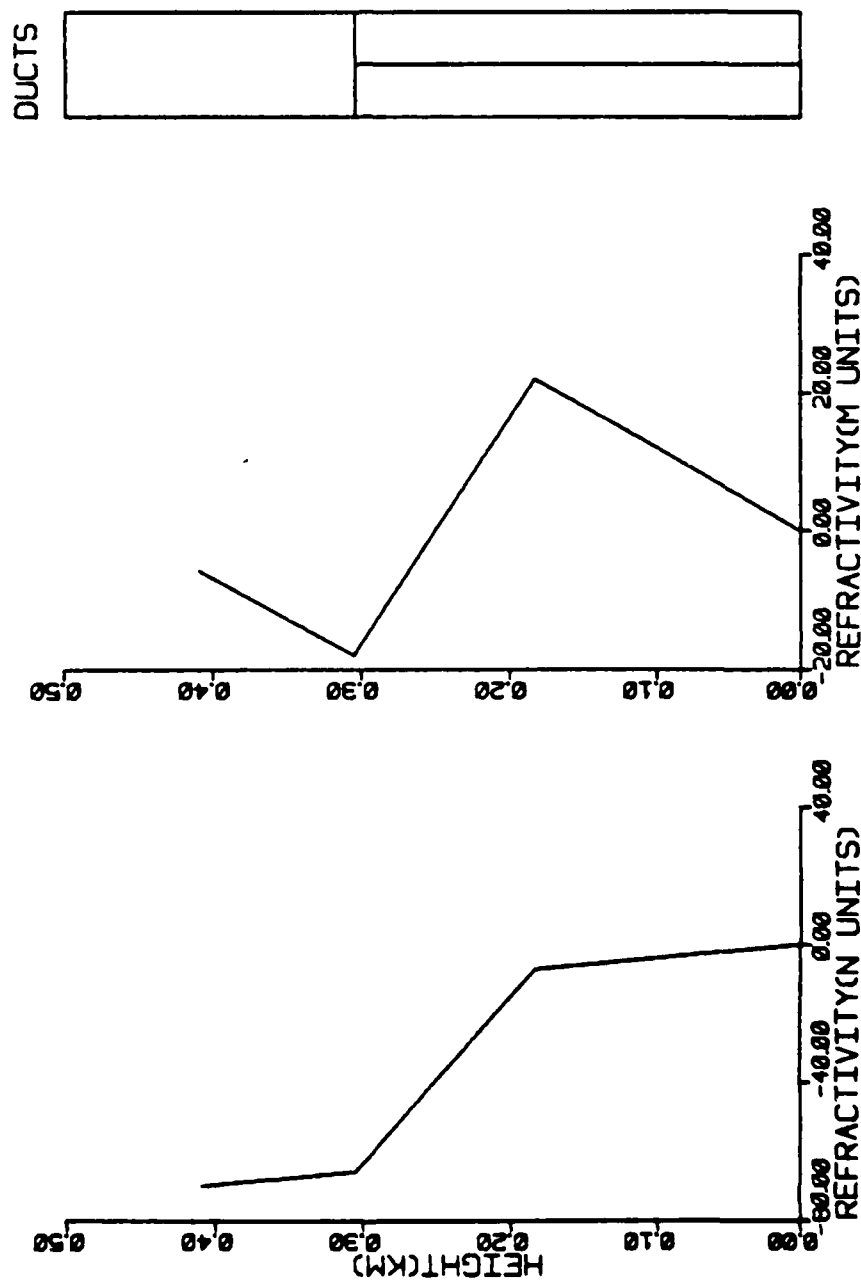
Figure 21. Refractivity profile producing elevated duct for comparison of DUCT predictions with measurements.
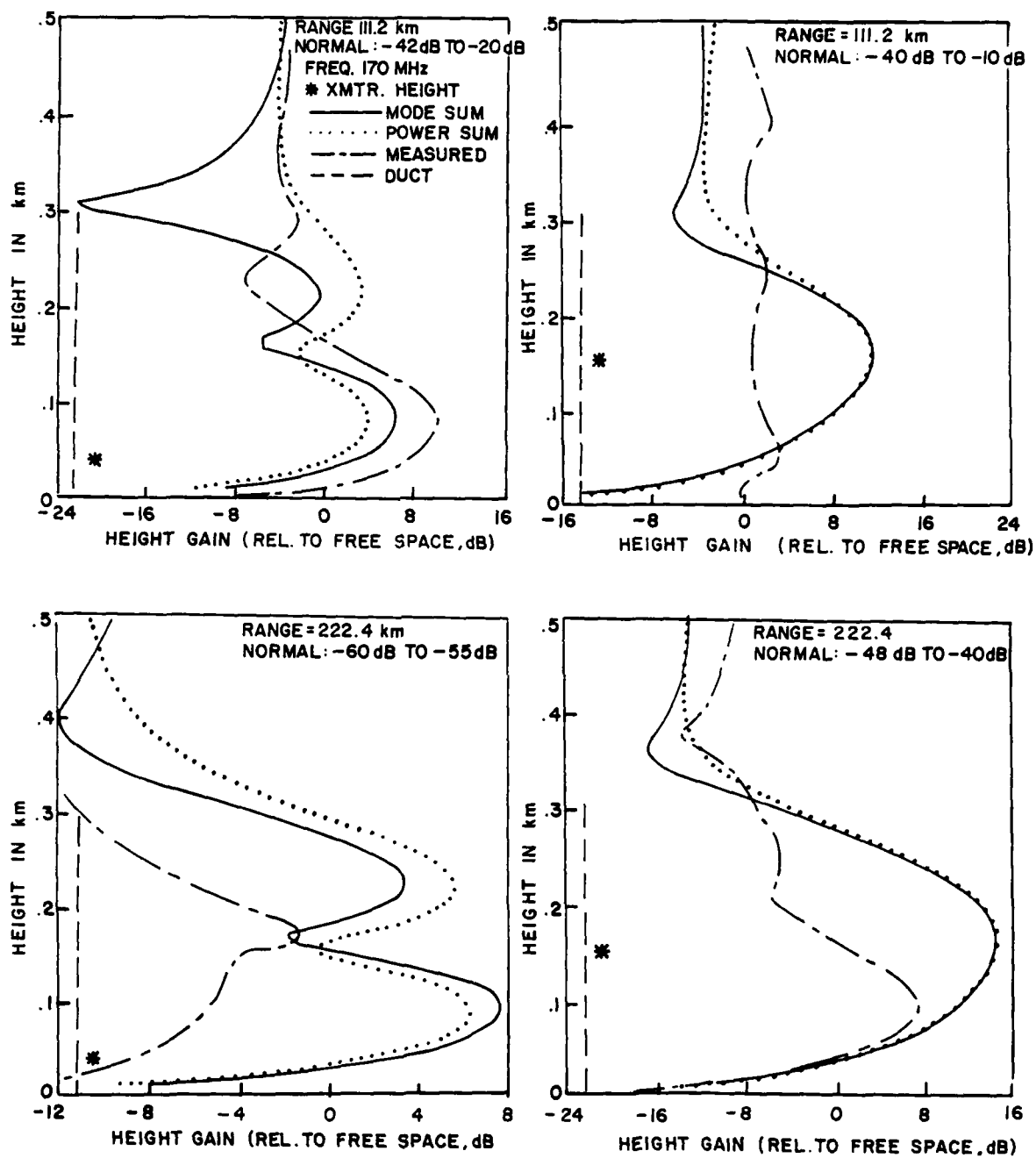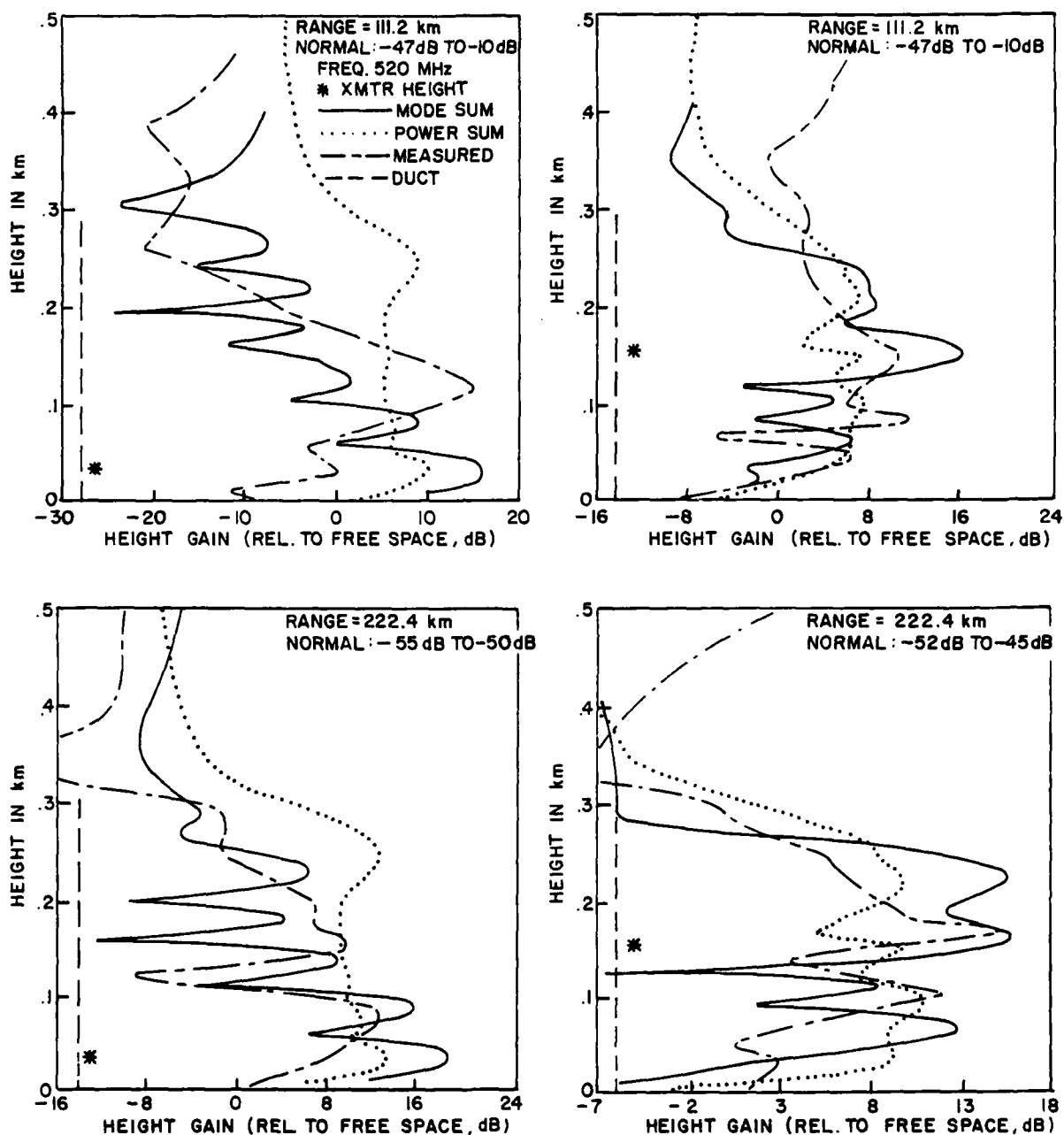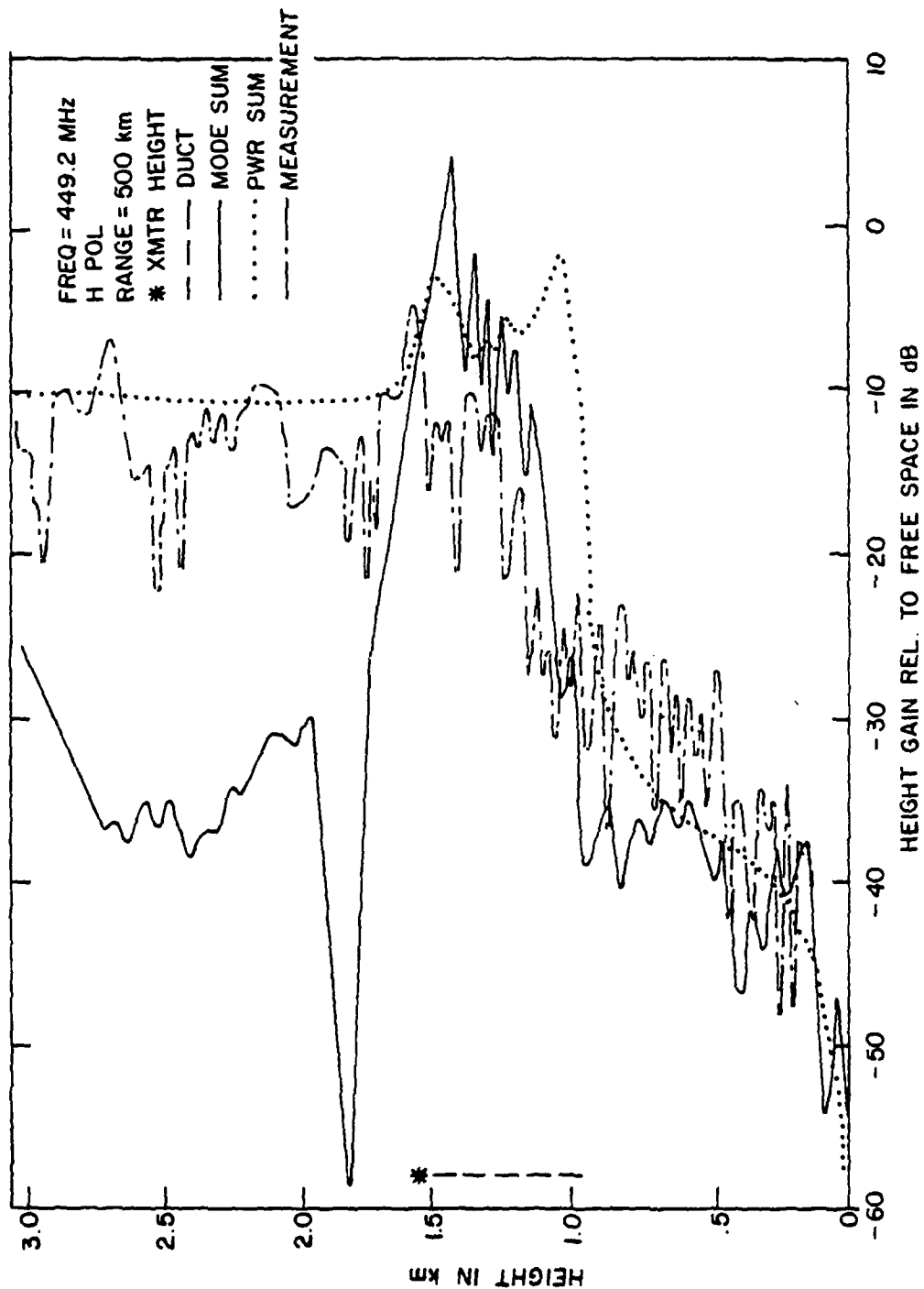
Figure 22. Comparison of predictions with measurements for elevated duct, f = 449.2 MHz.
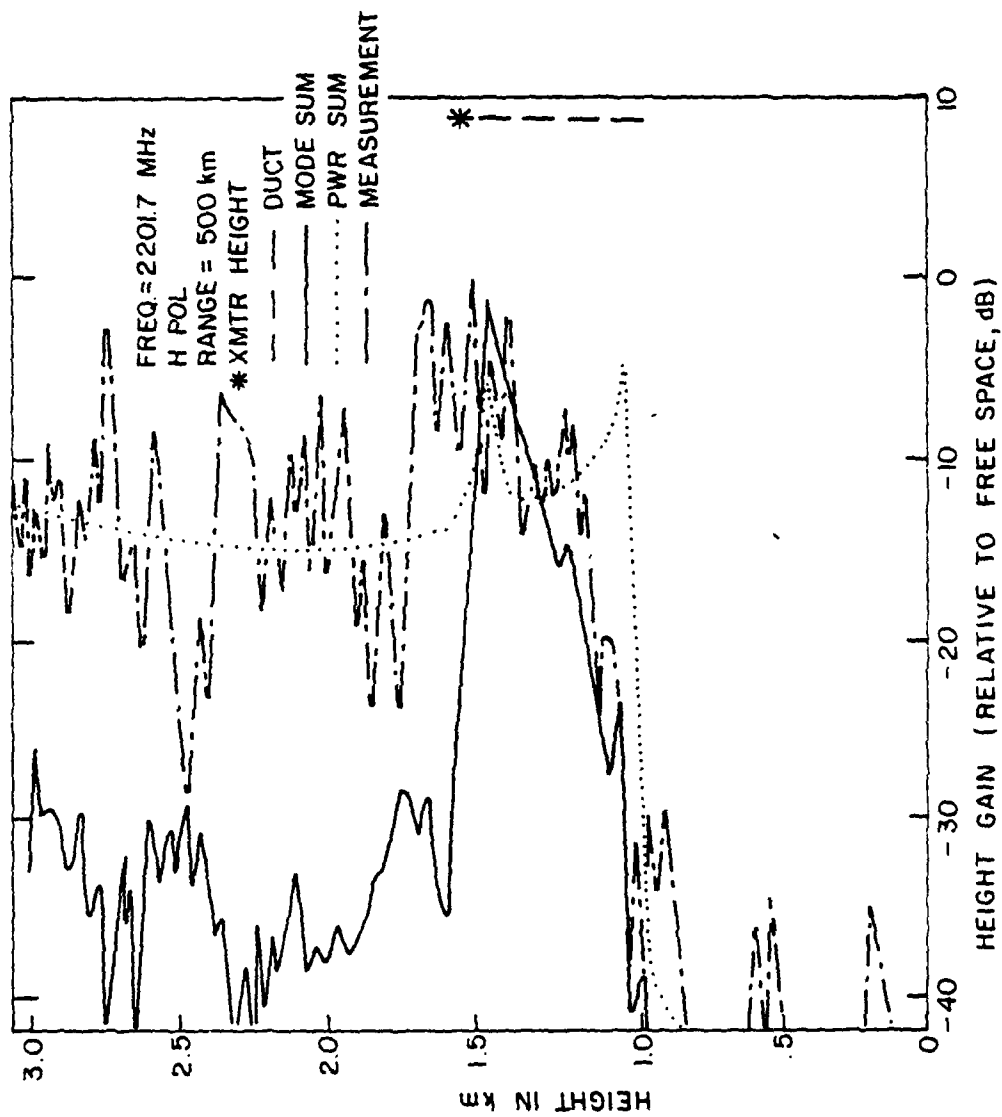
Figure 23.   Comparison of predictions with measurements for elevated duct, f = 2201.7 MHz.

SECTION 6

EIGENVALUE ANALYSIS

GENERAL
‾‾‾‾‾‾‾

In Section 3, a method is described for determining the roots, or
eigenvalues, of the modal Equation 91 in a complex space, referred to as q_{10}-
space. In this section, it will be seen that the locus of the eigenvalues in
q_{10}-space have certain distinct characteristics that can be predicted from the
refractivity profile. The roots in different portions of this locus may be
associated with different types of contributions to the fields in a duct.

The correspondence between the locations of roots in θ-space (see
Section 3) and specific types of field contributions (i.e., trapped waves,
chordal waves, multi-hop waves) was discussed by Skillman and Woods (Reference
9). As will been seen below, use of the q_{10}-space for this purpose along with
the formulation of the problem utilized in Section 2 make possible the
prediction of the location of the roots that contribute to trapped waves,
leaky (chordal) waves and multi-hop waves.

To determine the field contribution of a given (say nth) eigenvalue to
the field, the corresponding term in the field sum in Equation 66 is used.
Thus, the field contribution of the nth eigenvalue is given by:

$$A_n = \beta_o \left| \lambda_n E_n e^{-j\rho_n r} \right| \tag{195}$$

where the definitions of the terms are given in Section 2. From the
definition of the "power sum", Equation 67b, it is seen that the contribution
of the nth eigenvalue to the "power sum" field is identical to Equation 195.
Thus, separate data for "mode" and "power" results are not needed.

The parameter E_n is a function of the receiver height z_R and the transmitter height z_T, and can in principle be cast in the form of Equation 68:

$$E_n = u_n(z_R) \, u_n \, (z_T) \tag{196}$$

In order to determine the contribution of the nth mode to the field at a receiver height z_R, a transmitter height z_T must be specified. It is seen from Equation 196 that, regardless of the value of z_T, the variation of E_n (and therefore of A_n) will be the same except for a factor $u_n(z_T)$. When expressing the result in dB, the variation of ADB as a function of z_R will be the same for different values of z_T, except for an additive constant.

COMPUTED EIGENVALUE LOCATIONS - ELEVATED DUCTS

To determine the locations of the eigenvalues in the q_{10}-plane, the refractivity profile shown in Figure 24 will be assumed. The eigenvalues are determined using the methods described in Section 3, for four different propagation frequencies: 149 MHz (Figure 25), 449 MHz (Figure 26), 2.2017 GHz (Figure 27) and 10 GHz (Figure 28). (It is emphasized here that the eigenvalues are independent of the location of the transmitter and the receiver.) In each of these figures, the location of an eigenvalue is indicated by a dot on a graph of the q_{10}-plane in a portion of the figure. When the dots are sufficiently close together on the scale used, they will give the appearance of a continuous line or area. The eigenvalue plot in Figure 27 was shown in greater detail in Figure 11.

In each of the eigenvalue plots, the following regions may be identified:

1. A region in which the eigenvalues lie on or near the real axis (region A in Figure 11).
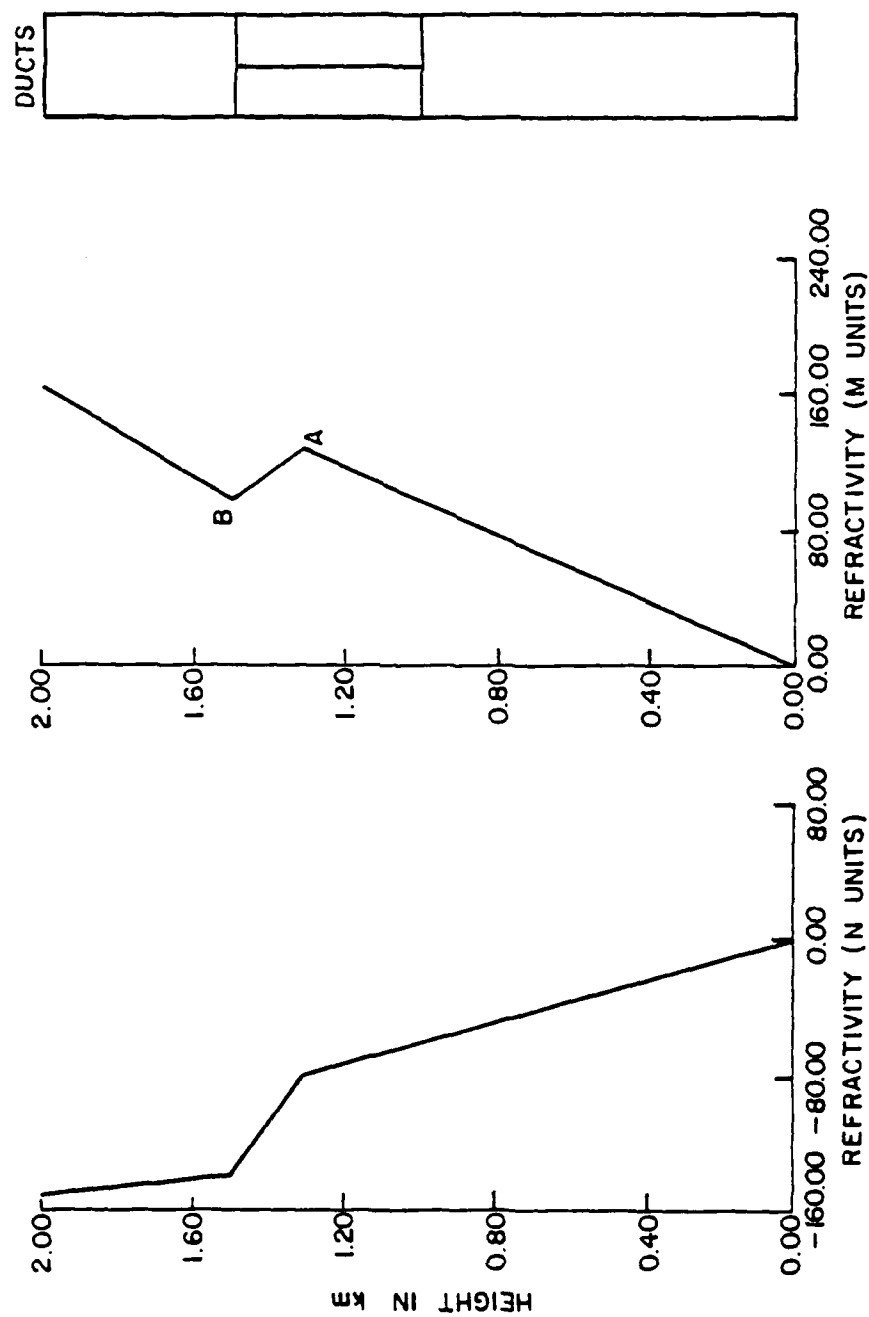
Figure 24. Refractivity profile producing single elevated duct for eigenvalue analyses.

ESD-TR-81-102
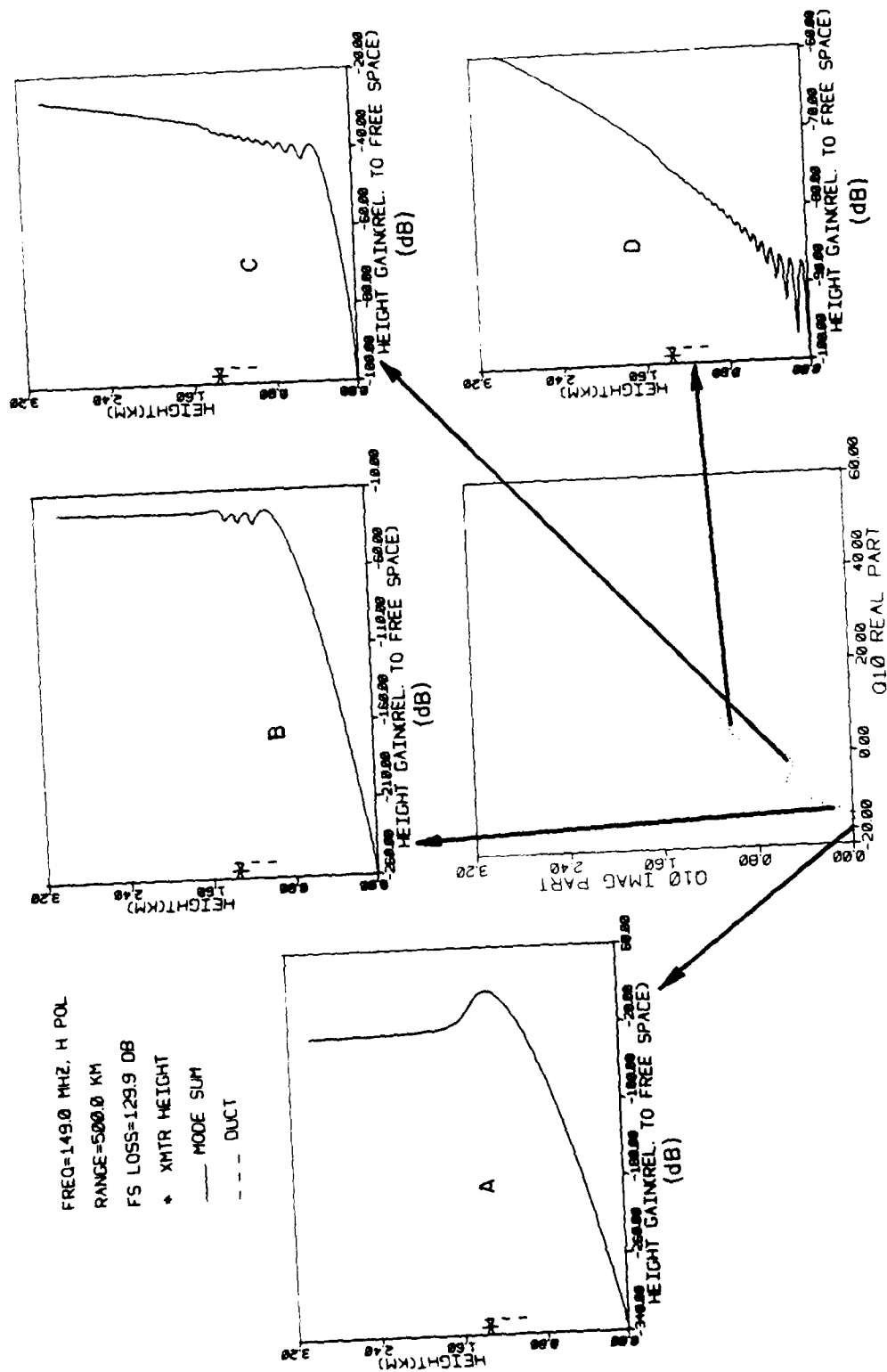
Figure 25. Eigenvalues and some of their field contributions for refractivity profile of Figure 24, f = 149 MHz.

FREQ=149.0 MHZ, H POL
RANGE=500.0 KM
FS LOSS=129.9 DB
+ XMTR HEIGHT
—— MODE SUM
- - - DUCT
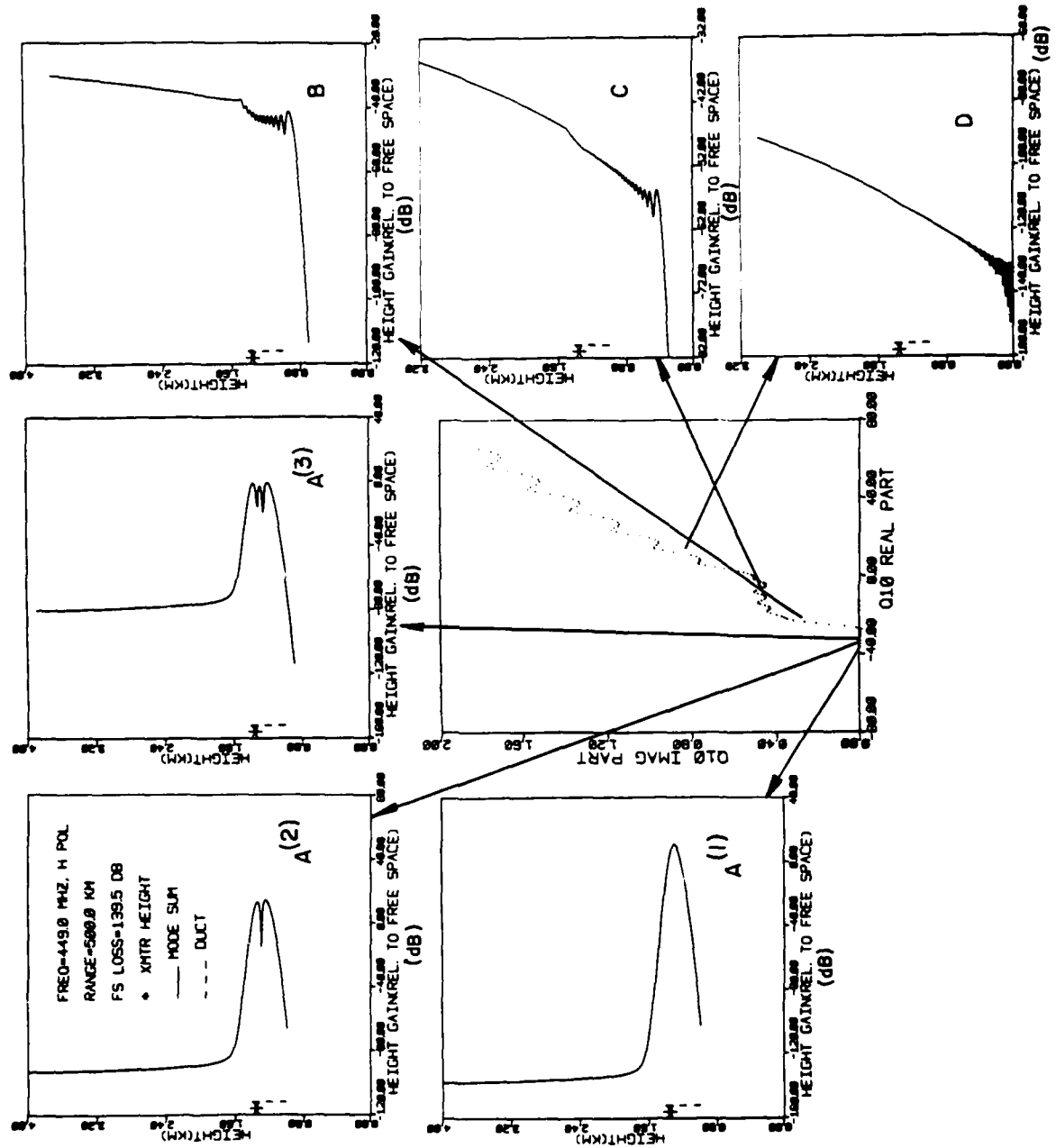
Figure 26. Eigenvalues and some of their field contributions for refractivity profile of Figure 24, f = 449 MHz.
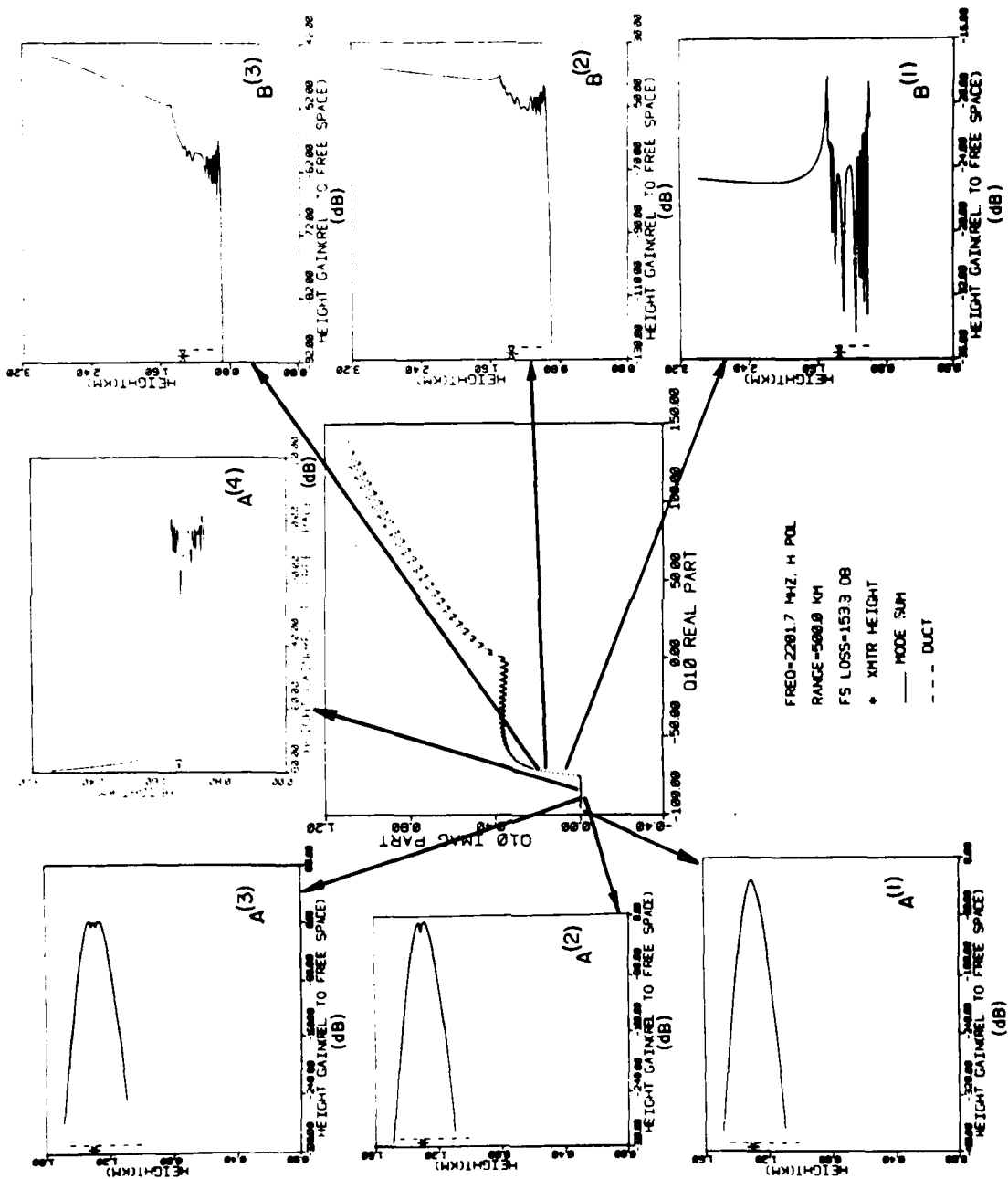
Figure 27. Eigenvalues and some of their field contributions for refractivity profile of Figure 24, f = 2201.7 MHz. (Page 1 of 2.)
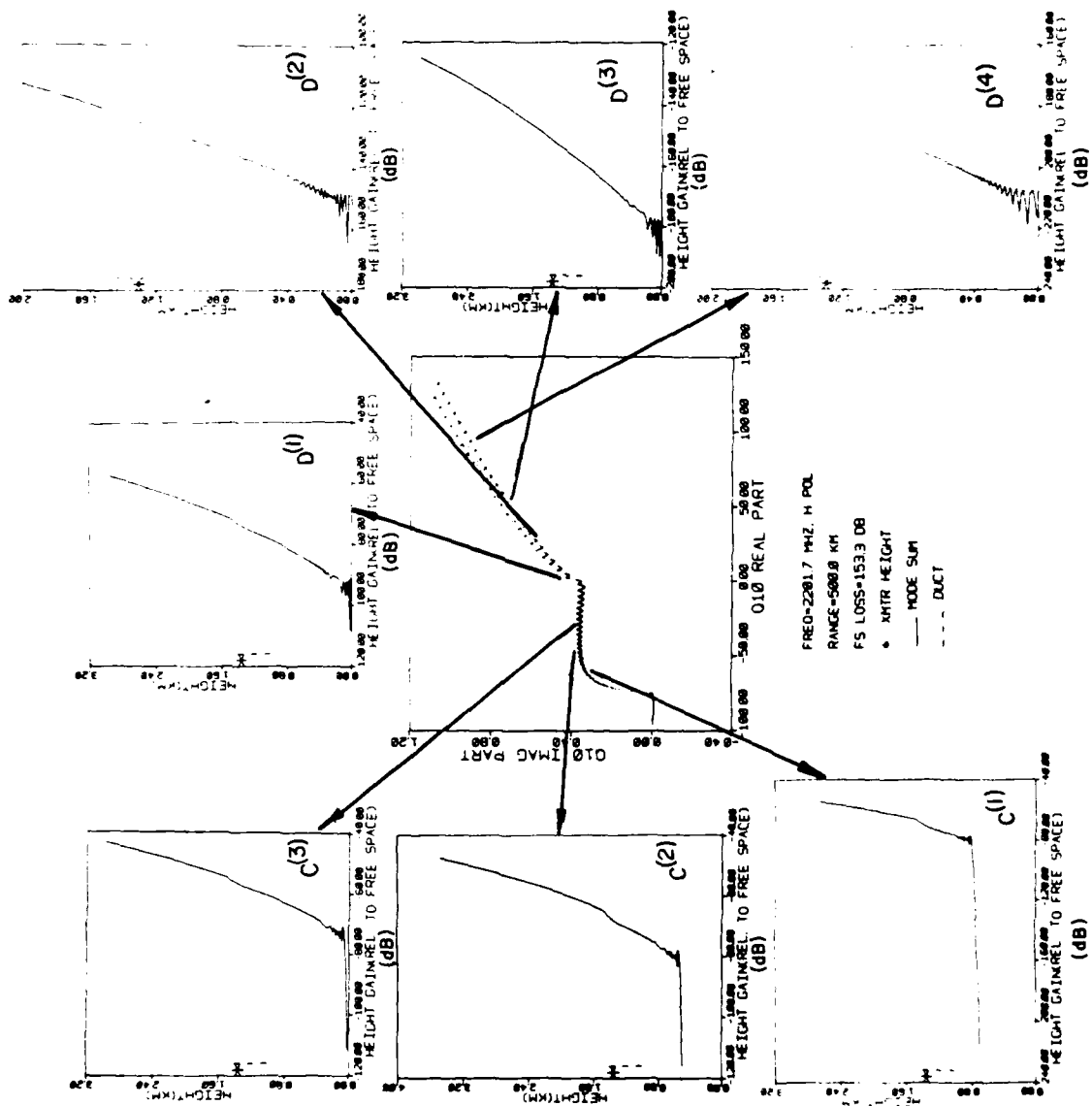
Figure 27 (Page 2 of 2). Eigenvalues and some of their field contributions for refractivity profile of Figure 24, f = 2201.7 MHz.
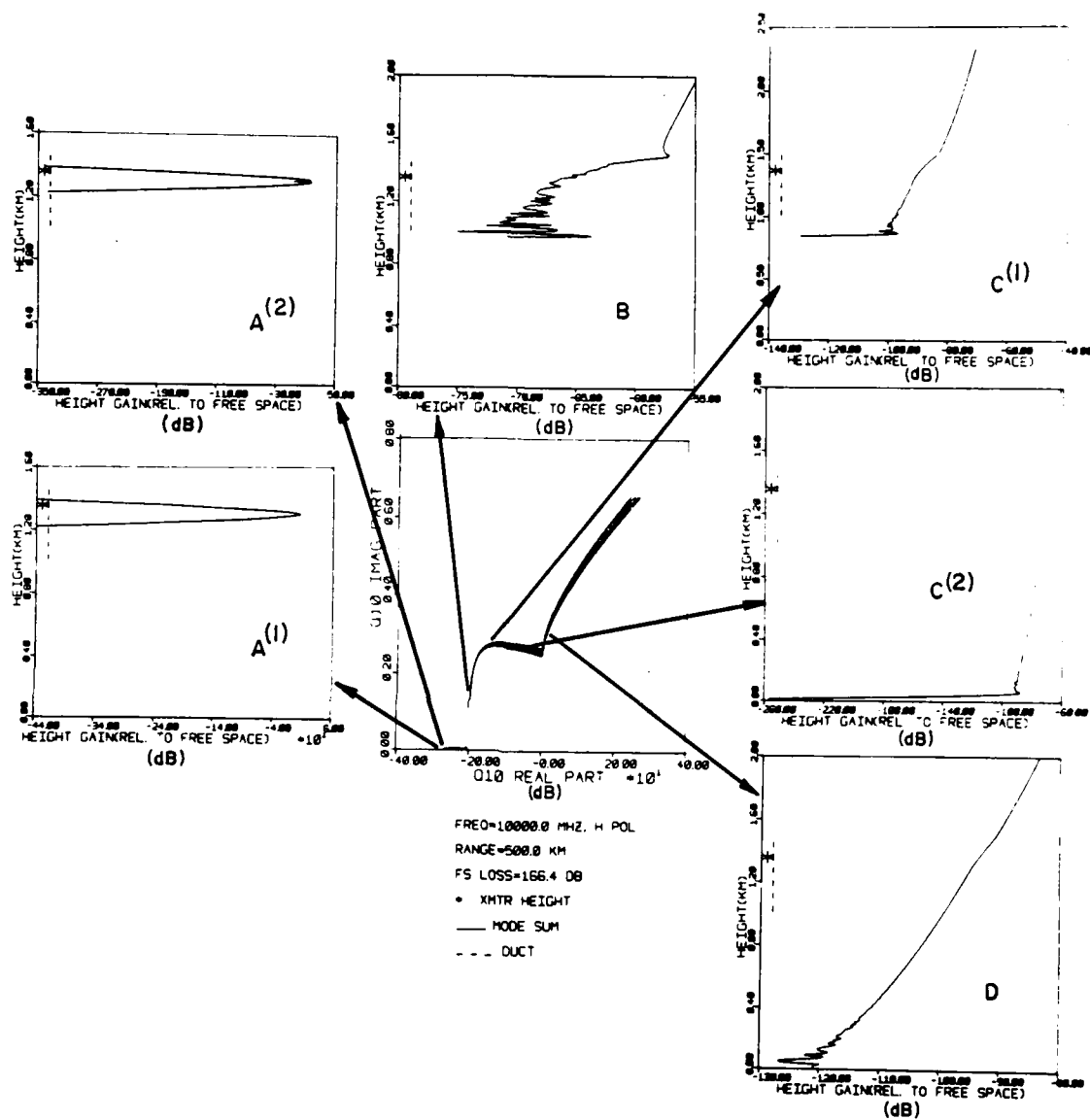
Figure 28.   Eigenvalues and some of their field contributions for refractivity
             profile of Figure 24, f = 10000 MHz.

2. A region in which the form of the locus of the eigenvalues is "wavy," but in which the overall trend is diagonal from lower left to upper right (region D in Figure 11). The lower left origin of this region corresponds approximately to $Re(q_{10}) = 0$.

The locus of the eigenvalues connecting the two regions above may be identified as consisting of two additional regions: one which has a wavy form and extends from $Re(q_{10}) = 0$ in the negative real direction (denoted as region C in Figure 11); and finally a region (denoted as region B in Figure 11) connecting the eigenvalues on the real axis with region C. The locus of the eigenvalues in region B is approximately linear.

FIELD CONTRIBUTIONS FROM EIGENVALUES IN DIFFERENT REGIONS OF THE q_{10}-PLANE

For the refractivity profile and frequencies considered above, it was shown that the locus of the eigenvalues in the q_{10}-plane is always composed of well-defined sections, or regions. It will now be shown that all eigenvalues in the same region will contribute to the propagated fields in a similar manner. This is accomplished in Figures 25 to 28 by indicating the field contribution of various eigenvalues. In each of these figures, the graph of the field contribution versus height corresponding to a given eigenvalue is joined to that eigenvalue (in the q_{10}-plane) by an arrow.

f=149 MHz

The 149-MHz case is considered first. The four different regions of the locus of the eigenvalues (Figure 25) are identifiable in this case, but they are not as distinct as for the higher frequency cases. The field contributions for modes in each of these regions are illustrated as a function of height in the figure.

In Figure 25, the eigenvalue that lies near the real q_{10}-axis and corresponds to plot A contributes principally within the duct with a small amount of leakage above the duct and even less below it. The single "bump" in the curve in plot A indicates that the corresponding eigenvalue represents the

"fundamental" waveguide mode of propagation.

The eigenvalue corresponding to plot B in Figure 25, which lies in what has been identified as "region B," produces a field which is as strong above as it is within the duct. It falls off quickly, however, as the receiver height decreases. The number of "bumps" in the curve indicates that the corresponding eigenvalue represents a waveguide mode of fourth order.

Plot C in Figure 25 shows the field contribution due to an eigenvalue in region C. Here, the field is largest above the duct and falls off slowly as the receiver height is decreased until a point is reached at which the field decreases much more rapidly.

The effect of an eigenvalue in region D is shown in plot D, which is similar to plot C except for the fact that in plot D, the decrease in field strength with a decrease in altitude is approximately the same at all heights, whereas in plot C there is a sudden drop-off prior to reaching the ground.

f=449 MHz

For the 449 MHz case, the field contributions are illustrated in Figure 26 (plots $A^{(1)}$, $A^{(2)}$, $A^{(3)}$, B, C, D) for six eigenvalues. It is seen that the eigenvalues contributing to plots $A^{(1)}$, $A^{(2)}$, and $A^{(3)}$ represent the fundamental, second order and third order waveguide modes, respectively. In each of these cases, the fields due to these eigenvalues are negligible everywhere except within the duct.

The field in plot B is shown to be largest above the duct, but falls off very rapidly at a height just below the duct bottom. The field shown in plot C is similar to that in plot B, but the "leakage" reaches further below the duct before it falls off rapidly. The rapid fall-off disappears entirely in the field of plot D in which the ground presence appears to play a role.

f=2201.7 MHz

The fields shown in plots $A^{(1)}$, $A^{(2)}$, $A^{(3)}$ and $A^{(4)}$ in Figure 27 are negligible everywhere except within the duct. Plots $A^{(1)}$, $A^{(2)}$ and $A^{(3)}$ represent the lowest order waveguide modes.

The fields shown in plots $B^{(1)}$, $B^{(2)}$ and $B^{(3)}$ are "leaky" above the duct, but little or no leakage occurs below the duct. Comparing plots $C^{(1)}$, $C^{(2)}$, $C^{(3)}$ and $C^{(4)}$ with the locations of their corresponding eigenvalues, it is seen that, as $Re(q_{10})$ increases, the height decreases at which the respective fields fall off rapidly. Once the eigenvalue region corresponding to plots $D^{(1)}$, $D^{(2)}$, $D^{(3)}$ and $D^{(4)}$ is reached, there is no rapid fall-off of the fields at any height. This is interpreted as indicating that the ground contributes to these fields through the mechanism of reflection.

f=10 GHz

The *field behavior indicated in plots* $A^{(1)}$, $A^{(2)}$, B, $C^{(1)}$, $C^{(2)}$ and D of Figure 28 are seen to be entirely analogous to those already observed in the field plots (Figure 27) for corresponding eigenvalue regions for the 2201-MHz case.

Based on observations for the four frequencies considered, it is concluded that, when an elevated duct is present, the portion of the eigenvalue locus on or near the real axis contains the eigenvalues that describe "trapped waves" existing almost exclusively within the duct. Since the modal attenuation with distance is given from Equation 195 as $\left| e^{-j\rho_n r} \right|$, this attenuation depends on $Im(\rho_n)$. From Equation 160 it is seen that $Im(\rho_n)$ would be very small for values of $q_{10}^{(n)}$ on or near the real axis. The trapped waves within the duct, therefore, propagate with little or no attenuation per unit length.

As the location of the eigenvalues in the q_{10}-plane moves in the positive real direction, the eigenvalues begin to represent leaky waves, first to the

region above the duct and then to the region below the duct. The leaky waves below the duct correspond to the chordal waves referred to by Skillman and Woods (Reference 9). The leakage reaches lower altitudes as $Re(q_{10})$ increases until, in the neighborhood of $Re(q_{10}) = 0$, the leakage reaches the ground. Beyond this point, ground reflection becomes important, and the modes can be associated with "multi-hop" waves.

The mathematical basis for $Re(q_{10}) = 0$ to represent the boundary in q_{10}-space between eigenvalues which produce ground-influenced fields (multi-hop modes) and eigenvalues which produce ground-independent fields (chordal modes) is presented below. Also presented is a criterion for determining the limits of $Re(q_{10})$ in the q_{10}-space enclosing the region of the eigenvalue locus representing trapped modes (region A).

BOUNDS ON TRAPPED AND MULTI-HOP EIGENVALUES

The eigenvalues of interest will generally lie in a region of q_{10}-space of the form shown in Figure 29, where the real dimension is much greater than the imaginary dimension. This was seen to be the situation in the cases considered above. Also shown in Figure 29 is the line representing $arg(q_{10}) = 2\pi/3$. As discussed in Section 3, the eigenvalues $q_{10}^{(n)}$ are the zeroes of the function:

$$G_1(q_{10}) = G_3(q_{10}, q_{11}, q_{21}, q_{22}, \ldots, q_{L,L-1}) = 0 \tag{197}$$

where G_1 is the value of the determinant in Equation 136. The q_{ij} are related to q_{10} through Equations 95, 96 and 155:

$$q_{ij} = q_{10}t_i + S_{ij} \tag{198}$$
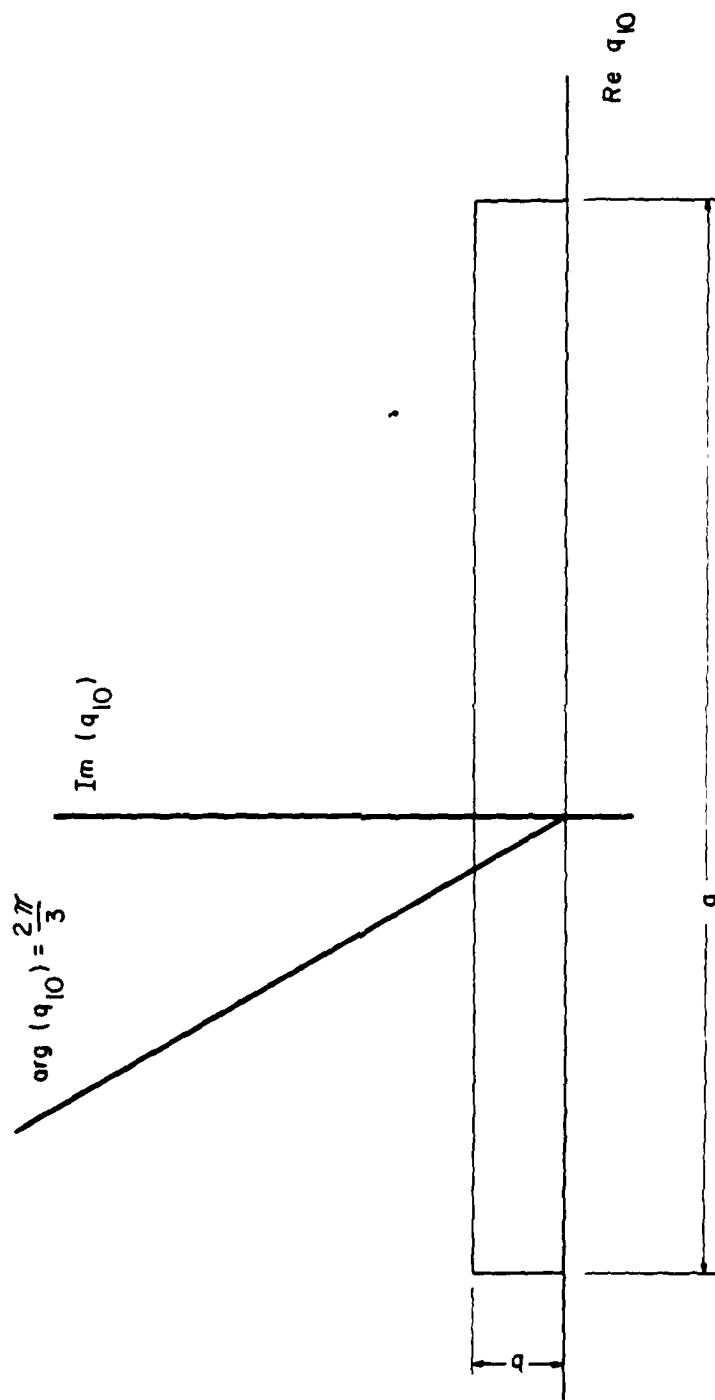
Figure 29. Schematic illustration of region of q_{10} plane containing eigenvalues of interest.

$$t_i = \left(\frac{|\tan \alpha_1|}{|\tan \alpha_i|} \right)^{2/3} > 0 \qquad\qquad\qquad (199)$$

$$S_{ij} = \left(\frac{k_0}{|\tan \alpha_i|} \right)^{2/3} 2\, M(z_j) \times 10^{-6}, \; S_{ij}\,\text{real} \qquad\qquad (200)$$

and the refractivity profile is assumed normalized to zero at the ground. Each parameter q_{ij} enters Equation 197 through $K_m(q_{ij})$, $m = 1, 2$, where K_m is a linear sum of modified Hankel functions. In APPENDIX A it was shown that, if $\text{Im}(q_{ij}) > 0$, the asymptotic behavior of each $K_m(q_{ij})$ for $\arg(q_{ij}) < 2\pi/3$ is different from its asymptotic behavior for $\arg(q_{ij}) > 2\pi/3$. Since $\text{Im}(q_{10}) \geq 0$, it follows from Equations 198 to 200 that $\text{Im}(q_{ij}) \geq 0$, so that the prior statement is valid for the case under consideration. Therefore, it is reasonable to assume that, for a particular q_{ij}, the behavior of the function G_3 in Equation 197 for $\arg(q_{ij}) < 2\pi/3$ would be different from the behavior of G_3 for $\arg(q_{ij}) > 2\pi/3$. If the functional behavior of G_3 is different when q_{ij} crosses the line $\arg(q_{ij}) = 2\pi/3$, then it is reasonable to assume that the locus of the roots of G_3 would be different as well.

Consider, for example, the refractivity profile shown in Figure 24, with a propagation frequency $f = 2201.7$ MHz. Using Equations 198 to 200, Figure 30 illustrates the locations of the q_{ij} for two values of q_{10}, such that only the q_{10} (and not the other q_{ij}) are on different sides of the line $\arg(q) = 2\pi/3$. The behavior of G_3 and the locus of its roots would be expected to be different for the two cases shown in Figure 30. Similarly, the locus of the roots of G_3 are expected to be different for the two cases shown in Figure 31.

Now if, in the vicinity of $\arg(q_{10}) = 2\pi/3$, the roots of $G_1(q_{10})$ occur for values of q_{10} for which $\text{Im}(q_{10})$ is small, then $\text{Re}(q_{10})$ would also be small for these roots. Since a different behavior of the locus of the roots of $G(q_{10})$ would be expected for values of q_{10} on either side of the line $\arg(q_{10}) = 2\pi/3$, this difference of behavior would appear to occur near $\text{Re}(q_{10}) = 0$. This would explain the location in Figure 11 of the boundary
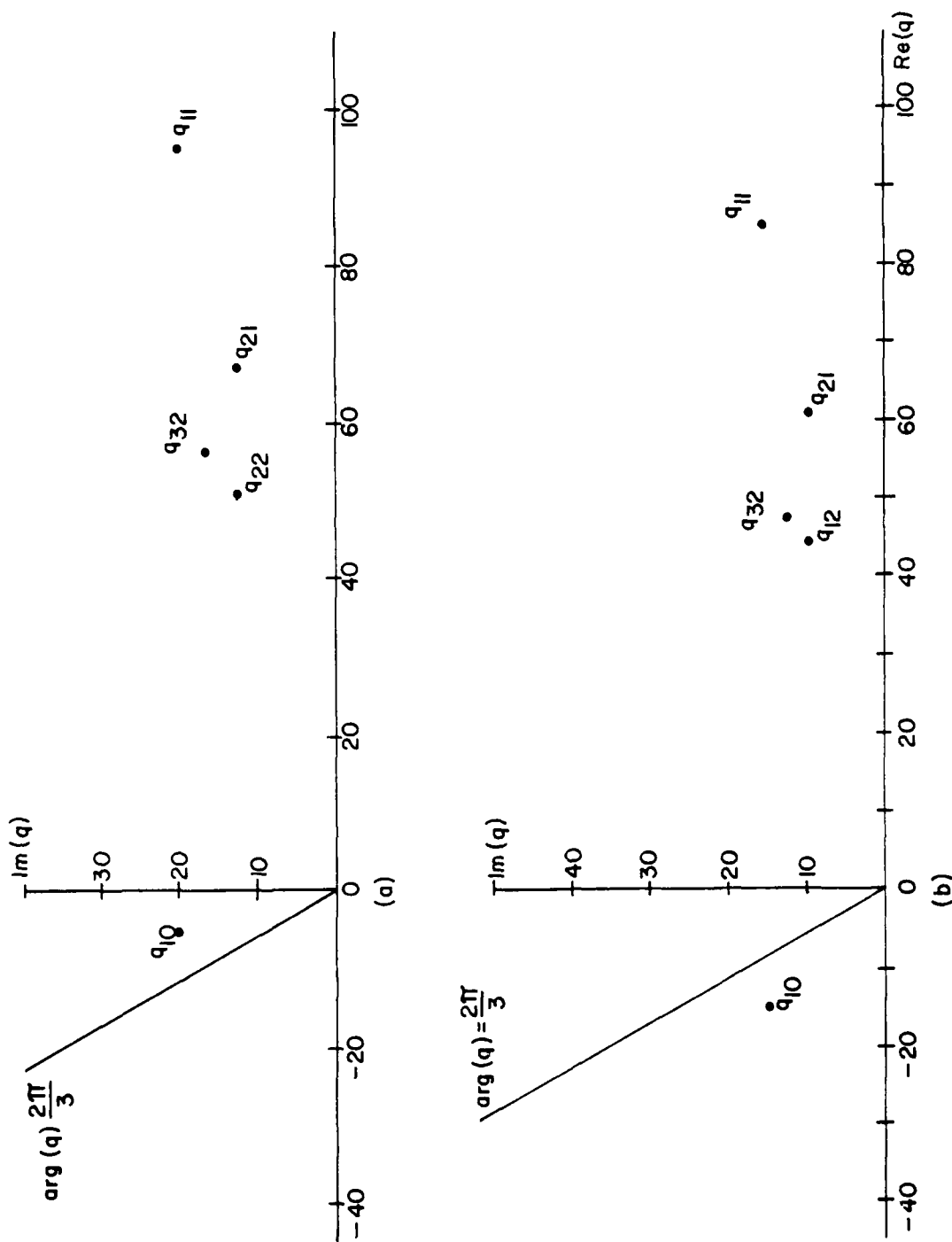
Figure 30. Locations in q-plane of q_{ij} for cases in which the q_{ij} lie on opposite sides of the line arg $(q) = \frac{2\pi}{3}$.
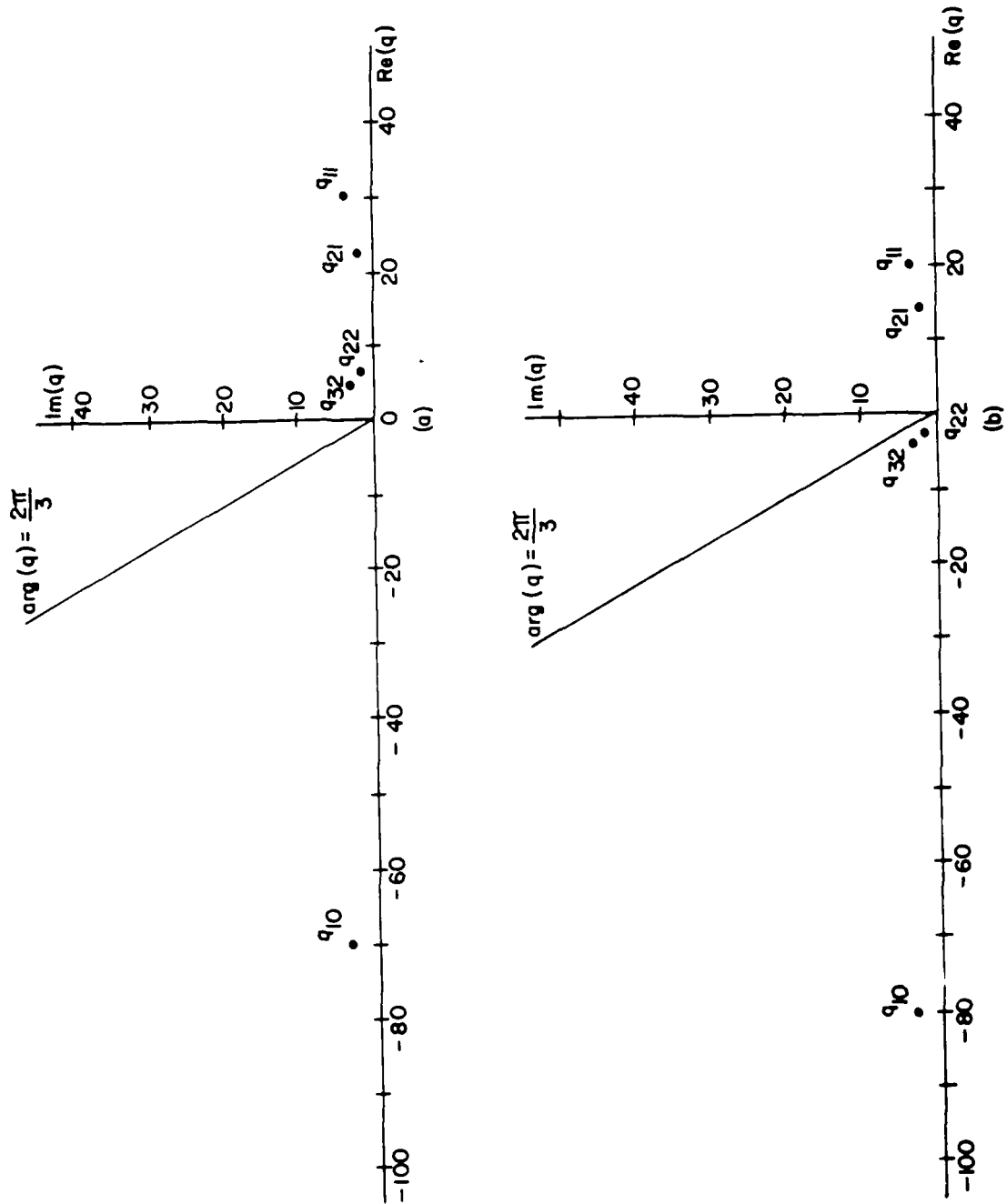
Figure 31. Locations in q-plane of q_{ij} for cases in which q_{32} and q_{22} lie on opposite sides of the line arg $(q) = \frac{2\pi}{3}$.

between region C and region D of the locus of the roots. A similar difference in behavior across $Re(q_{10}) = 0$ is observed in Figues 25, 26 and 28 as well. Since q_{10} is the value of q (Equation 26) at the ground, it is not at all surprising that the field contributions of the roots for which $Re(q_{10}) > 0$ would demonstrate a ground effect (e.g., plot D of Figure 28), whereas field contributions of the roots for $Re(q_{10}) < 0$ would not demonstrate a ground effect (e.g., plot $C^{(2)}$ of Figure 28).

The same reasoning would be expected to apply to the fields within the duct. As demonstrated in the previous subsection, these fields would receive their major contribution from the "trapped" modes, the eigenvalues $q_{10}^{(n)}$ of which lie on or near the real q_{10} axis. The duct boundaries in q-space are characterized by the values of q corresponding to the points A and B in the modified refractivity profile of Figure 24. These values of q are:

(1) Point A: either q_{11} or q_{21}

(2) Point B: either q_{22} or q_{32}

Since the eigenvalues contributing to the trapped waves in the duct satisfy:

$$Im(q_{10}) \approx 0, \text{ trapped modes} \tag{201}$$

then from Equations 198 to 200,

$$Im(q_{ij}) \approx 0, \text{ trapped modes} \tag{202}$$

It follows that, for trapped modes, the roots $q_{10}^{(n)}$ are such that, if any q_{ij} crosses the line $arg(q) = 2\pi/3$, it does so in the vicinity of:

$$Re(q_{ij}) \approx 0, \text{ trapped modes} \tag{203}$$

It follows from Equations 202 and 203 that, for trapped modes, the roots $q_{10}^{(n)}$ are such that if any q_{ij} crosses the line $arg(q) = 2\pi/3$, it does so in the vicinity of:

121

$$q_{ij} = 0 \qquad\qquad (204)$$

From Equations 198 to 200, the value of q_{10} at which Equation 204 holds is:

$$q_{10} = -\frac{S_{ij}}{t_i} = -\left(\frac{k_0}{\lceil \tan \alpha_1 \rceil}\right)^{2/3} 2\, M(z_j) \times 10^{-6} \qquad (205)$$

But since the right side of Equation 205 is dependent only on the index j and not on the index i, the value of q_{10} is the same for the two q_{ij}'s that characterize point A in Figure 24 (i.e., q_{11} and q_{21}), and is the same for the two q_{ij}'s that characterize point B (i.e., q_{22} and q_{32}).

The locations of the roots $q_{10}^{(n)}$ which represent the fields within the duct would thus be expected to be affected by the value of q_{10} for which q_{11} (or q_{21}) = 0, and by the value of q_{10} for which q_{22} (or q_{32}) = 0. To investigate the relationship between these values of q_{10} and the bounds of the region in the q_{10}-plane containing the eigenvalues representing trapped modes, consider TABLE-1. The information in the table is for the refractivity profile and frequencies used to obtain Figures 25 through 28. In the table, trapped modes are taken as those modes for which $Im(q_{10}) < .02$.

It is seen from TABLE-1 that, for the elevated duct profile and for the frequencies considered, the left boundary in the q_{10} plane of the $q_{10}^{(n)}$ representing trapped waves in the duct is approximated well by the value of q_{10} for which $q_{11} = 0$. Similarly, the right boundary of these trapped modes is approximated well by the value of q_{10} for which $q_{22} = 0$.

It is also interesting to note from TABLE-1 that the number of trapped modes between the right and left boundaries of the trapped-wave eigenvalues (density of the eigenvalues in q_{10}-space) increases only logarithmically with frequency. Therefore, mesh size in the numerical method descibed in Section 3 to locate the roots need not be altered appreciably for different frequencies.

TABLE 1

APPROXIMATED AND ACTUAL BOUNDS OF TRAPPED MODES IN THE q_{10}-PLANE FOR

REFRACTIVITY PROFILE OF FIGURE 34

Frequency (MHz)	q_{10} for $q_{11}= 0$	q_{10} for $q_{22}= 0$	Left Boundary of Computed $q_{10}^{(n)}$ for Trapped Modes	Right Boundary of Computed $q_{10}^{(n)}$ for Trapped Modes	No. of Trapped Modes	Mode Density
149	-16.2	-12.4	-15.0	-13.5	2	$\sim \dfrac{4}{3}$
449	-33.7	-25.8	-32.6	-27.3	6	$\sim \dfrac{6}{5}$
2201.7	-97.4	-74.5	-96.2	- 75.6	36	$\sim \dfrac{9}{5}$
10000	-267.1	-204.3	-265.9	-204.7	164	$\sim \dfrac{14}{5}$

123

APPLICATION OF EIGENVALUE ANALYSIS TO TWO-DUCT PROFILE

In order to verify the concepts described above for estimating the locations of trapped modes, the theoretical two-duct geometry illustrated in Figure 32 will be considered with a propagation frequency of 449 MHz. The computed eigenvalues are illustrated as the dots in the q_{10} plane in Figure 33. The eigenvalues in this figure appear to lie along two separate loci, one characterizing each duct. The trapped waves for each duct are easily identifiable as those lying near the real axis. Field plots in Figure 33 illustrate the field contributions for each of the labelled different eigenvalues. (Note that the labelling is not in any apparent sequence, but rather represents the number of the mode in the order in which it is calculated using the MODESRCH method described in Section 3).

In Figure 33, plots 82, 81 and 80 are shown to correspond to the trapped waves in the higher duct. Plot 56 represents a leaky wave from the same duct. Plots 44, 46, and 47 are shown to correspond to trapped waves in the lower duct. It is interesting to note that the eigenvalue corresponding to plot 82 (i.e., the leftmost eigenvalue) represents the fundamental waveguide mode for the system, and contributes to the field in the upper duct. Plot 44, on the other hand, represents a higher mode of the system, but is the fundamental mode of propagation in the lower duct.

Using Equation 205, the boundaries of the region in the q_{10} plane containing the trapped modes of the lower duct are approximated by:

$$q_{10} = -\frac{S_{11}}{t_1} = -11.7$$

and

$$q_{10} = -\frac{S_{22}}{t_2} = -7.3$$

124
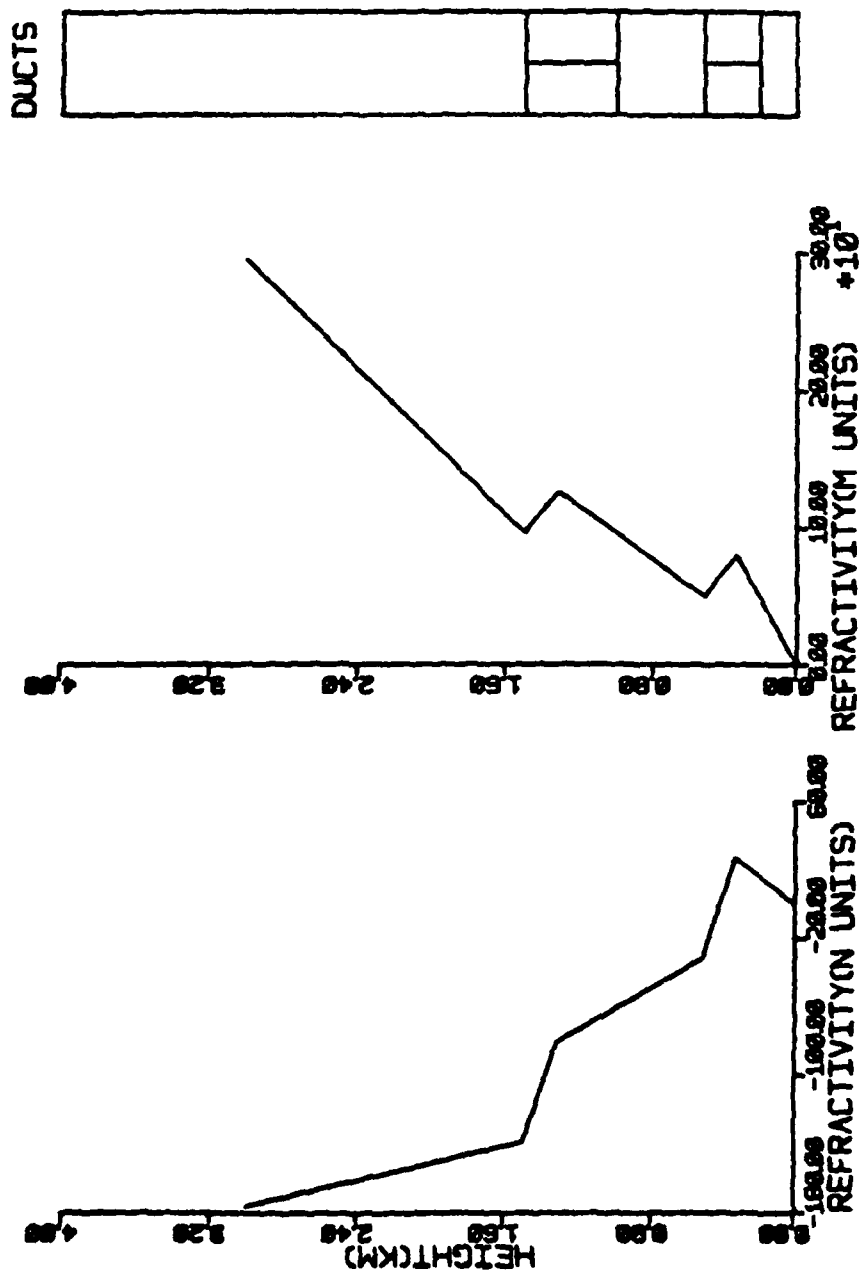
Figure 32. Refractivity profile producing two elevated ducts for eigenvalue analyses.

Figure 33.   Eigenvalues and some of their field contributions for refractivity profile of Figure 32, f = 449 MHz. (Page 1 of 2.)
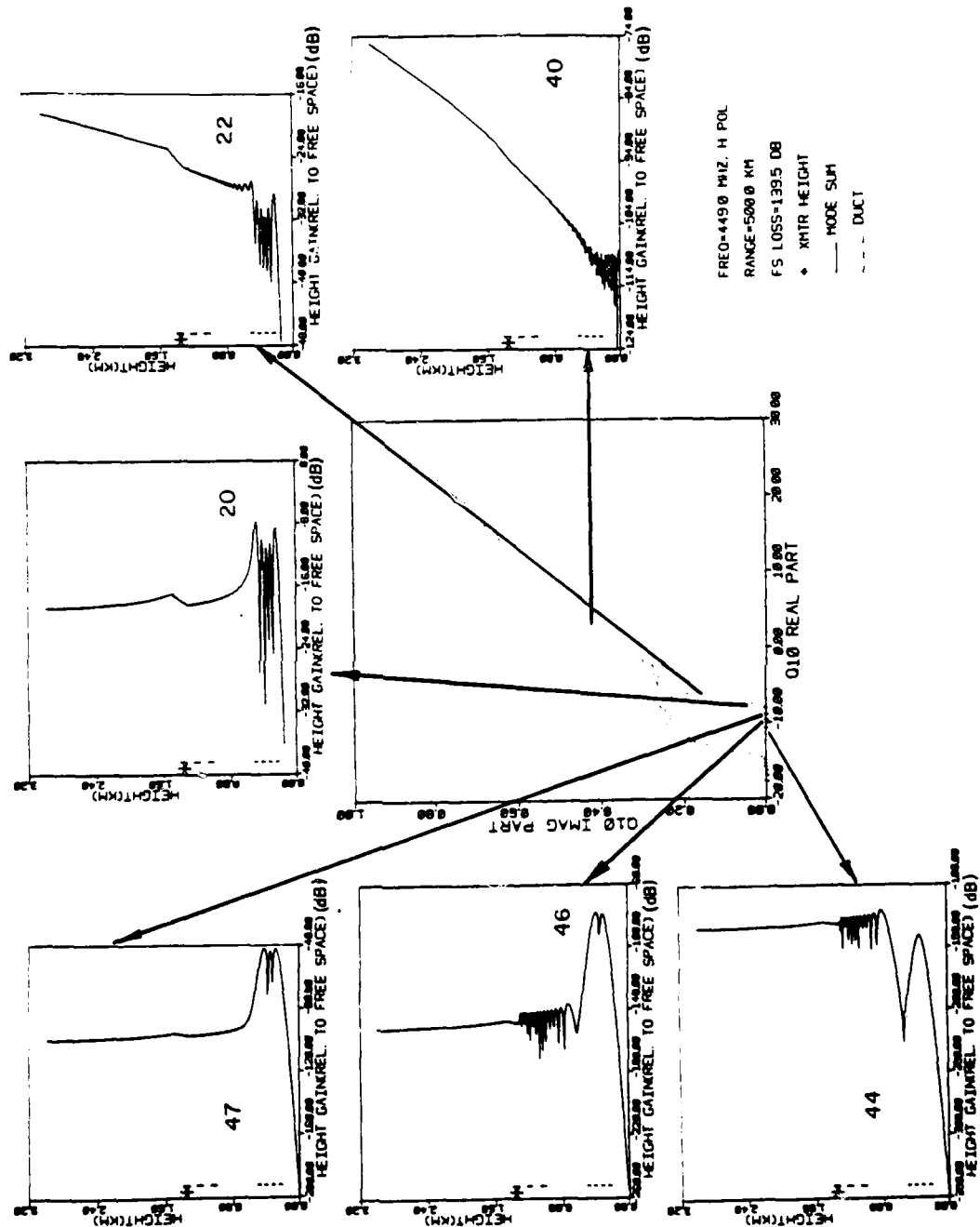
Figure 33. (Page 2 of 2)

127

while the corresponding actual boundaries for the eigenvalues shown in
Figure 33 are -10.8 and -8.1. The boundaries of the region containing the
trapped modes of the upper duct are approximated by:

$$q_{10} = - \frac{s_{33}}{t_3} = - 18.4$$

$$q_{10} = - \frac{s_{44}}{t_4} = - 14.1$$

while the corresponding actual boundaries for the eigenvalues are -17.7 and
-14.5.

The method described in the preceding subsections, for approximating the
boundaries of the region in the q_{10} plane that contains trapped modes, is thus
seen to have a more general validity. Its application to ground-based ducts
will be demonstrated in a later subsection.

COMPUTED EIGENVALUE LOCATIONS - SURFACE DUCTS

The locations of the eigenvalues in the q_{10}-plane will now be
demonstrated for the surface duct refractivity profile illustrated in
Figure 34 at four propagation frequencies: 65, 170, 520, and 3300 MHz.

The eigenvalue locations for the $_{\smile}$ lHz case is illustrated in Figure
35. Unlike the elevated cases, the locus of the eigenvalues appear to have
two branches: one including the eigenvalue which produces plot C and one not
including this eigenvalue. The field plots shown in Figure 35 illustrate the
field contributions of each of the modes. The modes that appear to be
affected by the presence of the duct are those corresponding to plots A and
C. Thus, in Figure 35, it would be reasonable to assume that plots A and C
correspond to eigenvalues that belong to another branch. Since the former
locus is associated with the ducted fields, it would be expected that the
latter locus is produced by a different propagation mechanism. It will be
demonstrated below for the 170-MHz case that this mechanism is likely to be
simple diffraction.
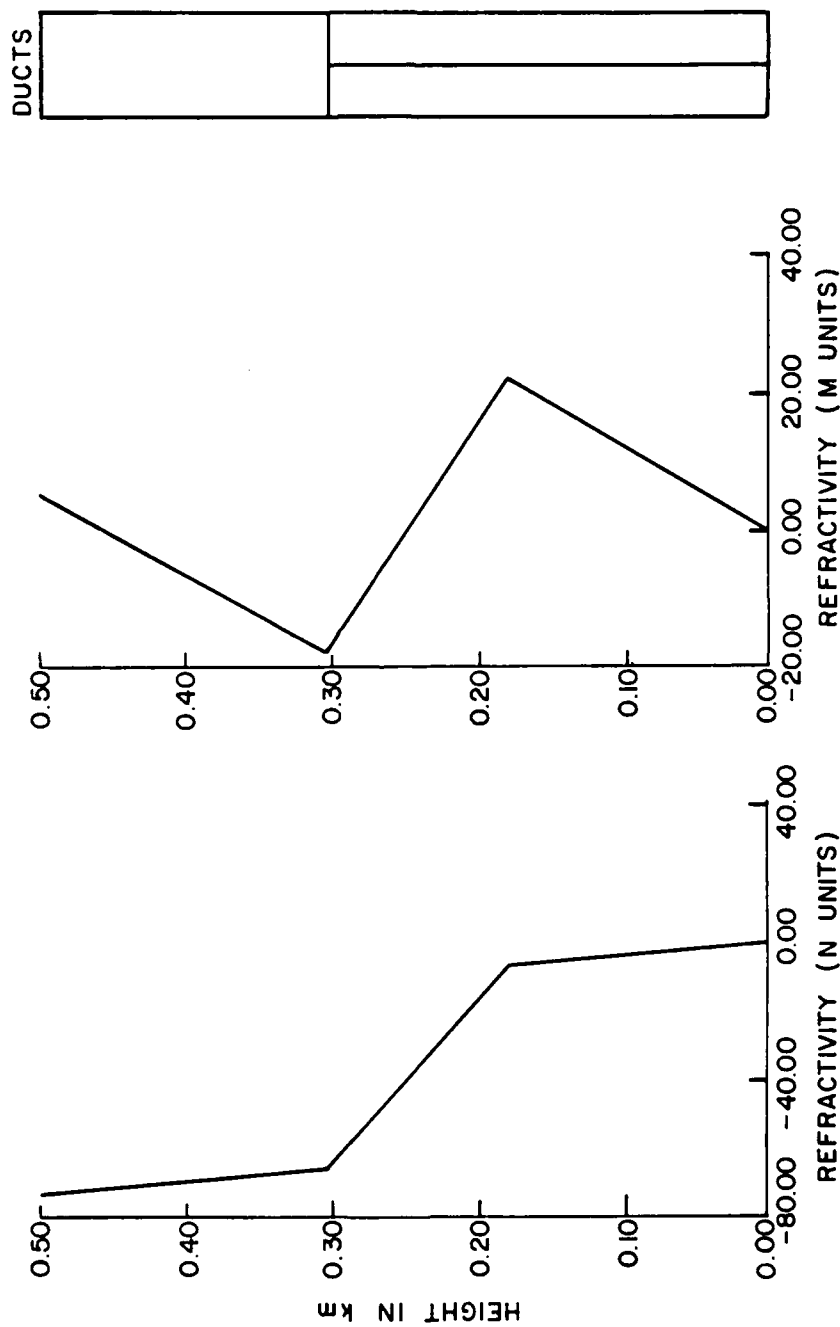
Figure 34. Refractivity profile producing surface duct for eigenvalue analysis.

Figure 35. Eigenvalues and some of their field contributions for refractivity profile of Figure 34, f = 65 MHz.

The eigenvalue locations for the 170-MHz case are illustrated in
Figure 36. Again, two distinct loci may be identified: one consisting of
eigenvalues corresponding to plots A, B, C, D, E, F, G; and the other
consisting of eigenvalues corresponding to plots H, I and J. The fields of
plots A, B, C, D, E, F and G are seen to be affected by the duct. However,
the fields in plots H, I, and J, seem unaffected.

It is interesting to note from Figures 35 and 36 that the loci of the
modes affected by the duct have a positive slope, while the loci of the modes
not affected by the duct have a negative slope. To ascertain the likely
source of the fields that are not affected by the duct, the "ductless"
refractivity profile shown in Figure 37 will be considered. The eigenvalues
produced by this profile for f = 170 MHz are shown in Figure 38. The form of
the field contribution for each of these eigenvalues is the same, a typical
one being illustrated by a single field plot in the figure. The form of this
field is seen to resemble that of those field plots in Figures 35 and 36 which
do not appear affected by the presence of the duct. The slope of the locus of
eigenvalues in Figure 38 is seen to be negative, resembling the loci of the
eigenvalues that are not affected by the duct in Figures 35 and 36. But when
the refractivity profile does not exhibit a duct, the fields at beyond-horizon
distances are caused by diffraction (since troposcatter has been ignored in
this formulation). The eigenvalues in Figures 35 and 36 that appear to be
transparent to the duct are, therefore, most likely associated with
diffraction fields.

Resuming the investigation of the eigenvalue locations for surface duct
environments, Figure 39 illustrates such locations for a propagation frequency
of 520 MHz and the duct profile shown in Figure 34. One eigenvalue
(corresponding to plot D) is now observed which does not lie on the locus of
the other eigenvalues. The eigenvalues corresponding to plots B and C, which
do not lie near the real q_{10} axis, are seen to be highly leaky to the region
above the duct. The field in plot D, which corresponds to an eigenvalue that
does not lie on the locus of the other modes, has the appearance of the
diffracted field shown in Figure 37 except for an oscillation in the curve
near the ground.
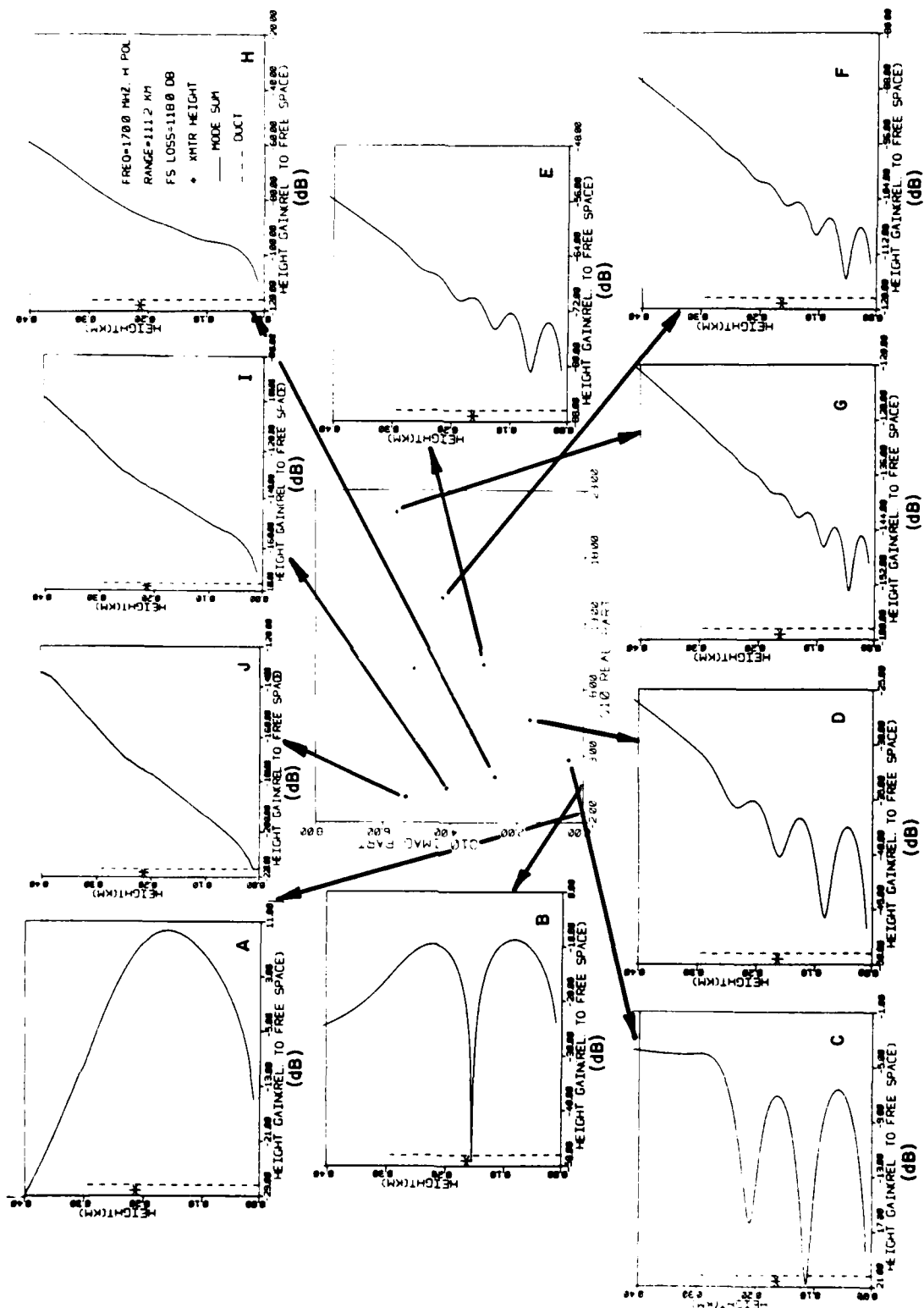
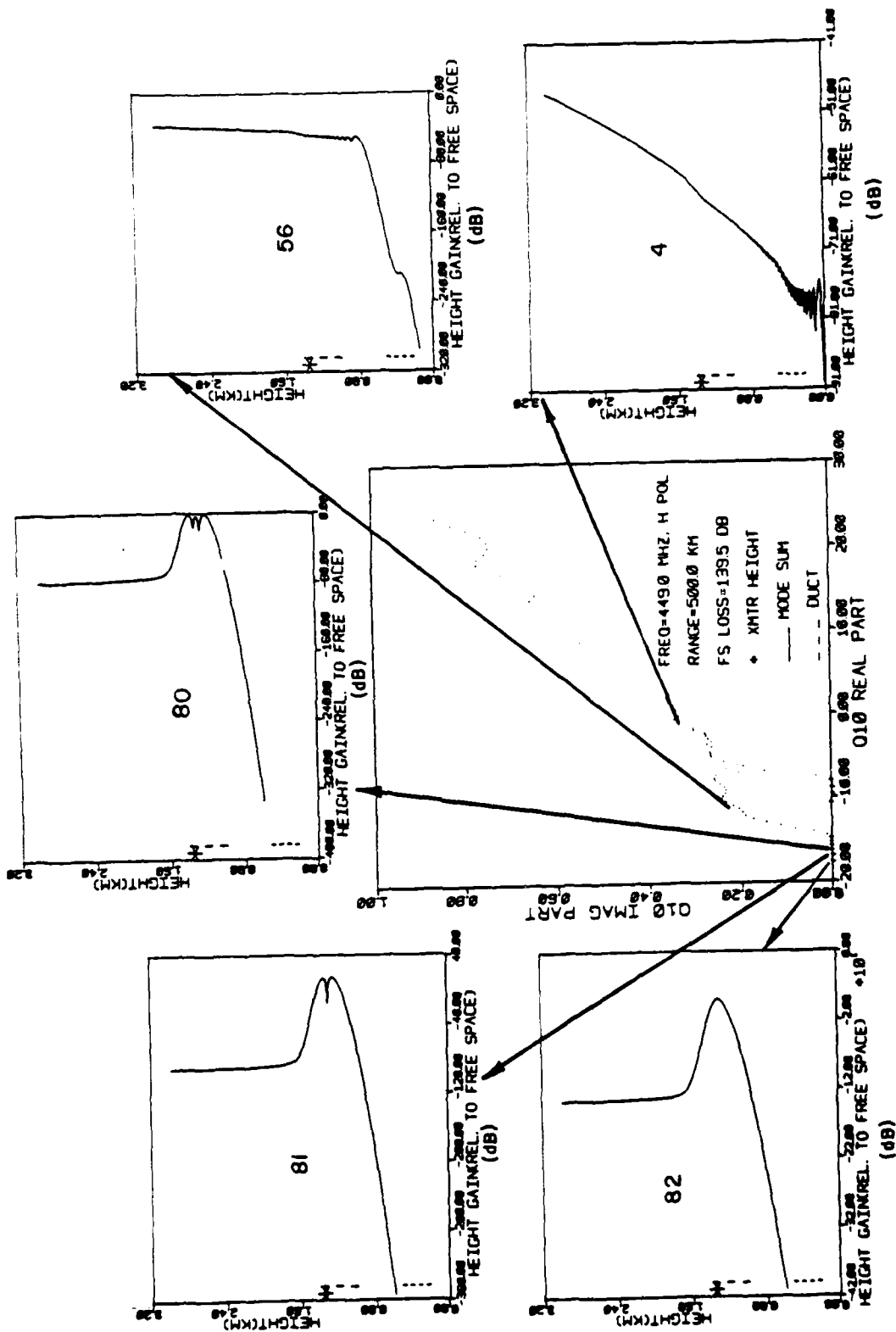Figure 36. Eigenvalues and some of their field contributions for refractivity profile of Figure 34, f = 170 MHz.
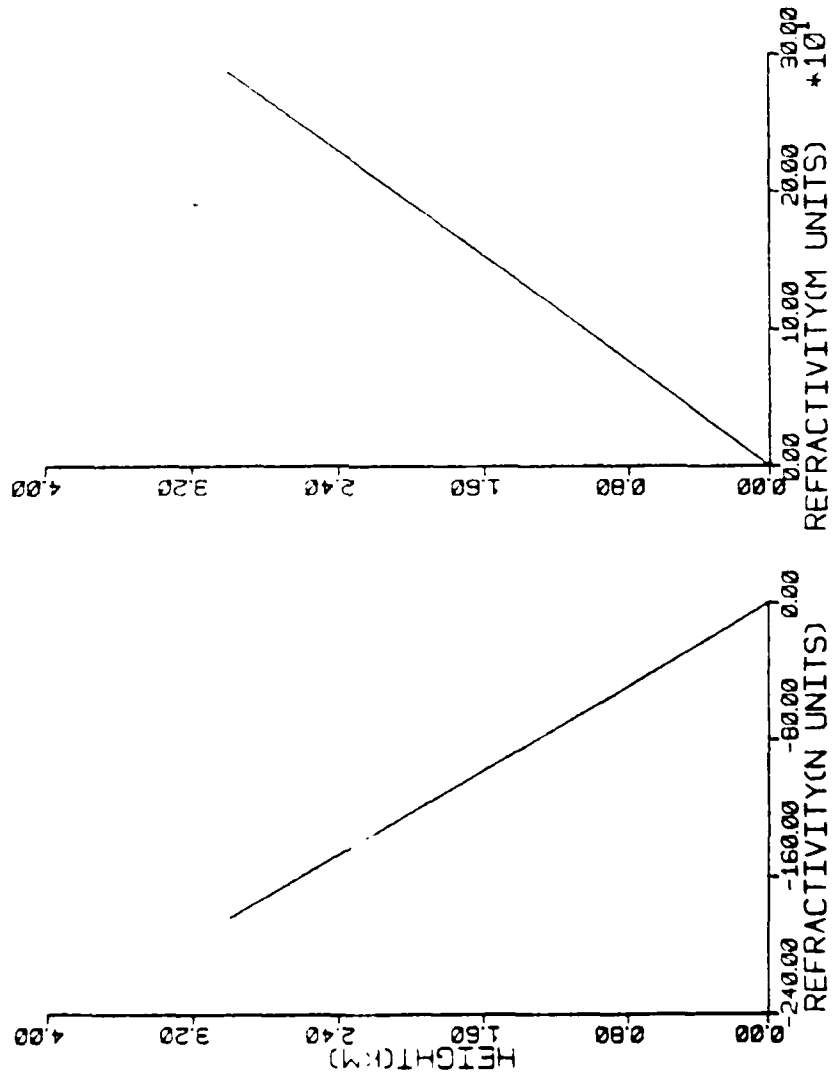
Figure 37. Ductless refractivity profile for eigenvalue analysis.
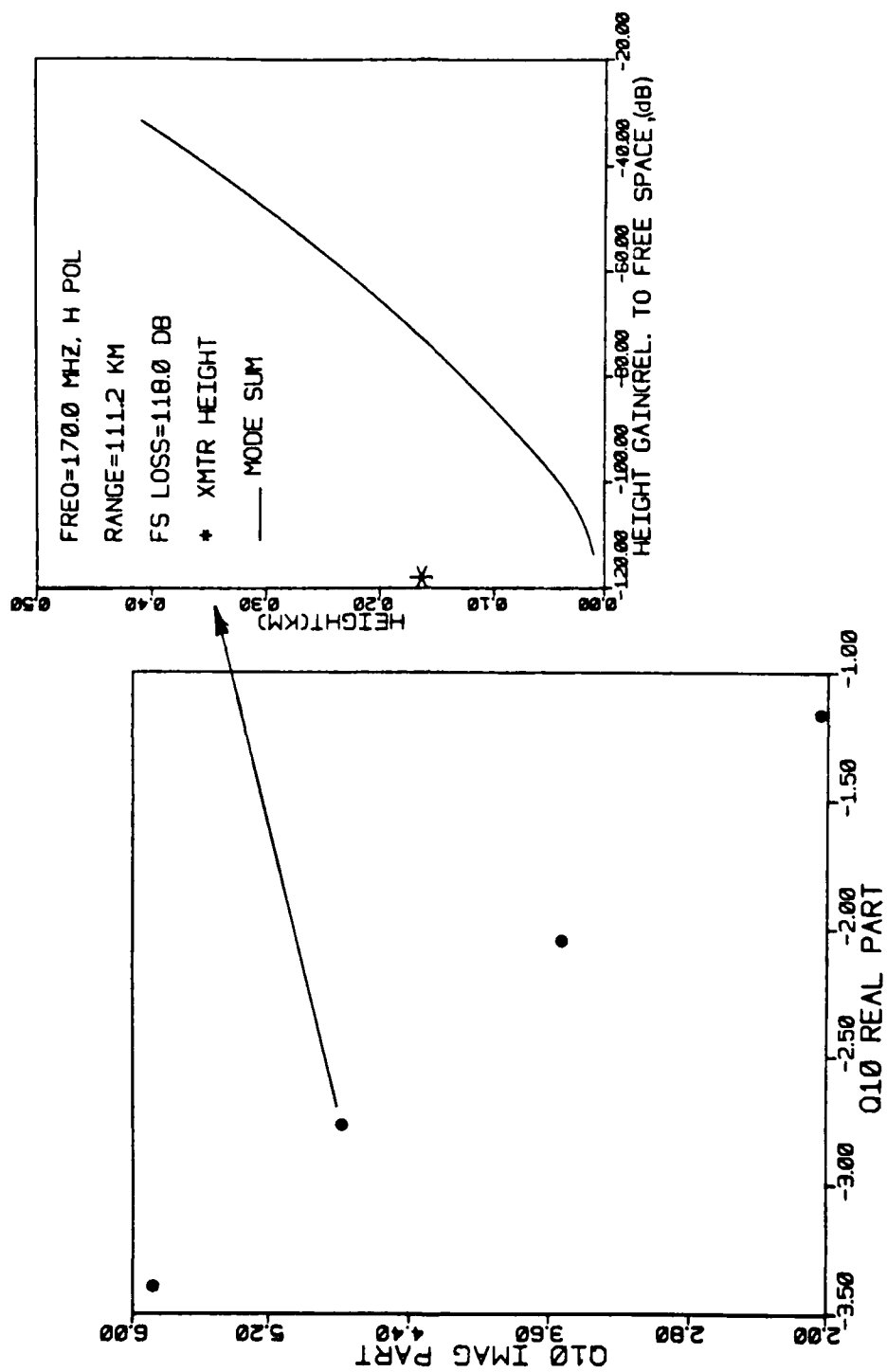
Figure 38.   Eigenvalues and a typical field contribution for refractivity profile of Figure 37,
f = 170 MHz.

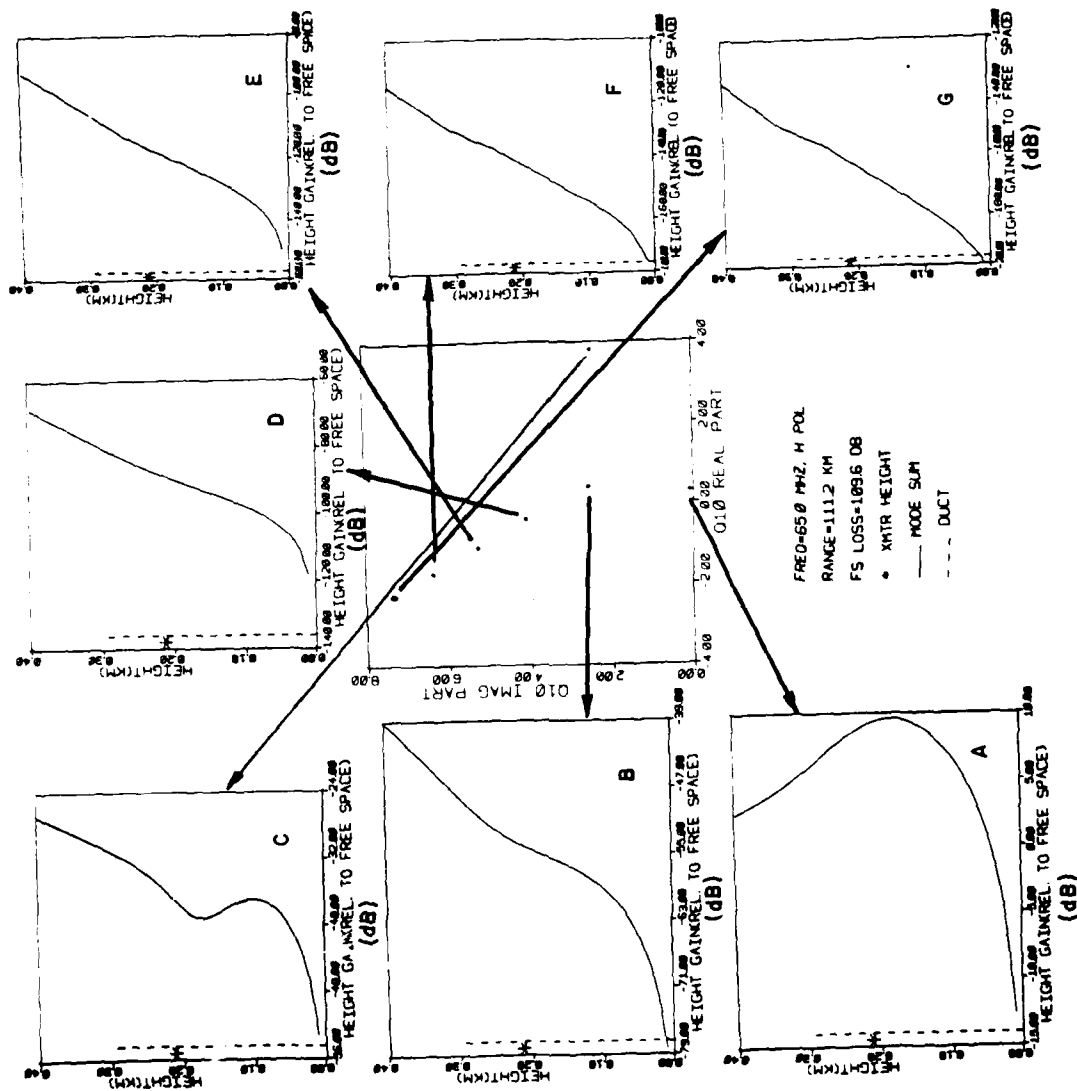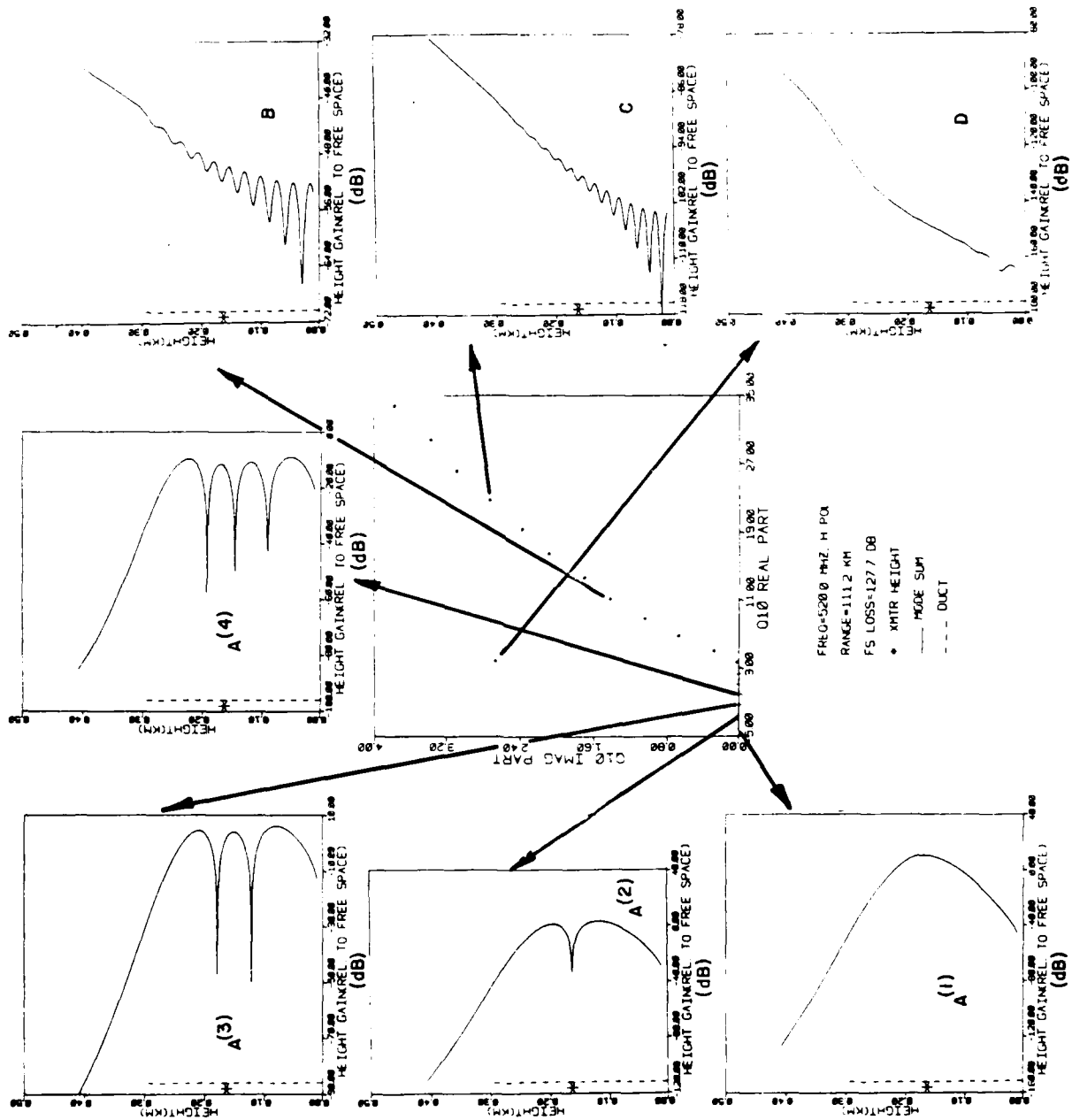Figure 39.   Eigenvalues and some of their field contributions for refractivity profile
             of Figure 34, f = 520 MHz.

The eigenvalues calculated for a frequency of 3300 MHz are illustrated in Figure 40. The field contributions of the first three trapped modes are shown in plots $A^{(1)}$, $A^{(2)}$ and $A^{(3)}$. The contribution of a mode located off the real axis is illustrated in plot B. It is seen that this mode still contributes significantly to the field within the duct, and leaks slightly above the duct and for only a short distance.

Just as in the case of elevated ducts (TABLE 1), the prediction method (Equation 205) for approximating the bounds of $Re(q_{10})$ for the trapped modes in the q_{10}-plane should apply for surface ducts as well. The predictions using this approximation are compared in TABLE 2 with the actual results calculated by the method of Sections 2 and 3 (and illustrated in Figures 35, 36, 39 and 40).

Notice that TABLE 2 shows no trapped modes for the 65-MHz case, whereas Figure 35 indicates the presence of a strong ducted field. There is no contradiction, however, since the trapped modes as defined for the purposes of TABLE 2 are non-leaky and are essentially unattenuated along the waveguide. The field contribution evident in Figure 35 is leaky and is attenuated along the waveguide. It is, however, appreciable at the distance for which the calculations were made for Figure 35.

Finally, note that no extreme change occurs in the locus of the eigenvalues in Figures 36, 39, and 40 in the vicinity of Re (q_{10}) = 0, as was the case for elevated ducts. For elevated ducts, it was shown that such a change occurs between modes that produce fields affected by the ground, and modes that produce fields unaffected by the ground. However, for surface ducts, the ground plays a role in the duct itself and, therefore, affects the trapped waves. This is demonstrated by the fact that the trapped modes lie on either side of q_{10} = 0.
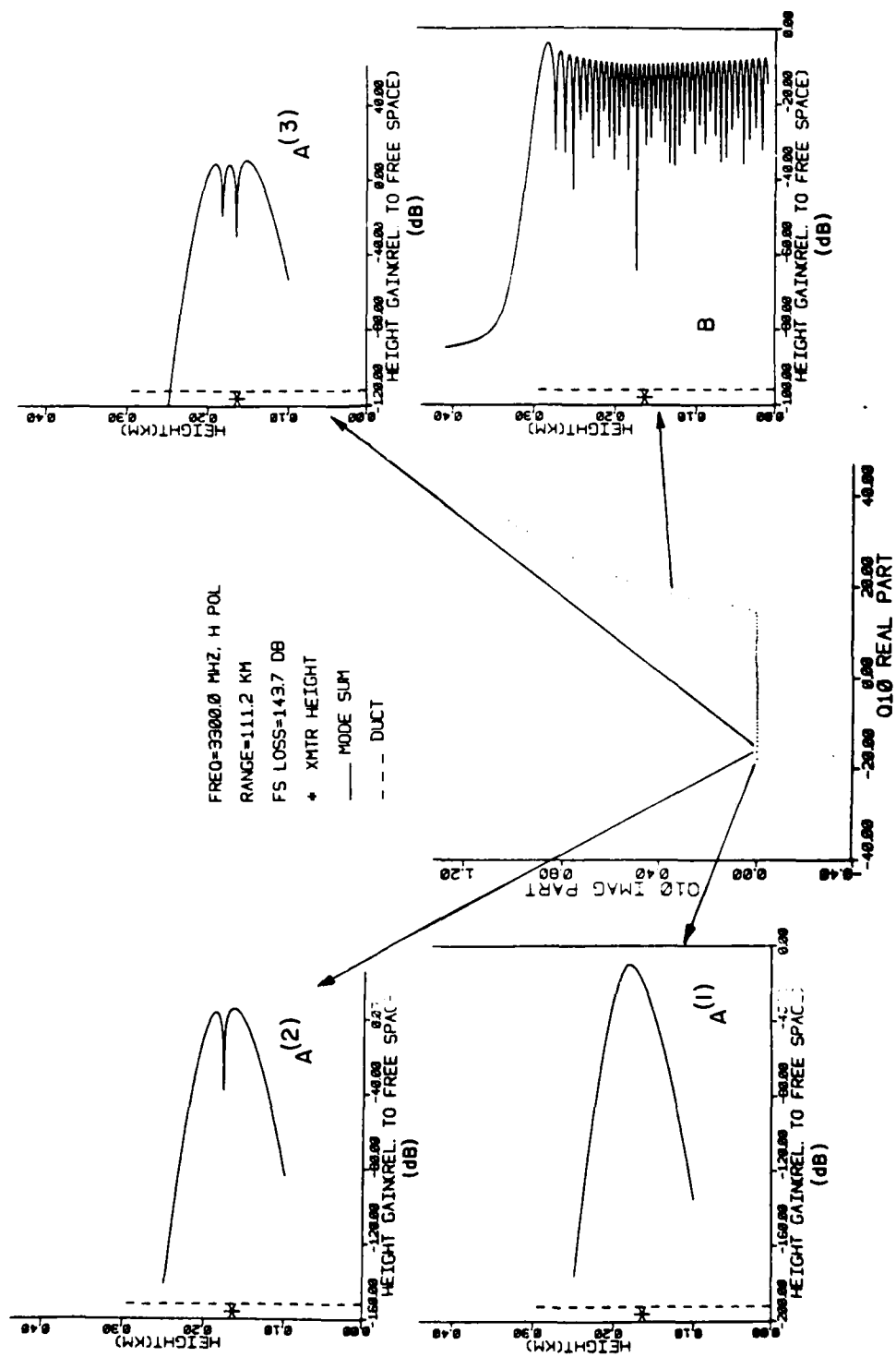
Figure 40. Eigenvalues and some of their contributions for refractivity profile of Figure 34, f = 3300 MHz.

TABLE 2

APPROXIMATED AND ACTUAL BOUNDS OF TRAPPED MODES IN THE q_{10}-PLANE FOR
REFRACTIVITY PROFILE OF FIGURE 34

Frequency (MHz)	q_{10} for $q_{11} = 0$	q_{10} for $q_{22} = 0$	Left Boundary of Computed $q_{10}^{(n)}$ for Trapped Modes	Right Boundary of Computed $q_{10}^{(n)}$ for Trapped Modes	No of Trapped Modes	Mode Density
65	-1.4	1.14	-	-	-	-
170	-2.7	2.17	-2.3	.78	2	~1
520	-5.6	4.6	-4.2	2.3	6	~1
3300	-19.2	15.7	17.8	14.3	45	$\sim \frac{45}{32}$

INFLUENCE OF DUCT HEIGHT

To illustrate the effects of the duct height on the locations of the roots of the modal equation in q_{10}-space, consider the refractivity profile shown in Figure 41. This profile (in M-units) is identical to that of Figure 24 except the center of the duct in Figure 41 is at about half the height of the one shown in Figure 24. The eigenvalues in q_{10}-space for a frequency of 449 MHz using the profile of Figure 41 are illustrated in Figure 42. The corresponding eigenvalues using the profile of Figure 24 are illustrated in Figure 26.

Comparing Figures 26 and 42, notice that the number of trapped modes (those near the real axis) is the same. These trapped modes appear at lower negative values of $Re(q_{10})$ in Figure 42 than in Figure 26 since, from Equation 205, the values of q_{10} at which q_{11} and q_{22} vanish have smaller negative values in the profile in which the duct height is lower. Although the number of trapped modes is the same, the number of all other modes (or the density of the other modes in q_{10}-space) is significantly smaller for the lower duct height than for the higher duct height. In addition, there are fewer and less intense fluctuations in the eigenvalue locus of Figure 42 than in the one in Figure 26. It is reasonable to assume that, when the duct height decreases to a point where the elevated duct becomes a surface duct, these fluctuations would disappear entirely, as was seen to be the case in, say, Figure 40.
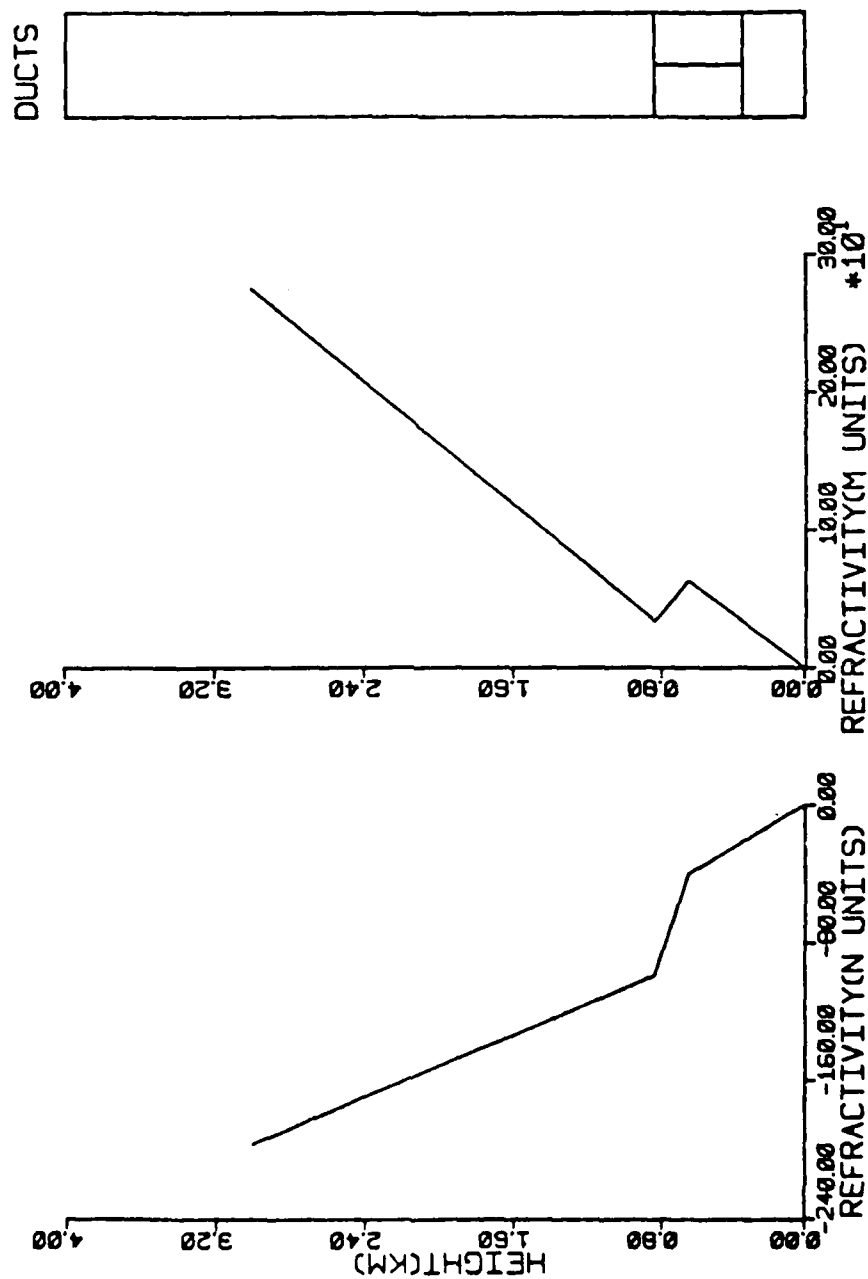
Figure 41. Refractivity profile producing a duct at about half the height of the duct of Figure 24.

140

FREQ=449.0 MHZ
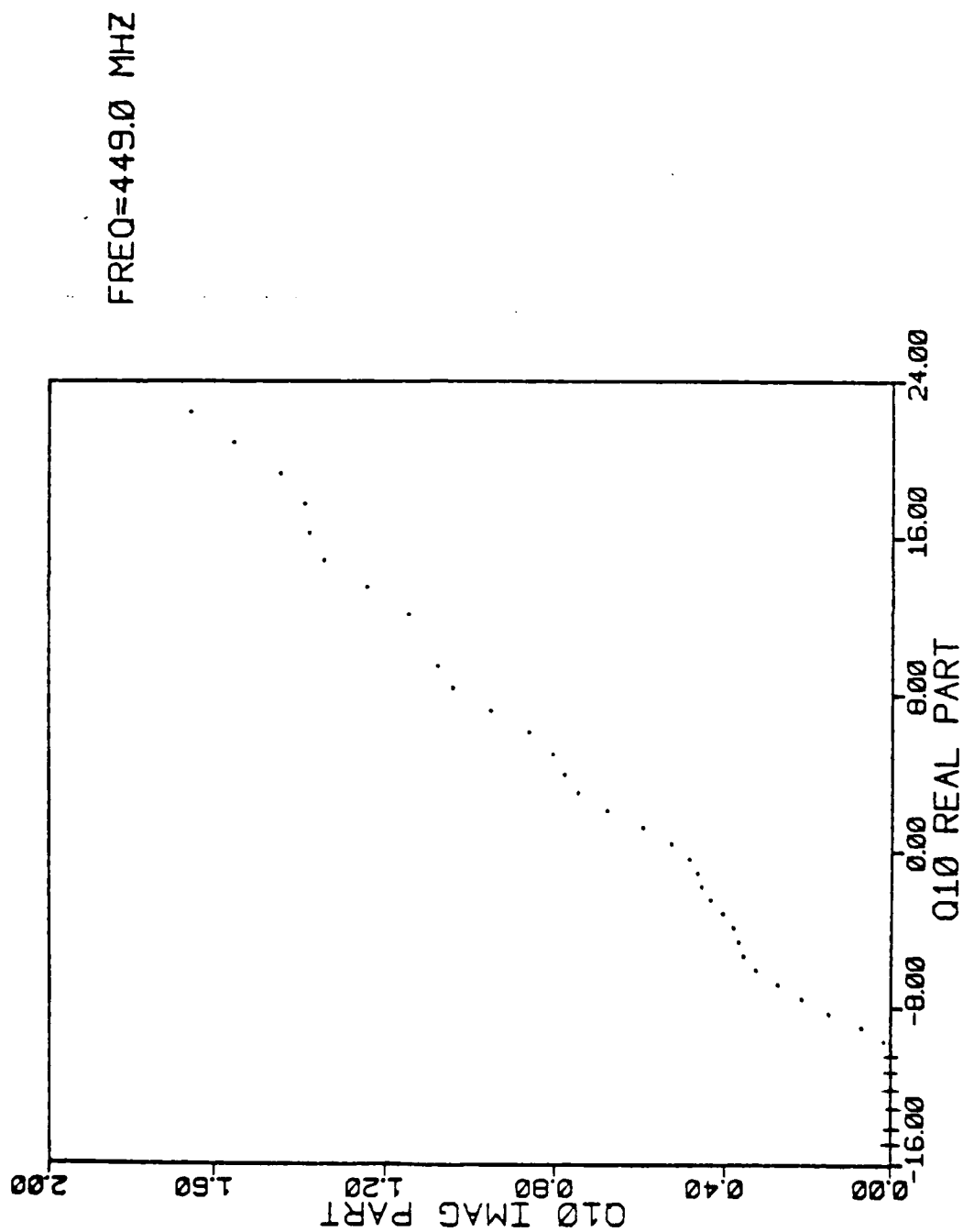
Figure 42. Eigenvalues produced by refractivity profile of Figure 41.

INFLUENCE OF DUCT THICKNESS AND INTENSITY

The propagation frequency of 449 MHz will be utilized to investigate the effect on the eigenvalue locus of a variation of duct thickness and intensity. Figures 43 through 48 provide illustrations of:

(1)   eigenvalue locations and

(2)   modal contributions

for ducts of decreasing thickness and intensity. In each case, the modified refractivity gradients in each region are the same as those in the profile of Figure 24. The boundary between region 2 and region 3, however, is lowered until, in Figure 48, region 2 disappears entirely.

As would be expected, Figures 43 and 48 show that the number of trapped modes decreases as the duct becomes less intense and narrower. The fluctuation in the eigenvalue locus also becomes subdued and disappears entirely when the duct disappears. The highest order modes become increasingly leaky as the duct strength diminishes. The fluctuation in the modal contributions to the field also becomes small, so that, in plot (B) of Figure 48, the inflection in the curve (see arrow in figure), which identifies the contribution as originating from the second order mode, is hardly distinguishable. In Figure 48, the lowest order mode from which plot (A) was constructed was the mode for which $Re(q_{10})$ is minimum -- this even though it does not have the lowest attenuation per kilometer (since it does not have the lowest value of $Im(q_{10})$). The contribution of the mode with lowest attentuation per kilometer is shown in plot (C) of the figure.
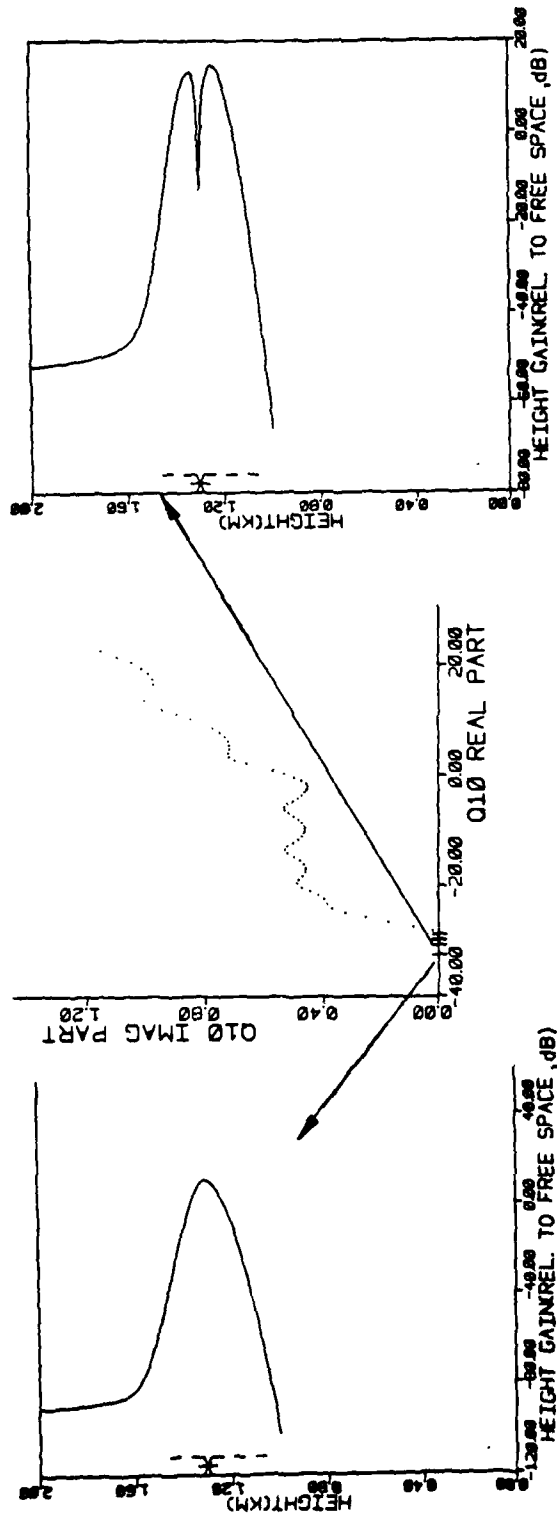
Figure 43. Eigenvalues and two of their field contributions for a refractivity profile with the same refractivity gradients and duct height as the profile of Figure 24, but with duct thickness = 0.4 km.

FREQ=449.0 MHZ, H POL

RANGE=500.0 KM

FS LOSS=139.5 DB

+   XMTR HEIGHT

___ MODE SUM
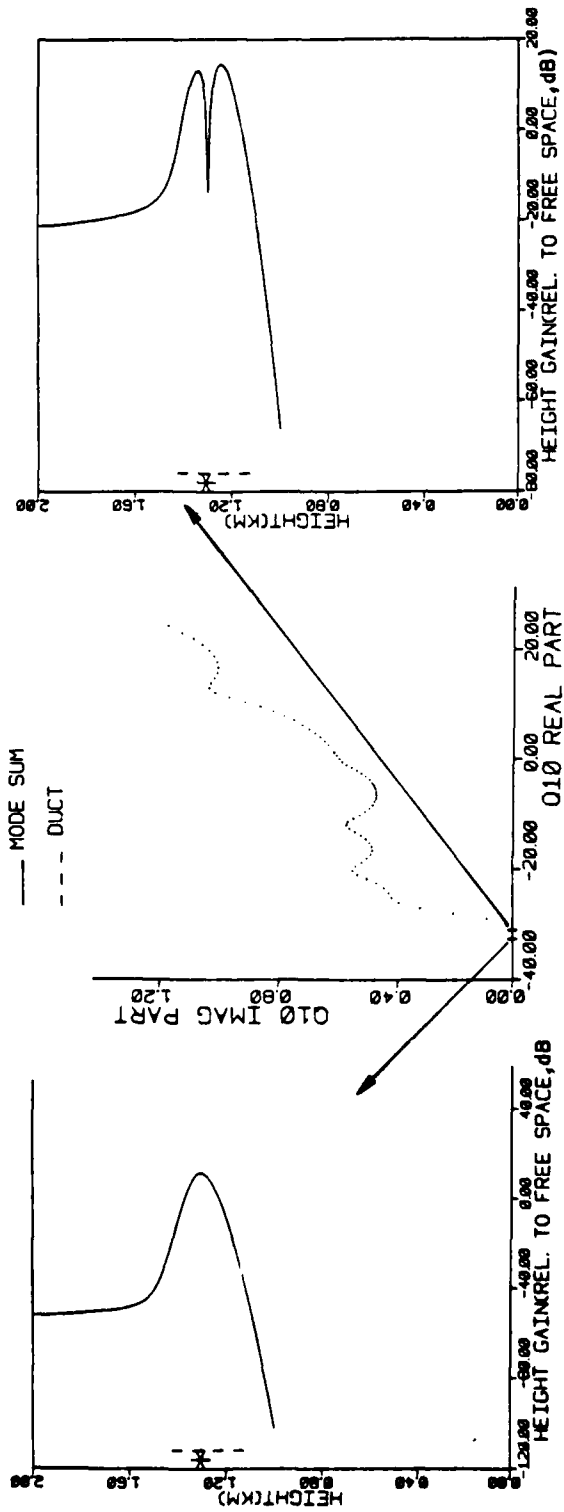
- - - DUCT

Figure 44.   Eigenvalues and two of their field contributions for a refractivity profile with the same refractivity gradients and duct height as the profile of Figure 24, but with duct thickness = 0.3 km.
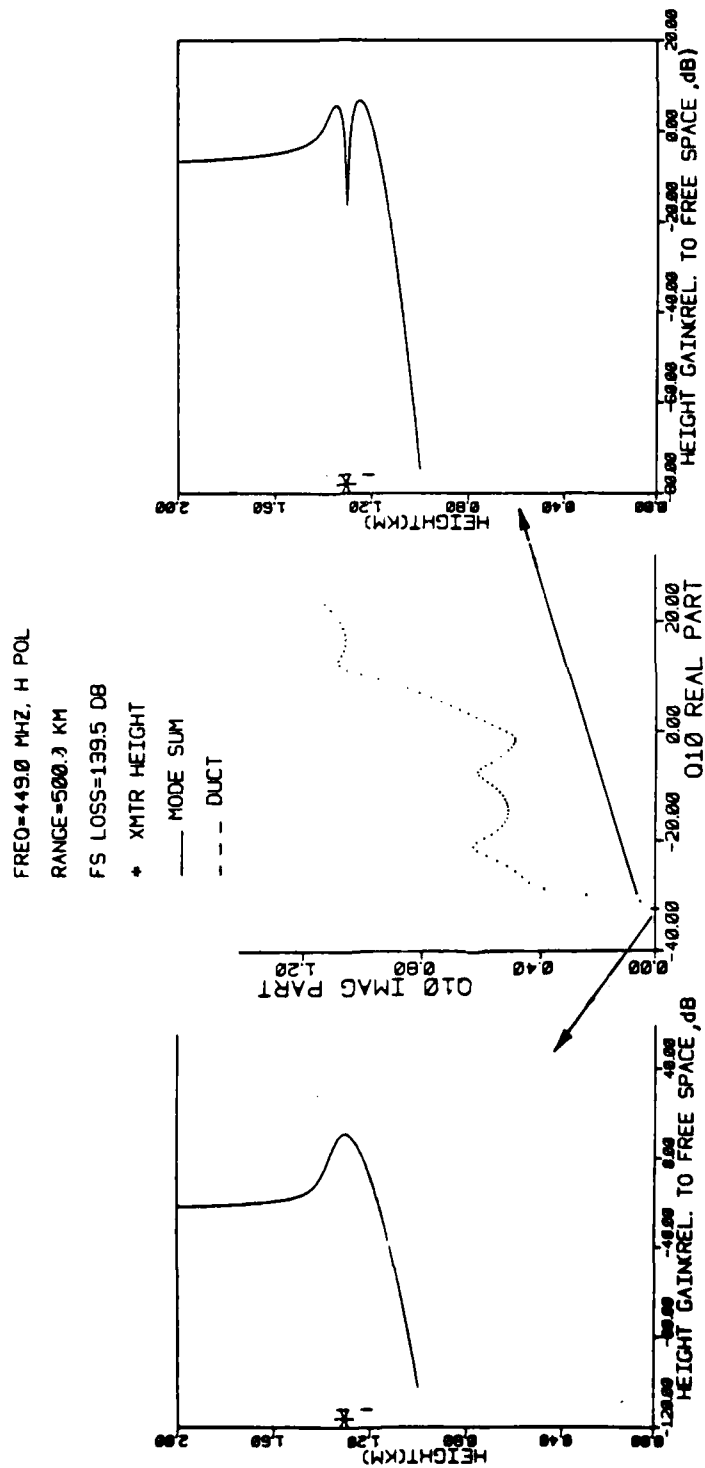
Figure 45. Eigenvalues and two of their field contributions for a refractivity profile with the same refractivity gradients and duct height as the profile of Figure 24, but with duct thickness = 0.2 km.
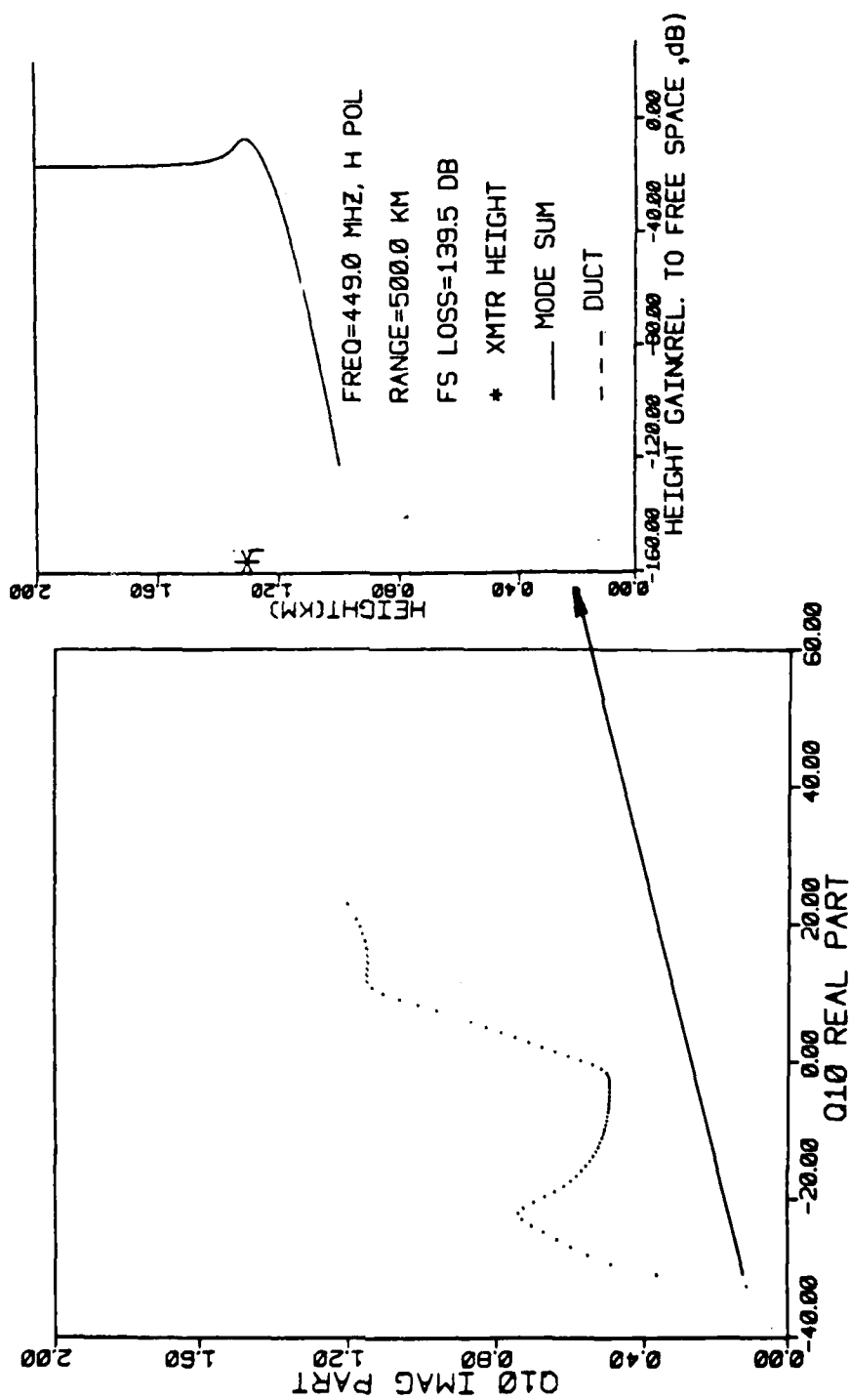
Figure 46.   Eigenvalues and fundamental mode field contributions for a refractivity profile with the same refractivity gradients and duct height as the profile of Figure 24, but with duct thickness = 0.1 km.
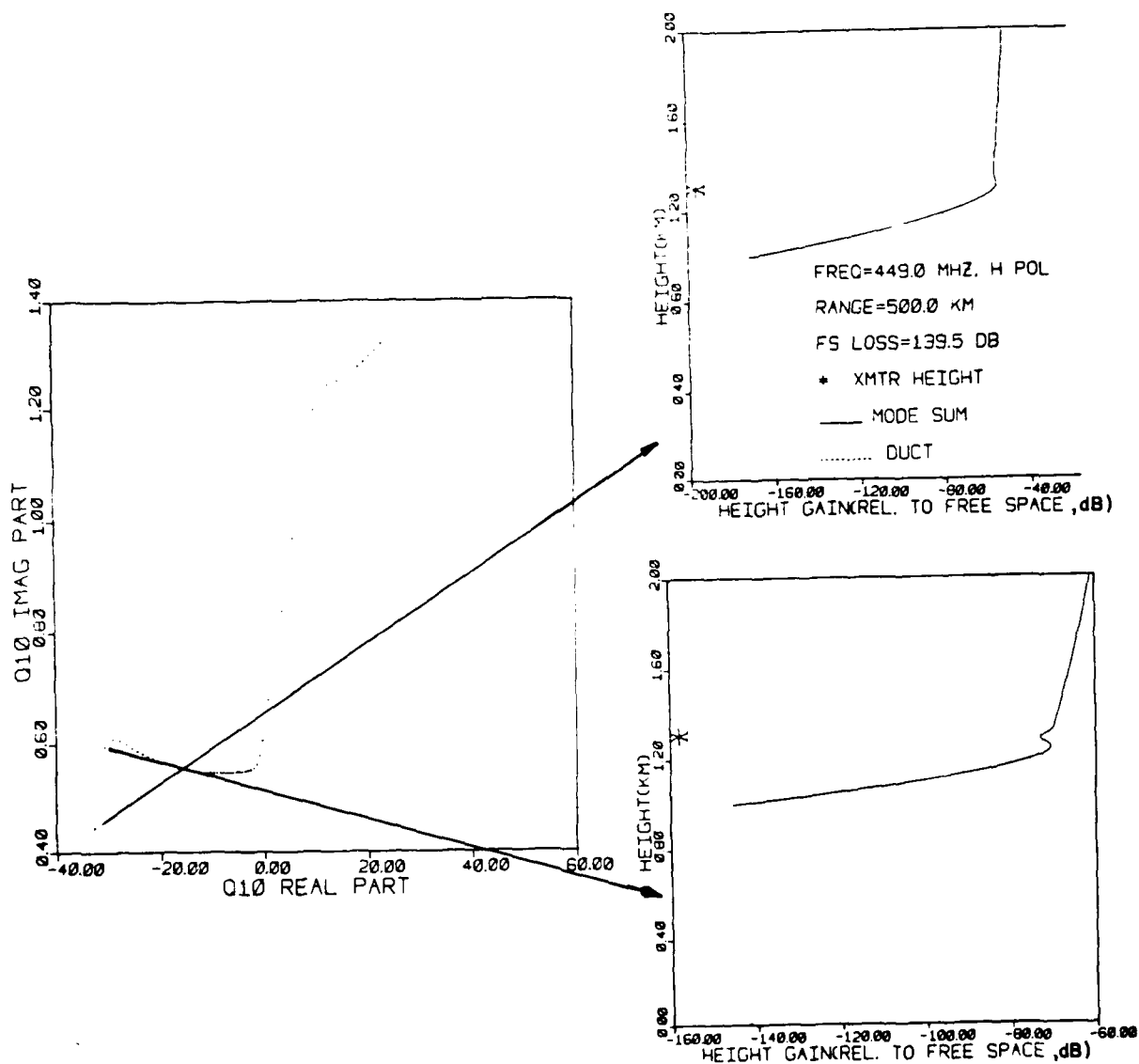
Figure 47. Eigenvalues and two of their field contributions for a refractivity profile with the same refractivity gradients and duct height as the profile of Figure 24, but with duct thickness = 0.05 km.

FREQ=449.0 MHZ, H POL

RANGE=500.0 KM

FS LOSS=139.5 DB   (B)

+ XMTR HEIGHT

—— MODE SUM

(A)

(C)
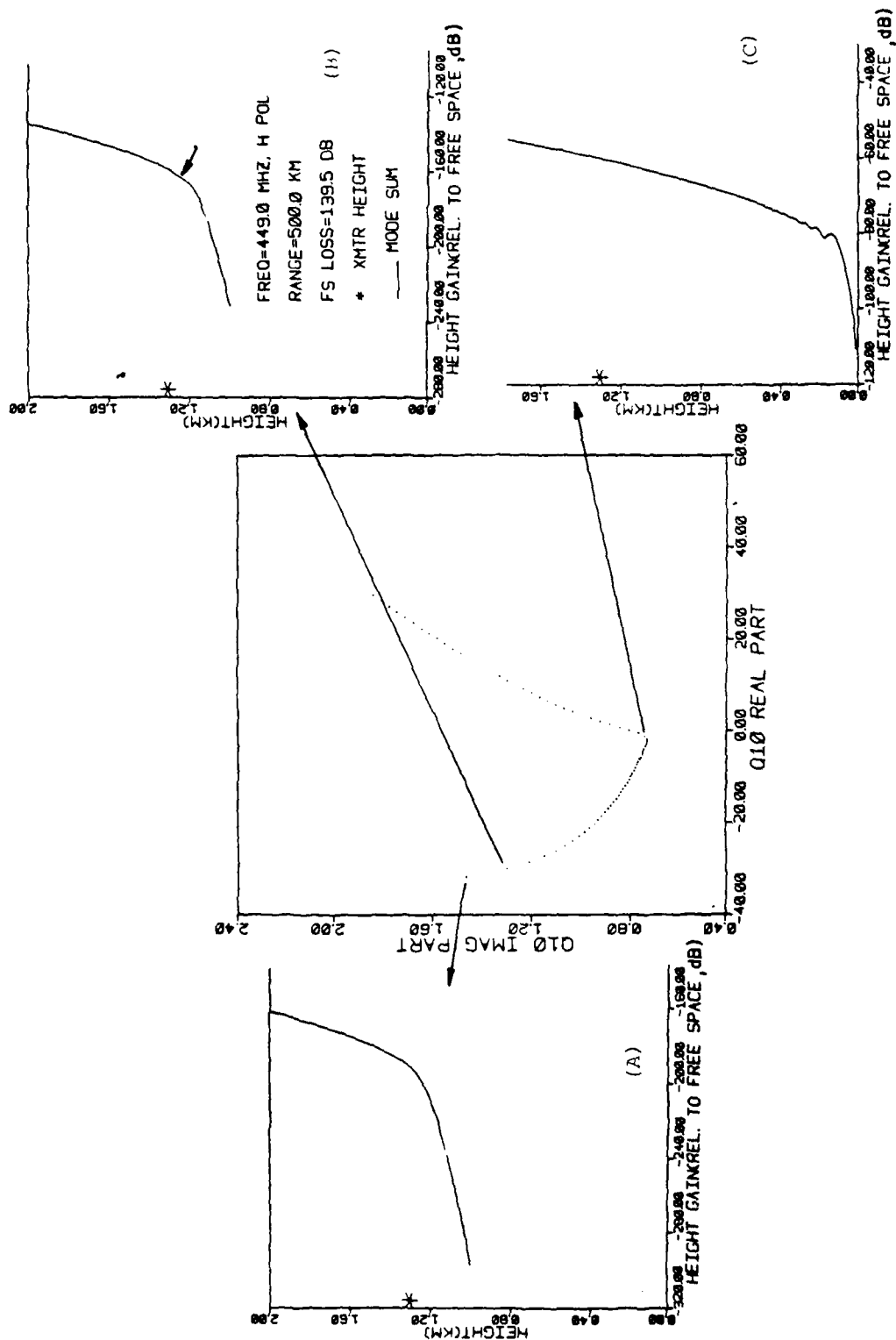
Figure 48.   Eigenvalues and some of their field contributions for a refractivity profile with the same refractivity gradients and duct height as the profile of Figure 24, but duct thickness = 0 km.

SECTION 7

ANALYSIS OF DUCTED FIELDS

FIELD SIMULATION BY PARTIAL MODE SUM

In the previous section, it was shown that specific types of propagation may be associated with different eigenvalues. Thus some eigenvalues will contribute only to trapped waves within the duct, some will contribute to leaky (or chordal) waves and some will be associated with multi-hop contributions caused by reflections from the ground. It was also shown that the locations of the eigenvalues in q_{10}-space that provide each type of contribution can generally be identified.

From Equations 67a and 68, the relative field may be written as:

$$A = \beta_o \left| \sum_n \lambda_n u_n(z_R) u_n(z_T) e^{-j\rho_n r} \right| \qquad (206)$$

where z_R and z_T are the receiver and transmitter heights, respectively, and the sum is over the eigenvalues. It will be noticed from Equation 206 that for each mode, there is reciprocity between the transmitter and receiver -- that is, the result remains unchanged if the transmitter and receiver heights are interchanged. Also, $u_n(z_R)$ characterizes the influence of the receiver height to the modal field contribution, and $u_n(z_T)$ characterizes the influence of the transmitter height to the modal contribution. This implies that, if both z_R and z_T are heights at which the same type of wave is dominant (e.g. trapped wave, chordal wave, multip-hop wave), then the dominant terms in the sum of Equation 206 will be those of the eigenvalues that contribute most to that type of wave. Thus, if both z_T and z_R are heights within the duct, the terms in Equation 206 representing the eigenvalues in region A (see Section 6) would contribute most significantly to the overall sum. Similarly, if z_T and

149

z_R are both near the ground, the dominant contributions in Equation 206 will be derived from the eigenvalues in region D.

If z_T is a height at which a particular type of wave is dominant, and z_R is a height at which a different type of wave is dominant, then the significant terms in the sum in Equation 206 would be those for the eigenvalues characterizing each of these types of waves.

The above considerations imply that, for certain specific propagation circuits of interest, it is possible to describe the relative fields by a relatively small number of eigenvalues. Since it is often possible to localize the region of the q_{10}-plane in which these eigenvalues lie (using the methods described in the previous sections), a significant saving in computation time may be realized.

Illustrating the point made above, consider the propagation in the duct in Figure 24. At 2201.7 MHz, the resulting eigenvalues were illustrated in Figure 27. A portion of these eigenvalues is shown in Figure 49. The location of the eigenvalues is independent of the transmitter and receiver heights. Assume the receiver and transmitter are both located within the duct. Then the dominant contribution to the field will derive from the eigenvalues close to the real axis in Figure 49. Figure 50 compares the field using all modes for which $Re(q_{10}) < -77$ with the total field using all the modes shown in Figure 27. It is seen that within the region of interest (i.e., within the duct), there is good agreement between the two cases. However, outside the duct, a large discrepancy between the two results is apparent, since eigenvalues that contribute to the regions outside the duct were not included in the partial mode sum. Figure 51 compares the field using all modes for which $Re(q_{10}) < -75$ (i.e., more modes than were used in Figure 50) with the total field using all modes. The agreement within the duct is even better than in the former case, and the field above the duct using the partial sum is closer to the total field than is the partial sum result in Figure 50.
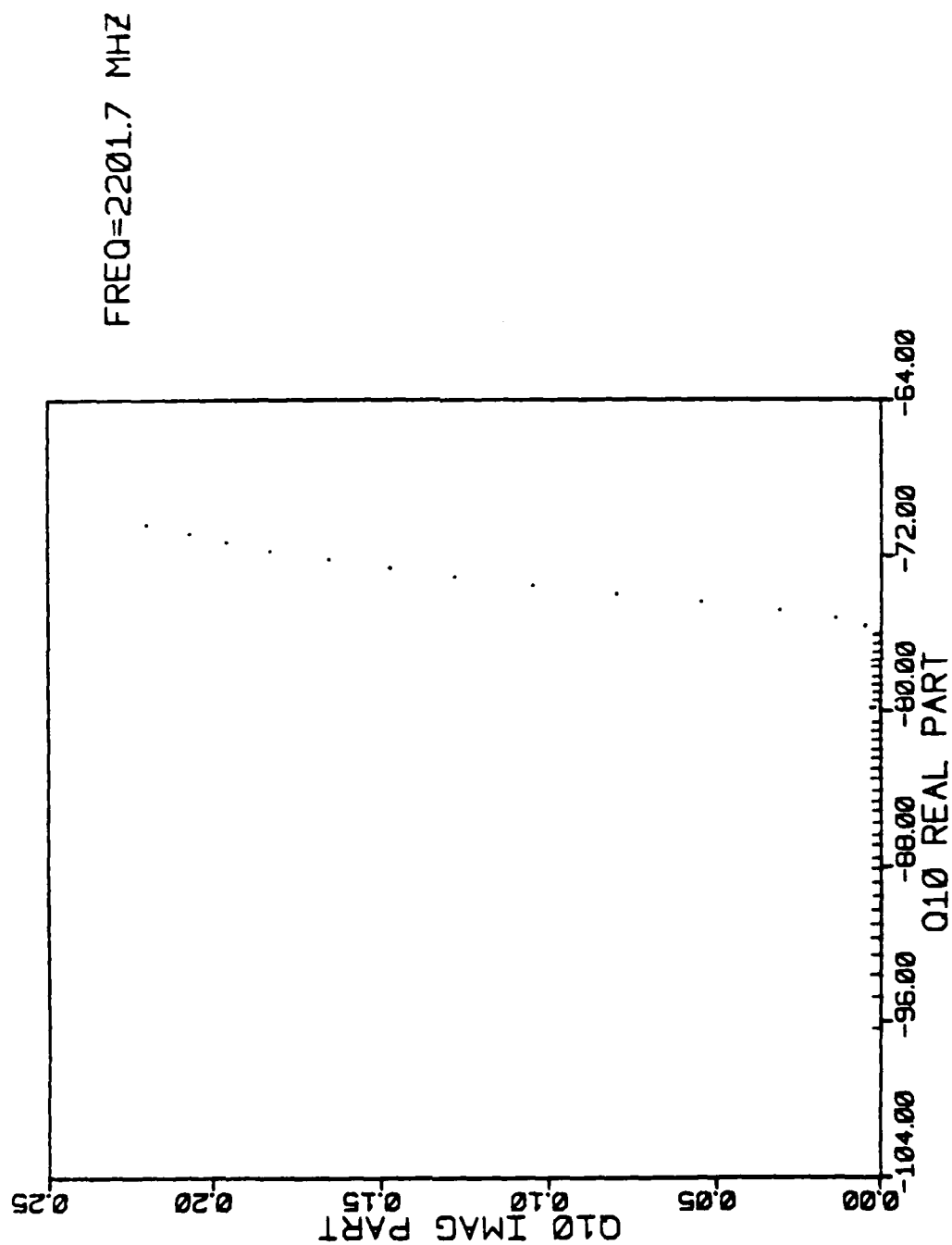
Figure 49. A portion of the eigenvalues shown in Figure 27.

FREQ=2201.7 MHZ, H POL

RANGE=500.0 KM

FS LOSS=153.3 DB

∗ XMTR HEIGHT

—— MODE SUM, MODES FOR WHICH RE(Q10) < -77

– – – DUCT

········ MODE SUM, ALL MODES

HEIGHT GAIN REL. TO FREE SPACE)
(dB)
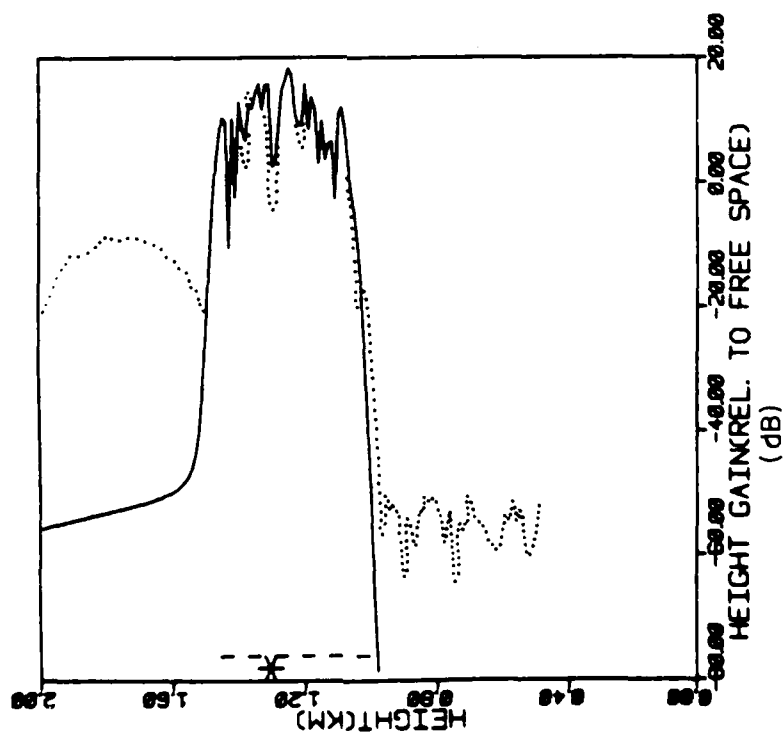
HEIGHT(KM)

Figure 50. Comparison of the fields calculated using all modes of Figure 27 with fields calculated using only the modes for which $Re(q_{10}) < -77$.

FREQ=2201.7 MHZ, H POL

RANGE=500.0 KM

FS LOSS=153.3 DB

＊ XMTR HEIGHT

——— MODE SUM, MODES FOR WHICH RE (Q10) < -75

– – – DUCT

……… MODE SUM, ALL MODES

HEIGHT GAINREL. TO FREE SPACE. dB)
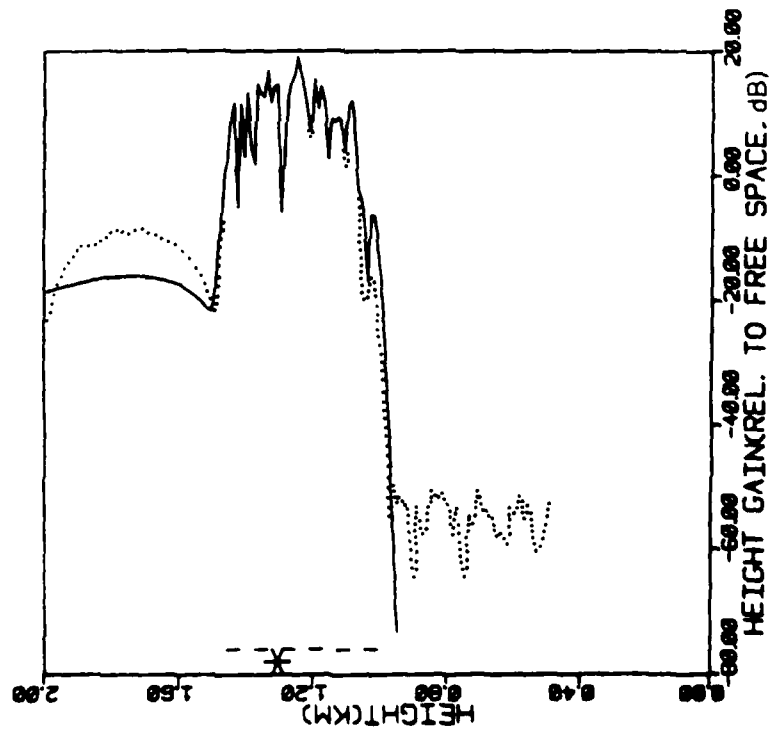
Figure 51. Comparison of the fields calculated using all modes of Figure 27 with fields calculated using only the modes for which $Re(q_{10})$ <-75.

DIFFERENCES BETWEEN MODE AND POWER SUMS - EFFECT OF PROFILE NORMALIZATION

In Section 5 it was seen that, in some cases, the "power sum" result (Equation 67d in Section 2) differed greatly from the "mode sum" result (Equation 67c). This difference was most obvious in Figures 22 and 23 in the region above the duct, and was apparently caused by extreme destructive interference between individual modal contributions that are significant at those heights. From the measured data shown in these figures, it appears that the power sum result is more realistic than the mode sum result. Since the mode sum is theoretically more accurate than the power sum, the question arises as to the reason for the discrepancy between the measurements and the mode sum results.

Skillman and Woods (Reference 9) suggested that the source of the problem might be a perturbation caused by horizontal refractivity inhomogeneities, or by inadequacy of the mathematical model. The fact that the problem seems to occur only at high altitudes might point more to the latter explanation. Pekeris (Reference 4) showed that the "earth-flattening" approximation used in this mathematical model (in which the curvature of the earth was taken into account by modifying the refractivity profile) would become less accurate as the altitude increases. This inaccuracy would affect both modal amplitudes and modal phases. Since phases would generally have a more dramatic influence on the calculated field than small differences in amplitudes, the solution that strictly accounts for these phases would be expected to go awry prior to the solution that assumes phase incoherency. This would explain the reason for the power sum solution providing predictions in Figures 21 and 22 that are superior to the mode sum predictions.

To illustrate the effect on the relative field strength of small differences in modal phases, it is interesting to compare the relative field strength results for the case of a "normalized" refractivity profile (see Section 3), with the case of an unnormalized refractivity profile. As

154

discussed in Section 3, the principal computational difference between these two cases appears in the value of ρ_n in the exponent in Equation 206. From Equation 94, for the unnormalized profile:

$$\rho_n = k_o \sqrt{1 - H_1 \tan \alpha_1 - \frac{q_{10}^{(n)}}{\left(\frac{k_o}{|\tan \alpha_1|}\right)^{2/3}}} \qquad (207)$$

while for the normalized profile,

$$\rho_n = k_o \sqrt{1 - \frac{q_{10}^{(n)}}{\left(\frac{k_o}{|\tan \alpha_1|}\right)^{2/3}}} \qquad (208)$$

Since $|\tan \alpha_1| \ll 1$, the difference between ρ_n as defined by Equation 207 and ρ_n as defined by Equation 208 is very small. Figure 52 provides results using the normalized refractivity profile of Figure 24 and using a corresponding unnormalized profile for a frequency of 449 MHz. In the unnormalized refractivity profile, the modified refractivity at the ground is taken as 300 (instead of zero). The power-sum results for both the normalized and unnormalized profiles are identical. However, these profiles produce different results using the mode sum. Note also that the results differ only in the region above the duct, but are the same within and below the duct.

FREQ=449.0 MHZ, H POL

RANGE=500.0 KM

FS LOSS=139.5 DB

* XMTR HEIGHT

——— MODE SUM, UNNORMALIZED PROFILE

. . . PWR SUM

– – – DUCT

–·–·– MODE SUM, NORMALIZED PROFILE
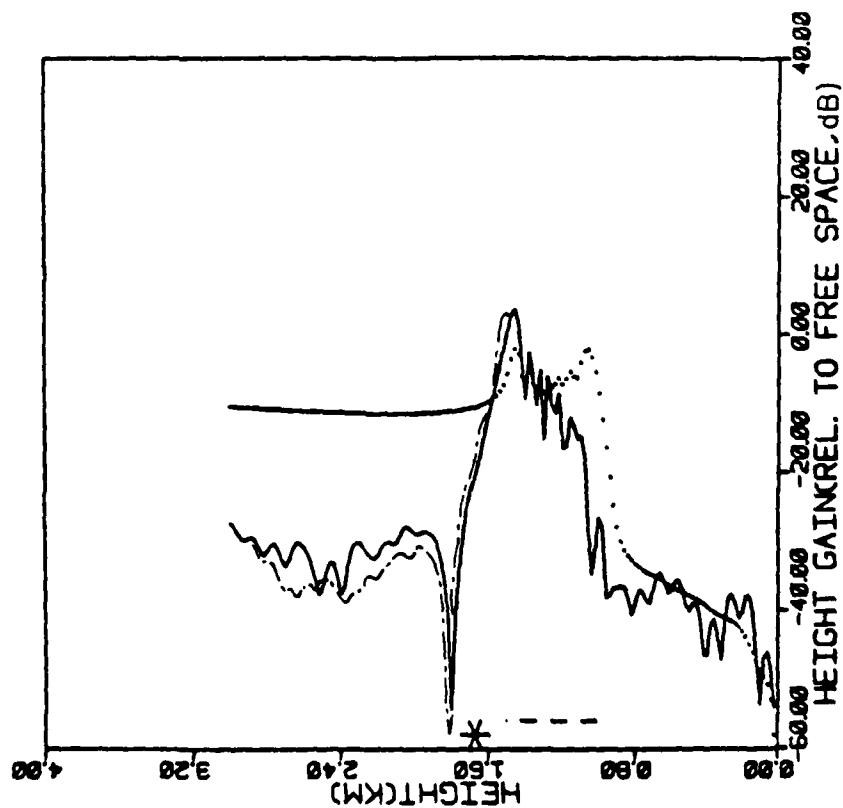
Figure 52. Comparison of fields using normalized and unnormalized refractivity profiles.

EFFECT OF TRANSMITTER HEIGHT - SINGLE DUCT

Elevated Duct

To investigate the effect of the transmitter height on the relative field
strength, the elevated duct profile of Figure 24 will be used for a frequency
of 2201.7 MHz. The mode-sum and power-sum results are presented in Figure 53
in order of decreasing transmitter height (indicated by an asterisk in the
left portion of each plot.) In Figures 53a and 53b, the transmitter is
located above the duct. The transmitter is within the duct in Figures 53c,
53d, 53e, and 53f. In Figures 53g and 53h, the transmitter is below the duct.

When the transmitter is above or in the duct, the fields in or above the
duct are relatively large. The optimum coupling of energy into the duct
occurs when the transmitter is near the duct center. When the transmitter is
above or in the duct, the fields are greatest within the duct. When the
transmitter is below the duct, field enhancement due to the presence of the
duct is negligible or absent entirely.

By reciprocity, the results cited above would hold if the receiver and
transmitter were interchanged. It may therefore be concluded that, under
suitable duct environments (i.e., environments in which the minimum trapping
frequency of the duct is less than the transmission frequency), the duct
serves to significantly enhance the fields when both the transmitter and
receiver are in or above the duct. If either terminal of the propagation
circuit is below the duct, the resulting fields would not be significantly
enhanced by the presence of the duct.

Surface Duct

The fields in a surface duct will now be considered for different
transmitter heights. The duct profile of Figure 34 will be used for

157
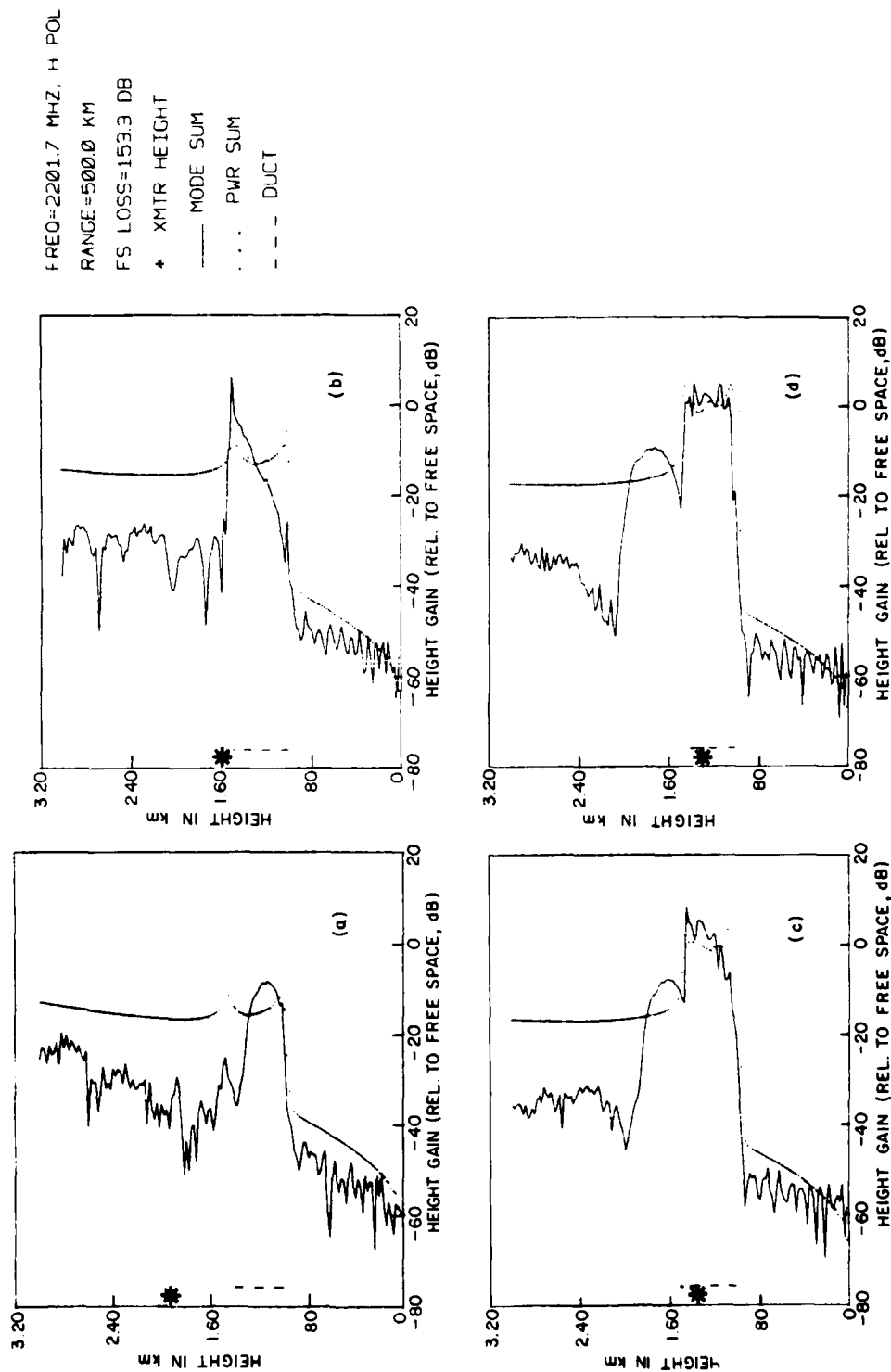
Figure 53. Fields calculated for different transmitter heights using the refractivity profile of Figure 34.

FREQ=2201.7 MHZ. H POL
RANGE=500.0 KM
FS LOSS=153.3 DB
* XMTR HEIGHT
——— MODE SUM
········· PWR SUM
— — DUCT
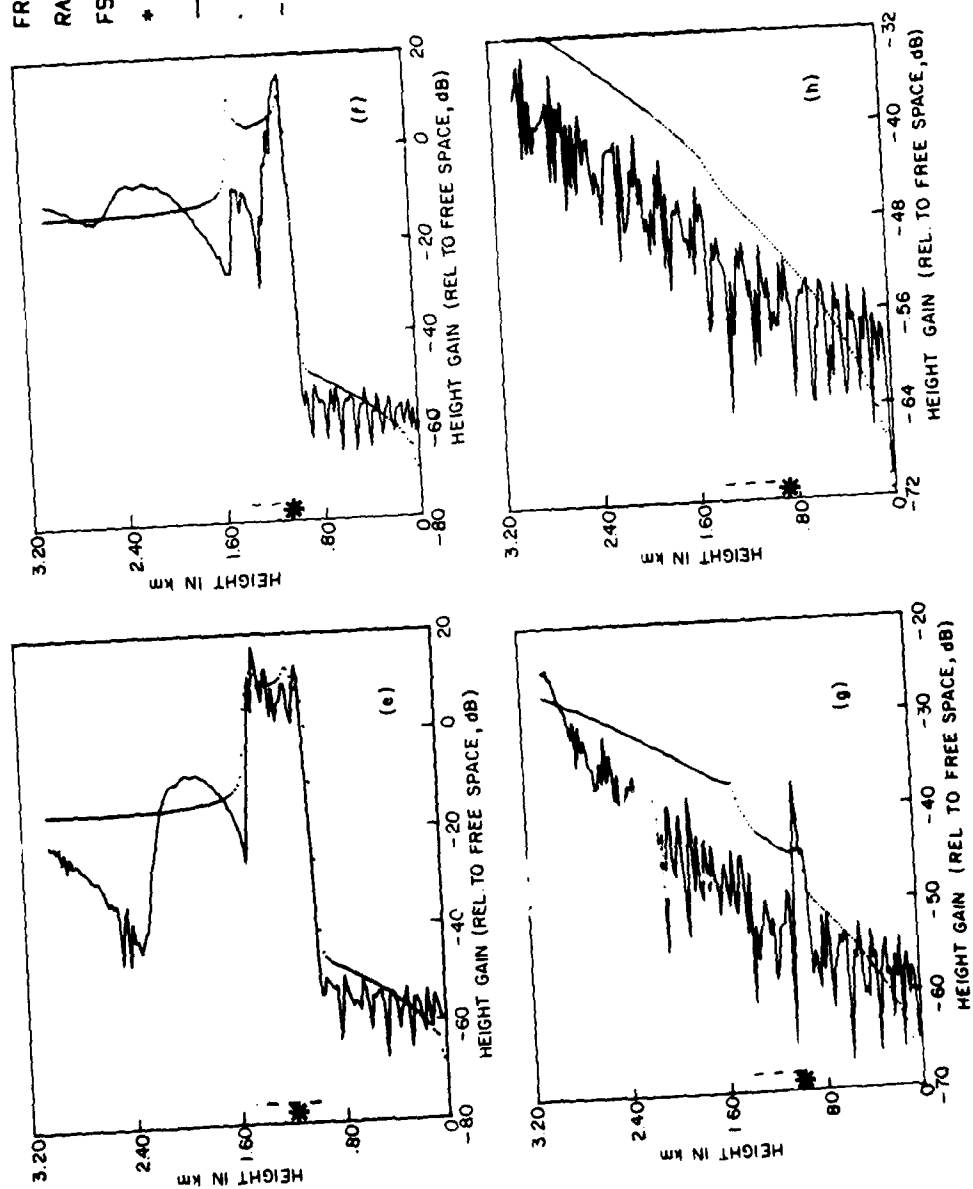
Figure 53. (Page 2 of 2).

a frequency of 3300 MHz. Figure 54a shows the fields calculated using the mode-sum series for three transmitter heights: one outside the duct and two within the duct. Figure 54b shows the corresponding fields using the power sum solution. Notice that, contrary to the case of elevated ducts, the field is weaker in the duct than above it when the transmitter is above the duct. This would be due to the fact that, when the source and observer are both above the duct and separated by a distance of 111.2 km, they are within line of sight of each other.

In Figures 54a and 54b, the transmission is taken as being vertically polarized. The results for this case were found to be identical to those using horizontal polarization.

FREQ=3300.0 MHZ, V POL

RANGE=111.2 KM

FS LOSS=143.7 DB

* XMTR HEIGHT

___ MODE SUM

_ _ _ DUCT
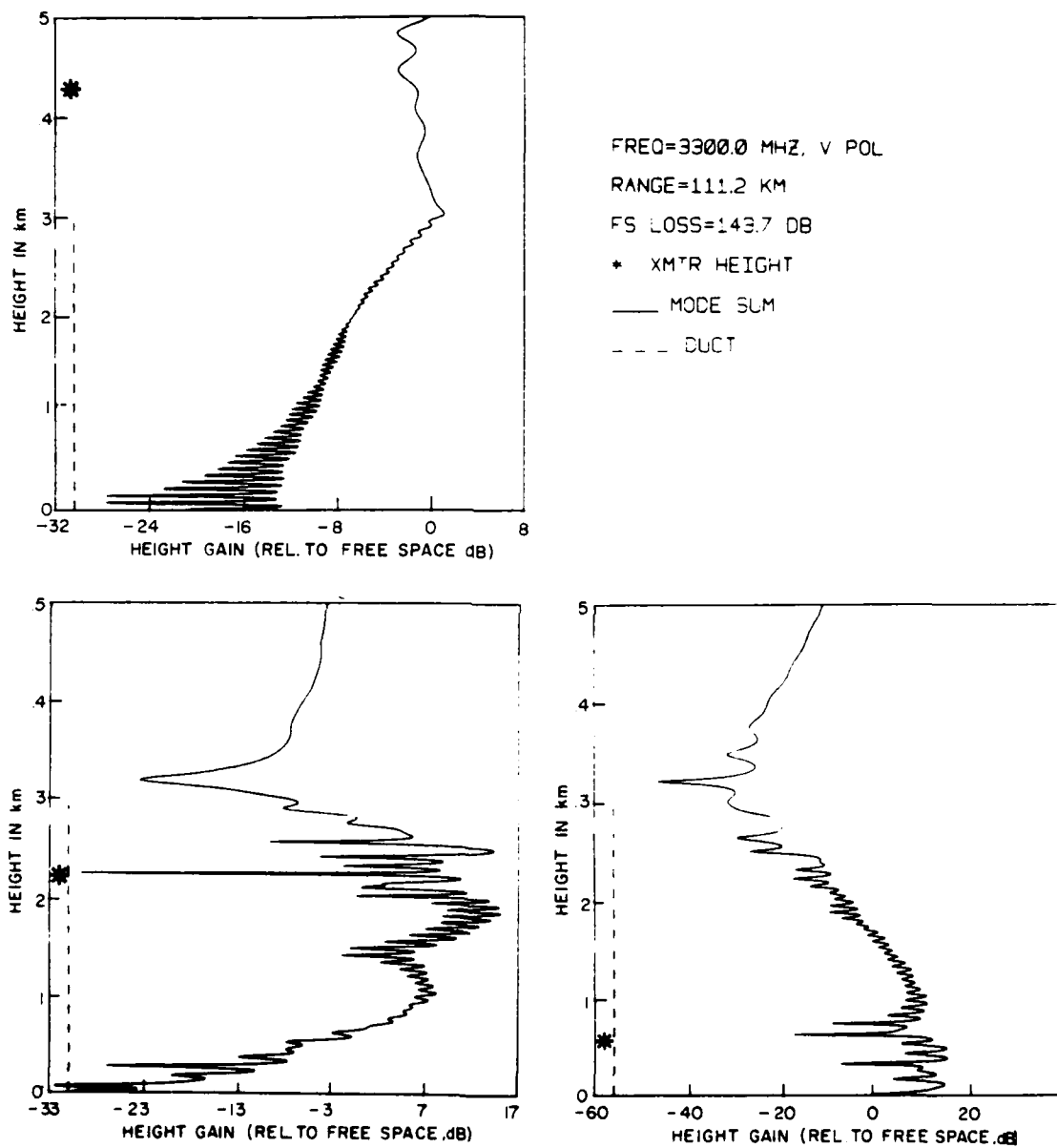
Figure 54a.   Mode sum fields calculated using the refractivity profile of
Figure 34 for different transmitter heights.

161

FREQ=3300.0 MHZ. V POL
RANGE=111.2 KM
FS LOSS=143.7 DB
- XMTR HEIGHT
— PWR SUM
... DUCT
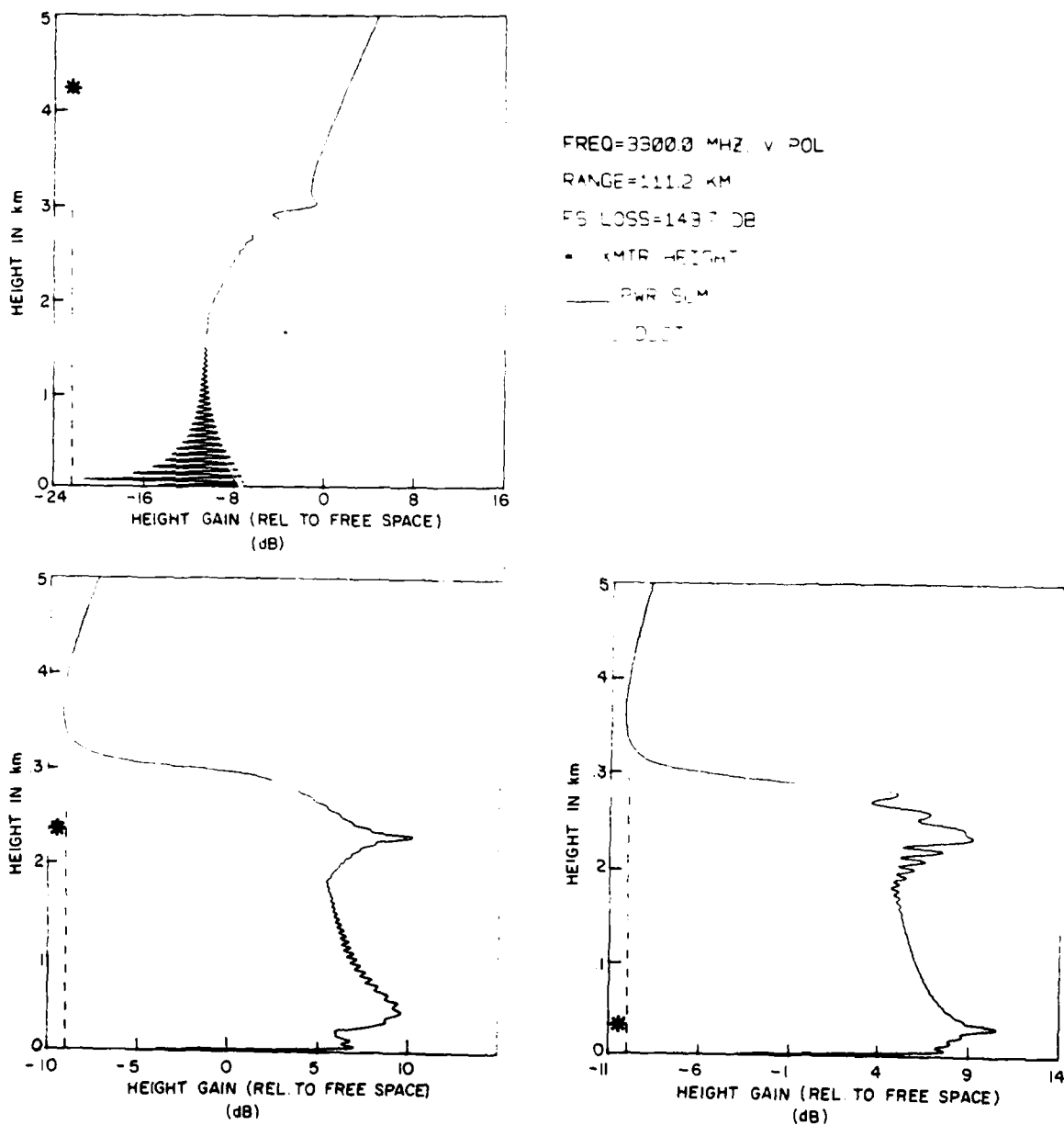
Figure 54b.   Power sum fields calculated using the refractivity profile of
               Figure 34 for different transmitter heights.

162

EFFECT OF TRANSMITTER HEIGHT - DOUBLE DUCT
──

The effect of transmitter height on relative field strength will now be
investigated for the two-duct refractivity profile illustrated in Figure 32
for a frequency of 449 MHz. The mode-sum and power-sum results are presented
in Figures 55a through 55d in order of decreasing transmitter height. In
Figure 55a, the transmitter is above the upper duct; in Figure 55b, the
transmitter is within the upper duct; in Figure 55c, the transmitter is
between the upper and lower ducts; and in Figure 55d, the transmitter is
within the lower duct. The effect of each duct (or lack of effect) is obvious
in each figure. It is clear that the field is greatest within each duct when
the transmitter is located within it. From Figures 55c and 55d, it is seen
that, when the transmitter is below the upper duct, the field in the upper
duct is similar to the field that would be expected if the upper duct were not
present. The lower duct, however, serves to enhance the field in these cases.

The conclusions drawn for the single duct environment may be generalized
to the two-duct environment: Each duct will significantly enhance the fields
when both the transmitter and receiver are in or above it. If either terminal
of the propagation circuit is below one duct (or both ducts), then the
resulting field will not be enhanced by the presence of that (those) ducts.
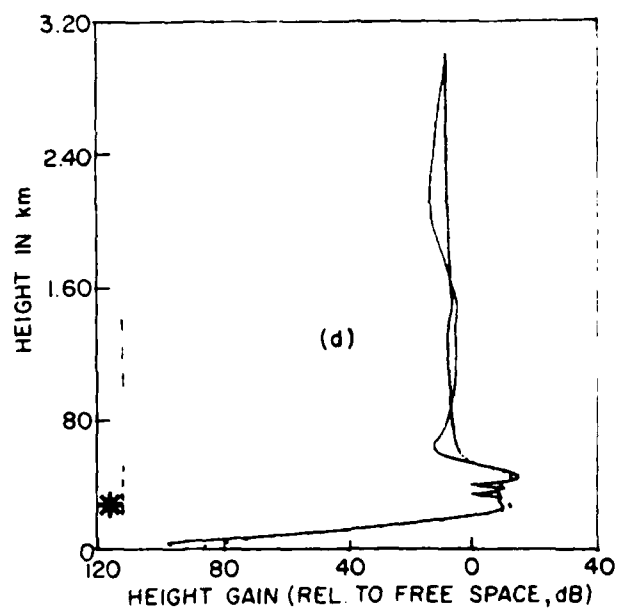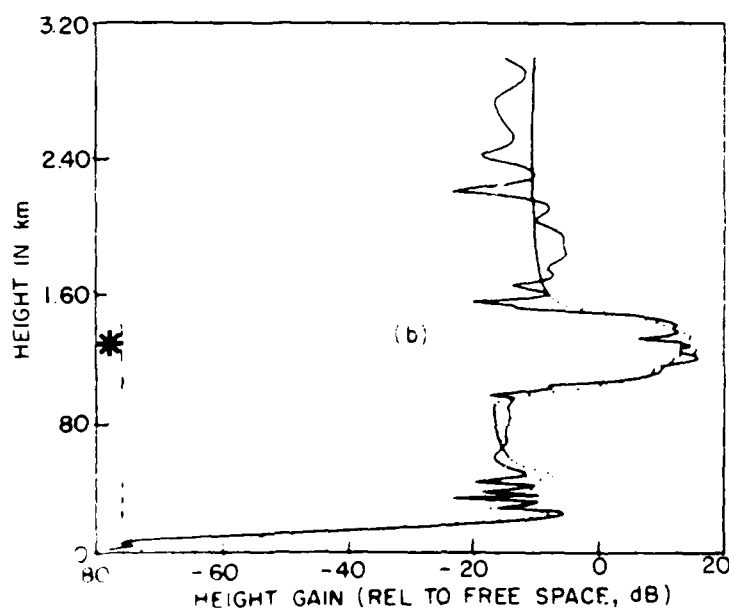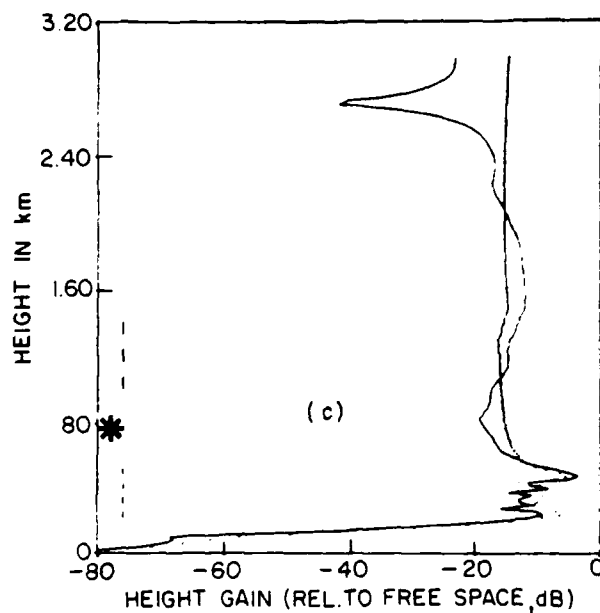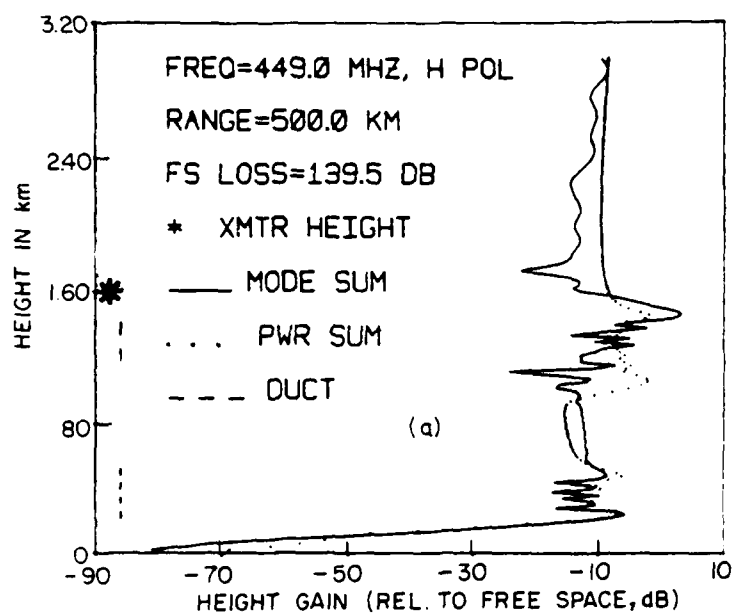
predicted using the refractivity profile of Figure 34
transmitter heights.

EFFECT OF DUCT THICKNESS AND INTENSITY

The propagation frequency of 449 MHz will now be utilized to investigate the effect on the calculated fields of a variation of duct thickness and intensity. In each case considered, the modified refractivity gradient in each region is the same as that in the profile of Figure 24. The variation in duct thickness and intensity is obtained by lowering the boundary between region 2 and region 3 until region 2 disappears entirely. This is accomplished for three different transmitter heights in Figures 56, 57 and 58, respectively. In Figure 56, the transmitter is located above the duct, in Figure 57 the transmitter is located within the duct, and in Figure 58, the transmitter is located below the duct. In each figure, relative field calculations are presented for different duct thicknesses (and intensities).

In Figures 56 and 57 (in which the transmitter is above the duct and within the duct, respectively) it is observed that, for the first two or three duct thicknesses considered, the maximum field within the duct remains about the same. The fields in the duct fall off rapidly for ...aller ducts. In Figure 58, the fields are very similar for all finite duct thicknesses, but are appreciably smaller in the limit of an absence of the duct.

The discrepancy in the figures between the mode-sum and the power-sum results for the smaller duct sizes was not investigated.
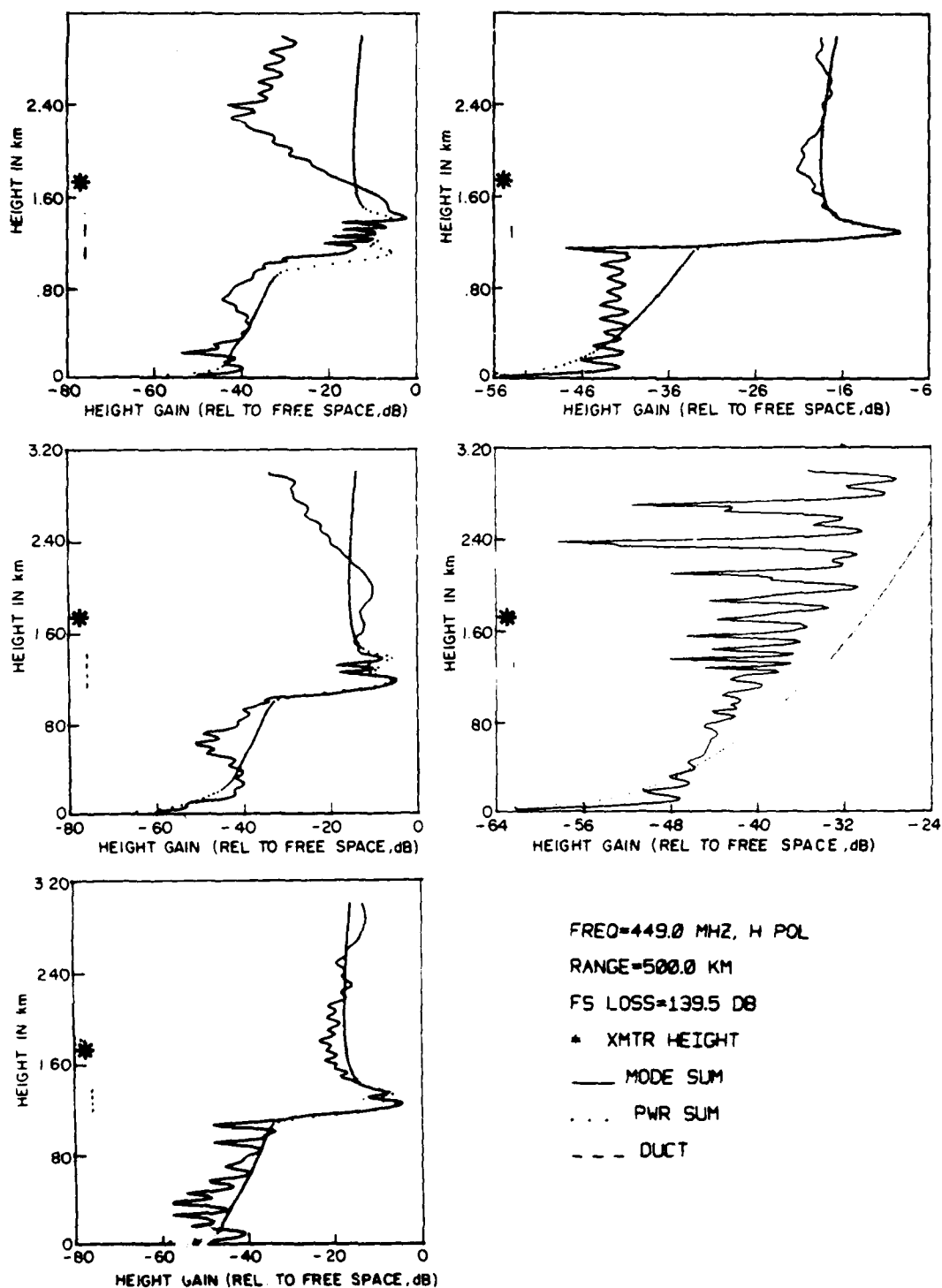
Figure 56. Fields calculated using a refractivity profile with the same refractivity gradients and duct height as the profile of Figure 24, for different duct thicknesses (transmitter above the duct).
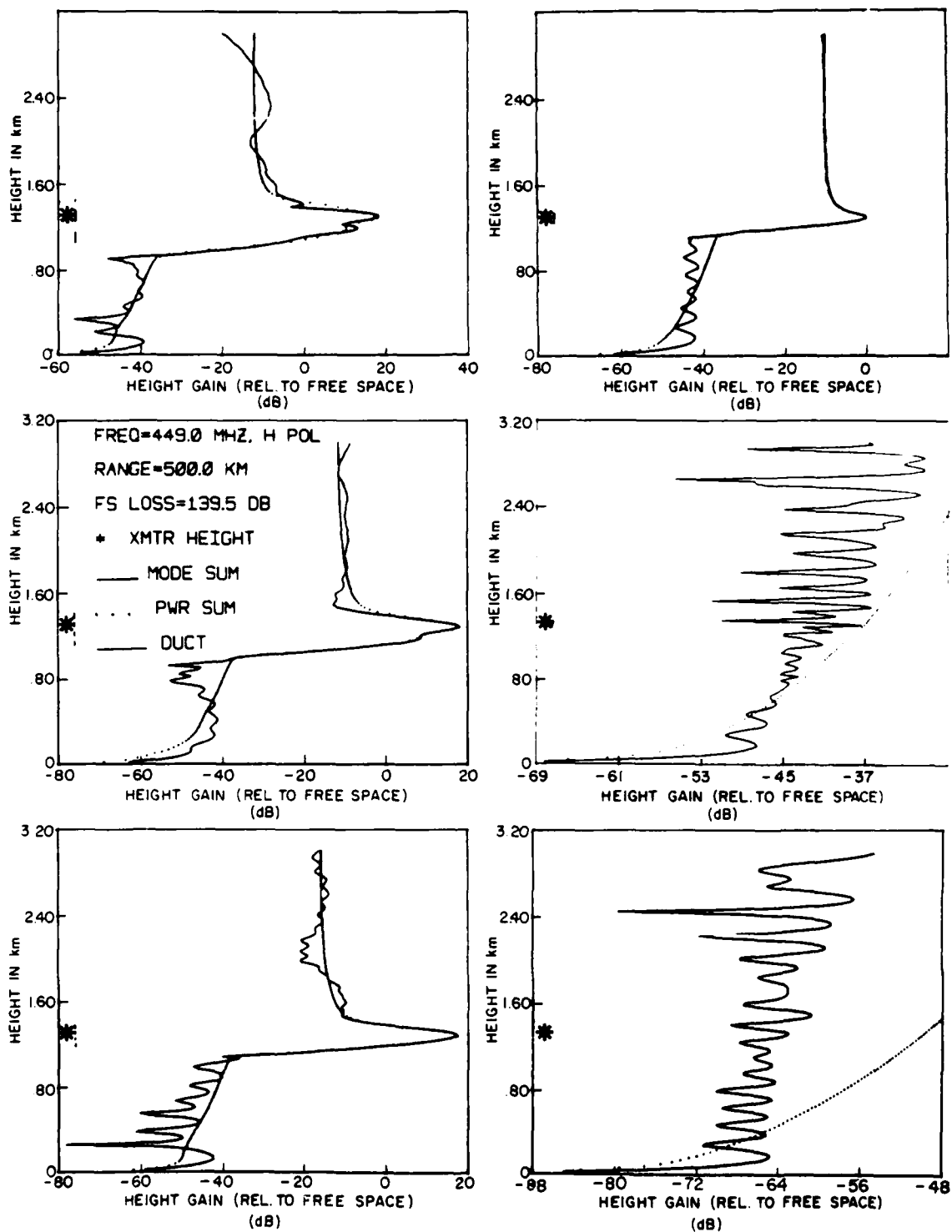
Figure 57.   Fields calculated using a refractivity profile with the same
             refractivity gradients and duct height as the profile of
             Figure 24, for different duct thicknesses (transmitter
             with the duct).

167
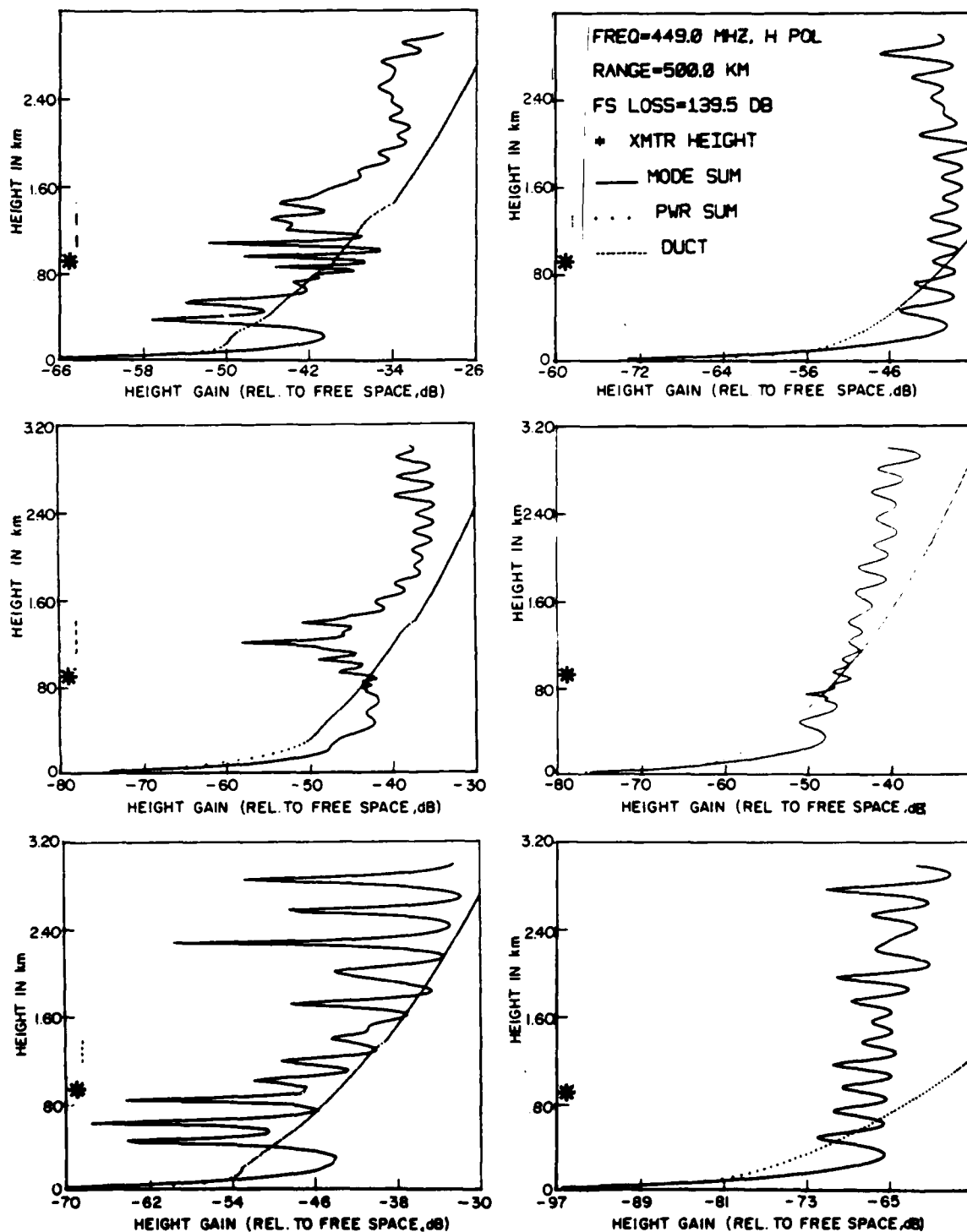
Figure 58.   Fields calculated using a refractivity profile with the same
             refractivity gradients and duct height as the profile of
             Figure 24, for different duct thicknesses (transmitter
             below the duct).

168

EFFECT OF FREQUENCY

The effect of frequency variation on the calculated field will now be investigated for the elevated duct profile of Figure 24. Measurements documented by Skillman and Woods (Reference 9) for a duct environment similar to this indicated that the relative field variation with height was similar for frequencies 449.2 and 2201.7 MHz. Their results were illustrated in Section 5. They succeeded in predicting the results for frequencies of 149.3 and 449.2 MHz using a computer program developed by Pappert and Goodhart (Reference 5).

In Figure 59, calculated results are presented for frequencies 149, 449, 2201.7 and 10000 MHz. The results for the 449 and 2201.7 MHz cases were compared in Section 5 with measurements documented by Skillman and Woods (Reference 9). It is seen here that not only are the 449 and 2201.7 MHz results similar to each other, but they are both similar to the results for 10000 MHz. This bears out the suggestion of Skillman and Woods that, in duct environments, it might be possible to utilize calculations at lower frequencies to determine relative fields at higher frequencies.
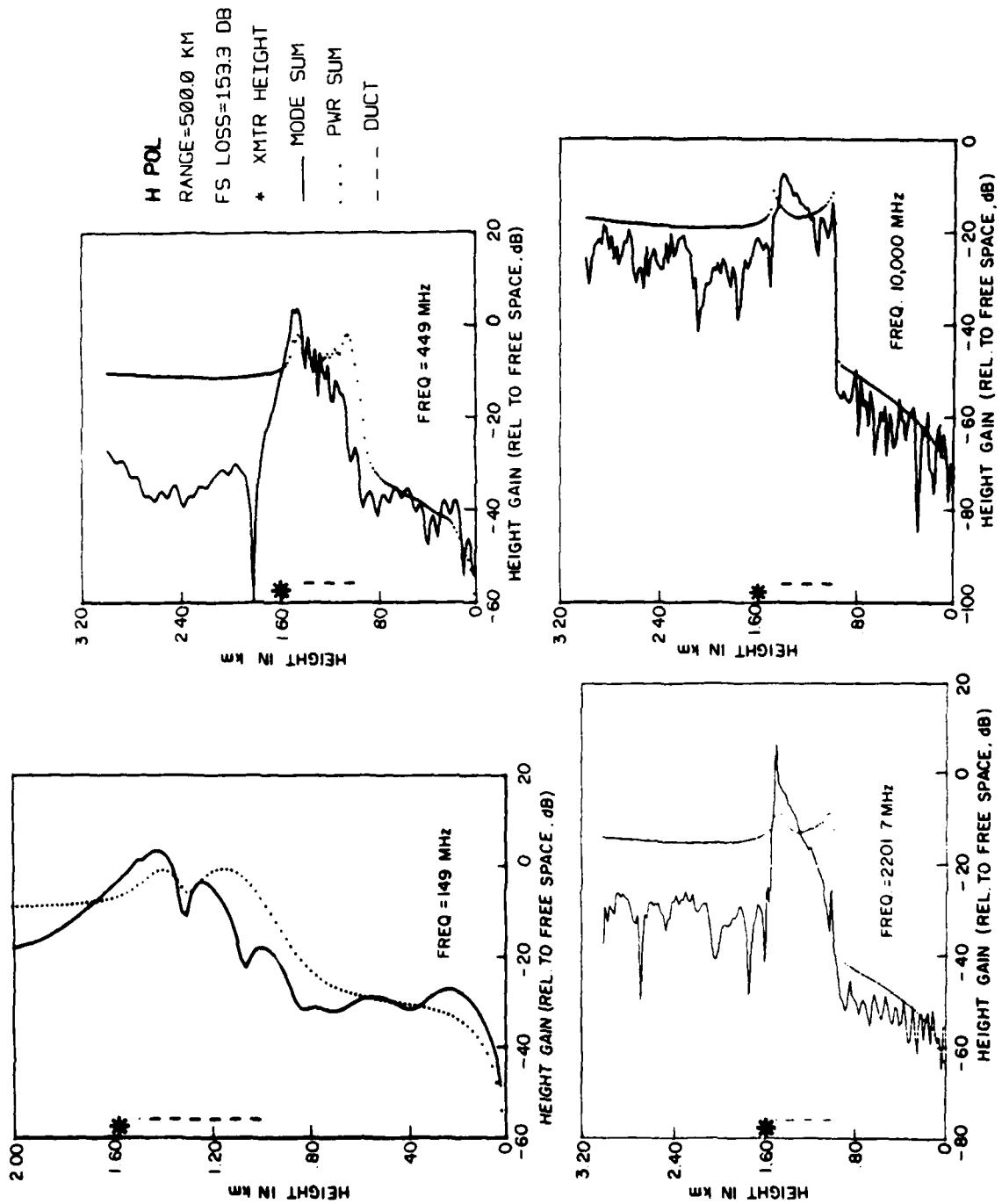
Figure 59. Fields calculated for different frequencies, using the refractivity profile of Figure 24.

SECTION 8

CONCLUSIONS AND RECOMMENDATIONS

CONCLUSIONS

1.   A reliable computer model, based on a waveguide mode
formulation, has been developed for calculating beyond-line-of-sight
electromagnetic fields in a horizontally stratified tropospheric duct
environment.

2.   The model is capable of evaluating fields for higher elevated
ducts and higher frequencies (i.e., through SHF) than were previously feasible
in other available models, which had numerical difficulties that precluded
computation of all significant eigenmodes of the system.

3.   The types of numerical difficulties encountered in other models
were eliminated by the use of a unique mathematical formulation that

        a.   Assures linear independence (Equations 104 to 106), even in
a "numerical sense", of the homogeneous form of the governing differential
equation; and

        b.   Provides flexibility for judiciously choosing the
particular solution (Equation 189) to the inhomogeneous form of the governing
differential equation.

4.   The model methodically and efficiently determines all
significant eigenvalues (Section 3) and corresponding fields (Section 4) for
elevated and surface ducts at all frequencies through SHF.

5.   Criteria have been developed (Equation 205) for associating
specific types of field contributions with eigenvalues in a specific portion
of the eigenvalue locus. These criteria have the potential for increasing the
computational efficiency of the model in certain circumstances.

6.   The model has been verified by comparing its predictions with measurements in both elevated and surface duct environments (Section 5).   It is the only known computer model that provides predictions which agree within a few dB with field strength measurements performed in an elevated duct environment at frequencies as high as 2201 MHz (Figure 23).

7.   The model is deemed to be a valid tool for predicting and studying electromagnetic fields in a tropospheric duct environment.

RECOMMENDATIONS

1.   Measured data on the probability of occurrence of ducts of various characteristics in various geographical locations should be analyzed and used in the deterministic model in a manner that would provide statistical loss values.   The results should specify the probability of loss as a function of geographical locations and seasons.   These statistical loss values should be used to revise the long-term power fading subroutine used in ECAC propagation models.

2.   The model should be extended to predict loss values at distances within line-of-sight.

3.   The model should be extended to account for the effect of obstructions in front of the antenna.

4.   The model should be extended to allow a nonhomogeneous horizontal refractivity.

APPENDIX A

ASYMPTOTIC BEHAVIOR OF $h_1(q)$ AND $h_2(q)$ AND $F(q)$ IN THE UPPER
HALF OF THE q-PLANE

Values of the real and imaginary parts of h_1 in the complex q-plane are
shown in Figures A-1 and A-2, respectively. The corresponding values for h_2
are given in Figures A-3 and A-4. When $|q|$ is small, h_1 and h_2 are both of
order unity, as must be $F(q)$, defined from Equation 98 as:

$$F(q) \equiv h_2(q) - e^{\frac{4}{3}\pi j} h_1(q) \tag{A-1}$$

$|h_1|$, $|h_2|$ and $|F|$ only become exponentially large or small when $|q|$ is
large. These functions may therefore be studied using their asymptotic
expansions. These asymptotic expansions will be defined according to
Reference 14. It is convenient to define the following:

$$u(q) = Aq^{-\frac{1}{4}} e^{-5\pi j/12} [1 + \sum_{m=1}^{\infty} (-j)^m C_m q^{-3m/2}] \tag{A-2}$$

$$v(q) = Aq^{-\frac{1}{4}} e^{5\pi j/12} [1 + \sum_{m=1}^{\infty} (j)^m C_m q^{-3m/2}] \tag{A-3}$$

173
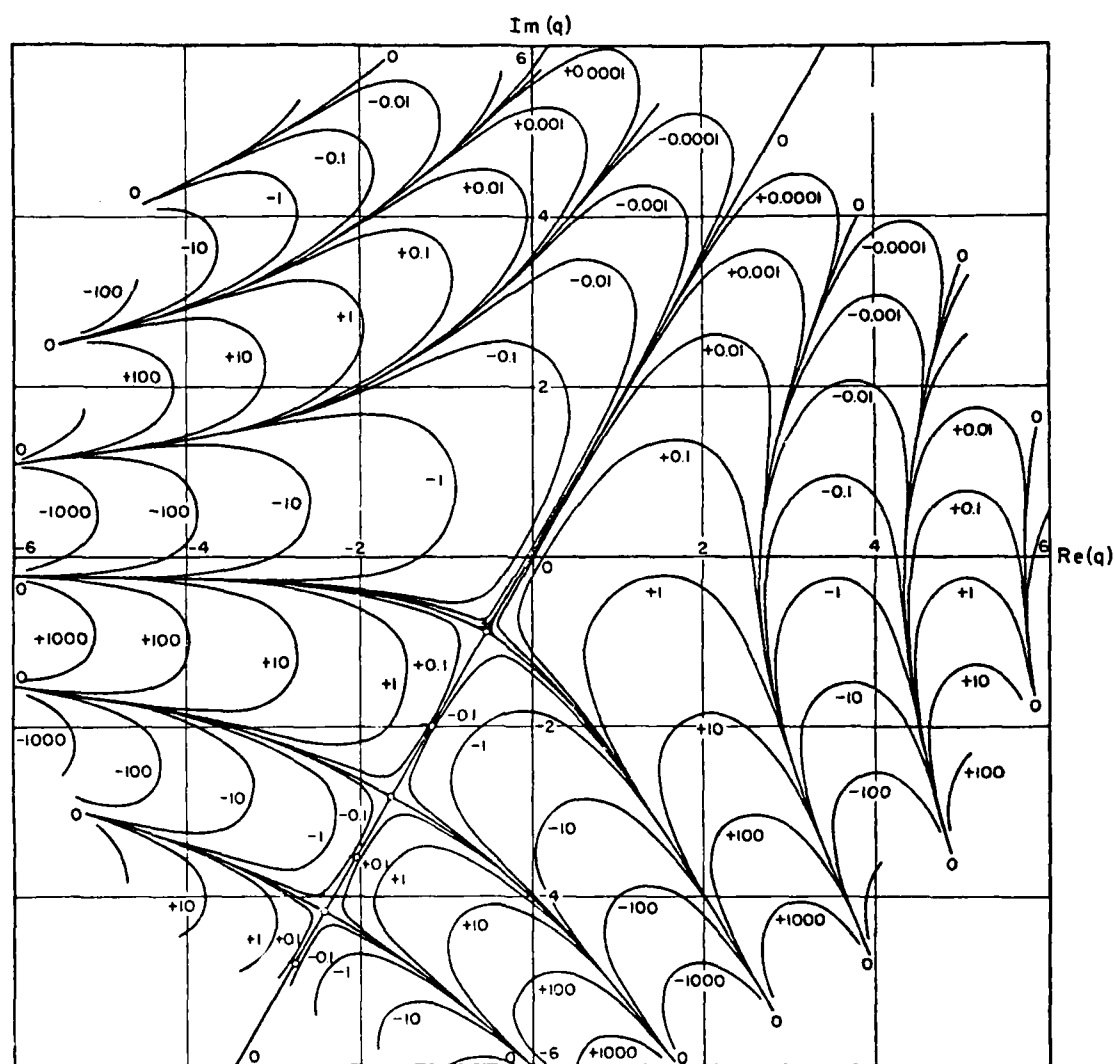
Figure A-1. Contours in the q-plane for $R_e(h_1)$ = constant (from Reference 14).
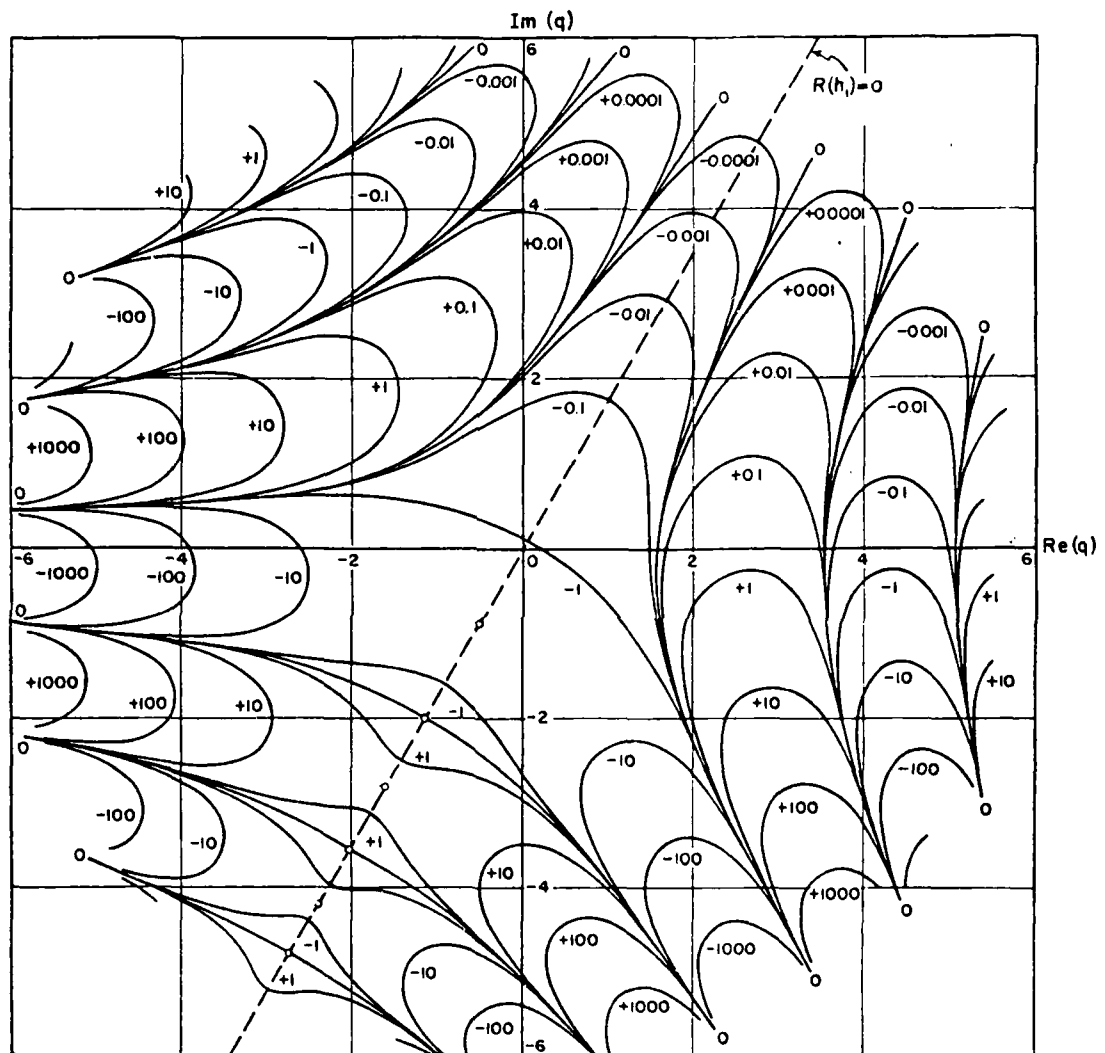
Figure A-2.   Contours in the q-plane for $I_m(h_1)$ = constant (from Reference 14).

175
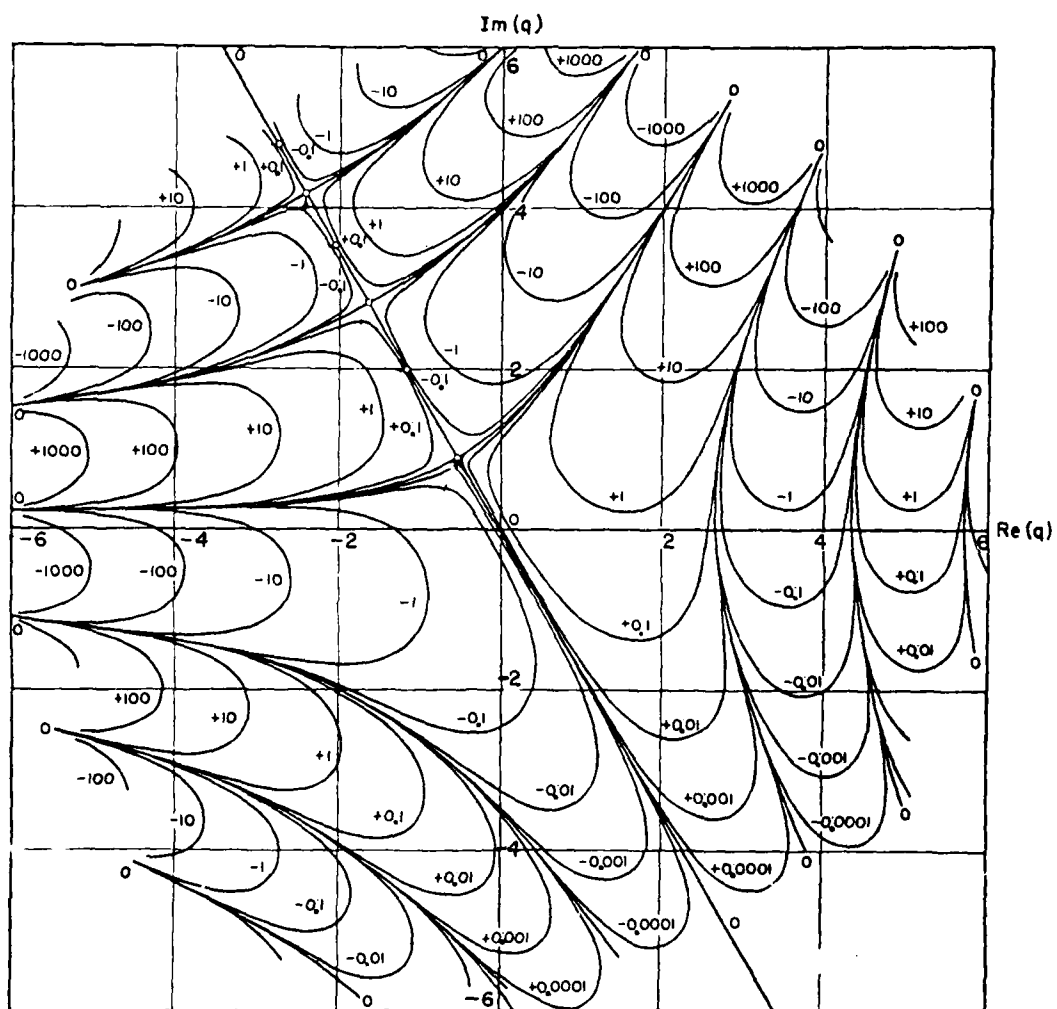
Figure A-3.   Contours in the q-plane for $R_e(h_2)$ = constant.

176
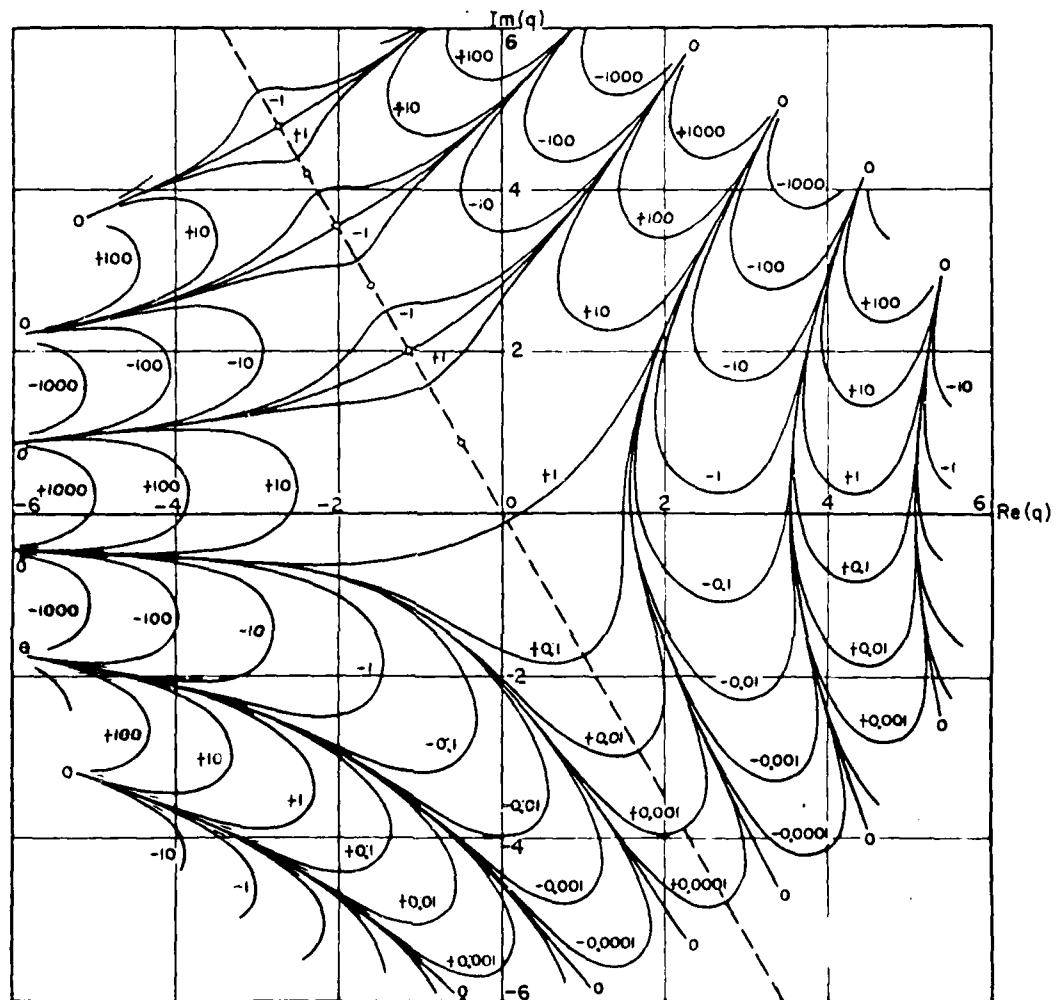
Figure A-4. Contours in the q-plane for $I_m(h_2) = $ constant.
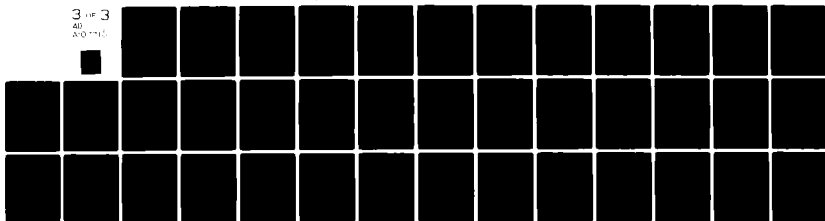
$$f(q) \;=\; e^{2/3\, jq^{3/2}} \tag{A-4}$$

$$g(q) \;=\; e^{-\frac{2}{3}\, jq^{3/2}} \tag{A-5}$$

where

$$A \;=\; 2^{\frac{1}{3}}\, e^{\frac{1}{6}}\, \pi^{-\frac{1}{2}} \;=\; 0.853667218838951$$

and

$$C_m \;=\; \frac{(9-4)\,(81-4)\;\cdot\;\cdot\;\cdot\;[9(2\,m-1)^2 - 4]}{2^{4m}\, 3^m\, m!}$$

Then:

$$h_1(q) \sim f(q)\, u(q), \quad 0 < \arg(q) < \pi \tag{A-6}$$

and

$$h_2(q) \sim g(q)\, v(q) + \begin{cases} 0 & , \ 0 < \arg(q) < \pi/2 \tag{A-7a} \\[2em] e^{4\pi j/3}\, f(q)\, u(q), & \frac{\pi}{2} < \arg(q) < \pi \end{cases}$$

$$\tag{A-7b}$$

The reason that different asymptotic expansions are needed in different regions of the complex plane (as in Equation A-7) is the fact that, although $h_1(q)$ and $h_2(q)$ are analytic for all finite values of q, these functions have branch cuts at infinity. Since the asymptotic expansion is essentially an expansion about a point at "infinity", the branch behavior becomes apparent in the asymptotic expansion. As discussed in Reference 14, Equation A-7a is valid in the region shown in Figure A-5a, while Equation A-7b is valid in the region shown in Figure A-5b. To avoid approaching the branch cut, it is convenient to use the region division used in Equation A-7.

From Equations A-1, A-6 and A-7:

$$F(q) \sim g(q)\, v(q) - \begin{cases} e^{4\pi j/3}\, f(q)\, u(q), & 0 < \arg(q) < \frac{\pi}{2} \tag{A-8a} \\[2em] 0 & , \ \frac{\pi}{2} < \arg(q) < \pi \end{cases}$$

$$\tag{A-8b}$$

Im(q)   Im(q)

(a)   (b)
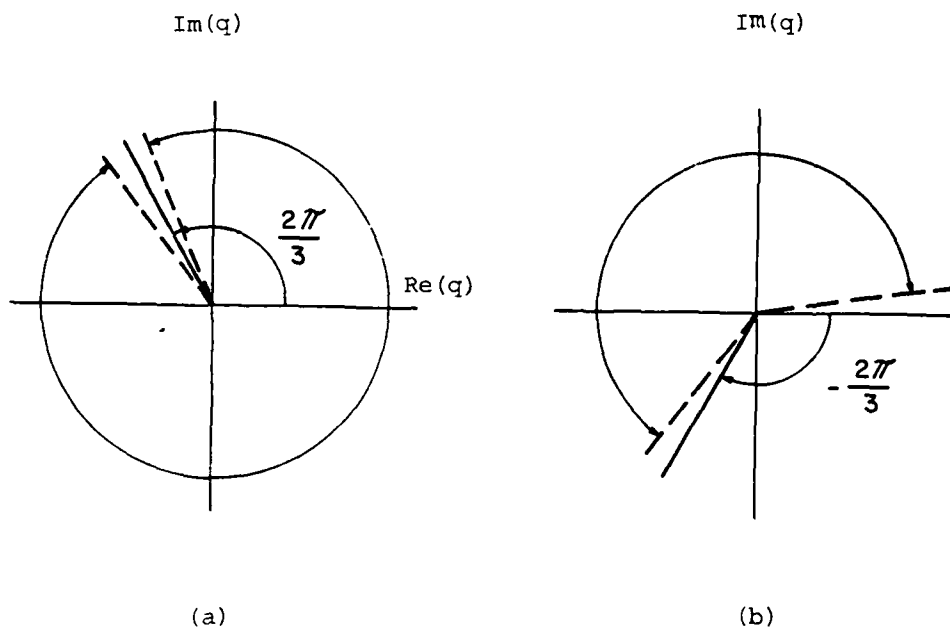
Region of validity of   Region of validity of
Equation A-7a   Equation A-7b

Figure A-5. Regions of validity of asymptotic expansions for h_2.

The exponential behavior of h_1, h_2 and F will enter through the variables f and g as defined by Equations A-4 and A-5. Letting:

$$q = \rho\, e^{j\theta} \tag{A-9}$$

where ρ and Θ are real, would produce:

$$q^{3/2} = \rho^{3/2} (\cos \frac{3}{2} \theta + j \sin \frac{3}{2} \theta) \tag{A-10}$$

so that

$$f = \alpha \, e^{j\beta}, \qquad g = \gamma \, e^{j\delta} \tag{A-11}$$

where

$$\alpha = e^{\frac{2}{3} \rho^{3/2} \sin \frac{3}{2} \theta} \, , \qquad \beta = \frac{2}{3} \rho^{3/2} \cos \frac{3}{2} \theta$$

$$\gamma = e^{\frac{2}{3} \rho^{3/2} \sin \frac{3}{2} \theta} \, , \qquad \varepsilon = - \frac{2}{3} \rho^{3/2} \cos \frac{3}{2} \theta \tag{A-12}$$

and α, β, γ and δ are real numbers. Since the modulus of $e^{j\beta}$ and $e^{j\delta}$ is unity, the magnitude of f and g may be obtained from α and γ, respectively. For a particular value of $\rho = |q|$, α and γ are determined by $\Theta = \arg (q)$. Whether α and γ are large or small would depend on the sign of the exponents in equation A-12, which in turn depends on the sign of $\sin \frac{3}{2} \Theta$. It is clear, though, that when α is exponentially large, γ is exponentially small, and vice versa. Now:

$$\text{sign} \left(\sin \frac{3}{2} \theta \right) = \begin{cases} 1, & 0 < \theta < 2\pi/3 \\ -1, & 2\pi/3 < \theta < \pi \end{cases} \qquad \text{(A-13)}$$

where only the values of $0 < \theta < \pi$ are considered since only the upper half of the q-plane is of interest. Therefore, for ρ large:

$$\begin{aligned} \alpha \ll 1, \qquad \gamma \gg 1, \qquad 0 < \theta < \frac{2\pi}{3} \\ \alpha \gg 1, \qquad \gamma \ll 1, \qquad \frac{2\pi}{3} < \theta < \pi \end{aligned} \qquad \text{(A-14)}$$

or

$$\begin{aligned} |f| \ll 1, \qquad |g| \gg 1, \qquad 0 < \theta < \frac{2\pi}{3} \\ |f| \gg 1, \qquad |g| \ll 1, \qquad \frac{2\pi}{3} < \theta < \pi \end{aligned} \qquad \text{(A-15)}$$

Therefore, from Equations A-6, A-7 and A-8,

$$\begin{aligned} |h_1(q)| \ll 1, \qquad 0 < \text{arg}(q) < \frac{2\pi}{3} \\ |h_1(q)| \gg 1, \qquad \frac{2\pi}{3} < \text{arg}(q) < \pi \end{aligned} \qquad \text{(A-16)}$$

$$|h_2(q)| \gg 1, \qquad 0 < \text{arg}(q) < \pi \qquad \text{(A-17)}$$

$$|F(q)| \gg 1, \qquad\qquad 0 < \arg(q) < \frac{2\pi}{3}$$

$$(A-18)$$

$$|F(q)| \ll 1, \qquad\qquad \frac{2\pi}{3} < \arg(q) < \pi$$

where, in Equations A-7b and A-8a, the fact was used that the sum of an exponentially large term and an exponentially small term is exponentially large. The inequalities in the above equations should be interpreted in terms of the "potential" for being much less than or greater than 1, since it is clear that as the boundary $\Theta = \arg(q) \to 2\pi/3$, the inequality would not necessarily hold.

From Equations A-16, A-17 and A-18, it is seen that $|h_1(q)|$ and $|h_2(q)|$ may both be exponentially large simultaneously in a portion of the upper half plane, whereas $h_1(q)$ and $F(q)$ cannot be large simultaneously in this region. This fact prompts the use of the functions $K_1(q) = h_1(q)$ and $K_2(q) = F(q)$ in the solution to the Stokes equation.

APPENDIX B

EVALUATION OF THE MODAL DETERMINANT

GENERAL

In searching for the roots of the modal determinant, this determinant must be evaluated many times. An efficient method for accomplishing this is, therefore, required. Standard elimination methods require many summing operations which should be avoided as much as possible if there are large differences in magnitude among the elements of the determinant. The evaluation method should also take maximum advantage of the presence of zero elements in the determinant. A method is described below to accomplish this. This will be done first for a simple 5-by-5 matrix. It will then be generalized to the N-by-N case.

5-by-5 MATRIX

When there are three atmospheric layers (L = 3), the modal determinant is given by Equation 136 which is written here as:

$$|A| = \begin{vmatrix} a_{11} & a_{12} & 0 & 0 & 0 \\ a_{21} & a_{22} & a_{23} & a_{24} & 0 \\ a_{31} & a_{32} & a_{33} & a_{34} & 0 \\ 0 & 0 & a_{43} & a_{44} & a_{45} \\ 0 & 0 & a_{53} & a_{54} & a_{55} \end{vmatrix} \qquad (B-1)$$

It is desired to evaluate this determinant.

The determinant in Equation B-1 can be written as a linear sum of cofactors:

$$|A| = a_{11} M(a_{11}) - a_{12} M(a_{12}) \qquad \text{(B-2)}$$

where the fact that $a_{13} = a_{14} = a_{15} = 0$ was used, and the determinants of the minors $M(a_{11})$ and $M(a_{12})$ are:

$$M(a_{11}) = \begin{vmatrix} a_{22} & a_{23} & a_{24} & 0 \\ a_{32} & a_{33} & a_{34} & 0 \\ 0 & a_{43} & a_{44} & a_{45} \\ 0 & a_{53} & a_{54} & a_{55} \end{vmatrix}$$

$$= - \begin{vmatrix} 0 & a_{22} & a_{23} & a_{24} \\ 0 & a_{32} & a_{33} & a_{34} \\ a_{45} & 0 & a_{43} & a_{44} \\ a_{55} & 0 & a_{53} & a_{54} \end{vmatrix} \qquad \text{(B-3)}$$

and

$$M(a_{12}) = \begin{vmatrix} a_{21} & a_{23} & a_{24} & 0 \\ a_{31} & a_{33} & a_{34} & 0 \\ 0 & a_{43} & a_{44} & a_{45} \\ 0 & a_{53} & a_{54} & a_{55} \end{vmatrix} = \begin{vmatrix} a_{21} & 0 & a_{23} & a_{24} \\ a_{31} & 0 & a_{33} & a_{34} \\ 0 & a_{45} & a_{43} & a_{44} \\ 0 & a_{55} & a_{53} & a_{55} \end{vmatrix}$$

(B-4b)

The final determinants in Equation B-4 were obtained by permuting the columns of the respective matrices.

Consider a system of four equations in four unknowns:

$$Bu = C \tag{B-5}$$

where B is the known, non-singular matrix formed from A as the minor of the a_{15} term:

$$B = M(a_{15}) = \begin{pmatrix} a_{21} & a_{22} & a_{23} & a_{24} \\ a_{31} & a_{32} & a_{33} & a_{34} \\ 0 & 0 & a_{43} & a_{44} \\ 0 & 0 & a_{53} & a_{54} \end{pmatrix} \tag{B-6}$$

u *is the unknown vector*

$$u = \begin{pmatrix} u_1 \\ u_2 \\ u_3 \\ u_4 \end{pmatrix} \tag{B-7}$$

and C is the known free vector formed by the negative of the last column of A excluding the first element:

$$C = \begin{pmatrix} 0 \\ 0 \\ -a_{45} \\ -a_{55} \end{pmatrix} \qquad (B-8)$$

Using Equations B-6 to B-8, the solution of u_1 is given by:

$$u_1 = - \frac{\begin{vmatrix} 0 & a_{22} & a_{23} & a_{24} \\ 0 & a_{32} & a_{33} & a_{34} \\ a_{45} & 0 & a_{43} & a_{44} \\ a_{55} & 0 & a_{53} & a_{54} \end{vmatrix}}{\begin{vmatrix} a_{21} & a_{22} & a_{23} & a_{24} \\ a_{31} & a_{32} & a_{33} & a_{34} \\ 0 & 0 & a_{43} & a_{44} \\ 0 & 0 & a_{53} & a_{54} \end{vmatrix}} = \frac{+ |M(a_{11})|}{|M(a_{15})|} \qquad (B-9)$$

and u_2 is given by:

$$u_2 = - \frac{\begin{vmatrix} a_{21} & 0 & a_{23} & a_{24} \\ a_{31} & 0 & a_{33} & a_{34} \\ 0 & a_{45} & a_{43} & a_{44} \\ 0 & a_{55} & a_{53} & a_{54} \end{vmatrix}}{|M(a_{15})|} = - \frac{|M(a_{12})|}{|M(a_{15})|} \qquad (B-10)$$

From Equations B-9 and B-10:

$$\left|M(a_{11})\right| = \left|M(a_{15})\right| u_1 \qquad\qquad (B-11)$$

and

$$\left|M(a_{12})\right| = - \left|M(a_{15})\right| u_2 \qquad\qquad (B-12)$$

so that Equation B-2 may be written:

$$\left|A\right| = \left|M(a_{15})\right| (a_{11}u_1 + a_{12}u_2) \qquad\qquad (B-13)$$

From Equation B-6, it is seen that the determinant of $M(a_{15})$ is simply the product of the determinant of the 2-by-2 submatrix in the upper left corner and the determinant of the 2-by-2 submatrix in the lower right corner. That is:

$$\left|M(a_{15})\right| = \begin{vmatrix} a_{21} & a_{22} \\ a_{31} & a_{32} \end{vmatrix} \cdot \begin{vmatrix} a_{43} & a_{44} \\ a_{53} & a_{54} \end{vmatrix} \qquad\qquad (B-14)$$

Substituting Equations B-6, B-7, and B-8 in Equation B-5 yields the system of equations:

$$a_{21} u_1 + a_{22} u_2 + a_{23} u_3 + a_{24} u_4 = 0 \tag{B-15a}$$

$$a_{31} u_1 + a_{32} u_2 + a_{33} u_3 + a_{34} u_4 = 0 \tag{B-15b}$$

$$a_{43} u_3 + a_{44} u_4 = -a_{45} \tag{B-15c}$$

$$a_{53} u_3 + a_{54} u_4 = -a_{55} \tag{B-15d}$$

It is clear from Equations B-15 that the values of u_3 and u_4 may be obtained by solving Equations B-15c and B-15d alone:

$$u_3 = \frac{\begin{vmatrix} -a_{45} & a_{44} \\ -a_{55} & a_{54} \end{vmatrix}}{\begin{vmatrix} a_{43} & a_{44} \\ a_{53} & a_{54} \end{vmatrix}} \tag{B-16}$$

$$u_4 = \frac{\begin{vmatrix} a_{43} & -a_{45} \\ a_{53} & -a_{55} \end{vmatrix}}{\begin{vmatrix} a_{43} & a_{44} \\ a_{53} & a_{54} \end{vmatrix}} \tag{B-17}$$

where it is assumed that the denominations have non-zero values.

Equations B-16 and B-17 may now be substituted into Equations B-15a and B-15b to obtain:

$$a_{21}\, u_1 + a_{22}\, u_2 = \cfrac{w_1}{\begin{vmatrix} a_{43} & a_{44} \\ a_{53} & a_{54} \end{vmatrix}} \qquad\qquad (B-18)$$

$$a_{31}\, u_1 + a_{32}\, u_2 = \cfrac{w_2}{\begin{vmatrix} a_{43} & a_{44} \\ a_{53} & a_{54} \end{vmatrix}} \qquad\qquad (B-19)$$

where

$$w_1 = a_{23} \begin{vmatrix} a_{45} & a_{44} \\ a_{55} & a_{54} \end{vmatrix} + a_{24} \begin{vmatrix} a_{43} & a_{45} \\ a_{53} & a_{55} \end{vmatrix} \qquad (B-20)$$

and

$$w_2 = a_{33} \begin{vmatrix} a_{45} & a_{44} \\ a_{55} & a_{54} \end{vmatrix} + a_{34} \begin{vmatrix} a_{43} & a_{45} \\ a_{53} & a_{55} \end{vmatrix} \qquad (B-21)$$

Equations B-18 and B-19 may be easily solved to yield:

$$u_1 = \cfrac{\begin{vmatrix} w_1 & a_{22} \\ w_2 & a_{32} \end{vmatrix}}{|M(a_{15})|} \qquad\qquad (B-22)$$

191

$$u_2 = \frac{\begin{vmatrix} a_{21} & w_1 \\ a_{31} & w_2 \end{vmatrix}}{|M(a_{15})|} \qquad\qquad (B\text{-}23)$$

where Equation B-14 was used.

Substituting Equations B-22 and B-23 in Equation B-13 results in:

$$|A| = a_{11} \begin{vmatrix} w_1 & a_{22} \\ w_2 & a_{32} \end{vmatrix} + a_{12} \begin{vmatrix} a_{21} & w_1 \\ a_{31} & w_2 \end{vmatrix} \qquad\qquad (B\text{-}24)$$

where w_1 and w_2 are given by Equations B-20 and B-21, respectively.

N-by-N MATRIX

The method utilized above for a 5-by-5 matrix will now be generalized. Consider the N-by-N matrix given by:

$$A = \begin{pmatrix} a_{11} & a_{12} & \cdots & \cdots & \cdots & a_{1N} \\ a_{21} & a_{22} & \cdots & \cdots & \cdots & a_{2N} \\ \vdots & \vdots & & & & \vdots \\ a_{N1} & a_{N2} & \cdots & \cdots & \cdots & a_{NN} \end{pmatrix} \qquad (B\text{-}25)$$

From the definition of the determinant of a matrix in terms of a cofactor expansion:

$$\left| A \right| = \sum_{i=1}^{N} (-1)^{i+1} \; a_{1i} \; \left| M(a_{1i}) \right| \qquad (B-26)$$

Define the following permutation operation on the columns of a square L-by-L matrix E: Let $P_\alpha^L(E)$ be the matrix formed by the operation of moving columns α, $\alpha+1$, $\alpha+2$, . . . ,L-1, L so that column L becomes column α, column α becomes column $\alpha+1$, column $\alpha+1$ becomes column $\alpha+2$, etc. Now:

$$\left| P_\alpha^L (E) \right| = (-1)^{L-\alpha} \left| E \right| \qquad (B-27)$$

In particular, let

$$E = M(a_{1i}) \qquad (B-28)$$

so that L = N - 1, and let α = i. Thus:

$$\left| E \right| = (-1)^{N-1-i} \left| P_i^{N-1} (E) \right| \qquad (B-29)$$

Then

$$\left| A \right| = \sum_{i=1}^{N-1} (-1)^{i+1} \; a_{1i} \; (-1)^{N-1-i} \left| P_i^{N-1} (M(a_{1i})) \right| + (-1)^{N+1} a_{1N} \left| M(a_{1N}) \right| \qquad (B-30)$$

$$= (-1)^N \sum_{i=1}^{N-1} a_{1i} \left| P_i^{N-1} (M(a_{1i})) \right| + (-1)^{N+1} a_{1N} \left| M(a_{1N}) \right|$$

Now consider the system of N-1 equations and N-1 unknowns:

$$Bu = C \tag{B-31}$$

where B is the known matrix formed from A as the minor of a_{1N}:

$$B = M(a_{1N}) = \begin{pmatrix} a_{21} & a_{22} & \cdot & \cdot & \cdot & \cdot & \cdot & \cdot & \cdot & \cdot & a_{2,\,N-1} \\ a_{31} & a_{32} & & & & & & & & & a_{3,\,N-1} \\ \vdots & \vdots & & & & & & & & & \vdots \\ a_{N1} & a_{N2} & & & & & & & & & a_{N,\,N-1} \end{pmatrix} \tag{B-32}$$

u is the unknown vector

$$u = \begin{pmatrix} u_1 \\ u_2 \\ \vdots \\ u_{N-1} \end{pmatrix} \tag{B-33}$$

and C is the known tree vector formed by the negative of the last column of A excluding the first element:

$$C = \begin{pmatrix} -a_{2N} \\ -a_{3N} \\ \vdots \\ -a_{NN} \end{pmatrix} \tag{B-34}$$

It is known that, if the matrix B is non-singular, the solution for u_i is obtained as:

$$u_i = \frac{|B^{(i)}|}{|B|} \, , \quad 1 \leq i \leq N-1 \tag{B-35}$$

so that

$$|B^{(i)}| = u_i \, |B| \, , \qquad 1 \leq i \leq N-1 \tag{B-36}$$

where $B^{(i)}$ is the matrix obtained by replacing the ith column of B with the free vector C. But some thought would show that:

$$|B^{(i)}| = -|P_i^{N-1} (M(a_{1i}))| \, , \qquad 1 \leq i \leq N-1 \tag{B-37}$$

Using Equations B-32 and B-37 in Equation B-36 leads to:

$$|P_i^{N-1} (M(a_{1i}))| = -u_i \, |M(a_{1N})| \, , \quad 1 \leq i \leq N-1 \tag{B-38}$$

Substituting Equation B-38 into Equation B-30 yields:

$$|A| = (-1)^N \left\{ -\sum_{i=1}^{N-1} a_{1i} u_i |M(a_{1N})| \right\} + (-1)^{N+1} a_{1N} |M(a_{1N})|$$

$$= (-1)^{N+1} |M(a_{1N})| \left\{ a_{1N} + \sum_{i=1}^{N-1} a_{1i} u_i \right\}$$

or

$$|A| = (-1)^{N+1} |M(a_{1N})| \sum_{i=1}^{N} a_{1i} u_i, \quad u_N \equiv 1 \qquad (B-39)$$

APPLICATION

At first glance, Equation B-39 looks more involved than its equivalents in Equations B-26 and B-30. Indeed, the form of Equation B-39 contains the unknowns in the vector u, which first must be solved through Equation B-31 before a *solution for* $|A|$ is obtained. Nevertheless, there exist matrices for which Equation B-39 represents a more efficient method for evaluating $|A|$ than does Equation B-26. Such a matrix would be one for which $B = M(a_{1N})$ would be relatively simple to evaluate even though $|A|$ is not.

Consider, for example, the N-by-N matrix A for which the submatrix $B = M(a_{1N})$ has the form illustrated in Figure B-1. About the diagonal of $M(a_{1N})$ are 2-by-2 and 3-by-3 submatrices which are each (except for those on the array boundary) flanked below and to the left by zero elements. There are, say, K such submatrices. The kth such matrix M_k will have N_k-by-N_k elements, so that:

$$\sum_{k=1}^{K} N_k = N-1 \qquad (B-40)$$

Define the determinant of M_k as:

$$D_k = |M_k| \qquad (B-41)$$

196
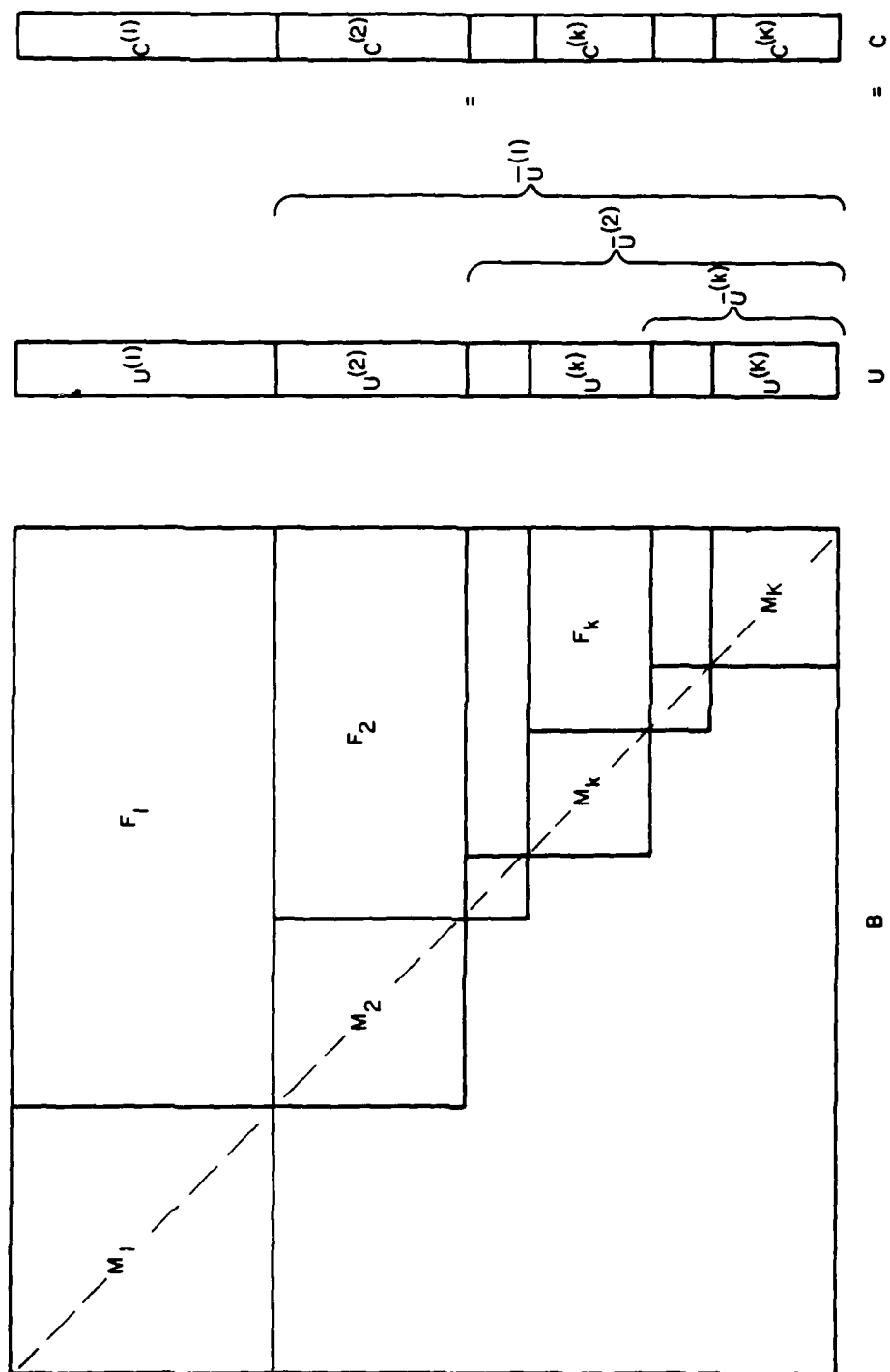
Figure B-1. Form of the matrices for the equation BU = C.

The rectangular matrix consisting of the elements of B to the right of M_k will be called the matrix F_k, $k = 1, 2 \ldots, K-1$. The elements of each F_k may be zero or non-zero. F_k will have N_k rows and $\overline{N}_k$ columns, where:

$$\overline{N}_k = \sum_{i=k+1}^{K} N_i \qquad\qquad (B-42)$$

Now define the subvectors $u^{(k)}$ of the unknown vector u as that portion of u corresponding to the matrix F_k (see Figure B-1). $u^{(k)}$ will contain N_k terms. Its first term will be the $n_I^{(k)}$ element of u, and its last term will be element number $n_F^{(k)}$ of u, where

$$n_I^{(k)} = \begin{cases} 1 + \sum_{i=1}^{k-1} N_i & , \quad k > 1 \\ 0 & , \quad k = 1 \end{cases} \qquad\qquad (B-43)$$

and

$$n_F^{(k)} = \sum_{i=1}^{k} N_i \qquad\qquad (B-44)$$

Similarly, define the subvectors $c^{(k)}$ of the free vector C.

Also define complementary subvectors $\overline{u}^{(k)}$ of the unknown vector u. $\overline{u}^{(k)}$ is the vector consisting of all terms in u beyond those which make up $u^{(k)}$. Thus the first term in $\overline{u}^{(k)}$ will be the term number $\overline{n}_I^{(k)}$ of u and the last term will be term number N-1 of u, where:

$$\overline{n}_I^{(k)} = n_F^{(k)} + 1 \qquad\qquad\qquad (B-45)$$

It is now clear that:

$$|B| = |M(a_{1N})| = \prod_{k=1}^{K} D_k \qquad\qquad (B-46)$$

Now the subvector $u^{(K)}$ may be solved using the equation:

$$M_K\, u^{(K)} = C^{(K)} \qquad\qquad\qquad (B-47)$$

so that

$$u_i^{(K)} = \frac{|M_K^{(i)}|}{D_K} \qquad\qquad\qquad (B-48)$$

where, again, $M_K^{(i)}$ is the matrix obtained by replacing the ith column of M_K with the vector $C^{(K)}$.

The subvector $u^{(K-1)}$ may be solved from the equation:

$$M_{K-1}\, u^{(K-1)} = C^{(K-1)} - F_{K-1}\, \overline{u}^{(K-1)}$$
$$\equiv \overline{C}^{(K-1)} \qquad\qquad\qquad (B-49)$$

so that

$$u_i^{(K-1)} = \frac{|M_{K-1}^{(i)}|}{D_{K-1}} \tag{B-50}$$

where $M_{K-1}(i)$ is the matrix obtained by replacing the ith column of M_{K-1} by the vector $\overline{C}^{(K-1)}$. The kth subvector $u^{(k)}$ may now be solved for through the equation:

$$M_k u^{(k)} = C^{(k)} - F_k \overline{u}^{(k)} \equiv \overline{C}^{(k)} \tag{B-51}$$

so that

$$u_i^{(k)} = \frac{|M_k^{(i)}|}{D_k} \tag{B-52}$$

This procedure may be continued until a solution is obtained for the subvector $u^{(1)}$. The values of u_i so calculated may be used along with Equation B-46 in Equation B-39 to obtain the determinant of A.

SINGULAR SUBMATRIX

The effect of one of the submatrices (say M_j) being singular is now considered. In solving this, an investigation is made into the manner in which D_j enters the final expression for A when D_j is small.

It is clear that D_j would not enter the successive calculations described in Equations B-51 and B-52 until the value of $u^{(j)}$ is to be evaluated. Then:

$$u_i^{(j)} = \frac{M_j^{(i)}}{D_j} = \frac{v_i^{(j)}}{D_j} \tag{B-53}$$

where the vector $v^{(j)}$ is defined:

$$v^{(j)} = \begin{pmatrix} |M_j^{(1)}| \\ \\ |M_j^{(2)}| \\ |M_j^{(3)}| \\ \vdots \\ |M_j^{(N_j)}| \end{pmatrix} \qquad\qquad (B-54)$$

The equation for $u^{(j-1)}$ is then:

$$M_{j-1}\, u^{(j-1)} = C^{(j-1)} - F_{j-1}\, \overline{u}^{(j-1)} \qquad\qquad (B-55)$$

But

$$\overline{u}^{(j-1)} = \begin{pmatrix} u^{(j)} \\ u^{(j+1)} \\ \vdots \\ u^{(K)} \end{pmatrix} = \begin{pmatrix} \dfrac{v^{(j)}}{D_j} \\ u^{(j+1)} \\ \vdots \\ u^{(K)} \end{pmatrix}$$

$$= \frac{1}{D_j} \begin{pmatrix} v^{(j)} \\ D_j\, u^{(j+1)} \\ D_j\, u^{(j+2)} \\ \vdots \\ D_j\, u^{(K)} \end{pmatrix} \equiv \frac{1}{D_j}\, \overline{v}^{(j-1)} \qquad (B-56)$$

Substituting this into Equation B-55 yields:

$$M_{j-1} u^{j-1} = \frac{1}{D_j} \left\{ D_j C^{(j-1)} - F_{j-1} \bar{v}^{(j-1)} \right\} \qquad (B-57)$$

As D_j becomes small, the first term in the brackets of Equation B-57 will vanish, as will all elements in the product $F_{j-1} \bar{v}^{(j-1)}$ containing the factor D_j. But this is the result that would be obtained if:

$$C^{(j-1)} = u^{(j+1)} = u^{(j+2)} = \ldots\ldots = u^{(K)} = 0$$

$$u^{(j)} = \frac{v^{(j)}}{D_j} \qquad (B-58)$$

Each term in the free vector in Equation B-57 will therefore be inversely proportional to D_j. In solving Equation B-57, each element of the vector $u^{(j-1)}$ will likewise be inversely proportional to D_j. The same reasoning may be used for $u^{(j-2)}$, $u^{(j-3)}$, $\ldots$, $u^{(1)}$ to show that each of these subvectors will be inversely proportional to D_j, and that the result obtained requires ignoring the subvectors $C^{(k)}$ and $u^{(k)}$, $j+1 \leq k \leq K$, in comparison to the other terms of the free vector. Using Equations B-58 and B-46 in Equation B-39 yields:

$$|A| = (-1)^{N+1} \prod_{k=1}^{K} D_k \sum_{i=1}^{N} a_{1i} u_i$$

$$\qquad (B-59)$$

$$= (-1)^{N+1} \prod_{\substack{k=1 \\ k \neq j}}^{K} D_k \sum_{i=1}^{N} a_{1i} \tilde{u}_i$$

where

$$
\tilde{u}_i = \begin{pmatrix} u^{(1)} \\ u^{(2)} \\ \vdots \\ u^{(j-1)} \\ v^{(j)} \\ 0 \\ \vdots \\ 0 \end{pmatrix}
$$

(B-60)

in which the factor D_j in the numerator and the denominator have been cancelled, and D_j does not appear in Equation B-59. The unknown $u^{(i)}$, $1 \leq i \leq j-1$ are assumed to be obtained using the successive method described by Equations 27 and 28, using:

$$
\begin{aligned}
C &= 0 \\
u^{(k)} &= 0, \qquad j + 1 \leq k \leq K
\end{aligned}
$$

(B-61)

and with $u^{(j)}$ replaced by $v^{(j)}$. Equation B-59 is the final value for the determinant when the jth submatrix M_j is singular.

In the event that both M_j and $M_{j-\alpha}$ are singular, where α is a positive integer, then the resulting value of $|A|$ would be:

$$
|A| = (-1)^{N+1} \prod_{\substack{k=1 \\ k \neq j,\ j-\alpha}}^{K} D_k \sum_{i=1}^{N} a_{1i} \tilde{u}_i
$$

(B-62)

where

where

$$\tilde{u}_i = \begin{pmatrix} u^{(1)} \\ u^{(2)} \\ \vdots \\ u^{(j-\alpha-1)} \\ \\ v^{j-\alpha} \\ 0 \\ \vdots \\ 0 \end{pmatrix} \qquad\qquad (B\text{-}63)$$

and the $u^{(k)}$, $1 \le k \le j- \alpha - 1$ are obtained as described above. The extension to any number of singular submatrices is straightforward.

PARTICULAR CASE

Of particular interest will be the matrix A with:

$$a_{1i} = 0, \qquad N_1 + 1 \le i \le N \qquad\qquad (B\text{-}64)$$

$$a_{iN} = 0, \qquad N - N_K + 1 \le i \le N \qquad\qquad (B\text{-}65)$$

and with

$$(F_k)_{\alpha\beta} = 0, \qquad \beta > N_{k+1} \qquad\qquad (B\text{-}66)$$

$$|A| = (-1)^{N+1} |M(a_{1N})| \sum_{i=1}^{N} a_{1i} u_i^1 \qquad (B\text{-}67)$$

From Equation B-65:

$$c^{(1)} = c^{(2)} = \ldots = c^{(K-1)} = 0 \qquad (B\text{-}68)$$

and from Equation B-66, the submatrix $M(a_{1N})$ is as shown in Figure B-2. The non-zero portion of the F_k will be called F_k', and will have N_k rows and N_{k+1} columns.

The first step in the solution procedure is determination of the elements of $u^{(K)}$ from Equations B-47 and B-48 to yield:

$$u^{(K)} = \frac{v^{(K)}}{D_K} \qquad (B\text{-}69)$$

where again $v^{(K)}$ is the vector, the ith term of which is the determinant of the matrix formed by replacing the ith column of M_K by the free vector $c^{(K)}$.

B =
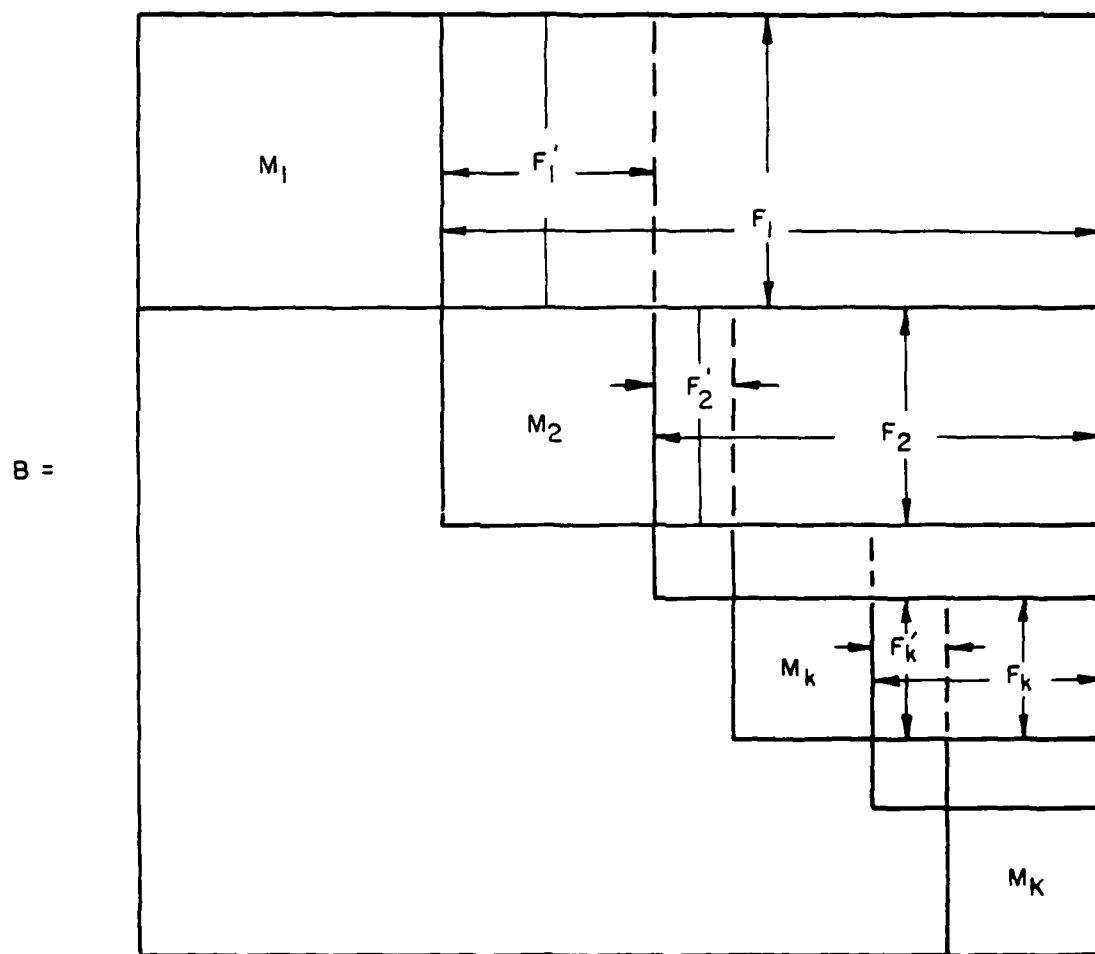
Figure B-2.   Submatrix $M(a_{1N})$.

From Equations B-49 and B-68, the elements of $u^{(K-1)}$ are given by:

$$M_{K-1} \, u^{(K-1)} \;=\; -F_{K-1} \, \overline{u}^{\,(K-1)} \;=\; -F_{K-1}' \, u^{(K)}$$

$$=\; F_{K-1}' \, \frac{v^{(K)}}{D_K} \;\equiv\; \frac{\overline{C}^{\,(K-1)}}{D_K} \qquad\qquad (B\text{-}70)$$

This has the solution:

$$u^{(K-1)} \;=\; \frac{v^{(K-1)}}{D_K \, D_{K-1}} \qquad\qquad (B\text{-}71)$$

where now $v^{(K-1)}$ is the vector, the ith term of which is the determinant of the matrix formed by replacing the ith column of M_{K-1} by the vector $\overline{C}^{\,(K-1)}$.

The elements of $u^{(k)}$ are given by:

$$M_k \, u^{(k)} \;=\; -F_k' \, u^{(k)} \;=\; -F_k' \, \frac{v^{(k-1)}}{D_K \, D_{K-1} \, D_{K-2} \, \cdots \, D_{k-1}}$$

$$=\; -F_k' \, \frac{v^{(k-1)}}{\displaystyle\prod_{i=k-1}^{K} D_i} \;=\; \frac{\overline{C}^{\,(k)}}{\displaystyle\prod_{i=k-1}^{K} D_i} \qquad\qquad (B\text{-}72)$$

with the solution:

$$u^{(k)} = \frac{v^{(k)}}{\prod\limits_{i=k}^{K} D_i} \tag{B-73}$$

The solution of $u^{(1)}$ will similarly be given by:

$$u^{(1)} = \frac{v^{(1)}}{\prod\limits_{i=1}^{K} D_i} \tag{B-74}$$

Substituting Equation B-46 and B-74 into Equation B-67 yields:

$$|A| = (-1)^{N+1} \sum_{i=1}^{N} a_{1i} v_i^{(1)} \tag{B-75}$$

Thus it is seen that, for this particular form of the matrix A, the determinants of the submatrices do not enter into the final expression for $|A|$. It follows that Equation B-75 also holds when any of the submatrices is singular.

EXAMPLE - FIELDS IN HOMOGENEOUS STRATIFIED LAYERS

Consider L layers of atmosphere over a ground, with each layer homogeneous and characterized by a parameter α. In acoustics, this parameter might be the medium density. In electromagnetics, this might be the permittivity ε. A field quantity E_i in the ith layer may be written as:

$$E_i(r, z) = \int \Psi_i(\alpha_i k, z) f(k,r) dk \tag{B-76}$$

where f is a known kernel and the integration is over a closed contour in the complex k-plane. Assuming the quantity Ψ_i satisfies a linear second-order differential equation, it may be written as:

$$\Psi_i(\alpha_i,k,z) = A_i \bar{h}_1(\alpha_i,k,z) + B_i \bar{h}_2(\alpha_i,k,z) + \delta_{ip} g(\alpha_i,k,z,z_T) \quad (B-77)$$

where

$\bar{h}_1$ and $\bar{h}_2$ are linearly independent functions,

g is a Green function, which is a particular solution of the governing differential equation that accounts for a source at the location

$z = z_T$ located in the pth layer,

δ_{ip} is the Kronecker delta function.

The unknowns A_i and B_i may be found by solving the system of linear equations representing the boundary conditions on the Ψ_i and $\Psi_i' \equiv \partial\Psi_i/\partial z$ at the layer interfaces ($z = z_i$, $1 \le i \le L-1$) and at the ground, ($z = z_o$) and the radiation conditions at $z \to \pm\infty$. For L = 4 This system will have the form:

$$
\begin{aligned}
A_1\, h_1(q_{10}) + B_1\, h_2(q_{10}) \qquad\qquad\qquad\qquad\qquad\qquad\qquad &= 0\\
A_1\, h_1(q_{11}) + B_1\, h_2(q_{11}) - A_2\, h_1(q_{21}) - B_2\, h_2(q_{21}) \qquad\qquad\qquad &- f_1\\
A_1\, h_1'(q_{11}) + B_1\, h_2'(q_{11}) - A_2\, h_1'(q_{21}) - B_2\, h_2'(q_{21}) \qquad\qquad\qquad &= f_2\\
A_2\, h_1(q_{22}) + B_2\, h_2(q_{22}) - A_3\, h_1(q_{32}) - B_3\, h_2(q_{32}) &= f_3\\
A_2\, h_1'(q_{22}) + B_2\, h_2'(q_{22}) - A_3\, h_1'(q_{32}) - B_3\, h_2'(q_{32}) &= f_4\\
A_3\, h_1(q_{33}) + B_3\, h_2(q_{33}) - B_4\, h_2(q_{43}) &= 0\\
A_3\, h_1'(q_{23}) + B_3\, h_2'(q_{33}) - B_4\, h_2'(q_{43}) &= 0
\end{aligned}
$$

$$(B-78)$$

where $h_m(q_{ji}) \equiv \bar{h}_m(\alpha_i,k,z_j)$, j=i, i+1, i > 0, $h_m(q_{10}) \equiv \bar{h}_m'(q_{10}) - G\bar{h}_m(q_{10})$, where G is a function of k and the ground parameters, and it has been assumed that p=2. The f_i are functions of k. Equation B-76 may be evaluated using residue theory, where the poles of Ψ_i are the values of k at which the determinant of the above system of equations vanishes. When the roots of this

determinant are evaluated numerically, the determinant must be evaluated many times, thus making an efficient means for such evaluation very useful.

The matrix has the form:

$$
A = \begin{pmatrix}
a_{11} & a_{12} & 0 & 0 & 0 & 0 & 0 \\
a_{21} & a_{22} & a_{23} & a_{24} & 0 & 0 & 0 \\
a_{31} & a_{32} & a_{33} & a_{34} & 0 & 0 & 0 \\
0 & 0 & a_{43} & a_{44} & a_{45} & a_{46} & 0 \\
0 & 0 & a_{53} & a_{54} & a_{55} & a_{56} & 0 \\
0 & 0 & 0 & 0 & a_{65} & a_{66} & a_{67} \\
0 & 0 & 0 & 0 & a_{75} & a_{76} & a_{77}
\end{pmatrix}
\tag{B-79}
$$

This matrix has the form of the matrix in Figure B-2, and the evaluation of its determinant may be accomplished using the algorithm described above. The total number of multiplication operations required is on the order of 8K where K is the number of 2nd-order submatrices. In the example above, K= 3, so that the number of multiplication operations is 24, or about the number of non-zero terms in the matrix. This compares with N! for the case of expansion of the determinant in cofactors, which, for the above example, would be over 5000.

In the event the submatrices were of order 3, then the number of multiplication operations would be on the order of 45K. If K= 2, in a 7-by-7 matrix such as Equation B-79, this number would be 90, which still is small compared with the 5000 operations required to evaluate the determinant of a 7-by-7 matrix using a cofactor expansion.

LIST OF REFERENCES

1. Ortenburger, L. N., Lawson, S. B. and Miller, G. K., <u>Radiosonde Data Analysis Summary Maps of Observed Data</u>, GTE Sylvania, Inc., December 1978.

2. Kerr, D. E., <u>Propagation of Short Radio Waves</u>, MIT Radiation Laboratory Series, Vol. 13, McGraw-Hill Book, New York, NY, 1951.

3. Pekeris, C. L., "Wave Theoretical Interpretation of Propagation of 10-Centimenter and 3-Centimeter Waves in Low-Level Ocean Ducts," <u>Proc. of the IRE</u>, May 1947, pp. 453-462.

4. Pekeris, C. L., "Accuracy of the Earth-Flattening Approximation in the Theory of Microwave Propagation," <u>Physical Review</u>, Vol. 70, Nos. 7 and 8, 1 and 15 October 1946, p. 518.

5. Pappert, R. A., and Goodhart, C. L., <u>Waveguide Calculations of Signal Levels in Tropospheric Ducting Environments</u>, TN 3129, Naval Electronics Laboratory Center, San Diego, CA, 25 February 1976.

6. Budden, K. G., <u>The Wave-Guide Mode Theory of Wave Propagation</u>, Prentice Hall, Englewood Cliffs, NJ, 1961.

7. Wait, J. R., and Spies, K. P., "Internal Guiding of Microwaves by an Elevated Tropospheric Layer," <u>Radio Science</u>, Vol. No. 4, April 1969, pp. 319-326.

8. Dresp, M. R., <u>Tropospheric Duct Propagation at VHF, UHF, and SHF</u>, MITRE Technical Report MTR-3114, Vols. I and II, MITRE Corporation, Bedford, MA, October 1975.

9. Skillman, J. L., and Woods, D. R., "Experimental Study of Elevated Ducts," <u>Proc. of Conference on Atmospheric Refractivity Effects Assessment</u>, Technical Document 260, Naval Ocean Systems Center, San Diego, CA, 15 June 1979.

10. Goodhart, C. L., and Pappert, R. A., <u>Application of a Root Finding Method for Tropospheric Ducting Produced by Trilinear Refractivity Profiles</u>, Technical Report 153, Naval Ocean Systems Center, San Diego, CA, 12 September 1977.

11. Cho, S. H., and Wait, J. R., <u>Analytical Study of Whispering Gallery Transmission in a Non-Uniform Tropospheric</u>, Interim Report, Cooperative Institute for Research in Environmental Sciences, University of Colorado, Boulder, CO, 30 December 1976.

12. Cho, S.H., Migliora, C. G. and Felsen, L. B., "Hybrid Ray-Mode Formulation of Tropospheric Propagation," <u>Proc. of Conference on Atmospheric Refractivity Effects Assessment</u>, Technical Document 260, Naval Ocean Systems Center, San Diego, CA, 15 June 1979.

LIST OF REFERENCES (Continued)

13. Tyras, G., _Radiation and Propagation of Electromagnetic Waves_, Academic Press, New York, NY, 1969.

14. Harvard Computational Laboratory, _Tables of Modified Hankel Functions of Order One-Third and of Their Derivatives_, Harvard University Press, Cambridge, MA, 1945.

15. Wait, J. R., _Electromagnetic Waves in Stratified Media_, Pergamon Press, New York, NY, 1962.

16. Churchill, R. V., _Introduction to Complex Variables and Applications_, p. 122, McGraw Hill Book Co., New York, NY, 1948.

17. Dresp, M. R., _Tropospheric Duct Propagation at VHF, UHF and SHF_, MITRE Technical Report MTR-3114, Vols. I and II, MITRE Corporation, Bedford, Ma, October 1975.

18. Morfitt, D. G., and Shellman, C. H., _MODESRCH, An Improved Computer Program for Obtaining ELF/VLF/LF Mode Constants in an Earth - Ionosphere Waveguide_, Interim Report 77T prepared for Defense Nuclear Agency, Naval Electronics Laboratory Center, San Diego, CA, 1 October 1976.

19. Pennington, R. H., _Introductory Computer Methods and Numerical Analysis_, Macmillian Co., p. 236 ff, New York, NY.

20. Pappert, R. A., and Goodhart, C. L., "Case Studies of Beyond-the-Horizon Propagation in Tropospheric Ducting Environments," _Radio Science_, Vol. 12, No. 1, pp. 75-87, January-February 1977.

21. Pappert, R. A., and Goodhart, C. L., "A Numerical Study of Tropospheric Ducting at HF," _Radio Science_, Vol. 14, No. 5, pp. 803-813, September-October 1979.

DISTRIBUTION LIST FOR
A MODEL TO CALCULATE EM FIELDS IN TROPOSPHERIC
DUCT ENVIRONMENT AT FREQUENCIES THROUGH SHF
ESD-TR-81-102

EXTERNAL   Copies

Special Projects

Director   2
National Security Agency
Attn: W36/Mr. V. McConnell
Ft. George G. Meade, MD 20755

Department of Transportation   1
Federal Aviation Administration
Attn: ARD-62
2100 Second St., S.W.
Washington, DC 20591

National Aeronautics &   1
Space Administration
Goddard Space Flight Center
Attn: Code 801/Jim Scott
Greenbelt, MD 20771

Army

CDR, USATECOM   1
Attn: DRSTE-EL (L. Doughty)
Aberdeen Proving Ground, MD 21005

USAAMSAA   1
Attn: (H. Dubin)
Aberdeen Proving Ground, MD 21005

Commander   1
US Army Signal Center & Fort Gordon
Attn: ATZHCD-SD (H. Siemen)
Fort Gordon, GA 30905

CDR, USAEPG   1
Attn: STEEP-MT-M
Fort Huachuca, AZ 85613

CDR, USACEEIA   1
Attn: CCC-EMEO (Mr. H. Merkel)
Fort Huachuca, AZ 85613

Copies

CDR, USACECOM   1
Attn: DRSEL-COM-RY-3 (P. Major)
Fort Monmouth, NJ 07703

CDR, USACECOM   1
Attn: DRSEL-SEI-A (S. Segner)
Fort Monmouth, NJ 07703

CDR, USAMICOM   1
Attn: DRSMI-RE (D. Smith)
Redstone Arsenal, AL 35809

ASD/XRE   1
Mr. E. G. Barthel
Wright-Patterson APF, OH 45433

Commander   1
US Army Forces Command
Attn: AFOP-PM
Fort McPherson, GA 30330

Air Force

HQ RADC/RBC   1
Griffiss AFB, NY 13441

Air University Library   1
Maxwell AFB, AL 36112

AFGL(SULR)   3
Hanscom AFB, MA 01731

Navy

Chief of Naval Operations (OP-941F)   1
Navy Department
Washington, DC 20350

Commander (ELEX-832)   1
Naval Electronic Systems Command
Washington, DC 20360

Copies

Superintendent   1
Naval Postgraduate School
Monterey, CA 93940

Commanding Officer   1
Fleet Numerical Oceanography Center
Monterey, CA 93940

Commander   1
Naval Ocean Systems Center
Attn: Dr. P. Li (Code 8112)
San Diego, CA 92152

Commander   1
Naval Ocean Systems Center
Attn: Dr. J. Rockway (Code 8105)
San Diego, CA 92152

Commander   1
Naval Ocean Systems Center
Attn: H. V. Hitney
San Diego, CA 92152

Commander   1
Naval Ocean Systems Center
Attn: R. A. Paulus
San Diego, CA 92152

DoD and Others

CDR, USAERADCOM   1
Attn: DRDCO-COM-RP-2CP
Fort Monmouth, NJ 07703

CDR, USAERADCOM   1
Attn: Dr. Haim Soicher
Fort Monmouth, NJ 07703

CDR, USACEEIA   1
Attn: CCCEMEO-MED (George Lane)
Fort Huachuca, AZ 85613

Copies

Robert Rose   1
Code 5321
Naval Ocean Systems Center
San Diego, CA 92152

Dr. George Hufford
National Telecommunications and Information Administration   1
Institute for Telecommunications Sciences
Boulder, CO 80303

Dr. Charles Rush   1
National Telecommunications and Information Administration
Institute for Telecommunications Sciences
Boulder, CO 80303

Prof. Nathan M. Reiss   2
Department of Meteorology and Physical Oceanography
Cook College
Rutgers University, NJ 08903

M. R. Dresp   1
MITRE Corp.
P.O. Box 208
Bedford, MA 01730

Dr. Bradford R. Bean   1
Chief, Propagation Research Branch
NOAA/ERL
Boulder, CO 80303

John L. Skillman   1
NSA/R521
Fort Meade, MD 20755

Douglas R. Woods   1
NSA/R521
Fort Meade, MD 20755

Frank T. Wu   1
Michelson Laboratory
Naval Weapons Center
China Lake, CA 93555

Copies

Perry Snyder   1
Code 5325
Naval Ocean Systems Center
San Deigo, CA 92152

Prof. James R. Wait   1
Department of Electrical Engineering
The University of Arizona
Tuscon, AZ 85721

Prof. L. B. Felsen   1
Department of Electrical Engineering
Polytechnic Institute of New York
Route 113, Farmingdale, NY 11735

R. A. Pappert   1
Naval Ocean Systems Center
San Diego, CA 92152

Prof. Ezekial Bahar   1
Electrical Engineering Department
University of Nebraska
Lincoln, NB 68588

Victor Tawil   1
Federal Communications Commission
Office of Chief Engineer/Research Division
2025 M St. N.W.
Washington, DC 20054

Jeffrey Knorr   1
Naval Post Graduate School
Monterey, CA 93940

William F. Daniel   1
Office of Chief Engineer/Research Div.
2025 M St. N.W.
Washington, DC 20054

Carl A. Bower   1
Chief, Systems Support Branch
USAF ETAC
Scott AFB, IL 62225

DISTRIBUTION LIST FOR
ESD-TR-81-102 (Continued)

Harry Ng   1
FSSM
National Telecommunications and Information Administration
179 Admiral Cochrane Dr.
Annapolis, MD 21401

W. Frazier
FSSM
National Telecommunications and Information Administration   1
179 Admiral Cochrane Dr.
Annapolis, MD 21401

H. T. Dougherty   1
National Telecommunications and Information Administration
Institute for Telecommunication Sciences
Boulder, CO 80303

Sherman Marcus, Ph.D.   7
Hatichon Street, 8A
Haifa, Israel

Defense Technical Information Center   12
Cameron Station
Alexandria, VA 22314

INTERNAL
SMDL   5
XM/J. Janoski   1
DO/S. Cameron   1
DO/R. Whiteman   1
SAB/L. Katz   1
SABN/S. Timerman   1
SAG/M. Aasen   1
SAGE/E. Freeman   1
SAGE/H. Hodes   3
SAGE/J. Preis   1
SMA/J. Cook   1
SMA/D. Baran   1
SMA/D. Madison   1
SMAD/A. Fitch   1
SAMD/E. Kaita   1
SMAD/K. O'Haver   1
SMAD/J. Powell   1
SMAD/H. Riggins   5

Copies

	Copies
SMAD/B. Stuart	6
SMAD/R. Meidenbauer	1
SMAM/M. Weissberger	1
SMAS/F. Ellis	1
SMAS/M. Gruendl	1
SMAS/A. Tomko	1
SMOA/J. Jones	1
SM-1	1

DAT
ILM